National Technical University of Athens

School of Civil Engineering

Institute of Structural Analysis and Antiseismic Research

OPTIMIZED DESIGN OF STEEL STRUCTURES UNDER SEISMIC LOADING

PhD Dissertation

Athanasia E. Zacharenaki

Advisor:

Professor Manolis Papadrakakis

Athens, September 2014

Εθνικό Μετσόβιο Πολυτεχνείο

Σχολή Πολιτικών Μηχανικών

Εργαστήριο Στατικής και Αντισεισμικών Ερευνών

Βελτιστοποιημένος σχεδιασμός μεταλλικών κατασκευών υπό σεισμικά φορτία

Διδακτορική Διατριβή

της

Αθανασίας Εμμ. Ζαχαρενάκη

Επιβλέπων:

Καθηγητής Μανόλης Παπαδρακάκης

Αθήνα, Σεπτέμβριος 2014

Dedicated to

my family

PhD Examination Committee

I certify that I have read this dissertation and that in my opinion it is fully adequate, in scope and quality, as a dissertation for the degree of Doctor of Philosophy.

Manolis Papadrakakis
Professor
(Advisor)
School of Civil Engineering
National Technical University of Athens

I certify that I have read this dissertation and that in my opinion it is fully adequate, in scope and quality, as a dissertation for the degree of Doctor of Philosophy.

Charalampos Gantes
Professor
(Member of the Advisory Committee)
School of Civil Engineering
National Technical University of Athens

I certify that I have read this dissertation and that in my opinion it is fully adequate, in scope and quality, as a dissertation for the degree of Doctor of Philosophy.

Konstantinos Spiliopoulos
Professor
(Member of the Advisory Committee)
School of Civil Engineering
National Technical University of Athens

I certify that I have read this dissertation and that in my opinion it is fully adequate, in scope and quality, as a dissertation for the degree of Doctor of Philosophy.

Ioannis Psycharis
Professor
School of Civil Engineering
National Technical University of Athens

I certify that I have read this dissertation and that in my opinion it is fully adequate, in scope and quality, as a dissertation for the degree of Doctor of Philosophy.

Nikos D. Lagaros
Assistant Professor
School of Civil Engineering
National Technical University of Athens

I certify that I have read this dissertation and that in my opinion it is fully adequate, in scope and quality, as a dissertation for the degree of Doctor of Philosophy.

Dimitrios Vamvatsikos
Lecturer
School of Civil Engineering
National Technical University of Athens

I certify that I have read this dissertation and that in my opinion it is fully adequate, in scope and quality, as a dissertation for the degree of Doctor of Philosophy.

Michalis Fragiadakis
Lecturer
School of Civil Engineering
National Technical University of Athens

Abstract

This dissertation has two goals; first goal is the examination of the accuracy of the incremental dynamic analysis (IDA) method and secondly to investigate the practicality of using of IDA within a structural optimization procedure. Incremental dynamic analysis involves a series of nonlinear response history analyses with a suite of incrementally scaled ground motion records. Although IDA is perhaps the most comprehensive seismic performance assessment method, it receives criticism because several ground motion records are scaled up until structural collapse. The scaling practice often results to unrealistic multipliers, -which modify the amplitude of the ground motion and introduce bias on the structural performance estimation. Record scaling is a common practice in earthquake engineering due to the lack of natural records corresponding to large magnitudes and/or small distances from the fault rupture location.

In this study we use a large number of ground motion records to compare the predictions of IDA with that of unscaled ground motions and we propose a new methodology in order to quantify the bias introduced in IDA. Apart from natural records, we have conducted broadband ground motion simulations for rupture scenarios of weak, medium and large magnitude events in order to expand our record database. The investigation is performed on a series of inelastic single-degree-of-freedom systems and on two multistorey steel moment frame buildings. The results pinpoint both qualitatively and quantitatively, for the full range of limit-states, the bias that IDA introduces on the structural performance estimation.

Furthermore, an algorithm is presented for the reliability-based seismic design of structures incorporating approximate performance estimation methods and structural optimization. The proposed algorithm allows the automatic optimized design of steel moment-resisting frames using reliability-based criteria and more specifically design criteria based on the mean annual frequency (MAF) that a limit-state is exceeded. Such criteria allow setting constraints with a clear engineering meaning and help to obtain building designs of improved performance and reduced cost. In this dissertation, we

propose a simplified approach that allows a quick calculation of the limit-state mean annual frequencies without significant loss of accuracy. More specifically, we use the static-pushover-to-incremental-dynamic-analysis (SPO2IDA) method, which is a fast and accurate method to estimate the seismic demand and capacity of single-degree of freedom systems and first-mode-dominated multi-degree-of-freedom systems in regions ranging from near-elastic to global collapse. SPO2IDA extracts information from the static pushover curve and produces estimates of the limit-state response statistics that are necessary to implement the reliability-based criteria on the limit-state MAF. The optimization problem at hand is solved with a specifically tailored genetic algorithm. A three and a nine-storey steel moment-resisting frame are used to demonstrate the efficiency of the proposed procedure, leading to efficient building designs within reasonable computing time.

The dissertation consists of eight chapters in total, plus one appendix at the end of it. Its structure is organized as follows: *Chapter 1* contains the introduction, *Chapter 2* presents natural, synthetic and artificial records and outlines the measures of ground motion intensity. *Chapter 3* describes seismic performance assessment methods starting from linear static analysis to incremental dynamic analysis. In *chapter 4* the uncertainty in structural engineering is discussed by presenting the PEER (Pacific Earthquake Engineering Research) framework and the SAC/FEMA (Federal Emergency Management Agency) approach. In *chapter 5* the assessment of the bias introduced in IDA due to scaling is considered with the LOESS (locally weighted scatterplot smoothing algorithm) enabling the composition of a curve described by an intensity measure (IM)- engineering demand parameter (EDP) and the bootstrap analysis investigating the significance of our numerical results. *Chapter 6* provides the theoretical basis of structural optimization encompassing single-objective optimization and genetic algorithms. *Chapter 7* presents the reliability-based optimum seismic design of structures using approximate performance estimation methods and especially static pushover to incremental dynamic analysis (SPO2IDA) method. In chapter 8 the conclusions of this research work are presented.

Περίληψη

Βελτιστοποιημένος σχεδιασμός μεταλλικών κατασκευών υπό σεισμικά φορτία

Στην παρούσα διδακτορική διατριβή προτείνονται μέθοδοι για τον βελτιστοποιημένο σχεδιασμό μεταλλικών κατασκευών υπό σεισμικά φορτία. Προς τούτο χρησιμοποιήθηκε η μέθοδος της Προσαυξητικής Δυναμικής Ανάλυσης (ΠΔΑ). Η μέθοδος αυτή εξετάστηκε ως προς την ακρίβειά της και έπειτα με την βοήθεια ενός αλγόριθμου βελτιστοποίησης χρησιμοποιήθηκε για τον βέλτιστο σχεδιασμό κτηρίων από χάλυβα. Ο τελικός σχεδιασμός είναι βέλτιστος καθότι αντιστοιχεί στον σχεδιασμό με τον ελάχιστο βάρος κατασκευής. Έτσι, αναπτύχθηκε μία μεθοδολογία που βασίζεται σε ένα γενετικό αλγόριθμο βέλτιστου σχεδιασμού με βάση ντετερμινιστικά και πιθανοτικά κριτήρια. Ο αλγόριθμος βελτιστοποίησης βασίζεται σε ελέγχους ικανοτικού σχεδιασμού, ροπής-αξονικής, γεωμετρικών περιορισμών, καθώς και έλεγχο για την κατηγορία της διατομής, και γενικά όλους τους απαιτούμενους έλεγχους κατά τον Ευρωκώδικα 3 (ΕΚ3).

Η μέθοδος της Προσαυξητική Δυναμική Ανάλυσης (ΠΔΑ) περιλαμβάνει μια σειρά από μη-γραμμικές δυναμικές αναλύσεις που γίνονται με σεισμούς που κλιμακώνονται σταδιακά. Αν και η ΠΔΑ είναι ίσως η ακριβέστερη μέθοδος αποτίμησης της σεισμικής απόκρισης, συχνά δέχεται κριτική επειδή οι σεισμικές καταγραφές κλιμακώνονται μέχρι να καταρρεύσει η κατασκευή. Η πρακτική της κλιμάκωσης συχνά οδηγεί σε μη ρεαλιστικούς πολλαπλασιαστές της σεισμικής καταγραφής, τροποποιώντας έτσι την εδαφική κίνηση και εισάγοντας σφάλμα στην εκτίμηση της απόκρισης. Λόγω της έλλειψης φυσικών καταγραφών που αντιστοιχούν σε σεισμούς μεγάλου μεγέθους και

σε μικρή απόσταση από το σημείο διάρρηξης του ρήγματος, η κλιμάκωση των σεισμών υπήρξε μια συνήθης πρακτική στην αντισεισμική μηχανική. Σε αυτή την έρευνα χρησιμοποιούμε ένα μεγάλο αριθμό σεισμικών καταγραφών ώστε να συγκρίνουμε την καμπύλη της ΠΔΑ με αυτή που προκύπτει μέσω μη-γραμμικής παλινδρόμησης με την μέθοδο LOESS από σεισμικές καταγραφές που δεν έχουν κλιμακωθεί.

Προτείνεται μια νέα μεθοδολογία ώστε, να ποσοτικοποιηθεί η στατιστική προκατάληψη (bias) που εισάγεται κατά την ΠΔΑ. Εκτός από φυσικές σεισμικές καταγραφές, χρησιμοποιήθηκαν και συνθετικές προσομοιώσεις της εδαφικής κίνησης για περιπτώσεις σεισμών με μικρή, μεσαία και μεγάλη ένταση, προκειμένου να διευρυνθεί το πλήθος των σεισμικών καταγραφών που χρησιμοποιήθηκαν. Η έρευνα πραγματοποιήθηκε σε μια σειρά από ανελαστικά μονοβάθμια συστήματα και σε δύο πολυώροφα μεταλλικά κτίρια. Οι μονοβάθμιοι ταλαντωτές ποικίλουν, από πολύ δύσκαμπτους έως εύκαμπτους με μεσαία και υψηλή ιδιοπερίοδο. Τα πολυβάθμια κτήρια που εξετάστηκαν είναι δύο γνωστά κτήρια από τη βιβλιογραφία. Τα αποτελέσματα δείχνουν τόσο ποσοτικά όσο και ποιοτικά για όλες τις οριακές καταστάσεις, την στατιστική προκατάληψη (bias) που εισάγεται από την ΠΔΑ στην εκτίμηση της απόκρισης της κατασκευής.

Εξετάστηκαν έξι μονοβάθμιοι ταλαντωτές με ιδιοπεριόδους αντίστοιχα: T=0.1, 0.3, 0.5, 0.7, 1.0, 1.5 sec και δύο πολυβάθμιες μεταλλικά πλαίσια με θεμελιώδεις περίοδους T_1 = 0.93s και T_1 = 2.34s για το τριώροφο πλαίσιο (LA3) και εννιαώροφο πλαίσιο (LA9) πλαίσιο, αντίστοιχα. Η απόκρισή των δύο κτηρίων ακολουθεί κυρίως την πρώτη ιδιομορφή, αν και το κτίριο LA9 έχει κάποια ευαισθησία σε υψηλότερες ιδιομορφές. Στις αναλύσεις μας έχουν συμπεριληφθεί γεωμετρικές μη-γραμμικότητες τύπου P-Δ. Η επίδραση των εσωτερικών πλαισίων βαρύτητας λαμβάνεται υπόψη με τη βοήθεια μιας στήλης στην οποία τοποθετούνται οι μάζες των εσωτερικών πλαισίων, όπως προτείνεται στις οδηγίες του κανονισμού FEMA P-695 (2009).

Για να διερευνηθεί η σημασία των αριθμητικών αποτελεσμάτων, χρησιμοποιήθηκε η μέθοδος επαναχρησιμοποίησης των ιδίων δεδομένων (bootstrap) που προτάθηκε από τους Efron και Tibshirani (1993). Η μέθοδος bootstrap είναι ένα εύχρηστο εργαλείο, το οποίο επιτρέπει τον υπολογισμό της στατιστικής προκατάληψης (bias) καθώς και το διάστημα εμπιστοσύνης μιας στατιστικής παραμέτρου της απόκρισης. Η μέθοδος υπολογίζει τις ιδιότητες μιας στατιστικής παραμέτρου της απόκρισης, με τυχαία δειγματοληψία και στην συνέχεια με αντικατάσταση στο αρχικό δείγμα. Για παράδειγμα, αν έχουμε ένα αρχικό πληθυσμό x = (x_1,..., x_n), θα γίνει δειγματοληψία με επανατοποθέτηση για να προκύψει ένας νέος πληθυσμός x^m = (x^1,..., $x_n{}^m$). Δειγματοληψία με επανατοποθέτηση σημαίνει ότι ορισμένα μέλη του διανύσματος **x**, μπορεί να εμφανίζονται περισσότερες από μία φορά στο x^m. Η στατιστική παράμετρος της απόκρισης που μας ενδιαφέρει υπολογίζεται για κάθε δείγμα x^m για την απόκτηση της bootstrap κατανομής, η οποία περιέχει πολύτιμες πληροφορίες για το σχήμα, το κέντρο και την διασπορά της κατανομής δειγματοληψίας της στατιστικής απόκρισης.

Η διαδικασία αυτή εφαρμόζεται και στο επίπεδο, σε συνδυασμό με μεθόδους μη-γραμμικής παλινδρόμησης. Το επίπεδο EDP-IM (Engineering Demand Parameter versus Intensity Measure, Παράμετρος μηχανικής ζήτησης και επίπεδο έντασης) έχει σαν συντεταγμένες του το μέτρο έντασης IM στον κατακόρυφο άξονα και στον οριζόντιο άξονα το μέτρο βλάβης EDP. Επίσης, η μέθοδος νέφους (cloud) είναι μέθοδος με την οποία οι σεισμοί που συλλέγονται στο επίπεδο EDP-IM δεν έχουν υποστεί κλιμάκωση σχηματίζοντας ένα ‘νέφος-cloud’ μη-γραμμικών δυναμικών αναλύσεων. Τόσο η ΠΔΑ όσο και η cloud ανάλυση μέσω της μεθόδου του νέφους χρησιμοποιούν μεθόδους μη-γραμμικής παλινδρόμησης σε σημεία του επιπέδου EDP-IM. Σε αυτή την περίπτωση, το **x** περιλαμβάνει τις συντεταγμένες των σημείων και η μη-γραμμική παλινδρόμηση πραγματοποιείται για κάθε δείγμα x^m. Μπορούν εύκολα να υπολογιστούν και τα διαστήματα εμπιστοσύνης.

Στα σχήματα 1 και 2 εμφανίζεται ο υπολογισμός της μέσης τιμής και των διαστημάτων εμπιστοσύνης 95% έναντι των αρχικών δεδομένων (σχήμα 1). Επίσης, παρήχθησαν 1000 καμπύλες αντίστασης, μετά από εφαρμογή της μεθόδου bootstrap επαναχρησιμοποίησης των ιδίων δεδομένων στα αποτελέσματα της cloud ανάλυσης νέφους (σχήμα 2).

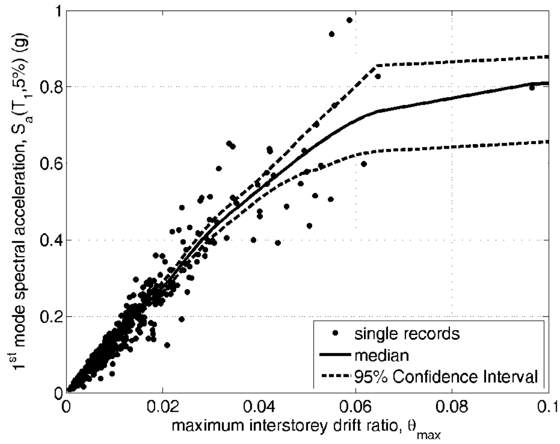

Σχήμα 1: Μέγιστη σχετική μετατόπιση ορόφου σε σχέση με τη φασματική επιτάχυνση για τα αρχικά σημεία της μεθόδου cloud.

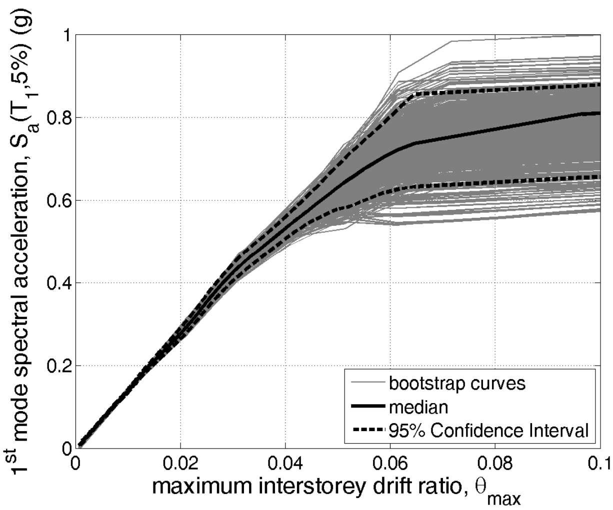

Σχήμα 2: Μέγιστη σχετική μετατόπιση ορόφου σε σχέση με τη φασματική επιτάχυνση για 1000 καμπύλες ικανότητας που παρήχθησαν έπειτα από bootstrapping επαναχρησιμοποίηση των ιδίων δεδομένων στα αποτελέσματα της μεθόδου νέφους-cloud.

Στα δύο διαγράμματα, τα διαστήματα εμπιστοσύνης 95% συμβολίζονται με διακεκομμένη έντονη γραμμή, όπως προέκυψε από την μέθοδο bootstrap, ενώ η συμπαγής έντονη γραμμή είναι η αντίστοιχη μέση καμπύλη όπως έχει ληφθεί μέσω της μη γραμμικής παλινδρόμησης με την μέθοδο LOESS (Local regression using weighted linear least squares), χρησιμοποιώντας γραμμικά ελάχιστα τετράγωνα και πολυωνυμικό μοντέλο δευτέρου βαθμού.

Τα σχήματα 1 και 2 δείχνουν τα διαστήματα εμπιστοσύνης της μεθόδου bootstrap όταν η cloud ανάλυση εφαρμόζεται στο εννιαώροφο μεταλλικό πλαίσιο (LA9). Στο σχήμα 1 εμφανίζονται τα αρχικά δεδομένα τα οποία έχουν ληφθεί μέσω cloud ανάλυσης, ενώ στο σχήμα 2 παρουσιάζονται οι 1000 bootstrap καμπύλες εκτυπωμένες ως γκρι γραμμές. Για τιμές θ_{max} πάνω από 0.06, τα αρχικά σημεία γίνονται ελάχιστα σε πλήθος (σχήμα 1). Εντούτοις, αυτό συμβαίνει για μεγάλες τιμές σχετικής μετατόπισης (drift) ή έντασης και κατά συνέπεια δεν επηρεάζει τις οριακές καταστάσεις που ενδιαφέρουν συνήθως.

Όλες οι καμπύλες ΠΔΑ λήφθηκαν από ένα σύνολο 30 σεισμών που περιλαμβάνει καταγραφές σχετικά μεγάλου μεγέθους M_w μέσα στο εύρος από 6.5 μέχρι 6.9 που έχουν καταγραφεί σε σκληρό έδαφος χωρίς σημάδια κατευθυντικότητας. Για την cloud ανάλυση τύπου νέφους χρησιμοποιήθηκαν φυσικές και συνθετικές καταγραφές. Συνολικά χρησιμοποιήθηκαν 1480 φυσικοί και συνθετικοί σεισμοί για τις μη-γραμμικές δυναμικές αναλύσεις της cloud ανάλυσης τύπου νέφους. Οι 1015 φυσικές καταγραφές που χρησιμοποιήθηκαν, διαλέχτηκαν από την βάση δεδομένων PEER database (PEER NGA Database 2008) ώστε να διασφαλίζεται η ομοιόμορφη επεξεργασία. Όπως έχει ήδη αναφερθεί, μόνο λίγοι σεισμοί έχουν καταγραφεί, με φασματική επιτάχυνση $S_a(T_1,5\%)$ η οποία να ξεπερνάει το 1g για περιόδους πάνω από 1 sec. Τέτοιες $S_a(T_1,5\%)$ εντάσεις δεν είναι αρκετά ισχυρές για να προκαλέσουν διαρροή ή κατάρρευση των κατασκευών μας. Έτσι, για να υπερβούμε αυτό το εμπόδιο, προσθέσαμε στις φυσικές και 465 συνθετικές καταγραφές.

Σε αυτή τη μελέτη οι 465 συνθετικοί σεισμοί οι οποίοι χρησιμοποιήθηκαν σε συνδυασμό με τις φυσικές καταγραφές αποτελούνται από μεγέθη σεισμών 6, 6.5, 7.5 κάθε μία από τις οποίες έχουν μέτρο έντασης (PGA) από 0.1 έως 2.0g. Επειδή από τους 3150 συνθετικούς σεισμούς μόνο οι 465 πληρούσαν τη συνθήκη να είναι το PGA από 0.1 εως 2.0g.

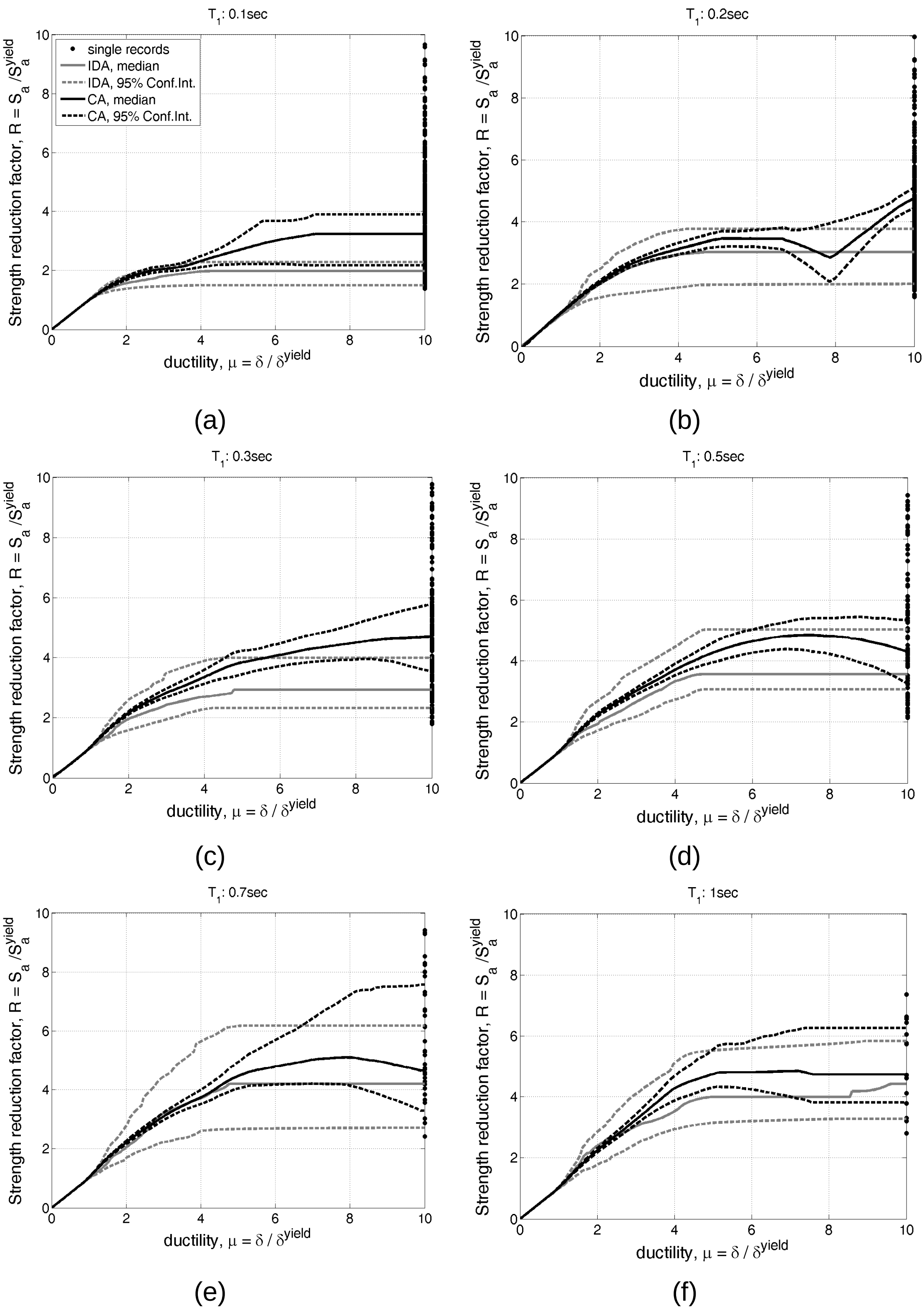

Σχήμα 3: Πλαστιμότητα ως συνάρτηση του συντελεστή απομείωσης αντοχής για (ductility versus strength reduction factor for) (a) T1=0.1sec (b) T1=0.2sec (c) T1=0.3sec (d) T1=0.5sec (e) T1=0.7sec (f) T1=1.0sec (g) T1=1.5sec.

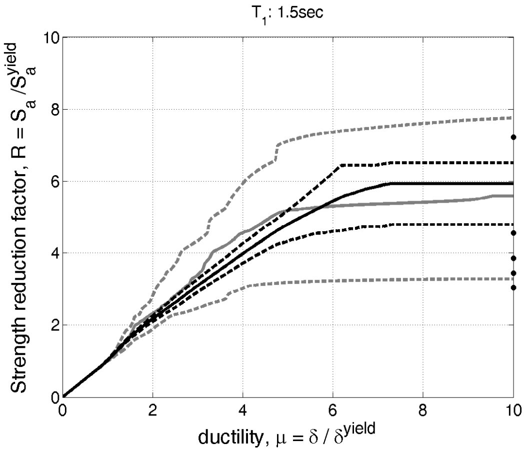

(g)

Σχήμα 3: (συνέχεια).

Το σχήμα 3 δείχνει τα αριθμητικά αποτελέσματα για τα επτά μονοβάθμια συστήματα. Οι μέσες καμπύλες ΠΔΑ και οι cloud καμπύλες τύπου νέφους, είναι κοντά για απαιτήσεις πλαστιμότητας ως το μ=3, για όλες τις περιόδους όπως φαίνεται στα παραπάνω σχήματα. Πιο συγκεκριμένα για μονοβάθμιους ταλαντωτές με T_1=0.1s, 0.3s, 0.5s συμπίπτουν μέχρι μ=2. Επίσης, για μονοβάθμιους ταλαντωτές T_1=0.7 s, 1.0s και 1.5s συμπίπτουν μέχρι μ=3, το οποίο αποτελεί πρακτικό όριο όπου ισχύει ο κανόνας των ίσων μετατοπίσεων. Πάνω από αυτή την τιμή πλαστιμότητας παρατηρούνται διαφορές στην αντοχή. Για τιμές πλαστιμότητας κοντά στο 4.5 οι καμπύλες αντίστασης αρχίζουν να γίνονται οριζόντιες, οπότε φαίνεται ότι το σύστημα έχει φτάσει τη μέγιστη αντοχή του.

Σύμφωνα με τα προηγούμενα αποτελέσματα (σχήμα 3), με την αύξηση της απαίτησης πλαστιμότητας οι διαφορές ανάμεσα στη μέση ΠΔΑ και τις καμπύλες της cloud ανάλυσης αυξάνουν. Γίνεται φανερό ότι για μικρές ιδιοπεριόδους T_1=0.1s και 0.3s, η ΠΔΑ υποεκτιμά τις αντοχές. Ενώ για μέσες προς μεγάλες ιδιοπεριόδους T_1=0.5s, 0.7s και 1.0s, η μέθοδος ΠΔΑ εξακολουθεί να υποεκτιμά την ικανότητα αλλά σε μικρότερο βαθμό. Για T_1=1.5s η διαφορά των καμπύλων είναι μικρή και η απαίτηση είναι ελαφρώς υπερεκτιμημένη για μ<6 και υποεκτιμημένη όταν μ>6. Για μ=6 έχουμε το σημείο τομής των μέσων καμπύλων της ΠΔΑ με την cloud ανάλυση τύπου νέφους.

Στο σχήμα 3 δείχνονται τα διαστήματα εμπιστοσύνης 95% έτσι, ώστε να έχουμε μια εκτίμηση της διασποράς. Σε γενικές γραμμές για T1>0.3, τα διαστήματα της ΠΔΑ είναι ευρύτερα σε σύγκριση με εκείνα της cloud ανάλυσης. Επιπλέον, το εύρος των διαστημάτων εμπιστοσύνης αυξάνεται όσο αυξάνεται η περίοδος. Στη γραμμική ελαστική περιοχή το εύρος είναι πρακτικά μηδενικό, αλλά αυξάνεται με ταχείς ρυθμούς για πλαστιμότητες: (α) πάνω από μ=1 για την ΠΔΑ και (β) μ=3 για την cloud ανάλυση. Αν θεωρήσουμε μια αυθαίρετη τιμή πλαστιμότητας (π.χ. μ=8), συγκρίνοντας ταλαντωτές με T_1 ίσο (α) με 0.1 και (β) 1.5sec, φαίνεται ότι το πλάτος των διαστημάτων εμπιστοσύνης της ΠΔΑ ποικίλλει σημαντικά. Αυτό σημαίνει ότι οι παρατηρήσεις σχετικά με τη μέση ΠΔΑ, ισχύουν περίπου, δεδομένου ότι μπορεί να υπάρχουν εδαφικές κινήσεις όπου η απαίτηση θα μπορούσε να βρίσκεται οπουδήποτε μέσα στο διάστημα εμπιστοσύνης.

Στα σχήματα 4 φαίνονται επίσης τα διαστήματα εμπιστοσύνης 95%, προκειμένου να παρασχεθεί μια εκτίμηση της διασποράς. Με βάση το σχήμα 4, τα διαστήματα είναι ευρύτερα στην περίπτωση της ΠΔΑ και σχετικά στενά για την cloud ανάλυση, εκτός στην περίπτωση που η πρώτη ιδιοπερίοδος ισούται με 0.1s. Γενικά, το εύρος των διαστημάτων εμπιστοσύνης αυξάνεται όσο αυξάνονται οι απαιτήσεις σε πλαστιμότητα και επίσης όσο αυξάνεται η περίοδος είτε είναι μονοβάθμια ή πολυβάθμια συστήματα με την περίοδο. Για τη γραμμική ελαστική περιοχή το πλάτος είναι μηδέν, αλλά αναπτύσσεται γρήγορα μετά την πλαστιμότητα μ=1. Στα παρακάτω σχήματα 4 φαίνονται οι μέσες καμπύλες ικανότητας και τα αντίστοιχα διαστήματα εμπιστοσύνης 95% για τετραγραμμικούς ταλαντωτές.

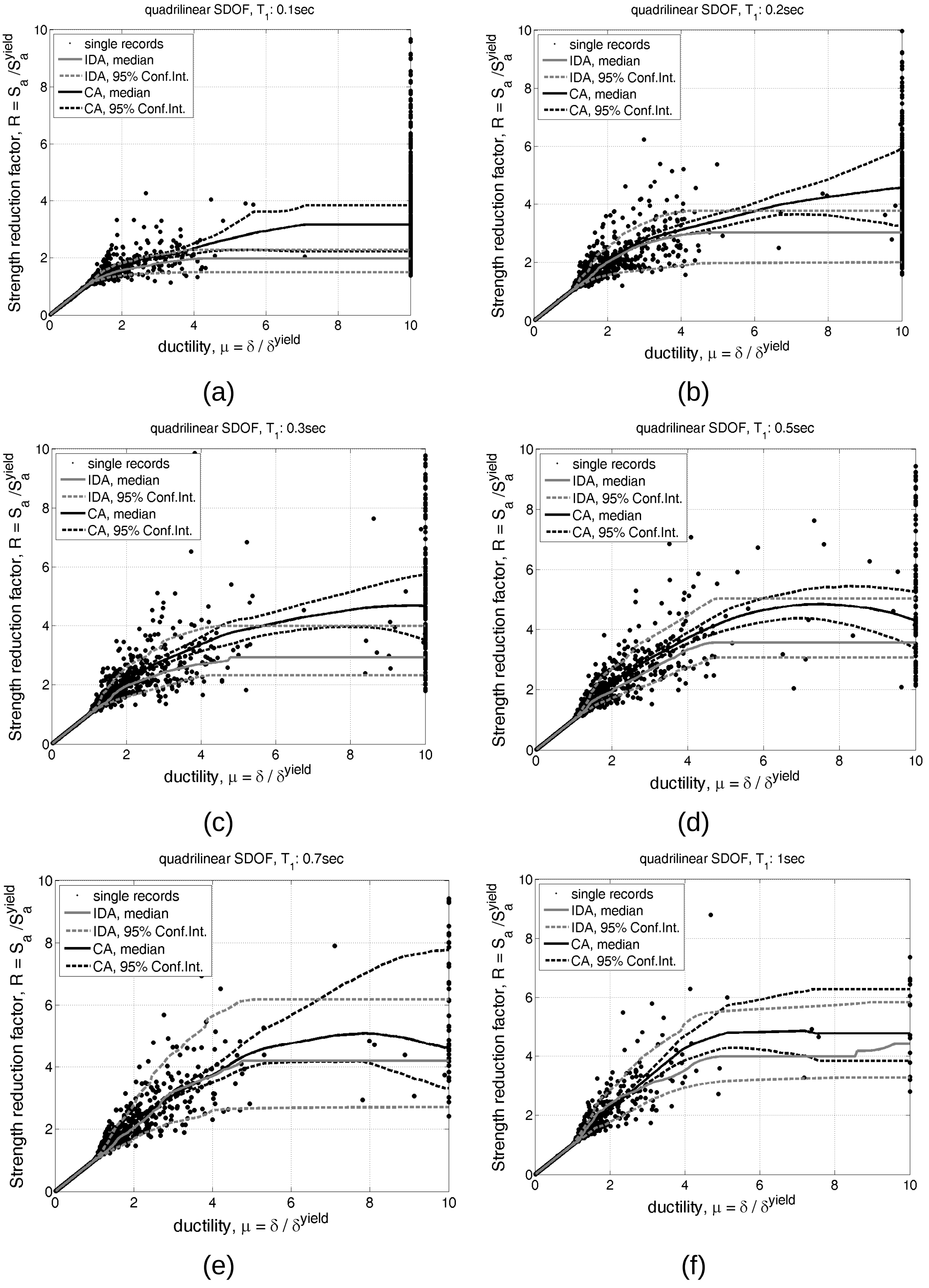

Σχήμα 4: Πλαστιμότητα μ σε σχέση με το συντελεστή απομείωσης αντοχής R (strength reduction factor) για τετραγραμμικούς μονοβάθμιους ταλαντωτές.

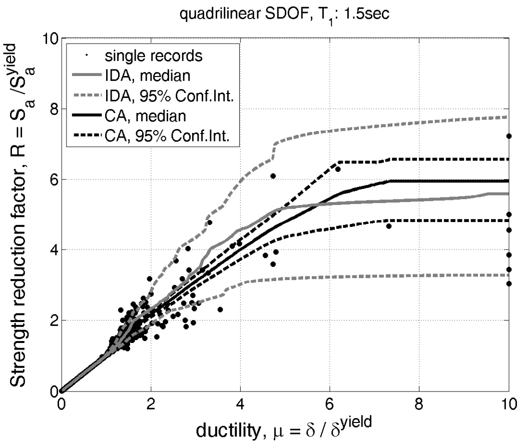

(g)

Σχήμα 4: (συνέχεια).

Παρατηρώντας τους τετραγραμμικούς μονοβάθμιους ταλαντωτές, μερικές κουκίδες φαίνονται να είναι συγκεντρωμένες στην κάθετη γραμμή μ=10. Γι' αυτούς τους σεισμούς, η απαίτηση για πλαστιμότητα είτε είναι πολύ κοντά είτε έχει ξεπεράσει το μ=10. Επίσης, για μεγάλες ιδιοπεριόδους (π.χ για T_1=1.5sec), ο αριθμός των κουκίδων που εμφανίζονται είναι μικρότερος, συγκρινόμενος με αυτό των μικρότερων ιδιοπεριόδων. Αυτό οφείλεται στην περιορισμένη διαθεσιμότητα σεισμών οι οποίοι έχουν μεγάλες τιμές φασματικής επιτάχυνσης $S_a(T_1,5\%)$, πάνω από 1s και είναι αρκετά ισχυροί για να προκαλέσουν μεγάλη απαίτηση πλαστιμότητας. Σε αυτή την περίπτωση, υπάρχουν επαρκή δεδομένα μόνο για τιμές πλαστιμότητας που δεν υπερβαίνουν τις τιμές 5 και 6 και επομένως πάνω από αυτές τις τιμές πλαστιμότητας δε μπορούμε να είμαστε σίγουροι για τα αποτελέσματά μας.

Άλλωστε, στα παραπάνω σχήματα 4a έως 4h όπου φαίνεται αντίστοιχα η περίπτωση τετραγραμμικού ταλαντωτή, αυθαίρετα επιλέχτηκε μια τιμή πλαστιμότητας (π.χ. μ=8). Το εύρος των διαστημάτων εμπιστοσύνης της ΠΔΑ ποικίλει από R=2 εως 6, για δύο ταλαντωτές με T_1=0.1sec και 2sec αντίστοιχα. Αυτό σημαίνει ότι οι παραπάνω παρατηρήσεις που σχετίζονται με την ακρίβεια της μέσης ΠΔΑ, είναι αληθείς κατά μέσον όρο, μια και μπορεί να υπάρχουν μεμονωμένες περιπτώσεις όπου οι μέσες ΠΔΑ μπορεί να διαφέρουν. Για T_1=0.1sec, 0.3sec και για μονοβάθμιους ταλαντωτές που ακολουθούν τον τετραγραμμικό νόμο υστέρησης, τα διαστήματα εμπιστοσύνης των καμπύλων LOESS που παρουσιάζονται δεν περιλαμβάνονται στα διαστήματα εμπιστοσύνης της ΠΔΑ.

Στα παρακάτω σχήματα 5a και 5b συγκρίνονται η μέση ΠΔΑ και η cloud ανάλυση για το τριώροφο και εννιαώροφο μεταλλικό πλαίσιο. Για το τριώροφο (LA3) μεταλλικό πλαίσιο, η μέση ΠΔΑ και η cloud συμπίπτουν έως θ_{max}=0.03. Πάνω από αυτή την τιμή η διαφορά αυξάνεται ως θ_{max}=0.12, ενώ πέρα από αυτήν την τιμή δεν μπορούμε να κάνουμε μια ασφαλή παρατήρηση.

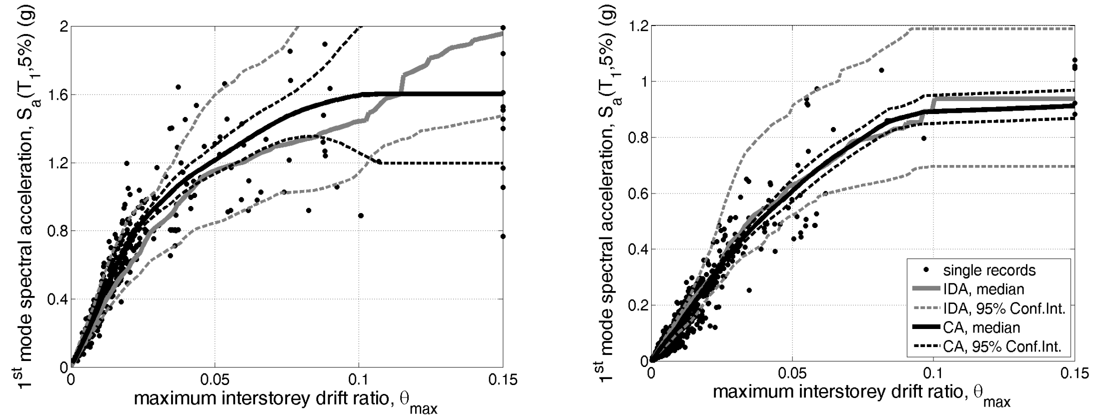

(a) (b)

Σχήμα 5: Μέσες καμπύλες αντίστασης και τα διαστήματα εμπιστοσύνης 95% (a) για το τριώροφο και (b) για το εννιαώροφο μεταλλικό πλαίσιο.

Για το εννιαώροφο μεταλλικό πλαίσιο και οι δύο καμπύλες τείνουν να συμπέσουν μολονότι, από θ_{max}=0.07 και πάνω από $S_a(T_1$,5%)=0.8g, τα δεδομένα μας σπανίζουν. Αυτό οφείλεται στην περιορισμένη διαθεσιμότητα σεισμικών καταγραφών για σεισμούς οι οποίοι να είναι επαρκώς ισχυροί, ώστε να προκαλέσουν μεγάλη απαίτηση σε σχετική μετατόπιση ορόφου (drift) σε αυτή την περίοδο, οπότε δε μπορούμε να φτάσουμε σε ασφαλή συμπεράσματα. Επιπλέον, για το εννιαώροφο πλαίσιο η μέση ΠΔΑ είναι ανάμεσα στα διαστήματα εμπιστοσύνης της cloud ανάλυσης, ενώ κάτι τέτοιο δε συμβαίνει στο τριώροφο πλαίσιο. Τόσο η ανάλυση cloud όσο και η ΠΔΑ παράγουν εκτιμήσεις των ικανοτήτων που είναι κοντά.

Υπολογισμός της στατιστικής προκατάληψης (Bias estimation)

Η στατιστική προκατάληψη (bias) μπορεί να θεωρηθεί, ως μια συστηματική υπό- ή υπέρ-εκτίμηση του R (ή του *Sa*(T_1,*5%)*) της αντοχής. Υπολογίζουμε τη στατιστική προκατάληψη (bias) θεωρώντας ότι η άνευ στατιστικής προκατάληψης απόκριση (unbiased response) είναι αυτή της cloud ανάλυσης τύπου νέφους, αφού αυτή η μέθοδος αφήνει τους σεισμούς ακλιμάκωτους. Έτσι, σχετικά με την ικανότητα της κατασκευής η στατιστική προκατάληψη (bias), υπολογίζεται ως ο λόγος:

$$\text{bias}=\frac{(R)_{IDA}}{(R)_{cloud}},\ \text{or}\ \ \text{bias}=\frac{\left(S_a\left(T_1,5\%\right)\right)_{IDA}}{\left(S_a\left(T_1,5\%\right)\right)_{cloud}} \qquad (1)$$

όπου $Sa(T_1,5\%)_{\mathrm{IDA}}$ είναι οι $Sa(T_1,5\%)$) αντοχές της ΠΔΑ και $Sa(T_1,5\%)_{\mathrm{cloud}}$ είναι οι αντοχές που λαμβάνουμε από την cloud ανάλυση. Προκειμένου να υπολογίσουμε τη στατιστική σημαντικότητα (statistical significance) της στατιστικής προκατάληψης (bias) και να υπολογίσουμε τα αντίστοιχα διαστήματα εμπιστοσύνης, εφαρμόζουμε τη μέθοδο bootstrap επαναχρησιμοποίησης των ιδίων δεδομένων πάνω στις τιμές της εξίσωσης 1. Είμαστε πλέον ικανοί να παρακολουθούμε τη στατιστική προκατάληψη (bias) για το πλήρες φάσμα των οριακών καταστάσεων (τιμές EDP). Τα διαστήματα εμπιστοσύνης της στατιστικής προκατάληψης (bias) προσφέρουν περισσότερη εμπιστοσύνη στις παρατηρήσεις που σχετίζονται με την επίδραση της κλιμάκωσης εντός του πλαισίου της ΠΔΑ.

Τα σχήματα 6 και 7 δείχνουν τα διαστήματα εμπιστοσύνης της στατιστικής προκατάληψης (bias) και επιτρέπουν μερικές γενικές παρατηρήσεις. Όταν όλα τα διαστήματα εμπιστοσύνης είναι τελείως πάνω ή τελείως κάτω από τη γραμμή της μονάδας, τότε είμαστε σίγουροι αντίστοιχα ότι η αντοχή έχει υπέρ ή υπό-τιμηθεί. Επίσης, αν τα διαστήματα εμπιστοσύνης εμπεριέχουν ομοιόμορφα τη μονάδα, τότε δεν έχουμε κάποιο στοιχείο που αποδεικνύει την ύπαρξή της στατιστικής προκατάληψης (bias).

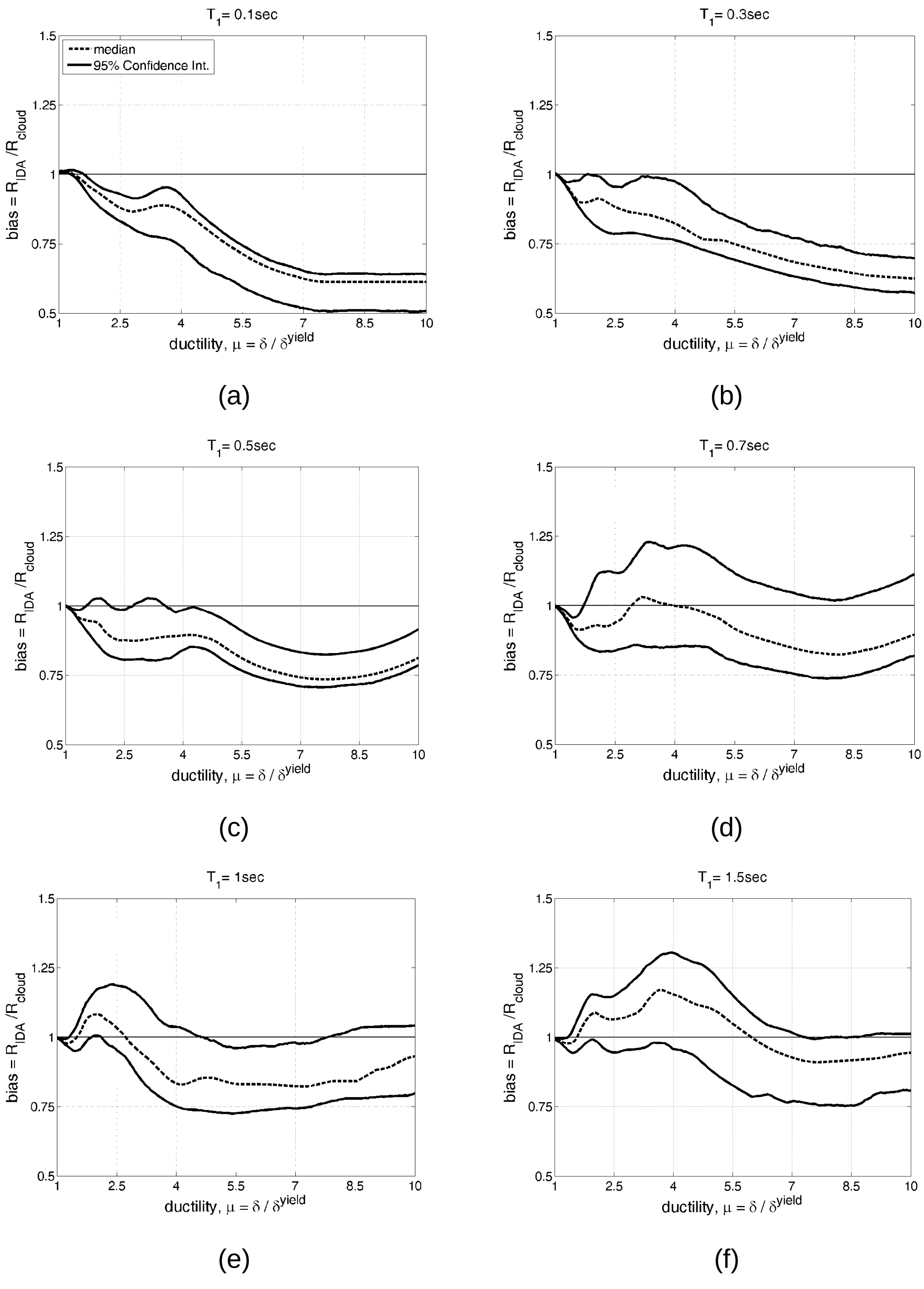

Σχήμα 6: Bias σε σχέση με την πλαστιμότητα για τετραγραμμικούς μονοβάθμιους ταλαντωτές με (a)T1=0.1sec, (b)T1=0.3sec, (c) T1=0.5sec, (d) T1=0.7sec, (e) T1=1.0sec, (f) T1=1.5sec.

Στο σχήμα 7 παρουσιάζονται τα αποτελέσματα της στατιστικής προκατάληψης (bias) για το τριώροφο (LA3) και το εννιαώροφο (LA9) μεταλλικό πλαίσιο. Για τα δύο πλαίσια η στατιστική προκατάληψη (bias) είναι περίπου σταθερή για όλο το εύρος των οριακών καταστάσεων. Για το τριώροφο κτήριο η απαίτηση υποεκτιμάται, περίπου 10%. Αυτό είναι μια μικρή στατιστική προκατάληψη (bias) αποδεκτή στη συνήθη πρακτική του μηχανικού, στο περιθώριο της ασφάλειας της κατασκευής. Επιπλέον, κάποια ευαισθησία παρατηρείται για τις αρχικές οριακές καταστάσεις, π.χ. θ_{max}=0.02. Εξάλλου, μικρή υπερεκτίμηση της απαίτησης παρατηρείται στο εννιαώροφο πλαίσιο. Σε αυτή την περίπτωση τα διαστήματα εμπιστοσύνης περιλαμβάνουν τη γραμμή της μονάδας, οπότε μπορούμε να θεωρήσουμε τους υπολογισμούς της αντοχής ως άνευ στατιστικής προκατάληψης (unbiased). Πάλι η μέση καμπύλη της μεθόδου bootstrap είναι το κέντρο των διαστημάτων εμπιστοσύνης. Η τιμή της είναι περίπου 0.9 για το τριώροφο και κυμαίνεται από 1.1 ως 0.98 για το εννιαώροφο μεταλλικό πλαίσιο. Επιπλέον, ποιοτικά διαπιστώνεται ότι τα αποτελέσματα στα πολυβάθμια συστήματα δίνουν παρεμφερή αποτελέσματα με τους μονοβάθμιους ταλαντωτές.

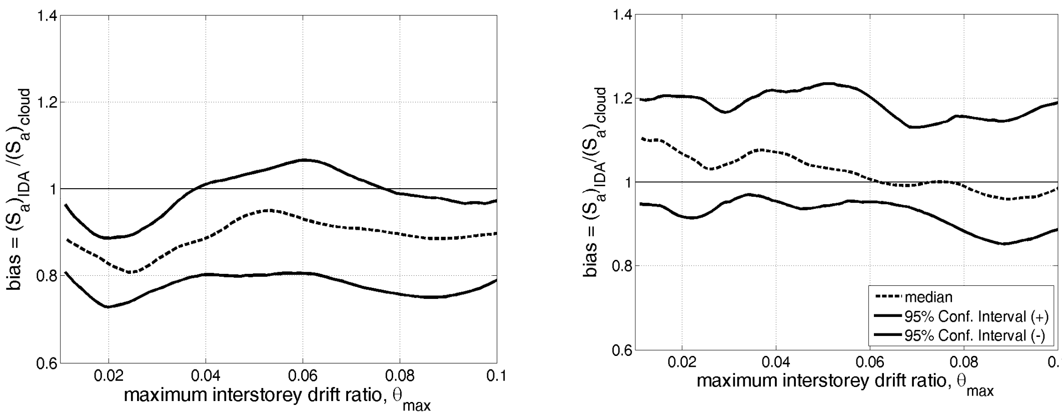

(a) (b)

Σχήμα 7: Bias σε σχέση με την μέγιστη σχετική μετατόπιση για (α) το τριώροφο LA3 και (β) το εννιαώροφο κτήριο LA9.

Γενετικός Αλγόριθμος Βελτιστοποίησης κατασκευής (GSO_IDA-SPO2IDA)

Στο πλαίσιο της διατριβής παρουσιάστηκε επίσης ένας αλγόριθμος βελτιστοποίησης για το σχεδιασμό των κατασκευών από χάλυβα με ντετερμινιστικα ή/και πιθανοτικά κριτήρια, ενσωματώνοντας ακριβείς και προσεγγιστικές μεθόδους εκτίμησης της απόκρισης της κατασκευής έναντι σεισμικών δράσεων. Πιο συγκεκριμένα, χρησιμοποιούνται τα κριτήρια σχεδιασμού που βασίζονται και στη μέση ετήσια συχνότητα (MAF) υπέρβασης της οριακής κατάστασης. Τέτοια κριτήρια επιτρέπουν να τίθενται περιορισμοί που είναι πιο κατανοητοί για το μηχανικό και οδηγούν σε κτηριακούς σχεδιασμούς αφενός μειωμένου κόστους και αφετέρου βελτιωμένης συμπεριφοράς. Σε αυτή τη διατριβή, προτείνεται μια απλοποιημένη προσέγγιση που επιτρέπει τον ταχύτερο υπολογισμό της μέσης ετήσιας συχνότητας οριακής κατάστασης, χωρίς σημαντική απώλεια ακρίβειας. Ειδικά, χρησιμοποιείται και η στατική-προσαυξητική-προς-προσαυξητική-δυναμική-ανάλυση (SPO2IDA) μέθοδος. Στην προτεινόμενη μέθοδο αναπτύχθηκε ένας γενετικός αλγόριθμος βέλτιστου σχεδιασμού με βάση ντετερμινιστικά και πιθανοτικά κριτήρια που ονομάζεται «GeneticStructuralOptimization_using_IDA-SPO2IDA» και συνοπτικά «GSO_IDA-SPO2IDA», όπου για πιθανοτικά κριτήρια μέσω της SPO2IDA λαμβάνονται πληροφορίες από τη στατική προσαυξητική καμπύλη ανάλυσης και παράγονται η μέση τιμή και η τυπική απόκλιση για διάφορες οριακές καταστάσεις. Οι υπολογισμοί αυτοί είναι απαραίτητοι για την εφαρμογή των πιθανοτικών κριτηρίων στη μέση ετήσια συχνότητα οριακής κατάστασης. Το πρόβλημα της βελτιστοποίησης που πρόκειται να αντιμετωπιστεί, προκειμένου να ευρεθούν οι βέλτιστες διατομές των πλαισίων, επιλύεται με ένα γενετικό αλγόριθμο «GSO_SPO2IDA». Ένα τριώροφο και ένα εννιαώροφο μεταλλικό πλαίσιο θεωρούνται ως παράδειγμα, για να φανεί η επάρκεια της μεθοδολογίας που προτείνεται και καταλήγει σε επαρκείς σχεδιασμούς μέσα σε ανεκτά χρονικά περιθώρια για το μηχανικό.

Η μέθοδος ‘static pushover to IDA (SPO2IDA)’ παρέχει μία κατά προσέγγιση εκτίμηση της μεθόδου ΠΔΑ χρησιμοποιώντας τις πληροφορίες από τον υπολογισμό της μεθόδου SPO (static pushover). Η SPO2IDA έχει επαληθευθεί ως μέθοδος για πολυάριθμους μονοβάθμιους ταλαντωτές και για πολυβάθμιες κατασκευές που κυριαρχούνται από την πρώτη ιδιομορφή. Δηλαδή, η στατική υπερωθητική μέθοδος (static pushover) προσεγγίζεται με μια τριγραμμική ή τετραγραμμική καμπύλη έτσι, ώστε να ληφθούν οι παράμετροι που περιγράφουν την καμπύλη SPO (SPO curve). Οι παράμετροι που εξήχθησαν δίνονται ως είσοδος στο πρόγραμμα SPO2IDA, ώστε αυτό να παράξει τα ποσοστημόρια (fractile) σε κανονικοποιημένες συντεταγμένες του συντελεστή μειωμένης αντοχής (strength reduction factor) *R* σε σχέση με την πλαστιμότητα μ. Οι τελικές προσεγγίσεις της ΠΔΑ λαμβάνονται μετά από μια σειρά υπολογισμών στα διαθέσιμα R-μ δεδομένα.

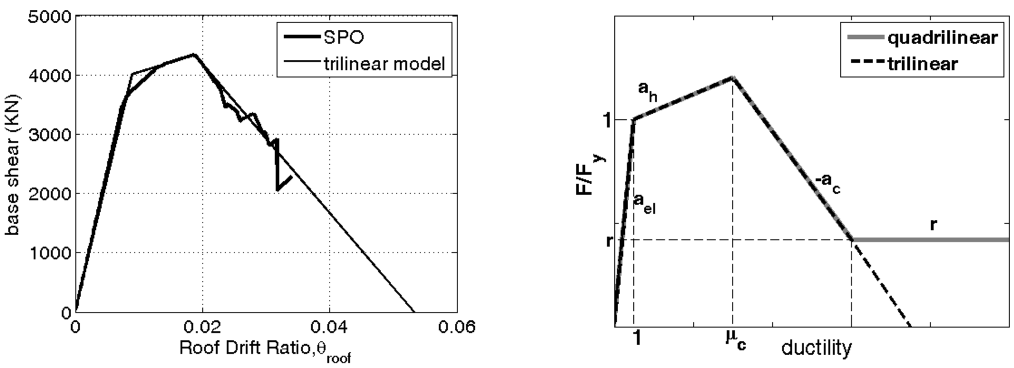

(a) (b)

Σχήμα 8 (a) Η pushover καμπύλη και η προσέγγισή της με ένα τριγραμμικό μοντέλο, (b) Ορισμός των παραμέτρων που καθορίζουν το κύριο μέρος (backbone) της pushover καμπύλης.

Συνοπτικά, η διαδικασία εξαγωγής μιας προσέγγιση της ΠΔΑ καμπύλης, από μία pushover στατική υπερωθητική ανάλυση, περιλαμβάνει τα ακόλουθα βήματα. Αρχικά εκτελείται μια static pushover ανάλυση με ένα σχήμα φόρτισης πρώτης ιδιομορφής (first-mode lateral load pattern) και έπειτα προσεγγίζεται με ένα τριγραμμικό μοντέλο. Κατόπιν από την SPO2IDA θα εξαχθούν οι καμπύλες ΠΔΑ σε κανονικοποιημένες (normalized) *R-μ* συντεταγμένες οι οποίες θα πρέπει να τροποποιηθούν σε φασματική επιτάχυνση $Sa(T_1,5\%)$ έναντι του $\boldsymbol{\theta}_{max}$. Αυτό απαιτεί την ελαστική κλίση της ΠΔΑ, όταν το $\boldsymbol{\theta}_{roof}$ είναι το μέτρο βλάβης (k_{roof}). Οι τελικές ΠΔΑ λαμβάνονται χρησιμοποιώντας την αντιστοιχία ανάμεσα στο $\boldsymbol{\theta}_{roof}$ και $\boldsymbol{\theta}_{max}$, που λαμβάνονται από τα αποτελέσματα της μεθόδου static pushover.

Για ένα εννιαώροφο μεταλλικό πλαίσιο ο υπολογιστικός χρόνος μειώνεται και από 2-3 ώρες που απαιτούνται για μια μοναδική (single IDA) ΠΔΑ, αρκούν μόνο λίγα λεπτά της ώρας που διαρκεί η επίλυση της SPO2IDA, δηλαδή απαιτείται χρόνος μικρότερος περίπου κατά δύο τάξεις μεγέθους, οπότε έχουμε μεγάλο κέρδος σε υπολογιστικό χρόνο.

Ο στόχος των προβλημάτων βελτιστοποίησης και διαστασιολόγησης είναι να μειωθεί η αντικειμενική συνάρτηση, που είναι ανάλογη προς το κόστος της κατασκευής. Η πιο συνήθης εφαρμοζόμενη αντικειμενική συνάρτηση για μεταλλικές κατασκευές είναι το βάρος τους, το οποίο συνδέεται άμεσα με το κόστος. Οι μεταβλητές σχεδιασμού έχουν επιλεγεί να είναι οι διατομές των μελών της κατασκευής, έτσι ώστε η αντικειμενική συνάρτηση να μπορεί να εκφραστεί ως ο γραμμικός ή μη γραμμικός συνδυασμός τους. Λόγω των απαιτήσεων του μηχανικού στην πράξη τα μέλη διαιρούνται σε ομάδες μεταβλητών σχεδιασμού. Έτσι, γίνεται μια εξισορρόπηση ανάμεσα σε παραπάνω υλικό και στην ανάγκη για συμμετρία και ομοιομορφία, για πρακτικούς λόγους. Μειώνεται επίσης το μέγεθος του προς επίλυση προβλήματος βελτιστοποίησης. Επιπλέον, λόγω περιορισμών κατασκευής, οι μεταβλητές σχεδιασμού δεν είναι συνεχείς αλλά διακριτές. Έτσι, εν προκειμένω ένα διακριτό ντετερμινιστικό πρόβλημα βέλτιστου σχεδιασμού (discrete deterministic-based structural optimization, DBO) μορφώνεται ως ακολούθως:

$$\begin{aligned} &\min F(\mathbf{s}) \\ &\text{subject to} \quad \begin{cases} g_i(\mathbf{s}) \geq 0, i = 1,...,l \\ s_j \in R^d, j = 1,...,m \end{cases} \end{aligned} \tag{2}$$

όπου $F(\boldsymbol{s})$ είναι η αντικειμενική συνάρτηση που θα ελαχιστοποιηθεί και g_i είναι οι l ντετερμινιστικοί περιορισμοί. R^d είναι ένα δοσμένο σύνολο διακριτών τιμών και s_j είναι το διάνυσμα των μεταβλητών σχεδιασμού που μπορούν να πάρουν τιμές από αυτό το σύνολο. Κατά τον ίδιο τρόπο, ένα διακριτό πρόβλημα βελτιστοποίησης με πιθανοτικά κριτήρια (RBO) μορφώνεται ως ακολούθως:

$$\begin{aligned} & \min F(\mathbf{s}) \\ \text{subject to} \quad & \begin{cases} g_i(\mathbf{s}) \geq 0, i = 1,...,l \\ s_j \in R^d, j = 1,...,m \\ h_k(v_{\text{EDP}}(\mathbf{s}) \leq v_{\text{EDP}}^{\lim}(\mathbf{s})), k = 1,...,n \end{cases} \end{aligned} \tag{3}$$

όπου h_k είναι οι n πιθανοτικοί περιορισμοί, v παριστάνει τη μέση ετήσια συχνότητα υπέρβασης (exceedance) του k_{th} στα επίπεδα απόδοσης (performance levels) και τέλος EDP υποδηλώνει ένα μέγιστο μέτρο βλάβης (EDP) που εδώ είναι η μέγιστη σχετική μετατόπιση ορόφων $\boldsymbol{\theta}_{max}$(maximum interstorey drift $\boldsymbol{\theta}_{max}$).

Σε αυτή τη μελέτη το πρόβλημα βελτιστοποίησης λύνεται με τη χρήση ενός γενετικού αλγορίθμου «GSO_IDA-SPO2IDA». Ο γενετικός αλγόριθμος είναι ένας αλγόριθμος αναζήτησης και βελτιστοποίησης και είναι εμπνευσμένος από την διαδικασία της φυσικής επιλογής (Goldberg 1989). Σήμερα είναι ο πιο ευρέως χρησιμοποιούμενος εξελικτικός αλγόριθμος.

Τα βήματα του γενετικού αλγόριθμου «GSO_IDA-SPO2IDA» που χρησιμοποιούνται για τον αντισεισμικό σχεδιασμό των κατασκευών παρουσιάζονται εδώ:

1. *Βήμα αρχικοποίησης*: Τυχαία παραγωγή ενός αρχικού πληθυσμού των διανυσμάτων της s_j μεταβλητών σχεδιασμού (j = 1,..., NPOP) τα οποία είναι κωδικοποιημένα ως δυαδικές συμβολοσειρές δηλαδή ως χρωμοσώματα ή γονότυποι.
2. *Βήμα ανάλυσης (Fitness evaluation):* Πρώτον, εκτέλεση ελέγχων που δεν απαιτούν ανάλυση για να διασφαλιστεί ότι ο σχεδιασμός είναι σύμφωνος με τη φιλοσοφία του ισχυρού υποστυλώματος - αδύναμης δοκού και ότι άλλες απαιτήσεις πληρούνται λεπτομερώς. Στη συνέχεια, εκτελείται γραμμική ελαστική ανάλυση για να ληφθεί υπόψη το αίτημα για τους μη σεισμικού φορτίου συνδυασμούς και στη συνέχεια εκτελείται Static Pushover στατική υπερωθητική ανάλυση για τις σεισμικές δράσεις. Το εργαλείο SPO2IDA χρησιμοποιείται για να

υπολογιστεί η υπό εξέταση οριακή κατάσταση. Για κάθε περιορισμό που παραβιάζεται, υπολογίζονται οι κυρώσεις, με μια διαδικασία ποινής και τροποποιείται η αντικειμενική συνάρτηση αναλόγως.

3. *Βήμα για γένεση, επιλογή, διασταύρωση και μετάλλαξη (generation, selection, crossover and mutation):* Εφαρμόζονται οι τελεστές του γενετικού αλγόριθμου για να δημιουργηθούν τα μέλη του επόμενου πληθυσμού t_j (j=1,…, *npop*).
4. *Τελικός έλεγχος:* Εάν ένας προκαθορισμένος αριθμό των γενεών έχει επιτευχθεί, στάση. Διαφορετικά επιστροφή στο βήμα 2.

Βέλτιστος σχεδιασμός με ντετερμινιστικά κριτήρια

Για προβλήματα δομικής μηχανικής υπό σεισμική φόρτιση, οι περιορισμοί που χρησιμοποιούνται σε αυτή την εργασία ακολουθούν το σχεδιασμό με βάση την επιτελεστικότητα. Η επιτελεστικότητα της κατασκευής αξιολογείται σε διαφορετικά επίπεδα σεισμικής έντασης. Τρία επίπεδα επιτελεστικότητας έχουν ληφθεί υπόψη: Άμεσης χρήσης (IO), Ασφάλεια ζωής (LS), και Αποφυγής κατάρρευσης (CP). Προκαταρκτικοί έλεγχοι γίνονται σε κάθε υποψήφιο σχεδιασμό. Αυτοί οι έλεγχοι περιλαμβάνουν την εξέταση που αφορά στο αν ο μηχανισμός ορόφου παράγεται από τις πλαστικές αρθρώσεις που γίνονται στα υποστυλώματα αντί στις δοκούς. Επίσης, γίνεται ένας έλεγχος που αφορά στις διατομές να είναι κλάσης 1 κατά τον Ευρωκώδικα. Αυτός ο έλεγχος είναι σημαντικός προκειμένου να εξασφαλιστεί ότι τα μέλη είναι σε θέση να αναπτύξουν την πλήρη πλαστική ροπή τους και την πλαστιμότητά τους. Επιπλέον, τίθενται γεωμετρικοί περιορισμοί που επιβεβαιώνουν τις σωστές συνδέσεις των δοκών στα υποστυλώματα. Επίσης γίνεται άλλος ένας έλεγχος ο οποίος επιβεβαιώνει ότι η καμπτική αντοχή των δοκών είναι επαρκής. Αν οι έλεγχοι δεν ικανοποιούνται ο σχεδιασμός τροποποιείται ελαφρώς, έτσι ώστε το πρόγραμμα «GSO_IDA-SPO2IDA» να ικανοποιεί τους περιορισμούς

Έπειτα γίνεται έλεγχος για αντοχή σε σεισμικά φορτία. Για τις τρεις οριακές καταστάσεις υπολογίζεται η $S_a(T_1,5\%)$ με τη βοήθεια του ελαστικού φάσματος. Στη συνέχεια καθορίζεται η απαιτούμενη μέγιστη σχετική μετατόπιση ορόφων (maximum interstorey drift demand) και τέλος με τη χρήση της SPO2IDA η μέγιστη σχετική μετατόπιση ορόφων συγκρίνεται με τις οριακές τιμές της μέγιστης σχετικής μετατόπισης που αντιστοιχούν στις οριακές καταστάσεις.

Όταν παραβιάζεται ένα κριτήριο επιτελεστικότητας (performance criterion), υπολογίζεται μια ποινή. Η μια συνάρτηση ποινής p, η οποία δίνει ένα μέτρο της απόκλισης της τιμής που δίνει η ανάλυση από το αποδεκτό όριο. Σε αυτή την εργασία η αντικειμενική συνάρτηση δέχεται τη συνάρτηση ποινής ως ακολούθως:

$$\overline{F}(\mathbf{s}) = \max(p) F(\mathbf{s}) \tag{4}$$

όπου το $\max(p)$ είναι η μέγιστη τιμή από τις τιμές ποινών των παραβιασμένων περιορισμών και $\overline{F}(\mathbf{s})$ είναι η τιμή της ποινικοποιημένης αντικειμενικής συνάρτησης. Η τιμή της ποινής που επιλέχθηκε για την i-th οριακή κατάσταση στο ντετερμινιστικό σχεδιασμό είναι:

$$p = \left| q - q_{\lim} \right| / q_{\lim} \tag{5}$$

όπου q_{lim} είναι η οριακή τιμή της ποσότητας στην οποία θέτουμε περιορισμό και q είναι η τιμή που επιλέχθηκε κατά τη διάρκεια της διαδικασίας της ανάλυσης.

<u>Σχεδιασμός χρησιμοποιώντας πιθανοτικά κριτήρια</u>

Οι έλεγχοι του σεισμικού σχεδιασμού μπορούν εναλλακτικά να εφαρμοστούν στη μέση ετήσια συχνότητα κάθε οριακής καταστάσεως αντί να εφαρμοστούν απευθείας στο μέτρο βλάβης. Ως εκ τούτου, κάθε στόχος επιτελεστικότητας (performance objective) πραγματοποιείται ως η πιθανότητα υπέρβασης ενός καθορισμένου επιπέδου επιτελεστικότητας (specified performance level). Ακολουθώντας αυτή τη λογική για κάθε συγκεκριμένο επίπεδο επιτελεστικότητας (performance level) υπολογίζεται μέση ετήσια πιθανότητα (MAF) υπέρβασης (v_{LS}). Η MAF μπορεί να υπολογιστεί χρησιμοποιώντας το θεώρημα ολικής πιθανότητας (total probability theorem):

$$v_{LS}(edp \le EDP) = \int_0^{+\infty} P(edp \le EDP \mid IM = im) \left| \frac{dv(IM)}{dIM} \right| dIM \tag{6}$$

όπου $P(edp \leq EDP \mid IM = im)$ είναι η πιθανότητα υπέρβασης μιας οριακής κατάστασης. Ονομάζεται επίσης και συνάρτηση ευθραυστότητας ή ευπάθειας (fragility or vulnerability function). $|dv(IM)/dIM|$ είναι η κλίση της καμπύλης σεισμικής επικινδυνότητας. Η απόλυτη τιμή χρησιμοποιείται για να αποφύγει την αρνητική τιμή που έχει η κλίση της καμπύλης επικινδυνότητας (hazard curve). Η παραπάνω εξίσωση περιγράφει το συνδυασμό της αβεβαιότητας στη σεισμική κίνηση του εδάφους όπως είναι δοσμένη μέσα από τη καμπύλη επικινδυνότητας (hazard curve) της περιοχής, με αβεβαιότητες που έχουν να κάνουν με την αντοχή των κατασκευών που αντιπροσωπεύονται από τη καμπύλη ευθραυστότητας (fragility curve).

Η παραπάνω εξίσωση υπολογίζεται αριθμητικά μια και η ολοκλήρωση δεν είναι πάντα δυνατή. Υπάρχουν δύο τρόποι για να υπολογιστεί η MAF. Ο πρώτος τρόπος είναι να υπολογιστεί η πιθανότητα ότι η απαίτηση υπερβαίνει την ικανότητα της κατασκευής, και ονομάζεται ευθεία μέθοδος ‘direct or EDP-based method’ ή εναλλακτικά χρησιμοποιείται και η έμμεση ‘indirect or IM-based’ προσέγγιση. Η τελευταία αναφέρεται στον υπολογισμό της πιθανότητας ότι το IM θα είναι πάνω από την τυχαία IM ικανότητα της κατασκευής. Σε αυτή την εργασία η δεύτερη μέθοδος χρησιμοποιείται, όπου:

$$P(edp \leq EDP \mid IM = im) = P\left(IM_C < IM \mid IM = im\right) \tag{7}$$

Η μέση ετήσια συχνότητα μιας οριακής κατάστασης υπολογίζεται με τη χρήση της στατιστικής από τις αποκρίσεις που λαμβάνουμε από τη SPO2IDA. Η SPO2IDA δίνει έναν υπολογισμό της μέσης τιμής και της διασποράς της απόκρισης που μπορούν να χρησιμοποιηθούν για να υπολογιστεί η σχέση 6. Η πιθανότητα υπέρβασης της IM ικανότητας της κατασκευής είναι έτσι υπολογισμένη και πολλαπλασιασμένη με την κλίση της καμπύλης επικινδυνότητας χρησιμοποιώντας την εξίσωση 7. Αν υποτεθεί λογαριθμοκανονική κατανομή και αν $\ln(\hat{\theta}_{max})$ και $\hat{\beta}$ είναι ο λογαριθμικός μέσος και η τυπική απόκλιση του $\hat{\theta}_{max}$ για μια δοσμένη ένταση $S_a(T_1,5\%)$, η ακόλουθη έκφραση μπορεί να χρησιμοποιηθεί (Vamvatsikos and Fragiadakis 2010):

$$\hat{\beta} = \frac{1}{2}\left(\ln S_a^{84\%} - \ln S_a^{16\%}\right) \approx \left(\ln S_a^{84\%} - \ln S_a^{50\%}\right) \qquad (8)$$

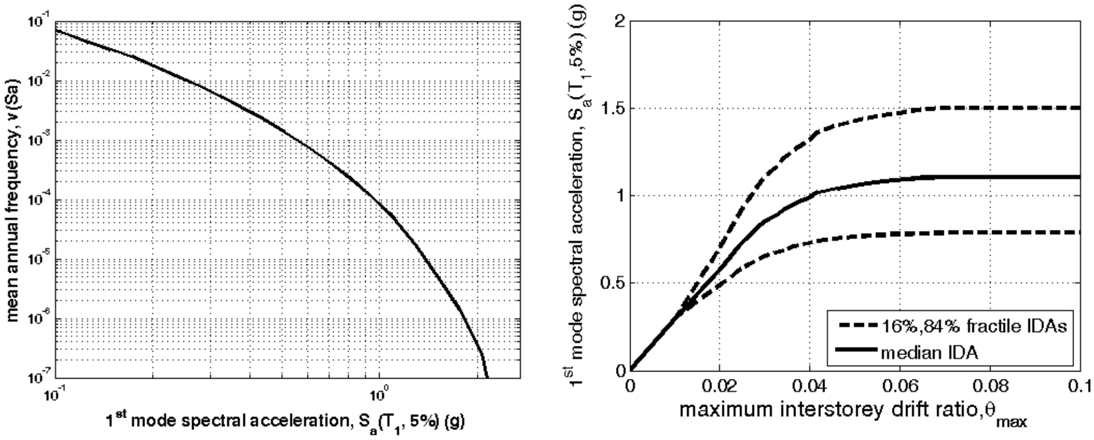

(a) (b)

Σχήμα 9 (α) Καμπύλες σεισμικής επικινδυνότητας για T1=0.93sec και (b) μέση καμπύλη SPO2IDA και οι καμπύλες του 16 ου και του 84ου ποσοστημόριου.

Οι πιθανοτικοί περιορισμοί εφαρμόζονται στον ετήσιο ρυθμό της σχετικής μετατόπισης του ορόφου που υπάρχει υπέρβαση (annual rate of the drift value being exceeded) για κάθε οριακή κατάσταση που λαμβάνεται υπόψη. Εν προκειμένω οι ρυθμοί που χρησιμοποιούνται για τα επίπεδα σεισμικής επικινδυνότητας (hazard levels) 50/50, 10/50 και 2/50 σχετίζονται με την περίοδο επαναφοράς δια της σχέσης $\tau_{LS}=1/v_{LS}$. Οι αντίστοιχες περίοδοι επαναφοράς είναι 72, 475, 2475 χρόνια αντίστοιχα. Αυτό οδηγεί στους ακόλουθους πιθανοτικούς περιορισμούς:

$$\begin{aligned} T_{DL} &\geq 72\text{yrs} \\ T_{SD} &\geq 475\text{yrs} \\ T_{NC} &\geq 2475\text{yrs} \end{aligned} \qquad (9)$$

Έτσι, με τους παραπάνω περιορισμούς το προτεινόμενο πρόγραμμα αντισεισμικού σχεδιασμού μεταλλικών κατασκευών με ντετερμινιστικά και πιθανοτικά κριτήρια «GSO_SPO2IDA», έχει το παρακάτω διάγραμμα ροής εφόσον χρησιμοποιείται το προσεγγιστικό πρόγραμμα ανάλυσης SPO2IDA. Στην περίπτωση που ζητείται η ακριβής επίλυση χρησιμοποιείται το πρόγραμμα ανάλυσης της IDA αντί της Static Pushover στο αντίστοιχο βήμα ‘Seismic Combinations Static Pushover’ του παρακάτω προγράμματος.

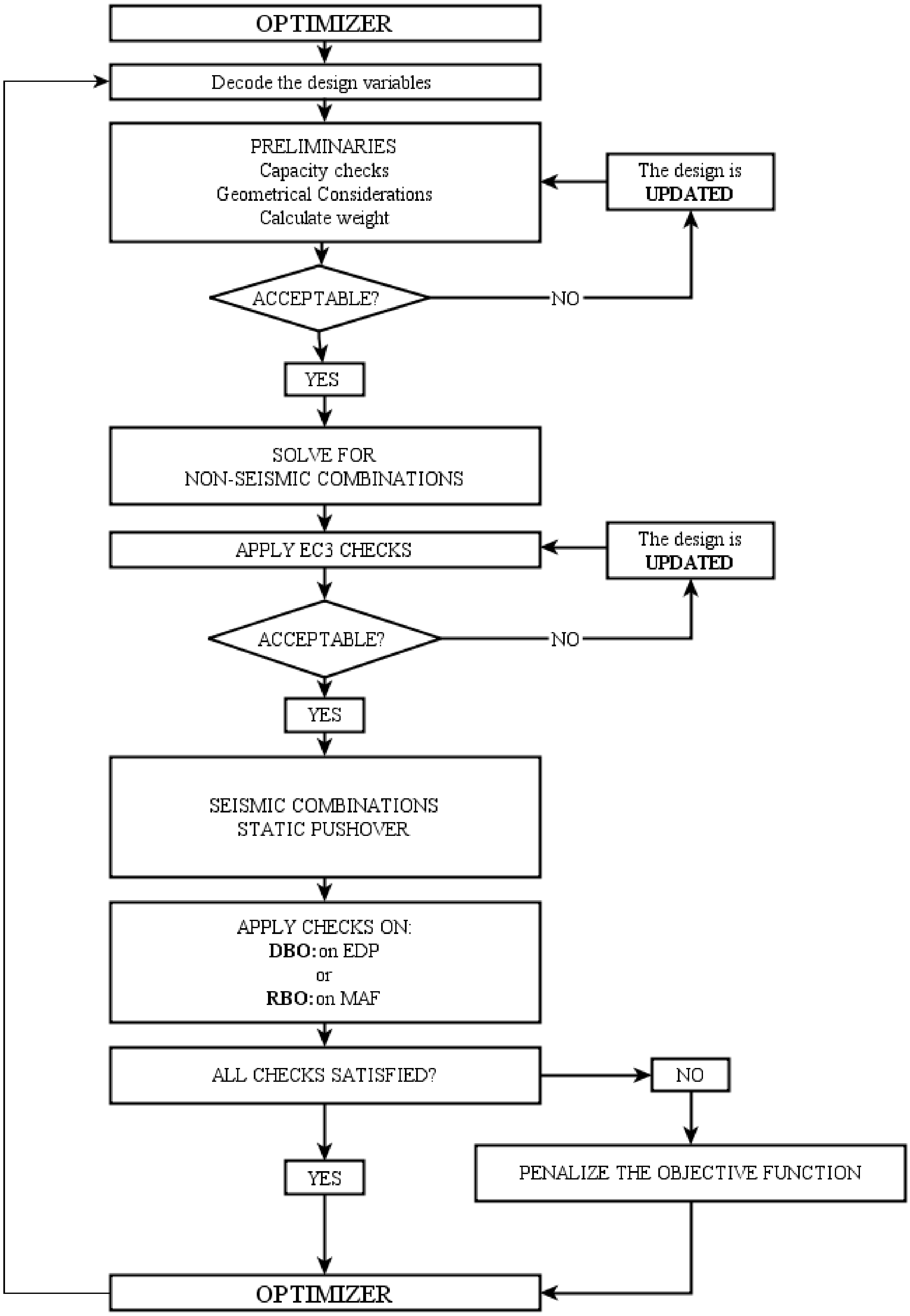

Σχήμα 10. Διάγραμμα ροής προγράμματος «GSO_SPO2IDA».

Αριθμητικά αποτελέσματα

Η προτεινόμενη μεθοδολογία «GSO_SPO2IDA» εφαρμόζεται σε ένα τριώροφο και ένα εννιαώροφο μεταλλικά πλαίσια. Τα πλαίσια έχουν σχεδιαστεί για την περιοχή του Los Angeles σύμφωνα με τον κανονισμό 1997 NEHRP (National Earthquake Hazard Reduction Program). Όλες οι αναλύσεις έγιναν στην πλατφόρμα του προγράμματος OpenSees.

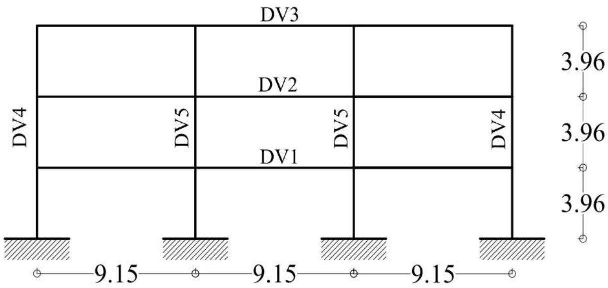

(α)

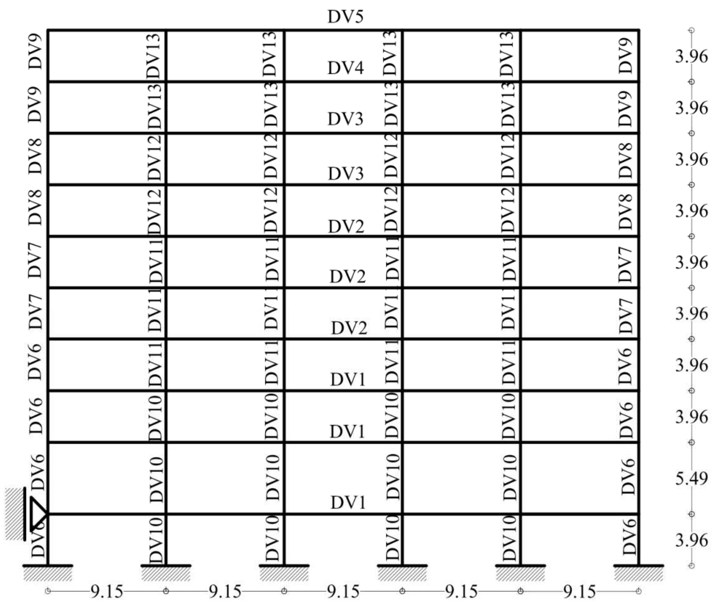

(β)

Σχήμα 11(α) Το τριώροφο (LA3) και (β)Το εννιαώροφο (LA9) μεταλλικό πλαίσιο.

Το μέτρο ελαστικότητας υποτέθηκε ότι είναι ίσο με 200GPa και η τάση διαρροής είναι f_y=235MPa. Όλες οι διατομές είναι από τους πίνακες του Αμερικάνικου Ινστιτούτου Σιδήρου και κατασκευής (American Institute of Steel and Construction, AISC). Το μόνιμο φορτίο έχει ληφθεί G=5KN/m^2 και το κινητό φορτίο είναι Q=2KN/m^2. Το μέτρο βλάβης που έχει ληφθεί είναι η μέγιστη γωνιακή παραμόρφωση ορόφου (maximum interstorey drift, θ_{max}) και τα όρια του είναι 0.6, 1.5, 3% για άμεση χρήση (IO), ασφάλεια ζωής (LS) και αποφυγή κατάρρευσης (CP), αντίστοιχα.

Ένα διακριτό ντετερμινιστικό πρόβλημα βελτιστοποίησης (DBO) και ένα διακριτό πρόβλημα βελτιστοποίησης με πιθανοτικά κριτήρια (RBO) επιλύθηκαν για τα δύο υπό εξέταση πλαίσια με το πρόγραμμα «GSO_SPO2IDA». Τα αποτελέσματα από τις βελτιστοποιημένες κατασκευές παρουσιάζονται στους πίνακες 1 και 2. Για το τριώροφο πλαίσιο οι βέλτιστοι σχεδιασμοί έχουν όγκους ίσους με 3.9m^3 και 4.10m^3 για το διακριτό ντετερμινιστικό (DBO) και για το πρόβλημα βελτιστοποίησης με πιθανοτικά κριτήρια (RBO) αντίστοιχα. Ενώ, για το εννιαώροφο πλαίσιο οι αντίστοιχοι σχεδιασμοί σε όγκο είναι 25.75m^3 και 27.34m^3. Είναι προφανές, ότι για τα δύο κτήρια η διαδικασία του ντετερμινιστικού σχεδιασμού οδηγεί σε σχεδιασμούς μικρότερου όγκου από τη διαδικασία με πιθανοτικά κριτήρια, επειδή η τελευταία λαμβάνει υπόψη της τις αβεβαιότητες του προβλήματος και για αυτό απαιτεί βαρύτερες διατομές ώστε να πληρούνται αυτές οι απαιτήσεις.

Στα σχήματα 12, 13, 14, 15 φαίνονται τα αποτελέσματα εφαρμογής του προτεινόμενου προγράμματος «GSO_IDA-SPO2IDA». Στο παραπάνω σχήμα 12α φαίνεται η σύγκριση ανάμεσα στους δύο σχεδιασμούς - ντετερμινιστικό και πιθανοτικό - σχεδιασμό για το τριώροφο πλαίσιο, με το προτεινόμενο πρόγραμμα «GSO_SPO2IDA». Παρατηρείται ότι ο RBO σχεδιασμός με πιθανοτικά κριτήρια έχει μεγαλύτερο βάρος σε σχέση με το ντετερμινιστικό σχεδιασμό DBO. Αυτό συμβαίνει γιατί στον RBO λαμβάνουμε υπόψη τις αβεβαιότητες. Στο σχήμα 12β παρουσιάζονται δύο καμπύλες χρησιμοποιώντας μέσα στο προτεινόμενο πρόγραμμα βελτιστοποίησης «GSO_SPO2IDA» :μια ως μέθοδο ανάλυσης την ΠΔΑ (IDA) «GSO_IDA» και μια την μέθοδο SPO2IDA (approximate IDA) για το τριώροφο πλαίσιο «GSO_SPO2IDA». Παρατηρείται ότι η προσεγγιστική μέθοδος ανάλυσης (SPO2IDA) έχει μικρότερο βάρος σε σχέση με την ακριβή μέθοδο IDA.

Πίνακας 1 Αποτελέσματα βέλτιστου σχεδιασμού για το τριώροφο κτίριο.

DBO optimized design (volume=3.9m^3 ή 30,62tn)					
Storey / Group	**Beams**	**Storey / Group**	**External columns**	**Storey / Group**	**Internal columns**
1 / DV1	W33×118	1 / DV4	W14×120	1 / DV5	W14×233
2 / DV2	W27×94	2 / DV4		2 / DV5	
3 / DV3	W21×57	3 / DV4		3 / DV5	
RBO optimized design (volume=4.1m^3 ή 32,18tn)					
1 / DV1	W33×118	1 / DV4	W14×145	1 / DV5	W14×257
2 / DV2	W27×84	2 / DV4		2 / DV5	
3 / DV3	W21×68	3 / DV4		3 / DV5	

Πίνακας 2 Αποτελέσματα βέλτιστου σχεδιασμού για το κτίριο εννέα ορόφων

DBO optimized design (volume=25.75m^3 ή 202,14tn)					
Storey / Group	**Beams**	**Storey / Group**	**External columns**	**Storey / Group**	**Internal columns**
0-2 / DV1	W36×182	0-3 / DV6	W14×398	0-3 / DV10	W14×398
3-5 / DV2	W33×241	4-5 / DV7	W14×370	4-6 / DV11	W14×370
6-7 / DV3	W27×178	6-7 / DV8	W14×132	7-8 / DV12	W14×132
8 / DV4	W21×201	8-9 / DV9	W14×132	8-9 / DV13	W14×132
9 / DV5	W21×223				
RBO optimized design (volume=27.34m^{3}ή 214,62tn)					
0-2 / DV1	W40×183	0-3 / DV6	W14×426	0-3 / DV10	W14×426
3-5 / DV2	W36×182	4-5 / DV7	W14×426	4-6 / DV11	W14×426
6-7 / DV3	W33×169	6-7 / DV8	W14×211	7-8 / DV12	W14×257
8 / DV4	W27×217	8-9 / DV9	W14×109	8-9 / DV13	W14×109
9 / DV5	W21×132				

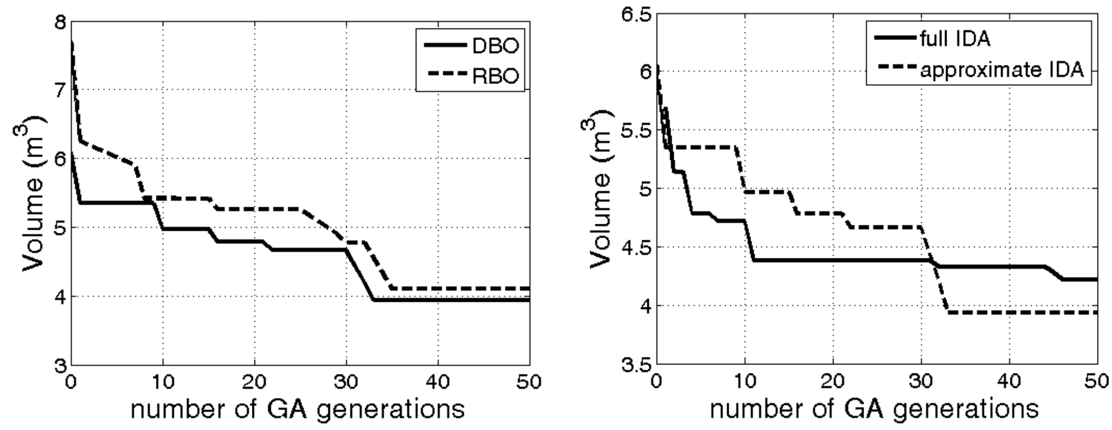

(α) (β)

Σχήμα 12(α): αριθμός γενεών έναντι του όγκου με το προτεινόμενο πρόγραμμα «GSO_IDA-SPO2IDA» για το τριώροφο πλαίσιο χρησιμοποιώντας: 12(α): την μέθοδο SPO2IDA με ντετερμινιστικά (DBO) και πιθανοτικά (RBO) κριτήρια, για τον DBO και τον RBO σχεδιασμό «GSO_ SPO2IDA» και 12(β) την ΠΔΑ (IDA) «GSO_IDA» και την μέθοδο SPO2IDA (approximate IDA) με ντετερμινιστικά κριτήρια «GSO_SPO2IDA».

Στο σχήμα 13 παρατηρούμε τους βέλτιστους σχεδιασμούς όταν έχουμε χρησιμοποιήσει στον κώδικά «GSO_IDA-SPO2IDA» της ανάλυσης αφενός την IDA και αφετέρου την SPO2IDA. Είναι προφανές ότι οι δύο σχεδιασμοί δίνουν παραπλήσια αποτελέσματα. Το σχήμα 15 παρουσιάζει για το εννιαώροφο μεταλλικό πλαίσιο αποτελέσματα σχεδιασμού που προέκυψαν από τον κώδικα «GSO_SPO2IDA»παρόμοια με αυτά του σχήματος 14. Σε αντίθεση με το τριώροφο, σημαντικές διαφορές έχουν παρατηρηθεί για το εννιαώροφο πλαίσιο. Ως εκ τούτου, για μεγαλύτερους και πιο πολύπλοκους σχεδιασμούς οι δύο διαδικασίες (DBO, RBO) είναι πιθανόν να συγκλίνουν σε σχεδιασμούς που διαφέρουν. Για τα θεωρούμενα τρία επίπεδα επιτελεστικότητας (performance levels considered), διαφέρει η κατανομή των καθ'ύψος σχετικών μετατοπίσεων (the height-wise drift distribution differs). Επίσης για τον DBO σχεδιασμό οι κρίσιμοι όροφοι είναι ο τρίτος και ο τέταρτος ενώ για τον RBO σχεδιασμό η μέγιστη απαίτηση παρατηρείται στην οροφή (έβδομο και όγδοο όροφο).

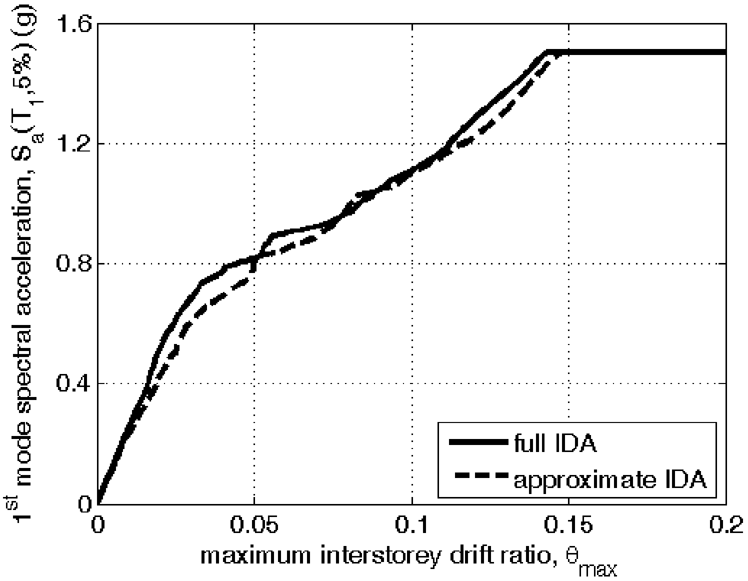

Σχήμα 13: Μέγιστη σχετική μετατόπιση ορόφου σε σχέση με τη φασματική επιτάχυνση κατά την πρώτη ιδιομορφή. Μέση καμπύλη βέλτιστου σχεδιασμού που προέκυψε από τον κώδικα «GSO_IDA-SPO2IDA» χρησιμοποιώντας την ακριβή ΠΔΑ και την προσεγγιστική SPO2IDA στο τριώροφο πλαίσιο.

Επιπλέον, για τα δύο κτήρια, τα όρια των σχετικών μετατοπίσεων έχουν προσεγγίσει τα όρια σε κάθε επίπεδο επιτελεστικότητας. Ο επόμενος πίνακας 3 δείχνει την οριακή κατάσταση της μέσης ετήσιας συχνότητας (the limit-state MAFs) και σε παρένθεση τις αντίστοιχες περιόδους επαναφοράς. Επίσης, με έντονο μαύρο χρώμα δείχνουμε τις περιπτώσεις όπου φαίνεται η αντίστοιχη μέση ετήσια συχνότητα (MAF) εκεί όπου υπάρχει υπέρβαση της αντίστοιχης μέσης ετήσιας συχνότητας. Για τα δύο πλαίσια οι RBO σχεδιασμοί που προέκυψαν από τον κώδικα «GSO_SPO2IDA» ικανοποιούν τους περιορισμούς της εξίσωσης 3 ενώ οι DBO σχεδιασμοί που προέκυψαν από τον κώδικα «GSO_SPO2IDA» τους παραβιάζουν για τις οριακές καταστάσεις δομικής βλάβης (SD) και κατάρρευσης (NC). Σε ότι αφορά τα πλαίσια που σχεδιάστηκαν με RBO όπως προέκυψε από τον κώδικα «GSO_SPO2IDA» έχοντας σαφή όρια σχετικά με τα επιτρεπόμενα της Μέσης Ετήσιας Συχνότητας υπέρβασης οριακής κατάστασης (MAF). Φαίνεται ότι η SD και NC οριακές καταστάσεις είναι κάπως κοντά στα κατώτατα όρια, δηλαδή 475 και 2474 χρόνια αντιστοίχως.

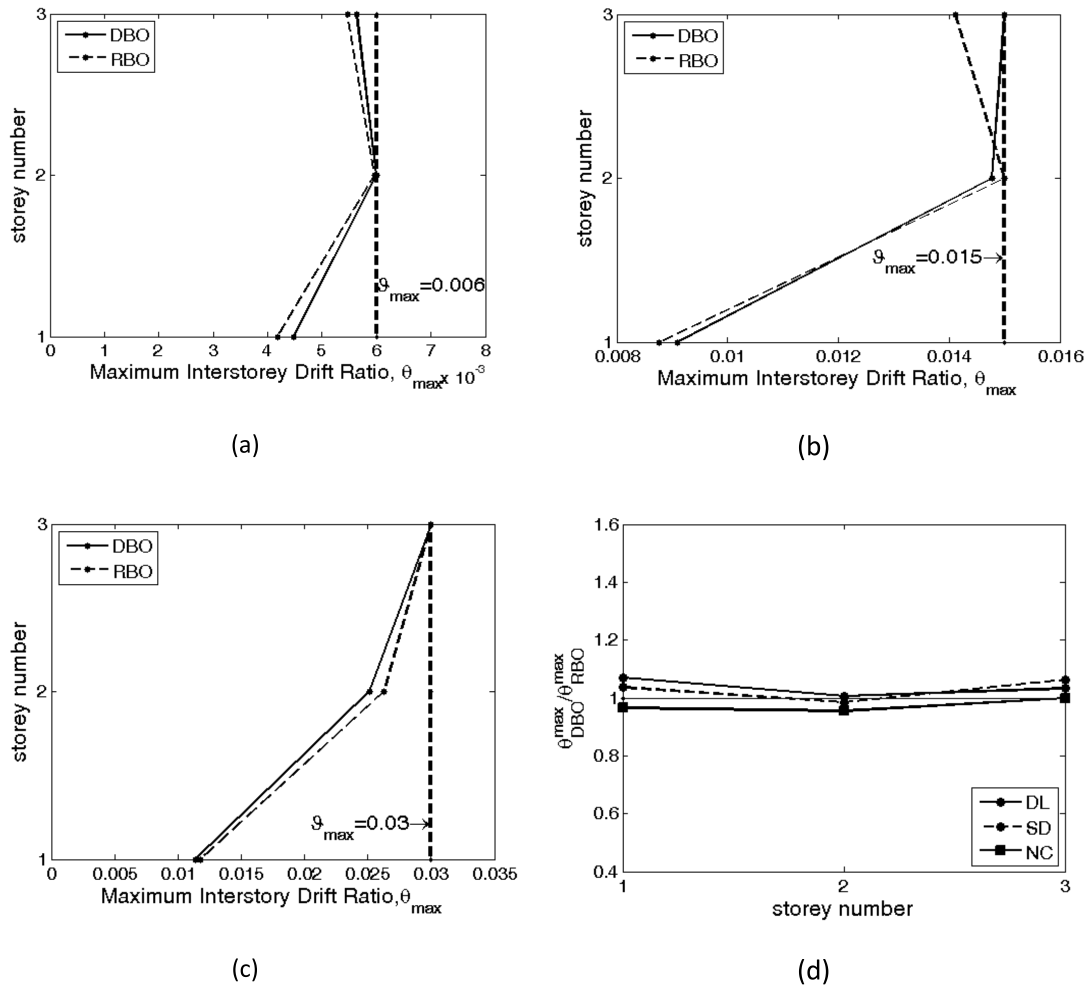

Σχήμα 14: Τριώροφο μεταλλικό πλαίσιο: Προφίλ της σχετικής μετατόπισης ορόφου για βέλτιστο σχεδιασμό που προέκυψε από τον κώδικα «GSO_SPO2IDA» για (a) οριακή κατάσταση περιορισμού των ζημιών(DL), (b) οριακή κατάσταση δομικής βλάβης (SD) (c) οριακή κατάσταση κατάρρευσης, (d) λόγος των DBO/RBO μέγιστης σχετικής μετατόπισης ορόφου για τις τρεις οριακές καταστάσεις. Η διακεκομμένη κάθετη γραμμή δείχνει τα (a), (b), (c) ντετερμινιστικά όρια σχετικής μετατόπισης ορόφου.

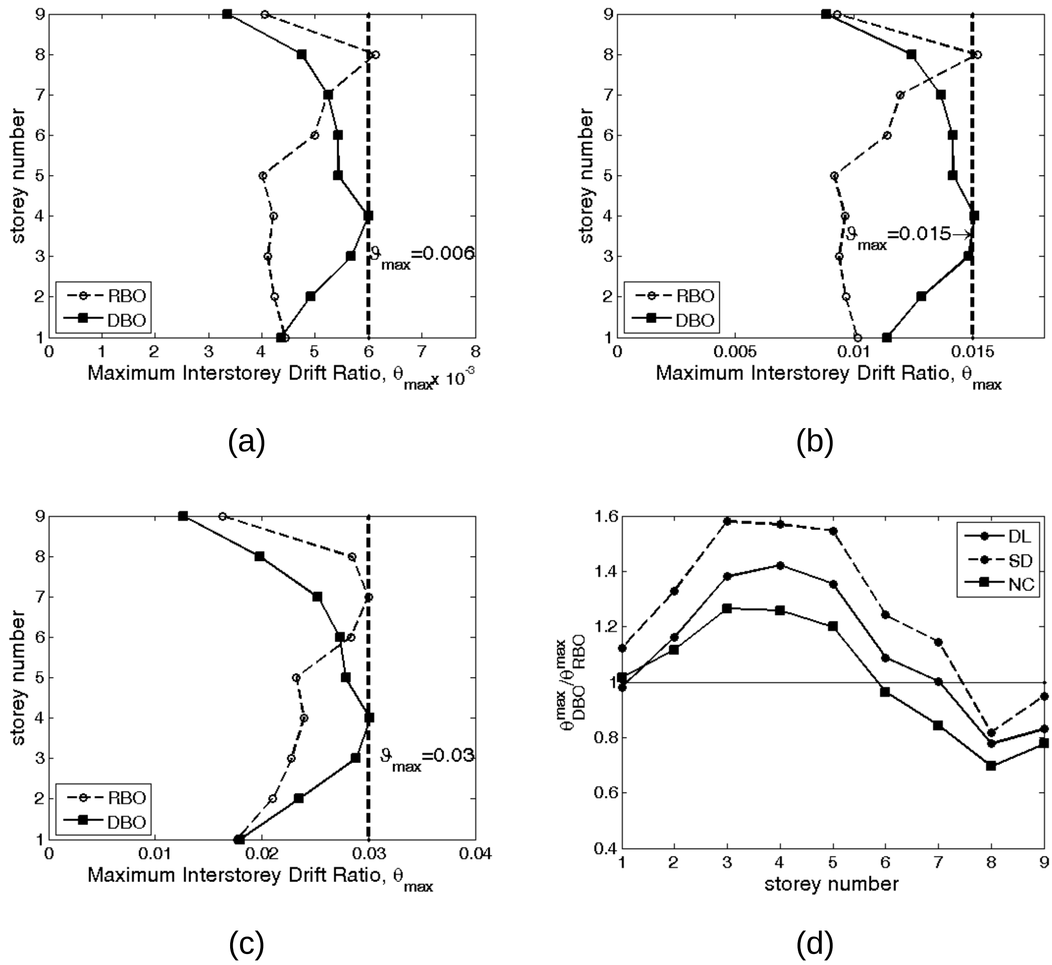

Σχήμα 15 Εννιαώροφο μεταλλικό πλαίσιο: Προφίλ των σχετικών μετατοπίσεων βέλτιστου σχεδιασμού που προέκυψε από τον κώδικα «GSO_SPO2IDA» για (a) οριακή κατάσταση περιορισμού των ζημιών(DL), (b) οριακή κατάσταση δομικής βλάβης (SD) (c) οριακή κατάσταση κατάρρευσης. (d) λόγος των DBO/RBO μέγιστη σχετική μετατόπιση ορόφου για τις τρεις οριακές καταστάσεις. Η διακεκομμένη κάθετη γραμμή δείχνει τα (a), (b), (c) ντετερμινιστικά όρια σχετικής μετατόπισης ορόφου.

Πίνακας 3: Μέσες ετήσιες συχνότητες για μόρφωση DBO και RBO.Στην παρένθεση δίδεται η αντίστοιχη περίοδος επαναφοράς τ.

Design objective **Στόχος σχεδιασμού (επιτελεστικότητα)**	**DBO**	**RBO**
Τριώροφο μεταλλικό πλαίσιο		
DL	0.00435 (230 έτη)	0.00425 (235 έτη)
SD	0.00183 (547 έτη)	0.00174 (575 έτη)
NC	0.00040 (2478 έτη)	0.00034 (2921 έτη)
Εννιαώροφο μεταλλικό πλαίσιο		
DL	0.0295 (340 έτη)	0.00142 (702 έτη)
SD	**0.0295 (340 έτη)**	0.00142 (702 έτη)
NC	**0.0012 (834 έτη)**	0.00040 (2530 έτη)

Συνοψίζοντας, στην παρούσα διατριβή εξετάστηκε η ακρίβεια της μεθόδου Προσαυξητικής Δυναμικής Ανάλυσης (ΠΔΑ-IDA, Vamvatsikos and Cornell 2002) με ικανοποιητικά αποτελέσματα και αναπτύχθηκε ένας γενετικός αλγόριθμος βέλτιστου σχεδιασμού με βάση ντετερμινιστικά και πιθανοτικά κριτήρια «GeneticStructuralOptimization_using_IDA-SPO2IDA» συνοπτικά «GSO_IDA-SPO2IDA» χρησιμοποιώντας ακριβείς και προσεγγιστικές μεθόδους ανάλυσης, δηλαδή αφενός τη μέθοδο Προσαυξητικής Δυναμικής Ανάλυσης «GSO_IDA» και αφετέρου την SPO2IDA «GSO_SPO2IDA» για τον σχεδιασμό μεταλλικών κατασκευών υπό σεισμικά φορτία με μεγάλο κέρδος σε υπολογιστικό χρόνο.

Acknowledgements

First of all, I would like to express my deepest gratitude to my advisor, Professor **Manolis Papadrakakis**, for giving me the opportunity to proceed to this PhD. I will always remember the fruitful conversations which led to a step forward in the scientific field that was chosen as subject for this dissertation.

I would also like to thank the members of the advisory committee, Professor **Ch. Gantes** and Associate Professor **K. Spiliopoulos** for their advice and assistance throughout this study.

Furthermore, I would like to thank Lecturer **Michalis Fragiadakis** for his invaluable support and assistance and his advice throughout this dissertation which will always be memorable for me.

Moreover, I would like to thank my Professors of the National Technical University of Athens for the knowledge they offered me through the Msc courses and the years of my PhD.

Generally I would like to thank the members of the laboratory of the Institute of Structural Analysis and Antiseismic Research of the School of Civil Engineering of the National Technical University of Athens for their encouragement during the preparation of this dissertation.

I want to thank my family who always support me to every step I choose to proceed. Their moral support is invaluable to me.

Finally, I would also like to mention that I am grateful to Professor Manolis Papadrakakis and the National Technical University of Athens for the financial support of this dissertation through the job he provided me in the pc-lab of the post graduate students.

Table of Contents

List of Figures

List of Tables

CHAPTER 1

Introduction

1.1 Motivation

The design and assessment of structural systems implies decision-making under uncertainty on the capacity of a structure to endure the uncertain demands of a future earthquake. To this direction, recent design codes and guidelines recommend the use of more advanced, nonlinear, static or dynamic, methods of analysis that allow a better insight on the system's demand and capacity that are able to provide accurate estimates of its reliability. Thus, engineering decisions can be based on improved analysis results, and, combined with the designer's experience, can lead to a variety of design solutions, with improved performance. The most direct approach to design a structure using more advanced analysis methods is a trial-and-error strategy. Since this process can often be cumbersome and time-consuming and can be influenced by several unforeseeable parameters, the development of an automatic seismic design procedure is appealing. Structural optimization algorithms have been applied successfully to obtain cost-effective design solutions. In an optimally designed structural system the structural members are chosen so as for the structure to exhibit increased capacity and improved performance.

The most accurate analysis method is the incremental dynamic analysis (IDA) method. Nonlinear response history analysis (NRHA) lies in the core of the incremental dynamic analysis method (IDA) (Vamvatsikos and Cornell 2002), where the structure is subjected to a suite of ground motion records. Each record is scaled to multiple levels of seismic intensity, producing the structure's capacity curve in terms of an intensity measure (IM) versus an engineering demand parameter (EDP). IDA provides a powerful performance estimation framework, which, however, is often questioned due to the scaling of records with scaling factors that considerably differ from one. This practice leads to ground motions that may not represent a realistic physical process and is responsible for under or over estimating the demand, or in other words, for introducing bias in the capacity estimation. The primary concern with record scaling is whether 'weak' records when scaled up will be representative of 'strong' records. The effect of record scaling also depends on the intensity measure adopted and the properties of the structure examined.

This research draws motivation from the presented issues, and systematically investigates the effect of record scaling providing a rational approach for measuring the bias introduced when IDA analysis is performed. This study provides also an assessment of response and performance of typical ductile SMRF structures, and develops an optimization procedure for obtaining for optimized design of steel structures.

1.2 Objectives and scope

The objectives of this study are two-fold: (i) The exploration of the accuracy of IDA with regard to the scaling procedure. This is illustrated with a comparison of IDA to a statistically extracted capacity curve using cloud analysis, and (ii) the possibility of using SPO2IDA (Static pushover to incremental dynamic analysis) within a structural optimizer in order to achieve cost-effective optimum designs with safety levels as the ones we would have obtained using IDA. Bearing in mind that IDA is a time consuming method we used an approximate performance estimation method static pushover to IDA (SPO2IDA method) which is considered as an IDA-based approximate performance estimation method to answer the last question.

In order to address these tasks efficiently, various algorithms have been considered. For the first objective a wide range of earthquake records have been used in order to perform nonlinear response history analysis. The results are inserted on a Cartesian plane with axes the intensity measure (IM)-and the engineering demand parameter (EDP) forming a ‘cloud’ of points. From this cloud of points with appropriate statistical analysis we obtain a curve. This curve is considered as more accurate compared to IDA. Because of the lack of records in high intensities, synthetic records have been used to track the curve in these intensities. For the second objective IDA seems to be time consuming and almost prohibitive for optimization problems and this is the reason for using an approximate performance estimation method reducing considerably the time needed for an optimization algorithm to reach the optimum design.

The optimum result obtained by a deterministic optimization formulation that ignores scatter of any kind of parameters affecting its response has limited value, as it can be severely affected by the uncertainties that are inherent in the model. The deterministic optimum can be associated with unacceptable probabilities of failure, or it can be quite vulnerable to slight variations of some uncertain parameters. Consequently, a deterministically optimum design may result in an infeasible design. In real-world conditions the significance of any “optimum” solution would be limited if the uncertainties involved in the geometric and material description of the structure as well as in the loading conditions are not taken into consideration. This is because real-world structures have always imperfections which induce deviations from the nominal state assumed at the analysis phase by the design codes. The reliability-based formulation requires the calculation of the mean annual frequency (MAF) for a number of prespecified limit-states. Usually in reliability-based optimization problems the thresholds are set on the limit-state probabilities, i.e. the probability of the near collapse limit-state should not be less than 90%. However, in earthquake engineering applications it is preferable to set the constraints on the limit-state MAF. The MAFs allow setting constraints with a clear engineering meaning thus providing a common language between engineers and stakeholders. More specifically, the reciprocal of the MAF is the return period, in years, that a limit-state is exceeded and the MAF provides how many times in one year a limit-state is exceeded.

1.3 Thesis organization and outline

This thesis consists of eight chapters in total, plus the bibliography and one appendix at the end of it. Its structure is organized as follows:

Chapter 1 is the introduction to the dissertation which provides a general description of the motivation, the goals pursued, as well as a brief description of the contents of each chapter.

Chapter 2 begins with a general view of natural recordings, following by a discussion the seismic loading of structures. Moreover, a review of accelerograms and accelerographs is presented. Furthermore, this chapter proceeds with describing the advantages and the disadvantages of natural, artificial and synthetic records. Due to the fact that even today with the large number of natural accelerograms recorded during the past three decades, it may still be difficult to find accelerograms that fulfill the requirements of certain magnitude and distance bins especially for large magnitudes and close distances, synthetic records are of great use. The intensity measures (IM) presented are peak ground motion, Arias intensity, Root mean square acceleration (RMS), duration, response spectra, spectrum intensity, I_v index, characteristic intensity and cumulative absolute velocity.

Chapter 3 The performance-based design concept is described in this chapter along with the seismic performance estimation methods. The chapter begins with the linear static analysis. Afterwards, the nonlinear static pushover (NSP) analysis with its pros and cons is studied along with the nonlinear response history analysis (NRHA). Furthermore, the most important nonlinear static (NSP) and nonlinear dynamic analysis (NDP) procedures are presented. In particular, the displacement coefficient method of ASCE-41, the capacity spectrum method of ATC-40, the N2 method of Eurocode 8 (EC8) are variations of the NSP procedures. Also, linear dynamic procedures are shown such as the spectral method and the time integration methods. Finally the seismic capacity of structures as seen through cloud analysis (CA), multi-stripe analysis (m-stripe) and incremental dynamic analysis (IDA) are examined.

Chapter 4 presents aspects of uncertainty in structural engineering. It begins describing the theoretical approach to uncertainty and how it can be assessed. Furthermore, the reliability analysis of structures is presented along with the basic approach giving the probability assessment formulation. The objective of the latter is to show how the demand and capacity factors γ and φ (Jalayer 2003), as well as v, the confidence factor in the SAC guidelines, have been derived by elementary probability theory from representations of the three random elements of the problem. These elements are: first-mode spectral acceleration $Sa(T_1,5\%)$, displacement demand D, and displacement capacity C calculating the limit-state mean annual frequency of exceedance.

Chapter 5 A methodology for the evaluation of the effect of scaling when Incremental Dynamic Analysis (IDA) is performed. The median capacity curve of IDA is compared to the capacity curve obtained using cloud analysis. Cloud analysis data contain results obtained using unscaled natural and synthetic ground motion records. Synthetic records were used due to the lack of a statistically significant number of natural records for large intensities. Nonlinear regression is performed with the aid of the Local Regression Smoothing Algorithm (LOESS) in order to post-process the results of cloud analysis. The primary difference between the two methods is that cloud analysis allows obtaining capacity curves without scaling the ground motion records, as opposed to the IDA algorithm. To investigate the statistical significance of this comparison, the bootstrap method is used. The bootstrap method is a powerful and easy-to-implement tool that allows calculating confidence intervals. Using bootstrap we are able to measure the bias introduced by record scaling when IDA is adopted. Thus, the bias is examined quantitatively and qualitatively for the full range of limit-states, yielding useful conclusions regarding scaling and its legitimacy in the context of IDA. A three-storey and a nine-storey steel moment resisting frames along with 12 single-degree of freedom oscillators are used for our case-study investigations.

Chapter 6 presents at the begining the history of optimization. Moreover, the concept of optimum structural design is discussed, followed by the formulation of a single objective optimization problem and some necessary definitions. The types of structural optimization problems and their aims are subsequently described. Furthermore, there is a brief review of genetic algorithms (GA) which is the algorithm used in the chapters to follow. Finally, two methods for handling the constraints are described: the method of static penalties and the method of dynamic penalties.

In **Chapter 7** a new approach for the performance-based seismic design of buildings using a deterministic and a reliability-based structural optimization framework is presented. To overcome the increased computing cost of Incremental Dynamic Analysis (IDA) we adopt an approximate seismic performance estimation tool, known as Static Pushover to IDA (SPO2IDA). The SPO2IDA tool is nested within the framework of a Genetic Algorithm resulting to an efficient seismic design procedure able to consider uncertainty. The genetic algorithm steps towards designs of improved performance, locating the most efficient design in terms of the minimum weight of the structure. Reliability-based constraints are considered in terms of the mean annual frequency of preset limit-states not being exceeded. A three- and a nine-storey steel moment resisting frames are used to demonstrate the design algorithm proposed. The methodology presented leads to efficient real-world building designs within acceptable computing time, directly considering the seismic risk.

The conclusions of this research are presented in **Chapter 8**. The contributions of this dissertation are clearly stated, together with the extensions of this work to future research on the subject of the dissertation.

CHAPTER 2

Earthquake loading and ground motion records

2.1 Introduction

The assessment of seismic response, in terms of non-linear dynamic analysis procedures, is performed using a number of accelerograms that correspond to seismic events of different earthquake magnitude and are recorded at a variety of soil conditions. The accelerograms are usually selected in terms of their first mode spectral acceleration. In case the response of a structure at limit states near collapse is studied, a limited strong motion database makes it difficult to find natural unscaled earthquakes at the desired intensity level. This is particularly evident for slender structures with large yielding acceleration where significant elastic spectral acceleration values may be needed to demand high ductility. This lack of natural recordings led to the need for artificial and synthetic records.

Three different types of strong ground motions are implemented in practice, i.e. natural, artificial and synthetic records. Natural accelerograms are the most preferable option to be used in nonlinear response history analysis (NRHA) since they are recorded during real seismic events. Natural records were relatively few in the past due to the insufficient instrumentation of seismic prone regions.

Various parameters are used in order to present, in a brief and clear way, the most important characteristics of strong ground motion. The selection of strong ground motion to be used in several types of seismic analysis is usually based on several earthquake parameters, given the fact that it is impossible to characterize strong motion accurately using any single parameter (Jennings J.E. (1985), Joyner W.B. and Boore D.M. (1988)). These parameters attempt to address the complex nature of strong seismic motion, including the energy and frequency content, the amplitude and the duration.

Recently, selected earthquake parameters the so-called intensity measures (IM), including peak ground acceleration (PGA) and Spectral acceleration to the first period ($S_a(T_1,5\%)$), have been applied not only to identify the salient characteristics of strong motion but also as a means to scale earthquake records at a desired level of intensity. Furthermore, intensity measures are applied for the selection of records to perform incremental dynamic analysis (IDA). In this chapter the most important intensity measures are presented, including those used in the present study, while a more extensive referencing on IMs may be found in the literature, e.g., (Krammer (1996), Acevedo (2003)).

2.2 <u>Seismic loading</u>

Due to the highly uncertain nature of earthquakes, the assessment of their magnitude, location and rate of occurrence is of paramount importance in earthquake engineering. The amplitude and the frequency content of seismic ground motions, as recorded at various sites, depends on the amount of seismic energy released during the fault rupture and its attenuation from source to site. Therefore, although the amount of energy released from the source depends on the size of the fault rupture, the properties of the seismic waves, as ultimately felt and recorded in the surface, depend also on the amount of energy dissipated due to anelastic absorption and geometric spreading. Moreover, local parameters such as superficial geology, site topography and the presence of structures, may also significantly affect the properties of the ground motions that are finally recorded at the site of interest. The various parameters that affect seismic ground motions, in general, are grouped into three categories. The first characterizes the source of energy release, the second the path along which the energy propagates and the last is the point of observation. The three categories are thus known as *source*, *path* and *site.* Magnitude, distance and soil properties are the most critical parameters and usually ground motion prediction equations are limited to them. However, a great number of other factors may also be of significance.

Seismic forces on a structure typically are inertia forces produced by the motion of the ground, or forces produced by the differential movement of the supports. For engineering purposes, and depending on the application, we seek simplified approaches to represent earthquake loading. Such approaches should be suitable to our needs and consistent with the associated uncertainties. Therefore, we merely have to be able to describe the characteristics of the ground motion that are of engineering significance, adopting metrics that can be extracted from the ground motions that reflect primarily: the *amplitude*, the *frequency content* and the *duration*. In seismic design codes and guidelines, earthquake loads are represented by the response spectrum of maximum absolute acceleration. However, the most faithful representation is achieved through the entire ground acceleration time-history. The representation of the seismic loading in the form of acceleration time-histories means that the hazard is defined in terms of all of the characteristics of the ground shaking. In addition to amplitude frequency, the energy and the duration of shaking are also significant and have to be considered (Bommer et al. (2000)). The latter information is lost when seismic loading is considered in the form of an elastic spectrum. Thus, depending on the problem and the analysis method at hand seismic loading may be defined using either response spectra, or acceleration time-histories. Both options require the knowledge of the seismic hazard, since the seismic loads, in principle, have to be compatible with the hazard conditions of the site. (Fragiadakis et al. 2013).

2.3 Natural (recorded) ground motion records

2.3.1 Accelerographs and accelerograms

Strong ground-motion is recorded by accelerographs, which are instruments that record the acceleration as a function of time. The first accelerographs were developed and installed in California in 1932 and recorded the strong ground-motion generated by the Long Beach earthquake in the following year.

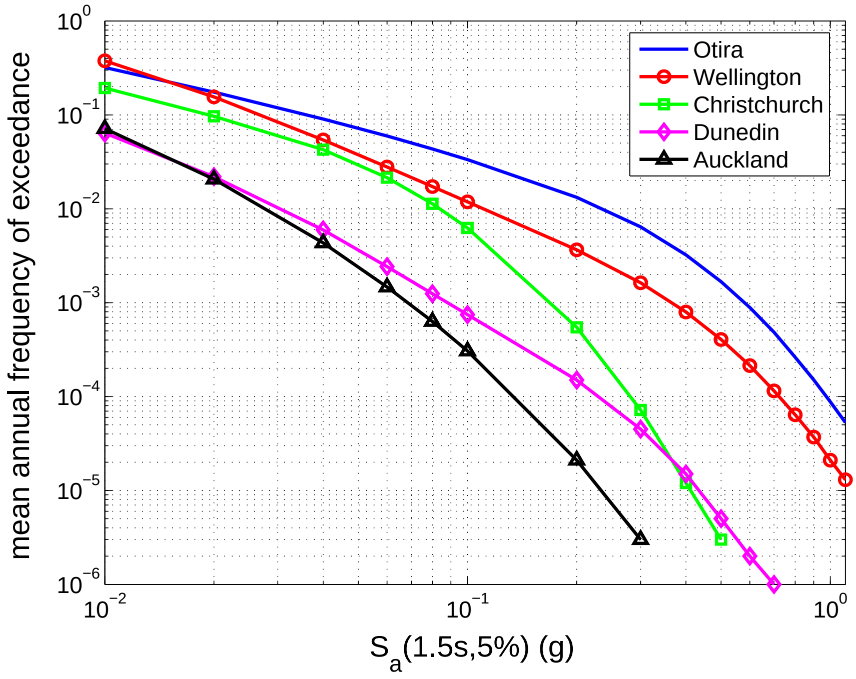

Figure 21. Seismic hazard curves for spectral acceleration for various New Zealand sites (adapted from Bradley, B.A. and Dhakal, R.P.2008).

The first generation of accelerographs is analogue instruments recording on film or paper. They do not record continuously; instead they remain on stand-by until triggered by a certain threshold level of acceleration. Therefore, the first wave arrivals that do not exceed the threshold value are not recorded. Since accelerographs only record strong shaking, they must be installed in those areas where earthquakes are expected. For these instruments, there is the necessity of digitizing the analogue record, which creates problems associated with the introduction of short- and long-period noise.

The second generation of accelerographs operates with a force-balance transducer and record digitally on to solid state or magnetic media. They are able to operate continuously and hence the first motions of the earthquake shaking are retained (Acevedo 2003).

Accelerographs usually record three mutually perpendicular components of motion in the vertical and two horizontal directions. The records obtained from the accelerographs are accelerograms, which are the most detailed representation of earthquake ground motion. They contain a wealth of information about the nature of the ground shaking in strong earthquakes and also about the highly varied characteristics that different earthquakes can produce at different locations (Acevedo 2003).

Accelerograms are the most detailed representation of earthquake ground motion and contain a wealth of information about the nature of the ground shaking. When time-histories are needed, they can be selected from database of real accelerograms or they can be generated synthetically. In all the cases, the accelerograms used in earthquake-resistant design should be compatible with the level of seismic hazard defined and they should reflect the nature of the expected ground motion at the site (Acevedo 2003).

2.3.2 Natural accelerograms

The use of natural (or “recorded”) ground motions is the most common and preferable option for nonlinear response history analysis. Ground motion databases were scarce in the past, but in the recent years the number of recorded accelerograms has increased considerably owing to the (increasingly) large number of events that took place in well-instrumented countries. The limitation of using natural records is that they are consistent with a hazard scenario of a past event at a given site, and thus it is often difficult to find records consistent with the problem at hand, especially when considering the collapse of well-designed structures. The reason is that instrument recordings are relatively recent compared to the time-scale of earthquake occurrences. Therefore the ground motion databases contain primarily small-to-moderate records. Records of earthquakes with larger magnitudes at close distances are scarce thus posing an additional difficulty when a full-range assessment is sought. The common practice for circumventing this problem is to “scale” their amplitude in order to match, in terms of intensity, the corresponding hazard scenario that is often represented by a target acceleration spectrum over a range of periods.

Over the years, various methods that process ground motion databases in order to optimally select records and compile them in bins have been presented (Dussom *et al.* (1991), Ferritto (1992)). Such algorithms may seek records that either individually, or on average, match a target spectrum (REXEL Iervolino *et al.* (2009)). More elaborate procedures have been also presented. For example, Naeim *et al.* (2004) proposed an approach based on an optimization algorithm in order to select a set of ground motions that minimizes the difference of the mean spectrum of the selected ground motions from the target design spectrum. Also, Jayram *et al.* (2011) proposed a procedure that probabilistically generates multiple response spectra from a target distribution and then selects recorded ground motions whose spectra match the target spectrum. Recently, Katsanos and Sextos (2013) proposed an algorithm for selecting ground motion records accounting for the variability of critical response quantities while also considering the properties of the structure studied.

Another process for using natural ground motions to obtain records consistent with a given scenario is “spectrum matching”, i.e., the modification through signal processing of the natural records to reproduce a particular (typically the design) acceleration spectrum. There are numerous such methods and the quality of the results always depends on the specifics of the modification approach. For example, Abrahamson (1992) and Hancock and Bommer (2007) have proposed a wavelet-based algorithm to adjust recorded ground motions to match a specific target response spectrum. This algorithm is implemented in SeismoMatch (2013) software.

To sum up, the advantage of using natural accelerograms is that they are genuine records of shaking produced by earthquakes. Therefore, they carry all the ground-motion characteristics (amplitude, frequency and energy content, duration and phase characteristics), and reflect all the factors that influence accelerograms (characteristics of the source, path and site). The disadvantages of natural accelerograms are that not all M-*d*-soil combinations are covered, and the spectra are generally not smoothed.

2.4 Synthetic accelerograms

Some of the models and methods currently used for the simulation of seismic actions are discussed in Pinto (2001). Apart from natural ground motions, ground motion records can be also defined in the form of: (i) random processes, (ii) simulated accelerograms compatible with a design response spectrum, and (iii) synthetic accelerograms on the basis of a model of the earthquake source. This is an area of intensive research where many new methods and approaches are constantly emerging. Therefore, we explain some common methods used for simulating broadband and narrowband ground motions.

Random processes is a helpful tool for understanding the features of the maximum response of structures in the elastic range, while simulated records can be used to ensure consistency with the code requirements, since they are generated from a smooth design code-based response spectrum such as those obtained with the SIMQKE software (Gasparini (1976), Pinto (2004)). The major shortcoming of these two methods is simply that they do not produce real seismic records and therefore cannot be adopted for the performance-based assessment of a given structure and a given site subjected to large inelastic deformations, since, contrary to linear elastic analysis, the number of cycles and their amplitude is important in this case. Regarding artificial accelerograms, the problems encountered from their use are discussed in Naeim and Lew (1995). Apart from SIMQKE, SeismoArtif (Seismosoft (2013)) can be used to obtain artificial records.

Synthetic accelerograms can be obtained using various approaches. State-of-the-art derivations based on numerical models of the fault rapture and wave propagation from the source to the site have been developed. This approach is complex and includes intensive calculations, and therefore its application for engineering purposes is not recommended. However, there are regions (e.g. Los Angeles basin) for which physically sound synthetic records have been produced, e.g., Liu *et al.* (2007). Kinematic fault models are a more widely used option. Such models are based on the Green's function techniques, which follows the idea that the total motion is equal to the sum of the motions produced by a series of individual ruptures of many small patches on the causative fault (Kramer (1996)).Thus the fault is divided to a finite number of patches, while their sequential rupture is described by Green's functions. Such functions describe the time variation of the slip displacement of every patch. Typically all above processes have to be supplemented with an appropriate model of the soil effect so that the natural record is consistent with the local site soil conditions.

Another method for generating synthetic ground motions is based on the time-domain generation of transient stochastic processes. The idea is multiplying a stationary, filtered white noise signal with a function that describes the envelope of a ground motion. This multiplication transforms the stationary white noise to a non-stationary process. This concept has been adopted by Shinozuka and Deodatis (1998) and also lies in the core of ARMA models (AutoRegressive Moving Average models), e.g. (Chang *et al*. (1982)).

A rational and easy to implement procedure for producing synthetic records is the stochastic method (Boore (2003)). In this case, the generation is performed in the frequency-domain (as opposed to the time-domain discussed above), using the ground motion radiation spectrum $Y(M_w,R,f)$, which is the product of quantities that consider the effect of source, path, site and instrument (or type) of motion. One of the products of $Y(M_w,R,f)$ contains the earthquake source spectrum, modelled with the ω-square model (Aki (1968)) or the specific barrier model (Papageorgiou (1983a), Halldorson (2005)). The former is commonly used, but it is a point source model and hence not appropriate for near-fault problems, while it may also not be appropriate for large sources. Both problems are sufficiently handled by the specific barrier model.

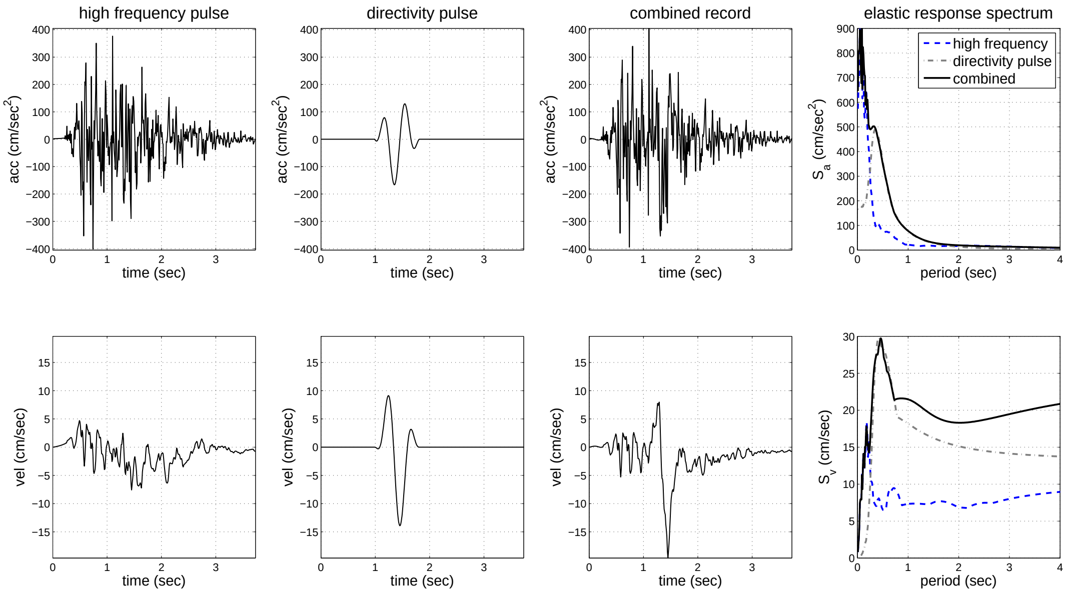

Figure 2.2. Generation of synthetic ground motion records. Upper row shows the acceleration and the bottom row the velocity time histories. The corresponding response spectra are shown at the further right column (Psycharis et al. 2013).

By separating the radiation spectrum $Y(M_w,R,f)$ to its contributing components, the models based on the stochastic method can be easily modified to account for different problem characteristics. The stochastic approach consists of first generating a white noise (Gaussian or uniform) for duration predicted by an appropriate ground motion prediction equation (GMPE). The noise is then windowed and transformed into the frequency domain using an envelope function $w(M_w,R,t)$ and subsequently transformed back into the time domain. The application of the stochastic method can be carried out with the aid of the SMSIM program (Boore (2003), Boore (1983), Boore (2005)) that is freely available from the web. An extension of SMSIM is EXSIM (Motazedian (2005)). EXSIM is able to consider information about the fault geometry and is appropriate for simulations of large earthquakes considering the sum of motions from subfaults distributed over a fault surface. The motions from each subfault are often given by SMSIM which is seen as a point-source simulation method. Boore in (Boore (2009)) compares the two programs and suggest simple modifications to SMSIM that render the two programs consistent (Fragiadakis *et al.* (2013)).

When near-fault ground motions are required, the procedure suggested by Mavroeides and Papageorgiou (2003) can be adopted in order to combine low frequency pulse models (Mavroeides and Papageorgiou (2003),Ricker (1944), Gabor (1946)) with high-frequency synthetic ground motion records. The procedure for combining low and high frequency components consists of first obtaining the Fourier transform of both the high- and the low-frequency components. Subsequently the Fourier amplitude of the pulse is subtracted from that of the high-frequency component of the ground motion and a synthetic acceleration time-history is constructed so that its Fourier amplitude is that of the previous step and its phase angle is that of the high-frequency record. The final synthetic record is obtained by adding the pulse time-history. The outcome of this procedure is shown schematically in

Figure 2.3, where the last column shows the corresponding acceleration and velocity response spectra. The velocity spectrum (bottom right figure) shows the impact of the directivity pulse, while looking at the third column, the effect of the pulse is clearly visible in the combined velocity time-history but difficult to discern when looking at the acceleration time-history (Fragiadakis *et al.* (2013)).

Iervolino *et al.* (2010) compared different procedures for obtaining sets of spectrum-matching accelerograms for nonlinear dynamic analysis of structures in terms of inelastic seismic response. The results of the analysis show that artificial, or adjusted, accelerograms may underestimate the displacement response when compared to original real records. The more recent work of Galasso *et al*. (2013) also compared response estimations obtained with natural and synthetic records and suggest that, apart from some exceptions (e.g. short periods), synthetic ground motions are able to sufficiently match recorded ground motions.

The intention of the discussion above is to outline some major approaches for generating ground motions records and is by no means exhaustive. Other approaches or variations/improvements of the above can be found in the literature. Moreover, various software are available for generating ground motions, each following a different approach. For example, some of the methods referenced above are available in the open source Broadband Platform software (BBP) (Southern California Earthquake Center 2013), and also in SeismoArtif (Seismosoft (2013)).

2.5 Artificial accelerograms

Except from natural and synthetic records another category is used: artificial records. Artificial records are usually generated to match a target response spectrum. This method leads to unrealistic high numbers of cycle of motion; thus, the artificial records should be used with caution.

Artificial accelerograms are generated to match a target response spectrum. Amongst the methods available is the SIMQKE program of Gasparini & Vanmarcke (1976). The use of these methods tend to generate artificial records that do not have the appearance of real earthquake accelerograms, with unrealistically high numbers of cycles of motion. This is due to the fact that the code spectrum is a uniform hazard spectrum (UHS), which is an envelope of the spectra corresponding to earthquakes in different seismic sources and the conservative scenario of earthquakes occurring in different seismic sources simultaneously is implicitly taken into account. The artificial records are problematic because they have to match the smooth code spectrum at all response periods. Additionally, in order to get other characteristics of artificial spectrum compatible record, such as duration, it is necessary to obtain supplementary information about the expected earthquake motion apart from the response spectrum.

2.6 Measures of ground motion intensity

Each of the following ground motion parameters can be considered as intensity measures within the plane of cloud analysis, or incremental dynamic analysis. Therefore we present some of them in the following sections.

2.6.1 Peak ground motion parameters

One of the parameters most widely associated with the severity of the ground motion is the PGA, which is obtained directly from the recorded data; it is the maximum absolute value of acceleration in a time-history. PGA is generally recognized as a poor parameter for characterizing the damage potential. Both a short-duration impulse of low-frequency may have the same peak ground acceleration value, producing very different response in structures.

Two other parameters also obtained directly from integration of the recorded data are the peak ground velocity (PGV) and the peak ground displacement (PGD). However, the integrated motions, especially the displacements, are highly sensitive to the processing applied to remove the digitization noise from the record, which tends to dilute high-frequency components of the motion and enhance low-frequency components. The reported values of velocity and displacements must always be interpreted with some caution, particularly the latter.

2.6.2 Arias Intensity

Arias intensity, AI, is a ground motion parameter that has been used to evaluate damage potential. It is defined as:

$$AI = \frac{\pi}{2g}\int_0^T a^2(t)dt \qquad (2.1)$$

Where a(t) is the acceleration time history of total duration T. The energy in the accelerogram can be quantified by the Arias intensity (Arias, 1969).

A Husid plot is a graph of the build-up of AI with time. It shows both the total amount of energy carried by the shaking and the rate at which it is imparted to structures. The rate of energy input over any interval t_1 to t_2 is related to another parameter called the root-mean-square acceleration, α_{rms}:

$$a_{rms}^2 = \frac{1}{(t_2 - t_1)^2} \int_{t_1}^{t_2} a^2(t)dt \qquad (2.2)$$

The level of damage produced by a ground motion will depend on both the total amount of energy and on the rate at which this energy is carried (Bommer, 2001).

2.6.3 Root-mean-square (RMS) acceleration

Another ground motion parameter that has been used to estimate the damage potential is the integral of the squared ground acceleration, which is a measure of the energy input capacity of the ground motion. Nevertheless, a strong short-duration ground motion could have the same RMS acceleration value than a weaker ground shaking of a very long duration.

α_{rms} is defined in equation 2.2, where t_2 -t_1 denotes the significant duration and α denotes the ground acceleration. For the significant duration defined by Trifunac and Brady (1975) t_2-t_1 corresponds to $t_{95} – t_5$.

2.6.4 Duration

The duration of the ground motion is related to the time required for rupture to spread across the fault surface, which is a function of the seismic moment or the magnitude. There is a wide number of duration measures commonly used. The value of the duration differs according to the measure used.

All the duration definitions can be grouped into three categories: bracketed, uniform and significant durations (Bommer and Martinez-Pereira, 1999). The most common measure is the bracketed duration, D_b, which is defined as the time between the first and the last exceedance of a defined threshold level of acceleration (usually 0.05g). The uniform duration, D_u, is defined as the sum of the intervals during which the acceleration exceeds a threshold level. Another measure is the significant duration, defined as the time interval across which a specified amount of energy in the accelerogram is distributed. A common measure of significant duration, D_s, is the duration defined by Trifunac and Brady (1975), related to the interval between 5% and 95% of AI. The time interval between 5% and 75% of AI is also commonly used.

2.6.5 Measures extracted from the response spectra

The response spectrum is the most important characterization of the seismic ground-motion in earthquake engineering. This parameter is obtained by passing the recorded data through a single-degree-of-freedom (SDOF) oscillator.

Acceleration response spectral ordinates represent the period-dependent peak acceleration response of SDOF elastic structure with a specified level of equivalent viscous damping. Acceleration response spectra are widely used in structural engineering, as the product of the spectral ordinate at the building period and the structural mass can be used to approximate the base shear in elastic structures. A limitation of response spectral ordinates is that they do not provide information on the duration of strong shaking.

2.6.6 Spectrum Intensity (SI)

The spectrum intensity, SI, is a measure of the intensity of shaking of an earthquake at a given site. The Housner spectrum intensity, SI, is defined as:

$$SI = \int_{0.1}^{2.5} SV(T,\xi)dT \qquad (2.3)$$

Where SV is the velocity spectrum curve and ξ is the damping coefficient. The limits of the integral were chosen by Housner because they include a range of typical periods of vibration of urban buildings.

2.6.7 Iv index

Fajfar et al. (1990) proposed a new intensity parameter for structures with fundamental periods in the medium-period range. This parameter, I_V, is defined as:

$$I_v = PGV \cdot D_S^{0.25} \tag{2.4}$$

where D_s is the significant duration defined by Trifunac and Brady (1975). The medium-period range is the region where the smoothed pseudo-velocity spectrum has its maximum values. This region has a lower and upper bound that varies for different ground motions and depend on the magnitude of the earthquake, the distance from the epicenter, and on the local soil condition (Acevedo 2003).

2.6.8 Characteristic intensity

The characteristic intensity is defined as:

$$I_c = a_{rms}^{1.5} T_d^{0.5} \tag{2.5}$$

Is related linearly to an index of structural damage due to maximum deformations and absorbed hysteretic energy (Ang (1990), Acevedo (2003)).

2.6.9 Cumulative absolute velocity

The cumulative absolute velocity is simply the area under the absolute accelerogram:

$$CAV = \int_0^{T_d} |a(t)|\, dt \tag{2.6}$$

The cumulative absolute velocity has been found to correlate well with structural damage potential. For example, a CAV of 0.3g-sec (obtained after filtering out frequencies above 10 Hz) corresponds to the lower limit for MMI VII shaking (Acevedo (2003)).

2.7 <u>Spectral acceleration.</u>

The concern of earth scientists with spectral acceleration is to predict the distribution of spectral acceleration at a site, given an earthquake with a particular magnitude, distance, faulting style, local soil classification, etc. This provision takes the form of an attenuation model. Many empirical attenuation models were developed using the analysis of recorded ground motions (see Abrahamson and Silva 1997, Boore et al.1997, Campbell 1997, Sadigh et al. 1997, and Spudich et al. 1999, among many others). This recorded data are scattered (due to path effects, variation in stress drop, and other factors that are not captured by the attenuation model), which must be dealt during development of the attenuation model.

The observed variability in spectral acceleration is well represented by a lognormal distribution (Abrahamson 2000). Thus, attenuation models work with the mean and standard deviation of the logarithm of *Sa*, which can be represented by a Gaussian distribution. The broad variability of the distribution hinders estimation of the mean value of ln*Sa* needed for the attenuation law. The log *Sa*'s of two perpendicular components of the ground motion are thus averaged, reducing the variance and allowing the mean value of ln*Sa* to be estimated with greater confidence. For example, it is seen that arbitrary-component spectra vary more about the estimated mean than their geometric mean does.

The exponential of the mean of the logarithms of two numbers is termed the "geometric mean" because it is the square root of their product. For conciseness, we will refer to the geometric mean of spectral acceleration of two components as $Sa_{g.m.}$, and the spectral acceleration of an arbitrary component will be referred to as Sa_{arb}. The logarithms of these values will be referred to as $\ln Sa_{g.m.}$ and $\ln Sa_{arb}$, respectively. The standard deviation of the mean of 2 uncorrelated random variables with common standard deviation (is equal to $\sigma/\sqrt{2}$).Calculating the standard deviation of $\ln Sa_{arb}$ thus takes an additional step of going back to the non-averaged data and examining the standard deviation there. Some researchers (e.g., Boore et al. 1997, Spudich et al. 1999) have taken this step, but many others have not because it was not recognized as important. However, the difference in standard deviations is in fact relevant for ground motion hazard analysis.

Structural engineers also utilize spectral acceleration as a basis for analysis of structural response. Let us first consider analysis of a single two-dimensional frame of a structure—a common situation in practice. In this case, only a single horizontal component of earthquake ground motion is needed for analysis. Therefore, spectral acceleration is computed only for the selected component at a period equal to the elastic first mode period of the structure, and that is used as the intensity measure. In most cases, no distinction is made between the two components of a ground motion, so using a single component in this case is equivalent to using Sa_{arb} as the intensity measure. To compute $Sa_{g.m}$. using both horizontal components of the ground motion, but then use only one of the components, the stronger or the weaker, for analysis would only introduce unnecessary scatter into the relationship between the IM and structural response. Prediction of response of a structure is made using both Sa_{arb} and $Sa_{g.m}$. to a model of an older seven-story reinforced concrete frame, described by Jalayer (2003) in previous papers. The larger dispersion implies that there is greater uncertainty in the estimate of median response (i.e., if $Sa_{g.m}$. is used as the IM, a greater number of analyses would need to be performed to achieve the same confidence in the mean ln). Thus the use of Sa_{arb} as the IM is preferable for the structural engineer in order to minimize the number of nonlinear dynamic analyses performed.

Many examples of the use of *Sa* as an intensity measure exist in the literature. For example, modal analysis (Chopra 2001), the SAC/FEMA methodology (SAC 2000a, b, c), and incremental dynamic analysis (Vamvatsikos and Cornell 2002) all use *Sa* as a predictor of structural response in some cases. In virtually every application of these procedures, Sa_{arb} (or $Sa_{g.m}$. which is used in FEMA P695 and several recent publications) is used as the intensity measure for analysis of a single frame of a structure.

Calculation of the risk to a structure from future earthquakes requires assessment of both the probability of occurrence of future earthquakes (hazard) and the resulting response of the structure due to earthquakes (response). The analysis of hazard is typically performed by earth scientists (e.g., seismologists or geotechnical engineering scientists), while the analysis of response is typically performed by structural engineers. The results from these two specialists must then be combined, and this is often done by utilizing an intensity measure (IM) (Banon et al. 2001, Cornell et al. 2002, Moehle and Deierlein 2004). Earth scientists provide the probability of occurrence of varying levels of the IM (through hazard maps or site-specific analysis), and structural engineers estimate the effect of an earthquake with given levels of the IM (using dynamic analysis or by associating the IM with the forces or displacements applied in a static analysis).

Spectral acceleration, *Sa*, is the most commonly used intensity measure in practice today for analysis of buildings. This value represents the maximum acceleration that a ground motion will cause in a linear oscillator with a specified natural period and damping level. In fact, the true measure is pseudospectral acceleration, which is equal to spectral displacement times the square of the natural frequency, but the difference is often negligible and the name is often shortened to simply "spectral acceleration." But *Sa* is often defined differently by earth scientists and structural engineers. The difference originates from the fact that earthquake ground motions at a point occur in more than one direction. While structural engineers often use the *Sa* caused by a ground motion along a single axis in the horizontal plane, earth scientists often compute *Sa* for two perpendicular horizontal components of a ground motion, and then work with the geometric mean of the *Sa*'s of the two components. Both definitions of *Sa* are valid. However, the difference in definitions is often not recognized when the two pieces are linked, because both are called "spectral acceleration." Failure to use a common definition may introduce an error in the results.

Although intensity measure–based analysis procedures have proven to be useful methods for linking the analyses of earth scientists and structural engineers, care is needed to make sure that the link does not introduce errors into the analysis. Two definitions of "spectral acceleration" are commonly used by analysts, and the distinction between the definitions is not always made clear. Because of this, a systematic error has been introduced into the results from many risk analyses, typically resulting in unconservative conclusions.

This problem is, however, merely one of communication, and not a fundamental flaw with the intensity measure approach. It is not difficult to use intensity measures in ways that produce correct results. For analysis of a single frame of a structure, there are three paths to the correct answer: 1. Use Sa_{arb} for both parts of the analysis; 2. Use $Sa_{g.m}$. for both parts of the analysis; and 3. perform hazard analysis with $Sa_{g.m}$., and structural response analysis with $Sa_{g.m}$ directly (even in 2D). No reason to go to Sa_{arb}. If a three-dimensional model of a structure is to be analyzed, the most straightforward method is to use $Sa_{g.m}$. as the intensity measure for both the ground motion hazard and the structural response. In the absence of a single standard procedure, both earth scientists and structural analysts are encouraged to explicitly state which *Sa* definition they are using for evaluation, in the interest of transparency.

The methods described above will all produce valid estimates of the annual frequency of exceeding a given structural response level. In the future it would be desirable to have attenuation models that estimate the dispersion of both $Sa_{g.m}$. and Sa_{arb}, in order to allow flexibility in the definition of the spectral acceleration used for analysis. Finally, vector-based methods of hazard and response analysis should improve upon the current situation.

2.8 Conclusions

This chapter includes the theory needed for the seismic loading of structures. It begins with a general reference in the history of loading, then lists the intensity measures and closes with the different interpretations that is given by earth scientists and engineers in the first mode spectral acceleration ($Sa(T_1,5\%)$). Also, the seismic hazard curve of spectral acceleration is presented. The seismic records are presented and the three types of accelerograms considered in practice are: natural, synthetic and artificial. Emphasis is given in the natural records because they are the most representative of strong ground motion. Furthermore, a limited strong motion database makes it difficult to find natural unscaled earthquakes at the desired intensity level when it is studied near collapse. Results show that the use of synthetic records covers the insufficiency of natural accelerograms in high intensities. Finally, the intensity measures are presented distinguishing the first-mode spectral acceleration, which is usually used as the main intensity measure when the structure experiences seismic loading.

2.9 References

Abrahamson, N.A. (1992). “Non-stationary spectral matching”, Seismological Research Letters, 63(1), 30

Abrahamson, N. A., and W. J. Silva (1997), Empirical Response Spectral Attenuation Relations for Shallow Crustal Earthquakes, Seismological Research Letters, 68(1), 94-127.

Abrahamson, N.A. (2000). “Effects of rupture directivity on probabilistic seismic hazard analysis”, Proc. 6th Int. Conf. on Seismic Zonation, Palm Springs, California.

Acevedo, A.B. (2003). “Seismological criteria for selecting and scaling real accelerograms for use in engineering analysis and design”, PhD dissertation submitted in Rose school, European school of advanced studies in Reduction of seismic risk Rose school.

Ang, A.H.S. (1990). “Reliability bases for seismic safety assessment and design”, Proceedings, Fourth U.S. National Conference on Earthquake Engineering, Earthquake Engineering Research institute, Palm Springs, 1: 29-45.

Arias, A. (1969). “A measure of earthquake intensity”, In Hansen, R. J. (ed.), Seismic Design of Nuclear Reactors, MIT Press, 438-483.

Aschheim, M., Tjhin, T., Comartin, C., Hamburger, R., Inel, M. (2007). “The scaled nonlinear dynamic procedure”, Engineering Structures, 29(7): 1422-1441.

Baker, J.W., Cornell C.A. (2006). “Vector-Valued Ground Motion Intensity Measures for Probabilistic Seismic Demand Analysis”, John A. Blume Earthquake Engineering Center. Report No. 150 Report#150, Stanford, CA.

Banon, H., Cornell, C.A., Crouse, C. B., Marshall, P., Nadim, F., and Younan, A., (2001). “Seismic design guidelines for offshore platforms”, Proceedings, 20th OMAE, OMAE 2001/ S&R-2114, Rio de Janeiro.

Bommer, J. J. and Martinez-Pereira A. (1999). "The effective duration of earthquake strong motion", Journal of Earthquake Engineering. 3: 127-172.

Bommer, J.J. and C. Ruggeri (2002) "The specification of acceleration time-histories in seismic design codes," European Earthquake Engineering. 1, 3-17.

Bommer, J.J., Scott, S.G., Sarma, S.K. (2000). "Hazard Consistent Earthquake Scenarios", Soil Dynamics and Earthquake Engineering 19: 219-231.

Boore, D. M., Joyner, W. B., and Fumal, (1997). "Equations for estimating horizontal response spectra and peak acceleration from western North American earthquakes: A summary of recent work", Seismol. Res. Lett. 68, 128–153.

Boore, D.M. (2003a). "Simulation of ground motion using the stochastic method", Pure and Applied Geophysics, 160: 635-676.

Boore, D.M. (1983). "Stochastic simulation of high-frequency ground motions based on seismological models of the radiated spectra", Bulletin of the Seismological Society of America, 79: 1865–1894.

Boore, D.M. (2005). "SMSIM-Fortran Programs for Simulating Ground Motions from Earthquakes: Version 2.3—A Revision of OFR 96-80", A U.S. Geol. Surv. Open-File Report 00-509.

Boore, D.M. (2009). "Comparing stochastic point-source and finite-source ground-motion simulations: SMSIM and EXSIM", Bulletin of the Seismological Society of America, 99: 3202-3216.

Campbell, K.W. (1997). "Empirical near-source attenuation relationships for horizontal and vertical components of peak ground acceleration, peak ground velocity, and pseudo-absolute acceleration response spectra", Seismological Research Letters, 68(1): 154 -179.

Chang, M., Kwiatowski, H., Nau, R., Oliver, R., Pister, K. (1982). "ARMA models for earthquake ground motions", Earthquake Engineering and Structural Dynamics, 10: 651-662.

Chopra K.A., (2012) "Dynamics of Structures: Theory and Applications to Earthquake Engineering, 4th Edition", Prentice Hall, Englewood Cliffs, New Jersey.

Cornell, C.A., Jalayer, F., Hamburger, R. O., and Foutch, D. A., 2002. Probabilistic basis for 2000 SAC federal emergency management agency steel moment frame guidelines, J. Struct. Eng. 128 (4), 526–533.

Dussom, K.B., Hadj-Hamou, T., Bakeer, R. (1991). “QUAKE: An expert system for the selection of design earthquake accelerogram” ,Computers and Structures 40(1): 161-167.

EN 1998-1:2003 (2003). “Eurocode 8: Design of structures for earthquake resistance. Part 1: General rules, seismic actions and rules for buildings”, Commission of the European Communities, European Committee for Standardization, October

FEMA-440 (2005): Improvement of Nonlinear Static Seismic Analysis Procedures. Federal Emergency Management Agency: Washington, DC.

Ferritto, J.M. (1992). “Optimized earthquake time history and response spectra”, User’s guide, Report UG-0025, Naval Civil Engineering Laboratory, Port Hueme, California.

Fragiadakis M., Vamvatsikos D., Karlaftis M., Lagaros N., Papadrakakis M. (2014). “Seismic assessment of structures and lifelines”, Journal of Sound and Vibration, http://dx.doi.org/10.1016/j.jsv.2013.12.031.

Gabor, D. (1946). “Theory of communication. I. The analysis of information”, IEEE 93: 429–441.

Galasso, C., Zhong, P., Zareian, F., Iervolino, I., Graves, R.W. (2013). “Validation of ground-motion simulations for historical events using MDOF systems”, Earthquake Engineering and Structural Dynamics, 42(9): 1395-1412.

Gasparini D.A. and Vanmarcke E.H. (1976). “Simulated earthquake motions compatible with prescribed response spectra”, Dept. of Civil Engineering, Research Report R76-4, Massachusetts Institute of technology.

Halldorsson, B., Papageorgiou, A.S. (2005). “Calibration of the specific barrier model to earthquake of different tectonic regions”, Bulletin of the Seismological Society of America, 95(4): 1276-1300.

Hancock, J., Bommer, J.J. (2007). “Using spectral matched records to explore the influence of strong-motion duration on inelastic structural response”, Soil Dynamics and Earthquake Engineering, 27: 291-299.

Iervolino, I. Galasso, C. , Cosenza E. (2009). “REXEL: computer aided record selection for code-based seismic structural analysis”, Bulletin of Earthquake Engineering, 8: 339-362.

Iervolino, I., De Luca F., Cosenza, E. (2010). “Spectral shape-based assessment of SDOF nonlinear response to real, adjusted and artificial accelerograms”, Engineering Structures, 32(9): 2776-2792.

Jayram, N., Lin, T. Baker, J.W. (2011). “A computationally efficient ground-motion selection algorithm for matching a target response spectrum mean and variance”, Earthquake Spectra 27(3): 797-815.

Jennings, J.E. (1985). “Ground motion parameters that influence structural damage” in Scholl R.E. and King J.L. eds. Strong Ground motion simulation and Engineering Applications, EERI publications 85-02, Earthquake Engineering Research Institute, Berkeley, California.

Joyner W.B., Boore D.M. (1988). “Measurement, characterization and prediction of strong ground motion” in Earthquake Engineering and Soil Dynamics II – Recent Advances in Ground Motion Evaluation, Geotechnical Special Publication 20, ASCE, New York, 43-102.

Katsanos, E.I., Sextos, A.G. (2013). “ISSARS: An integrated software environment for structure-specific earthquake ground motion selection”, Advances in Engineering Software doi: 10.1016/j.advengsoft.2013.01.003.

Katsanos, E.I., Sextos, A.G., Manolis, G.D. (2010). “Selection of Earthquake Ground Motion Records: a State-of-the-art review from a structural engineering perspective”, Soil Dynamics and Earthquake Engineering, 30(4): 157-169.

Kottke, A. Rathje, E.M. (2008). “A semi-automated procedure for selecting and scaling recorded earthquake motions for dynamic analysis”, Earthquake Spectra, 24(4): 911-932.

Kramer, S. L. (1996) “Geotechnical Earthquake Engineering”. Prentice Hall.

Liu, P.C., Archuleta, R.J., Hartzell, S.H. (2007). “Prediction of broadband ground motion time histories: Hybrid low/high-frequency method with correlated random source parameters” Bull. Seismol. Soc. Am. 96: 2118–2130.

Luco, N. and Bazzurro, P. (2007). “Does amplitude scaling of ground motion records result in biased nonlinear structural drift responses?” Earthquake Engineering and Structural Dynamics, 36(13): 1813-1835.

Maniatakis, Ch.A., Spyrakos, C.C, A new methodology for elastic displacement spectra determination in the near-fault region, Soil Dynamics and Earthquake Engineering, Vol. 35, pp. 41-58 (2012).

Martinez-Rueda, J.E. (1998). “Scaling procedure for natural accelerograms based on a system of spectrum intensity scales”, Earthquake Spectra, 14(1): 135-152.

Mavroeidis, G.P., Papageorgiou, A.S. (2003). “A Mathematical Representation of Near-Fault Ground Motions”, Bulletin of the Seismological Society of America, 93(3): 1099–1131.

Moehle, J. & Deierlein, G. (2004). “A framework methodology for performance-based earthquake engineering.” In International Workshop on Performance-Based Engineering, Bled, Slovenia.

Motazedian, D., Atkinson, G.M. (2005). “Stochastic finite-fault modeling based on a dynamic corner frequency”, Bulletin of the Seismological Society of America, 95: 995–1010.

Naeim, F., Lew, M. (1995). “On the use of design spectrum compatible time histories”, Earthquake Spectra, 11: 111-127.

Naeim, F., Alimoradi, A., Pezeshk, S. (2004). “Selection and scaling of ground motion time histories for structural design using genetic algorithms” Earthquake Spectra, 20: 413–426.

Nau, J.M. and Hall W.J. (1984). “Scaling methods for earthquake response spectra” Journal of Structural Engineering, 110: 1533-1548.

Papageorgiou, A.S., Aki. K. (1983a). “A specific barrier model for the quantitative description of inhomogeneous faulting and the prediction of strong ground motion, part I: description of the model.”, Bulletin of the Seismological Society of America, 73: 693–722.

Pinto, P.E. (2001). “Reliability methods in earthquake engineering.” Prog. Struct. Eng. Mater, 3: 76–85.

Pinto, P.E., Giannini, R., Franchin, P. (2004). “Seismic Reliability Analysis of Structures”, IUSS, Pavia.

Ricker, N. (1944). “Wavelet functions and their polynomials”, Geophysics, 9: 314-323.

Sadigh, K., C. -Y. Chang, J. A. Egan, F. Makdisi, and R. R. Youngs (1997), “Attenuation relationships for shallow crustal earthquakes based on California strong motion data”, Seismological Research Letters, 68(1), 180-189.

Seismosoft, SeismoArtif. (2013). “A computer program for generating artificial earthquake accelerograms”.

Shinozuka, M., Deodatis, G. (1988). “Stochastic process models for earthquake ground motion” Journal of Probabilistic Engineering Mechanics 3(3): 187-221.

Shome, N., Cornell, C.A., Bazzurro, P., Carballo, J.E. (1998). “Earthquakes, records, and nonlinear MDOF responses.” Earthquake Spectra, 14(3), 469–500.

Spudich, P., W. B. Joyner, A. G. Lindh, D. M. Boore, B. M. Margaris, and J. B. Fletcher (1999), “SEA99: A revised ground motion prediction relation for use in extensional tectonic regimes”, Bulletin of the Seismological Society of America, 89(1), 1156-1170.

Spyrakos CC, Maniatakis Ch.A., Taflambas J, Evaluation of near-source seismic records based on damage potential parameters. Case study: Greece, Journal of Soil Dynamics and Earthquake Engineering. Volume 28, Issue 9, September 2008, Pages 738-753.

Trifunac, M. D. and A.G. Brady. (1975). “A study on the duration of strong earthquake ground motion”, Bull. Seis. Soc. Am.65: 581-626.

Vamvatsikos, D., Cornell, C.A. (2002). “Incremental dynamic analysis”, Earthquake Engineering and Structural Dynamics, 31(3): 491–514.

Watson-Lamprey, J., Abrahamson, N. (2006). “Selection of ground motion time series and limits on scaling”, Soil Dynamics and Earthquake Engineering, 26(5): 477-482.

CHAPTER 3

Seismic performance assessment methods

3.1 Introduction

In this chapter performance assessment methods are presented. These methods lead to a capacity curve that can be measured within the frameworks of performance-based design (PBD). The aim of this chapter is to present the frameworks of contemporary methods of analysis for the determination of the capacity of a structure that is subjected to seismic actions. Emphasis is given in the non-linear performance assessment methods which can predict more accurately the performance of a structure. The last years these assessment methods are widely used for the performance of existing buildings. Thus, for building new structures their application is usually based on the trial and error technique. In the chapters to follow the application of the performance analysis procedures for the design of new structures of steel will be presented with the aid of a genetic algorithm for achieving optimized designs.

The contemporary methods of analysis have as a target the design which is performance-based. The response of the structure is checked for several performance levels with the use of static or dynamic methods of analysis. In the chapters to follow emphasis is given to nonlinear methods of analysis which permit to determine directly the response without the mediation of simplified assumptions that lead to conservative solutions. For example, if during the analysis care is taken for second order effects then the checks for ultimate limit states are not based on the reduced axial strength which result from the buckling curves of EC3 (1993). The design checks based on which engineers can decide whether the response of the structure is satisfying, differ according to the method of analysis chosen. The checks of the Eurocode which are based on linear methods of analysis examine every design from the allowable maximum strength perspective. The nonlinear methods of analysis use checks that are based on inelastic structural response.

3.2 Performance-based earthquake engineering

Extensive damages which were observed in relatively recent earthquakes in Japan and in the USA led the engineers rethink the adequacy of current modern seismic regulations. Even though the number of human lives that were lost was relatively small, the economic cost was very substantial. Given that the primary target of today's antiseismic regulation is the protection of human life, this leads to the conclusion that other targets should be considered for the design of structures. In order to improve the regulations to this direction the performance-based design concept is introduced.

The performance-based design is presented in various guidelines that have been issued mostly in the United States (e.g., FEMA-356 (2000), Vision (2000), ATC-40 (1996)), while for Greece in draft form is the new Greek Code of Structural Interventions (G.C.S.I) (2002). These instructions exhibit differences in their details but in essence they adopt the same concepts (Krawinkler (1999)).The aim of the regulations is to formulate a framework where the assessment and capability of new buildings, or buildings that have already been constructed, for every level of seismic loading, is achievable. Performance-based design permits the structures to be designed so that they have a reliable and quantifying behavior for several levels of seismic intensity. In this way, several performance levels are defined corresponding to the respective limit states adopted in Eurocode 8 (EC8) (1992), where for every limit state the maximum extent of allowable damage is defined. Thus the engineer, or the owner of the structure, can have the choice to select the desirable behavior of the building for every performance level.

Eurocode 8 (1992), as other contemporary antiseismic regulations, takes onto consideration two performance levels: the ultimate limit state and the serviceability limit state. In essence it is a simplified form of performance-based design. Generally, performance-based design refers to the control of the full range of response i.e. for each level of seismic intensity. Since this is in practice not possible to take place, the usual practice is the selection of some discrete levels of performance. For example FEMA-356 (2000) suggests three performance levels: operational performance level, life safety performance level, collapse prevention performance level. For ordinary engineering structures the life safety performance level corresponds to serviceability limit states. There is also a correspondence between some of the performance level of FEMA-356 and limit states of Eurocode 8. Figure 3.3 shows that a performance level may correspond to different seismic intensity levels depending on the importance of the structure. Note that the seismic intensity is defined as a function of the probability of exceedance of the design earthquake during the lifetime of the structure which is usually taken equal to 50 years.

Most of the current seismic design codes belong to the category of limit-state design procedures (or prescriptive design procedures), where a number of checks, expressed in terms of force (most frequently) and deformation limits, should be satisfied in order for the structure to be considered safe, since it fulfils the safety criterion against collapse. A typical limit-state based design implements either the ultimate strength (one limit-state approach) or a two limit-state approaches (i.e., serviceability and ultimate strength). Existing seismic design procedures are based on the principle that a structure will avoid collapse if it is designed to absorb and dissipate the kinetic energy that is induced in it during a seismic excitation. Most modern seismic norms express the ability of the structure to absorb energy through inelastic deformation by using a reduction on the applied loads, expressed by the behavior factor, that depends on the material and the structural system used (Mitropoulou (2011)).

The frameworks of antiseismic performance-based design (FEMA-356 (2000)) distinguish the capacity and the demand. With the term “demand” is meant the imposed displacements (or alternatively, deformations, curvatures, member rotations and interstorey drifts) due to seismic loading. The term “capacity” corresponds to the maximum displacement (or alternatively deformations, curvatures, interstorey drifts) that a structure, a member or a section can sustain.

Performance-based design has the following distinct features with respect to the prescriptive design codes: (i) allows the structural engineer to choose both the appropriate level of seismic hazard and the corresponding performance level of the structure, (ii) the structure is designed to meet a series of combinations of hazard levels in conjunction with corresponding performance levels. The PBD process implemented in this dissertation is a displacement-based procedure where the design criteria and the capacity demand comparisons are expressed in terms of displacements rather than forces (Priestley *et al.* (2007)).

Performance-Based Earthquake Engineering (PBEE) implies the design, evaluation, construction and maintenance of engineering facilities in order to meet the objectives set by the society and the owners/users of the facility (Krawinkler and Miranda (2004)). In the case of earthquakes, the aim is to make structures having a predictable and reliable performance, or in other words, they should be able to resist earthquakes with quantifiable confidence. Therefore, the modern conceptual approach of seismic structural design is that the structures should meet performance-based objectives for a number of different hazard levels ranging from earthquakes with a small intensity and with a small return period, to more destructive events with large return periods. The current state of practice in performance-based earthquake engineering is defined by the US guidelines [ATC-40, 1996; ASCE-41, 2006; ASCE-41, 2013]. These guidelines do not differ conceptually and introduce procedures that can be considered as the first significant diversification from prescriptive building design codes. Many of the current codes for the design of new buildings are only partially performance-based, since they attempt to tie all design criteria to one performance level, usually to that of life safety or collapse prevention.

In nonlinear structural analysis procedures it is essential to formulate structural models that incorporate all the essential characteristics of the problem to be examined and can estimate the demand within acceptable accuracy. In order to evaluate the demand, appropriate EDPs are necessary. As an EDP any response variable can be used, such as stress resultants, displacements, chord rotations, among others. According to ASCE-41 the actions can be either force or deformation-controlled depending on the capacity of the members to deform inelastically. The capacity of deformation-controlled actions should be assessed using an appropriate EDP. EDPs may be interstorey drifts, inelastic deformations, section curvatures, floor accelerations and velocities, etc (Fragiadakis and Papadrakakis (2008), Mitropoulou *et al.* (2010)). The main concern in a performance-based seismic design procedure is the definition of performance objectives that will be used. Throughout this study the EDP used is the maximum interstorey drift, θ_{max} (Figure 2).

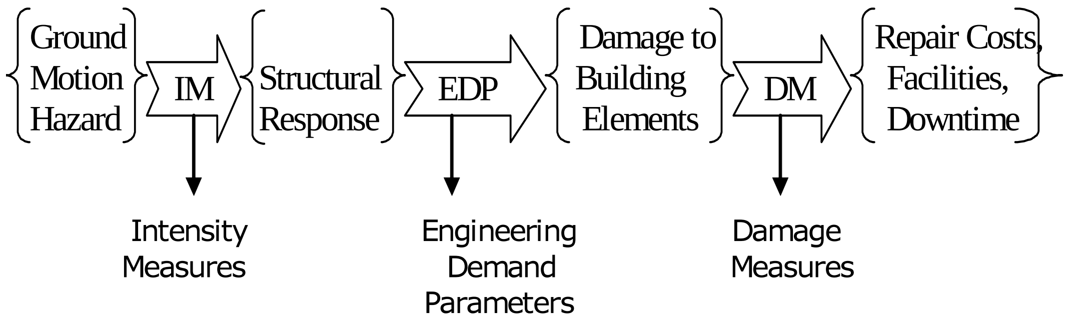

Figure 3.1. Schematic illustration of performance-based earthquake engineering Model and pinch points IM(Intensity Measures), EDP(Engineering Demand Parameters), and DM(Damage Measures). (Baker J.W and Cornell C.A. (2006)).

A performance objective is defined as the combination of a performance level for a specific hazard level. The first step in the definition of the performance objectives is the selection of the performance levels. The implemented performance levels are the following:

1. Operational: the overall damage level is characterized as very light. No permanent drift is encountered, while the structure essentially retains original strength and stiffness.

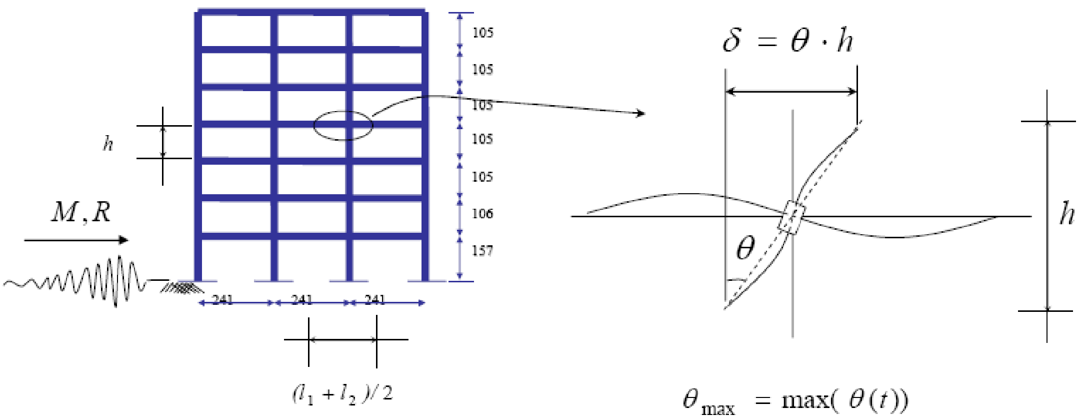

Figure 3.2: Structural response parameter maximum interstorey drift, θ_{max}.

2. Life safety: the overall damage level is characterized as moderate. Permanent drift is encountered while strength and stiffness reserves are encountered in all stories. Gravity-load bearing elements continue to function while there is no out-of plane failure of the walls. The overall risk of life-threatening injury as a result of structural damage is expected to be low. It should be possible to repair the structure; however, for economic reasons this may not be practical.
3. Collapse prevention: the overall damage level is characterized as severe. Substantial damage has occurred to the structure, including significant degradation in the stiffness and strength of the lateral-force resisting system. Large permanent lateral deformation of the structure and degradation in vertical-load bearing capacity is encountered. However, all significant components of the gravity load-resisting system continue to carry their gravity load demands. The structure may not be technically practical to be repaired and is not safe for reoccupancy, since aftershock activity could induce collapse.

The second step in the definition of the performance objectives is to determine the earthquake hazard levels. The structural design provisions of the building codes directly address earthquake hazards. Ground shaking hazards are typically characterized by a hazard curve, which indicates the probability that a given value of ground motion parameter, for example peak ground acceleration, will be exceeded over a certain period of time. The ground shaking hazard levels that have been considered are the following:

i. Occasional earthquake hazard level: with probability of exceedance 50% in 50 years with mean return period 72 years.
ii. Rare earthquake hazard level: with probability of exceedance 10% in 50 years with a mean return period 475 years.
iii. Maximum considered Event earthquake hazard level: with probability of exceedance 2% in 50 years with a mean return period 2475 years. (Not always defined like this. Definition will change depending on the document).

The combination of one performance level with an earthquake hazard level results in a performance objective. Figure 3.3 depicts the performance objectives for three classes of facilities. (i) For Standard Occupancy Facilities three performance objectives are defined (ii) For Emergency Response Facilities two performance objectives are defined (iii) For Safety Critical Facilities one performance objective is performed. It can be seen that the PBD step is performed as soon as the structure has satisfied the serviceability limit-state checks. In the current study the performance objectives for the standard occupancy buildings are employed.

3.3 Linear static analysis

The linear static analysis method as it is described within FEMA-356 corresponds to the simplified spectrum method of EC8. Based on this method of analysis, the seismic base shear is distributed along the height of the building and then the internal forces and displacements are determined by linear elastic analysis. The base shear V_b results from the elastic design spectrum (figure 3.4), after having previously determined the fundamental period of the structure *T*. The calculation of the fundamental period can be made: (a) analytically solving the full eigenvalue problem for the numerical

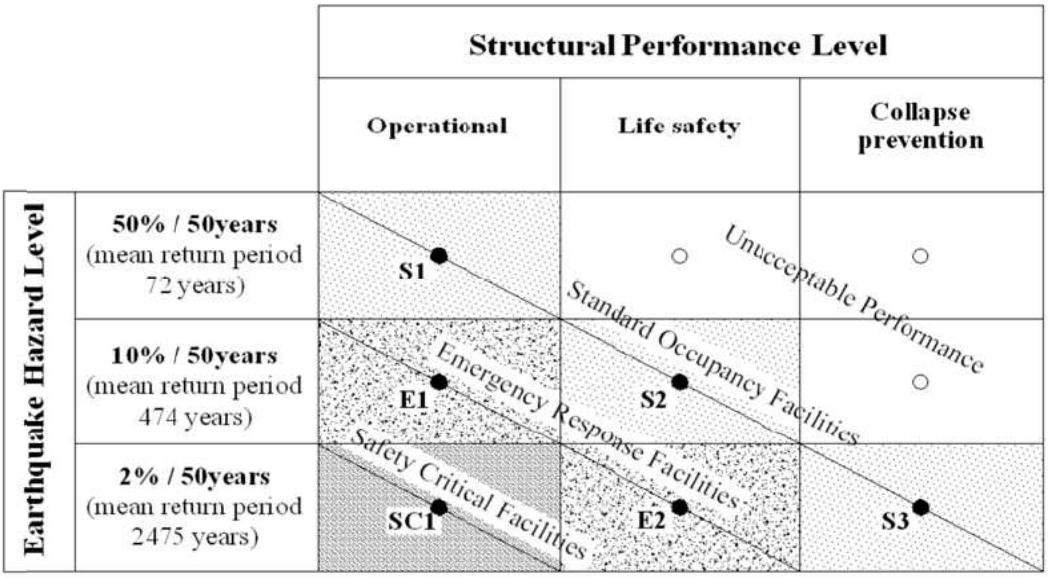

Figure 3.3 Performance objectives given by Visio 2000.

model of construction, (b) empirically through approximate relations or (c) approximated e.g., method Rayleigh. The empirical formulas for determining the fundamental period, are the following:

$$T = C_t h_n^{\beta} \qquad \text{(FEMA-356)} \qquad (3.1)$$

$$T = C_t h_n^{3/4} \qquad \text{(EC8)} \qquad (3.2)$$

where h_n is the height of the building (in m or in *ft*) and C_t, β are parameters that depend on the kind of the structure. If *W* is the total weight of a structure, then the base shear results from the acceleration of the design spectrum Sa(T):

$$V_b = S_a W \qquad (3.3)$$

The relation (3.3) gives the base shear of EC8. The corresponding relation of FEMA-356 additionally uses a weighting approach in order for the base shear to be more accurate. The relation of FEMA-356 is of the form:

$$V_b = C_1 C_2 C_3 C_m S_a W \tag{3.4}$$

where C_1: factor that relates the expected maximum inelastic displacements to displacements resulting from the linear elastic analysis, where:

$$C_1 = \begin{cases} 1.5, T < 0.10 \sec \\ 1.0, T \geq T_s \end{cases} \tag{3.5}$$

where Ts is the characteristic period of the design spectrum corresponding to the point of intersection of the acceleration spectrum with the velocity speed range.

C_2: is the factor taking into account the influence of the shape of the hysteresis loop, the stiffness reduction, and the reduction of durability. For the linear methods this factor is always taken equal to 1.0.

C_3: is the factor taking into account the increase in displacements due to P-delta effects. The factor obtained depending on the value of the parameter stability:

$$\theta_i = \frac{P_i \delta_i}{V_i h_i} \tag{3.6}$$

where P_i is the percentage of total weight, Vi is the base shear in the floor i, h_i is the height of the storey i and δ_i floor and the difference of the horizontal displacement of floor i to that floor i-1. For values of less than 0.1 the C_3 is assumed to be 1.0, otherwise it may be calculated by the relation:

$$C_3 = 1 + \frac{5(\theta - 0.1)}{T_1} \tag{3.7}$$

where θ is the maximum value θ_i of the parameter of stability of all the floors. C_m: is the equivalent mass factor used to take into account the influence of higher modes. This coefficient depending on the type of construction takes values from 0.8 to 1.0, while for T greater than 1 sec it is equal to the one.

The total weight W of the structure in equation (2.4) is obtained from the sum of the total permanent load and a proportion of live loads which in EC8 assumed to be 30%.

The seismic force to the floor i results from the seismic base shear according to the relationship:

$$F_i = C_{vi} V_b \tag{3.8}$$

For a building with N floors, C_{vi} coefficient is calculated as a function of the vector modes of φ, using the relationship:

$$C_{vi} = \frac{\varphi_i W_i}{\sum_{j=1}^{N} \varphi_j W_j} \tag{3.9}$$

In a more simplified manner the relation used should be:

$$C_{vi} = \frac{h_i^k W_i}{\sum_{j=1}^{N} h_j^k W_j} \tag{3.10}$$

where h_i is the distance of the floor i from the base of the building. Coefficient k in EC8 is taken equal to unity while in FEMA-356 is given by:

$$k = \begin{cases} 2.0, \text{ for } T \geq 2.5 \text{ sec} \\ 1.0, \text{ for } T \leq 0.5 \text{ sec} \end{cases} \tag{3.11}$$

In relation (3.11) for values of T between 0.5 and 2.5 sec linear interpolation is allowed.

In the simplified spectral method only the fundamental period of construction on the two main directions is taken into account. Thus, this process is suitable for buildings which can be analyzed as two flat panels, one for each main direction where the response should not be affected significantly by the higher forms of oscillation. This criterion is satisfied by structures which are normal in plan view and in height or they are normal only in height and the strength and mass centers of all stories are at about the same vertical line. Also, the fundamental period in any direction should not exceed 2 sec.

3.4 Nonlinear static pushover analysis method

3.4.1 Description of the method

The static pushover (SPO) analysis is the most widely used nonlinear method of seismic demand. The method is approximate, since the earthquake is a dynamic phenomenon, but given the fact that we are talking about a non-linear method, the analysis takes into account the nonlinear behavior in terms of material and geometry.

The mathematical model of the structure "is pushed" by a distribution of horizontal lateral loads. The horizontal loads are applied while the structure is loaded with the vertical gravity loads under seismic load combination which is specified by antiseismic regulation (EC8 (2003)). The distribution of loads increase proportionally until the displacement of the characteristic node becomes equal to the target displacement. A characteristic node is chosen as the node which lies in the center of mass on the roof of the building. The target displacement is the displacement of the characteristic node during the design earthquake and its calculation is presented in a next chapter. For the performance-based design the value of target displacement depends on the performance level under consideration.

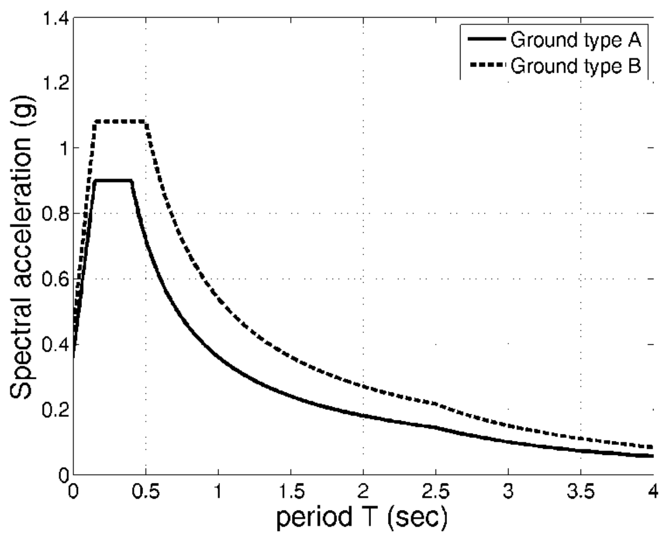

Figure 3.4. The elastic design spectrum of Eurocode 8.

According to FEMA-356 during the pushover analysis at least two side-load distributions of lateral loads should be taken into account. These distributions must be selected from the following two sets of distributions:

1. Choose one of the following modal distributions:
   - The lateral load pattern given by equation (3.9), when mass percentage of the fundamental eigenvalue is at least 75% of the total mass.
   - The pattern given by equation (3.10), when mass percentage of the fundamental form is of at least 75% of the total mass, and if a second uniform load pattern is also used. According to ASCE-41 (2006), apart from a first-mode based lateral load pattern, the use of a uniform along the height pattern is also suggested.
   - For buildings with a period greater than 1sec, the distribution is calculated using a combination of shear forces resulting from dynamic spectral analysis with a suitable design spectrum. The number of forms is such as to take account the 90% of the total mass.
2. The second distribution is selected from the following:
   - Uniform distribution where horizontal loads are proportional to the mass of each floor.
   - An adaptive distribution that changes as the structure is displaced. This load allocation should be adjusted according to the inelastic response.

The use of at least two distributions is due to the fact that during analysis the first eigenvalue changes continuously as the stiffness changes. The purpose is to identify the possible range of the response since it is considered that the uniform distribution better simulates actual loads in case the structure has undergone some degree of damage (Mwafy and Elnashai (2001)). As seismic demand the maximum sizes derived from each distribution are considered.

Alternatively it is proposed to use an adaptive procedure, where the shape of the distribution is altered during analysis. The adaptive procedures proposed in the literature vary. For example Fajfar and Fischinger (1988) suggested using a distribution that follows the profile of the deformed structure, Eberhartd and Sozen (1993) proposed the use of probability distributions which follow eigenmodes that are calculated from the shear stiffness (secant stiffness) at each loading step while Bracci et al. (1997) proposed the use of distributions depending on the distribution of shear forces at each load step.

Besides changing the shape of the distribution in many cases should take into account the participation of additional forms of deformation beyond the first. Chopra and Goel (2002) suggested Modal Pushover Analysis (MPA). During this process the distributions of important eigenmodes is calculated and pushover analysis is performed for each important eigenmodes. The results of analysis (displacements or interstorey drifts) are combined with the method SRSS. The theoretical background of the method is based on the observation that the eigenmodes of construction are coupled but this coupling is weak. The reliability of MPA over other analytical procedures have been studied in a large number of studies, while Goel (2005) shows a comparative investigation of the reliability of MPA compared with FEMA procedure described in the previous paragraphs. Having the same target Antoniou and Pinho (2004) proposed the displacement-based adaptive pushover. In construction a distribution which is based on the profile of the important modes as derived from after the modal analysis method combined with the SRSS is applied. This procedure is advantageous over the classical method because after every step the loading profile is updated and the applied displacements are based on the results of modal analysis avoiding the use of the relation (2.9).

3.4.2 Target displacement

In order to determine the target displacement in multiple hazard levels required by the performance-based design framework, typically one of the following methods is adopted: the Capacity Spectrum method of ATC-40 (1996), the Coefficient method of ASCE-41 (2006) and the N2 method of EC8 (2004).

(1) The displacement coefficient method (ASCE-41)

The target displacement, which is the displacement during a given seismic event of a characteristic node on the top of a structure, typically the roof, is defined with the aid of the formula:

$$d_t = C_0 C_1 C_2 C_3 \frac{T_e^2}{4\pi^2} g \tag{3.12}$$

where C_0, C_1, C_2 and C_3 are modification factors. C_0 relates the spectral displacement to the building roof displacement. C_1 relates the expected maximum inelastic displacements to the displacements calculated for linear elastic response. C_2 represents the effect of the hysteresis shape on the maximum displacement response and C_3 accounts for the P-Δ effects. T_e is the effective fundamental period of the building in the direction under consideration and Sa the response spectrum acceleration, corresponding to the T_e period, normalized by *g.* The FEMA-440 (2005) guidelines introduce updated expressions for the calculation of the effective damping and the fundamental period and also for scaling the demand spectrum based on the hysteretic model of the system.

(2) The capacity spectrum method (ATC-40)

The capacity spectrum method (CSM) was initially proposed by Freeman (1998). The method compares the capacity of a structure to resist lateral forces to the demand given by a response spectrum in a graphical manner. The response spectrum represents the demand while the pushover curve (or the “capacity curve”) represents the available capacity. Both curves are converted and plotted against an acceleration-displacement graph (AD graph) making easy the evaluation of the point of equal demand and supply, also known as performance point. Among the three variations of the method discussed in ATC-40, the procedure A was examined. The steps of the method are briefly summarized as follows:

1. Perform pushover analysis and determine the capacity curve in base shear (V_b) versus roof displacement of the building (D). This diagram is then converted to AD terms using an equivalent SDOF. The conversion is performed using the first mode participation factor C_0 ($D^*=D/C_0$) and the modal mass ($A=V_b/M$).

2. Plot the capacity diagram on the same graph with the 5%-damped elastic response spectrum that is also in AD format.

3. Select a trial peak deformation demand d_t^* and determine the corresponding pseudo-acceleration A from the capacity diagram, initially assuming ζ=5%.

4. Compute ductility $\mu=D^*/u_y$ and calculate the hysteretic damping ζ_h as $\zeta_h=2(\mu-1)/\pi\mu$.

The equivalent damping ratio is evaluated from a relationship of the form:

$$\zeta_{eq}=\zeta_{el}+k\zeta_h \tag{3.13}$$

where k is a damping modification factor that depends on the hysteretic behavior of the system. Update the estimate of d_t^* using the elastic demand diagram for ζ_{eq}.

5. Check for convergence the displacement d_t^*. When convergence has been achieved the target displacement of the MDOF system is equal to $d_t = C_0 d_t^*$

Note that this has been found to be inaccurate and changed considerably by FEMA-440. ATC-40 is no longer used per se.

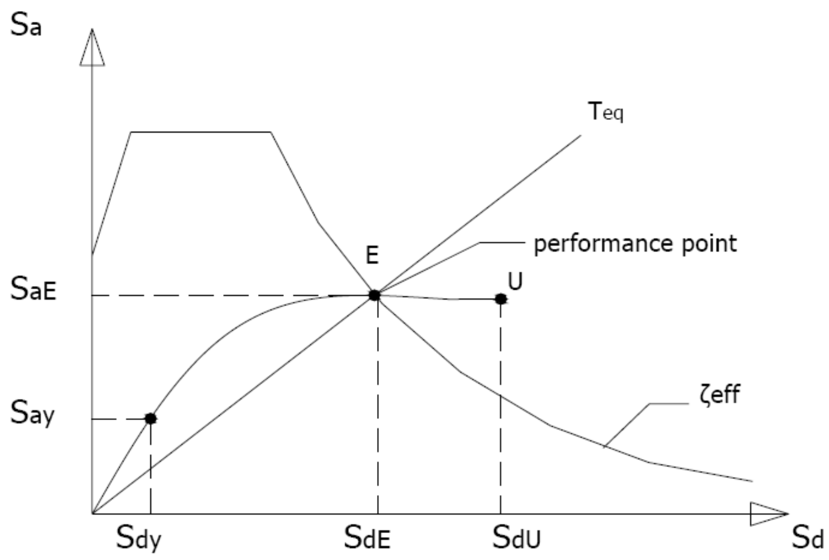

Figure 3.5: The Capacity Spectrum method (ATC-40).

(3) The N2 method (EC8)

The N2 method was initially proposed by Fajfar (Fajfar and Fiscinger, 1988), (Fajfar and Gaspersic, 1996) and was later expressed in a displacement-acceleration format (Fajfar, 1999). Recently, the method has been included in the Eurocode 8 (2003). Conceptually the method is a variation of capacity spectrum method that instead of highly damped spectra uses an R-μ-T relationship. The method, as implemented in EC8, consists of the following steps:

I. Perform pushover analysis and obtain the capacity curve in V_b-D terms,

II. Convert the pushover curve of the MDOF system to the capacity diagram of an ESDOF system and approximate the capacity curve with an idealized elasto-perfectly plastic relationship to get the period T_e of the ESDOF,

III. The target displacement is then calculated as:

$$d^{*}_{et} = S_a(T_e)\left[\frac{T_e}{2\pi}\right]^2 \tag{3.14}$$

where $S_a(T_e)$ is the elastic acceleration response spectrum at the period T_e. To determine the target displacement d_t^*, different expressions are suggested for the short and the medium to long-period ranges:

$T^* < T_c$ (short period range): If $F_y^* / m^* \geq S_a(T_e)$, the response in elastic and thus $d_t^* = d_{et}^*$ and $d_t = C_0 d_t^*$. Otherwise the response is nonlinear and the ESDOF maximum displacement is calculated as:

$$d_t^* = \frac{d_{et}^*}{q_u}\left(1 + (q_u - 1)\frac{T_c}{T_e}\right) \geq d_{et}^* \tag{3.15}$$

where q_u is the ratio between the acceleration in the structure with unlimited elastic behavior $S_a(T^*)$ times the modal mass m* over its yield force, or simply:

$$q_u = S_a(T_e) m^* / F_y^* \tag{3.16}$$

$T^* \geq T_c$ (medium and long period range): The target displacement of the inelastic system is equal to that of an elastic structure, thus $d_t^* = d_{et}^*$. The displacement of the MDOF system is always calculated as $d_t = C_0 d_t^*$.

3.4.3 Bilinear approximation of the capacity curve

Both in the capacity spectrum method and in the displacement coefficient method it is necessary for the capacity curve to be bilinear approximately in order to calculate various parameters such as the equivalent stiffness K_e, the shear yield strength V_y the equivalent elastic period T_e rate.

The bilinear approximation of the capacity curve is generated so as for equal areas of above and below the intersection points of the actual and the idealized curves are shown in figure 3.6. The intersection of the two branches

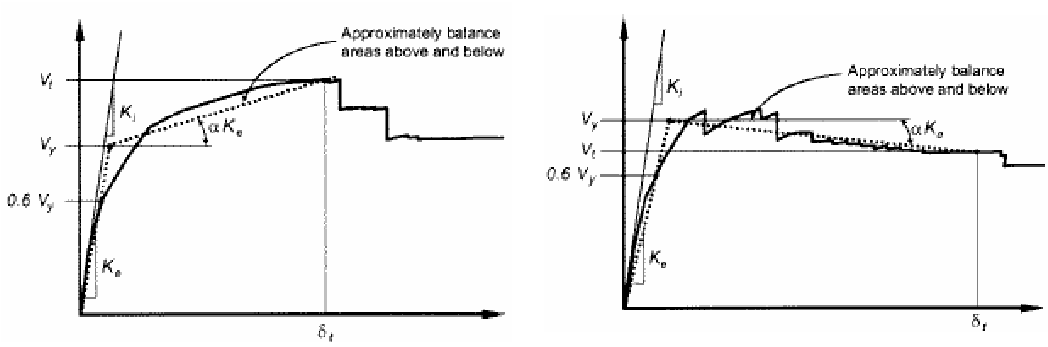

Figure 3.6. Transformation of the capacity curve into a bilinear curve (FEMA-356 (2000))

of the bilinear curve gives the yield base shear V_y, while the equivalent stiffness K_e is given by the shear stiffness for base shear equal to 60% of V_y. If K_i is the initial elastic stiffness and T_i is the corresponding fundamental period, then the equivalent period is given by:

$$T_e = T_i \sqrt{\frac{K_i}{K_e}} \tag{3.17}$$

3.4.4 Advantages and disadvantages of the method

The SPO takes directly into account the nonlinear nature of the response. Below are summarized the advantages of the method (Krawinkler and Seneviratna (1998)):

- Realistic estimates of the demand in potentially brittle members such as the axial demand in columns in requirement, the moment demand in beam-column connections or shear forces in walls and around short columns.

- Estimates of the displacement demand of members that deform inelastically in order absorb seismic energy and direct calculation of the angles relative movement, allowing the control and the reduction of damage to non-structural elements. Moreover, the method gives the opportunity to take into account the contribution of non-structural elements ability.

- Assessment of the effects of reducing the resistance of some members in the overall carrying capacity of the structure.
- Identification of critical regions where inelastic deformations are expected to be high. When calculating the capacity curve the series of plastic hinges until the creation of the collapse mechanism are identified.

Apart from the above advantages pushover analysis has a series of disadvantages which in many cases require attention in order to avoid use of the method in cases that are not appropriate. The disadvantages of the method can be summarized as follows:

- The theoretical background of the method is incomplete and, in many cases, it is difficult to be supported. The main hypothesis that the response of a system of many degrees of freedom can be correlated with the response of a single degree of freedom system responding to the fundamental eigenmode in many cases is not applicable. Also, the fundamental eigenmode is not constant and changes depending on the inelastic deformations. Thus, in cases where higher eigenmodes are important, the method can give misleading results.
- There is difficulty in applying the method to 3D buildings, especially in structures with non-normal plan. Generally there is no consensus in the research community on how to apply the horizontal lateral loads to 3D buildings.
- The distribution of horizontal lateral loads does not take into account the reduction of stiffness and therefore the modification of fundamental eigenmode due to inelastic response.
- The energy is absorbed by inelastic deformations and the energy absorption due to hysteretic behavior depends on the R-μ-T that you use. Also, the influence of the duration of the earthquake and the number of cycles is more difficult.

- The capacity of the structure and the seismic demand are taken separately into account, while it is known that the demand is always dependent on the dynamic characteristics of the structure.

The pushover analysis is used in order to assess the structural performance in terms of strength and deformation capacity for the whole structure, as well as at the element level.

3.5 Linear Dynamic approach

The linear dynamic process as described in FEMA-356 contains two procedures: the spectral method and the method of time integration. The spectral method is based on the modal superposition method and uses the spectrum of regulation (Figure 3.4). The method of time integration is based on the integration of the equations of motion of the structure due to the enforcement of seismic records. The main difference between the two procedures relates to the different way of application of seismic design actions.

3.5.1 The spectral method

The spectral method corresponds to the method of dynamic spectrum of EC8 and in general it includes (EAK (2000)):

- Modal analysis, i.e. calculation of the eigenmode’s shapes and the corresponding natural periods. The eigenmodes are calculated numerically solving the complete eigenvalue problem.
- Determine the modal response. Based on the response spectrum the peak responses that correspond to every type of oscillation for every main direction of the building are calculated (displacements, intensity measures). Depending on the period of the structure, the spectrum acceleration is calculated for every eigenmode and then the corresponding response.
- Modal response superposition. For each direction extreme seismic actions are calculated through superposition of responses. The superimposition may be done either by simple quadratic superposition,

i.e. the method SRSS (Square Root of the Sum of Squares), or by full square superposition wherein the method is known as CQC (Complete Quadratic Combination). The first procedure is computationally simpler but applies only if the modes are well distinct (well-spaced), while the CQC method can be applied in all cases.

- Spatial superposition, where the potential peak value of the seismic response for simultaneous action of three components of the earthquake is taken into consideration.

Detailed descriptions of the method can be found in the literature (e.g., Penelis and Kappos (1997), Chopra (2001)). The dynamic spectral method is suitable for the case where the spectral simplified method cannot be used.

3.5.2 Time integration method

During the time integration process the response of the structure is calculated at discrete time steps using natural or artificial seismic records. Performing the time integration can be done either through direct integration of the equations of motion (e.g., methods type Newmark) or with a superposition of modes assuming that the behavior of the building is linear.

The FEMA-356 requires both spectral and time integration methods to be multiplied by the coefficients C_1, C_2 and C_3 which presented in section 3.3.

3.6 Nonlinear Dynamic Approach

Nonlinear dynamic analysis takes into account the nonlinear structural response during the direct integration of the equations of motion of a seismic record. It is the most accurate method of analysis but the computational cost is still high regarding the other methods of analysis. Since the response of the structure is often sensitive to the characteristics of the seismic record, this approach it requires a multitude of seismic records in order to give more accurate results. This section outlines procedures that are based on the dynamic nonlinear analysis for the calculation of the seismic requirement for various performance levels.

3.6.1 Scaling of recorded ground motions

There is a definition proposed by Vamvatsikos and Cornell (2002) regarding the scale factor of recorded ground motions which goes as follows: “The scale factor (SF) of a scaled accelerogram, $\alpha_{\lambda,}$ is the nonnegative scalar $\lambda \epsilon [0,+\infty)$ that produces α_λ when multiplicatively applied to the unscaled (natural) acceleration time history, α_1. Note how the SF constitutes a one-to-one mapping from the original accelerogram to the scaled one. A value of $\lambda=1$ signifies the natural accelerogram, $\lambda>1$ corresponds to a scaled up accelerogram and $\lambda<1$ corresponds to a scaled down accelerogram.”

Therefore, the procedure in which a suite of accelerograms are multiplied by a number, called scaling factor, and performs nonlinear time history analysis with the ‘scaled accelerograms’, is called scaling procedure.

3.6.2 Cloud analysis

With this method, the structure is subjected to a set of ground motions. The records are either left unmodified, or all records are scaled by a constant factor if the unmodified records are not strong enough to induce the structural response level of interest.

The set of IM values and their associated *EDP* values resulting from nonlinear dynamic analysis are sometimes referred to as a “cloud” of points forming a rough ellipse when plotted (see fig. 3.8). Regression can be used on this cloud of data in order to compute the conditional mean and standard deviation of *EDP* given IM. A linear relationship may provide a reasonable estimate of the mean value of *EDP* for example:

$$lnEDP=a+b\ lnIM \quad (3.18)$$

where *a* and *b* are the intercept and the slope of the linear regression function, respectively, to be determined from the analysis. This “power law” is what is typically used.

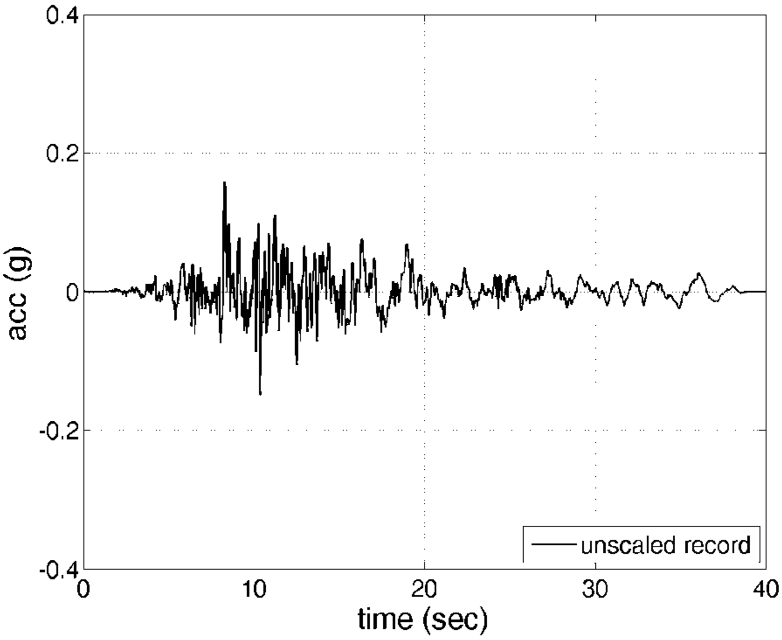

Figure 3.7a: Unscaled accelerogram

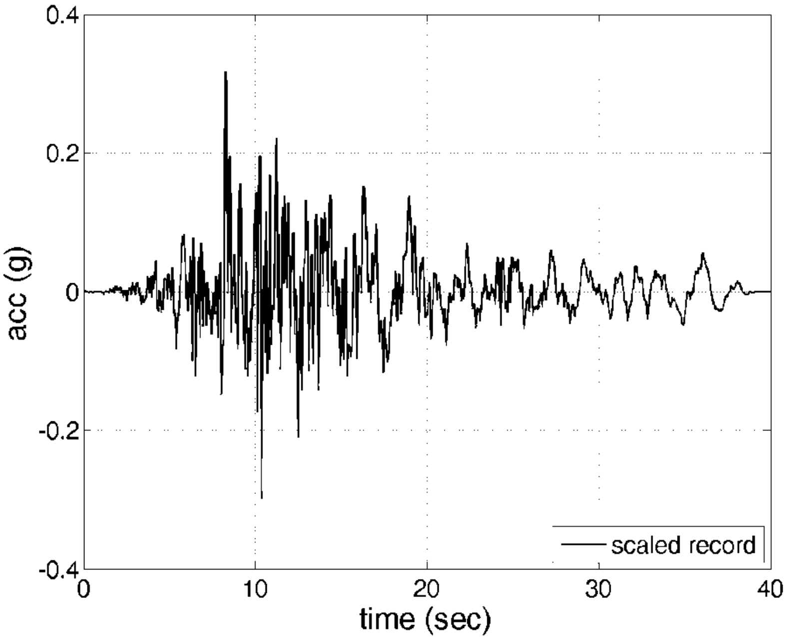

Figure. 3.7b: Scaled accelerogram by a scaling factor of two.

Figure 3.8 shows the cloud of EDP-IM data, where $Sa(T_1,5\%)$ is selected as the IM and θ_{max} is selected as EDP. The θ_{max} values have been obtained from nonlinear time history analysis (NLTHA) using unscaled records.

3.6.3 Seismic demand evaluation methods based on nonlinear dynamic analysis.

Methods of estimating seismic demand by dynamic non-linear analysis are divided into processes where the demand is estimated for a specified performance level and methods in which the response is determined for every performance level. In the second case from the analytical procedure the dynamic capacity curve results to a curve similar to the one resulting from the capacity curve of incremental static analysis. For the description of the methods presented in this paragraph the measure of seismic intensity is

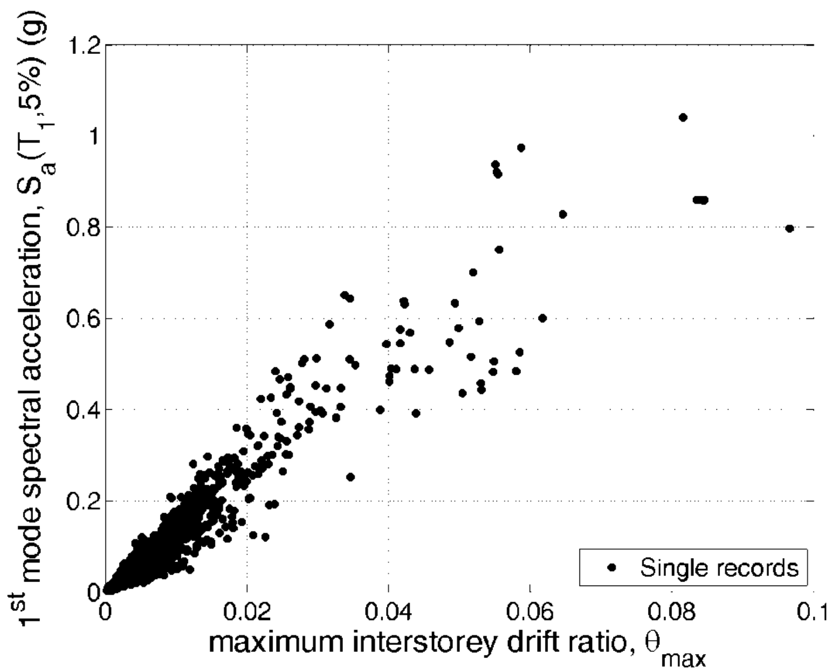

Figure 3.8 Cloud analysis of *EDP-IM* data.

spectral acceleration for the fundamental period for 5% damping and denoted by S_a (T_1, 5%). As a global measure of damage to the structure the maximum interstorey drift, θ_{max}, is selected. The selection of these measures of damage and intensity is based on the recommendations of FEMA-350 and is suitable for building structures as those analyzed in this thesis. In practice, however, depending on the kind of the problem any other measure of intensity (e.g., peak ground acceleration) or of damage (e.g., plastic rotations, required plasticity) can be used. These procedures beyond the determination of the mean value of demand have as a target the determination of other important parameters of the response such as the dispersion around the median or the slope of the curve of dynamic capacity.

3.6.4 Procedures for determining the demand for one performance level.

The procedures that are relatively limited in scope require a small number of non-linear dynamic analysis. If the spectral acceleration $S_a(T1,5\%)$ is used as a measure of seismic intensity, then the demand can be determined either by scaling all seismic records which possess the same spectral acceleration or by using a single scaling factor for all records. In the second case in order to calculate the value of the demand, θ_{max}, a linear regression of the results at the $S_a(T_1,5\%)$- θ_{max} plane is performed.

In both previously mentioned procedures the spectral acceleration $S_a(T_1,5\%)$ is initially determined from the seismic hazard curve. The determination of the demand when the records are scaled in order to have a uniform intensity can be seen in figure 3.9(a), while the determination of the demand with the use of a single scaling factor can be seen in figure 3.9(b). For the second case through linear regression a relation of this form:

$$\theta_{max} = \alpha \left[S_a(T_1, 5\%)\right]^{\beta} \tag{3.19}$$

may be obtained by Jalayer 2003 (figure 3.9b). This relation connects linearly the logarithms of the intensity measure and the damage measure of θ_{max} by means of the parameters α and β, as shown in figure 3.9(b) and on the 3.20 equation.

$$\theta_{\max} = \alpha \cdot Sa^{\beta} \Rightarrow \log\theta = \log a + \beta \cdot \log Sa \tag{3.20}$$

As shown in figure 3.10, the two procedures allow the determination of the dispersion of capacity around the mean. If the dispersion is small then there is greater confidence around the mean and generally requires fewer non-linear analyses for the mean value to be determined. The dispersion is usually measured in statistics with the help of standard deviation σ. In practice it has been observed that the results of dynamic analysis with seismic records follow the lognormal distribution (Benjamin and Cornell (1970)). Thus, in this case a variance measure may be used as the standard deviation of the natural logarithms of the maximum displacements. The dispersion is useful in various practical applications, for example in the case where instead of the average we need the 84th percentile (84th-percentile) of response. The 84th percentile corresponds to a value not exceeding capacity of 84% of recordings and is a more conservative value for the seismic demand in relation to the median. The 84th percentile can be calculated by multiplying the median with the dispersion raised to the base of natural logarithms (e^{δ}).

3.6.5 Procedures for determining the demand for every performance level

The demand for every performance level can be calculated if the procedure of the previous paragraph is repeated for monotonically increasing magnitude values of intensity $S_a(T_1,5\%)$. This procedure is known as multi-stripe analysis. Similar to the multi-stripe analysis is the incremental dynamic analysis (IDA) in which every record is scaled separately in different values of intensity $S_a(T_1,5\%)$.

The multi-stripe analysis is depicted in the figures 3.10, 3.12, 3.13. As the records are scaled the capacity curve that corresponds to median values is generated. Figure 3.10 also shows the capacity curves of 16% and 84% percentile. If the median lies in the 50% percentile, then, in proportion with the case that average and mean are the same values, the above percentiles (16% and 84%) depict the average plus-minus the standard deviation ($\mu \pm \sigma$). The two curves show the dispersion of values of θ_{max} with the mean curve. The dynamic capacity curve shows the capacity whose intensity is valued by measure of $S_a(T_1,5\%)$ for a specific value of θ_{max}. If this information is combined with a hazard curve, then return period of earthquake is generated for which the specific degree of damage is exceeded. Similarly, for a given value of $S_a(T_1,5\%)$, the demand results are expressed as the maximum interstorey drift θ_{max}.

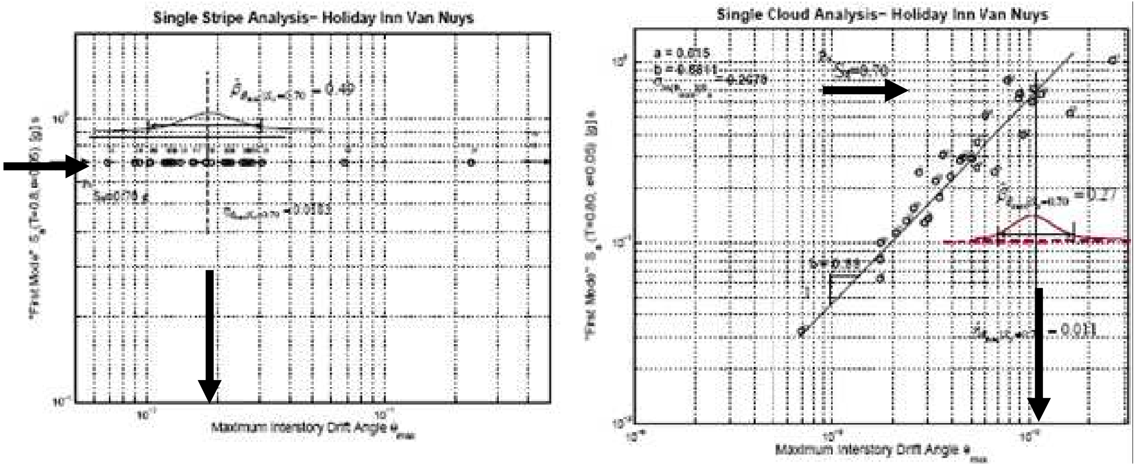

(a) (b)

Figure 3.9: (a) Scaling of records that have unified $S_a(T_1,5\%)$ and (b) scaling of records with a single scaling factor (Source: Jalayer (2003)).

In order to estimate engineering demand parameter (EDP) distributions at a range of intensity measure (IM) values, repeats of single-stripe analysis at a range of IM values (either at every IM value of interest, or by analyzing a few IM values and interpolating) is required. Multiple stripes of data are shown in figure 3.10 (using a suite of 20 ground motions scaled to 10 spectral acceleration levels between 0.005g and 1g). From this figure it can be seen that the standard deviation of EDP is not constant over the range of IM considered here. It also appears that the mean value of EDP is not a linear function of IM.

In this study we used accelerograms that were taken from the PEER strong motion database [PEER NGA Database 2008]. At first, twenty records were chosen arbitrarily. Then we scaled them in order to reach a certain spectral acceleration level up to 1.00g. We begun with 0.01g, 0.12g, 0.23g, 0.34g, 0.45g, 0.56g, 0.67g, 0.78g, 0.89g, 1.00g. This was done in order to introduce the desired forces to the structure. The responses obtained are demonstrated at figure 3.10.

In figure 3.10 the records are run at a suite of spectral acceleration stripes. In this case the single stripe results (median ,84th percentile and 16th percentile, and values without the outliers) beyond at figure 3.10 are repeated for each level and the values are connected level to level, forming approximate functional relations between, for example, the median drift and spectral acceleration. Also, in figure 3.11 the profile of the maximum interstorey drift of each of the nine floors for the nine-storey SAC building and for the median values of figure 3.10 is presented.

Multi-stripe analysis is closely connected to the incremental dynamic analysis in the sense that both are using the scaling technique but in a different way different. In multi-stripe analysis the scaling factor is augmented with a certain step every time that is selected by the user while in IDA the hunt-and-fill algorithm proposed by Vamvatsikos & Cornell (2004) finds the scaling factor automatically with the privilege of performing the least required nonlinear dynamic analysis.

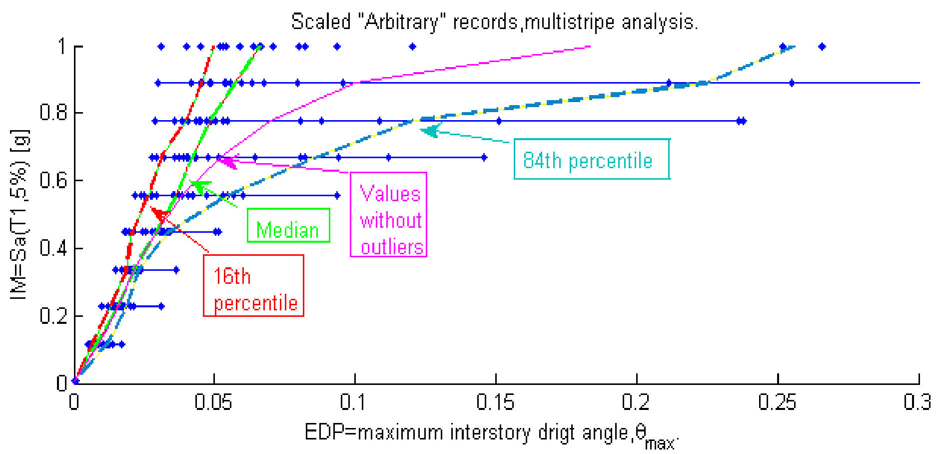

Figure 3.10: Multiple stripes of data using the same 20 records scaled at each of the 10 different levels.

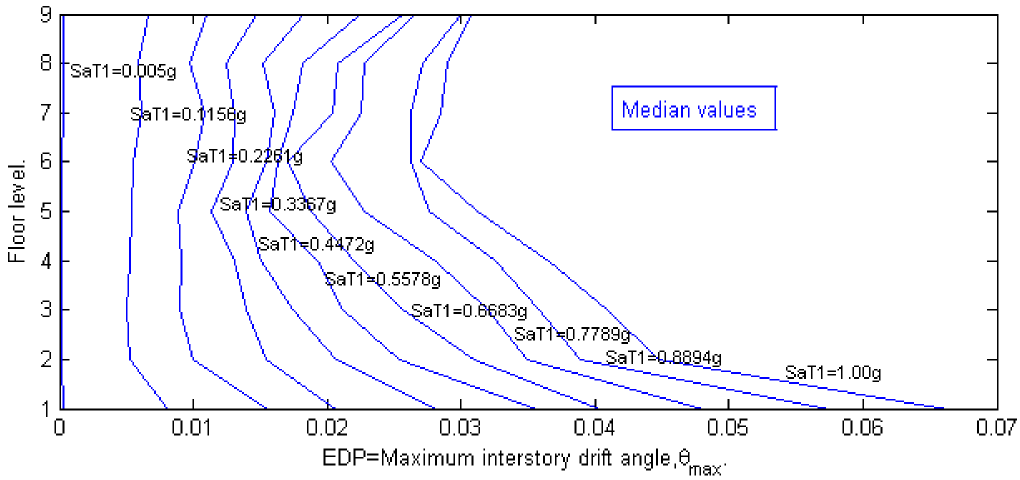

Figure 3.11: The maximum interstorey drift for a suite of ten different *Sa*(T_1,5%) over the nine floors of the SAC building.

Figure 3.12 presents a multi-stripe analysis using as intensity measure the maximum incremental velocity versus max interstorey drift ratio θ_{max}. It is obvious from this figure that the step of incremental dynamic analysis is constant. Each record is scaled to multiple levels of intensity, producing the structure's capacity curve in terms of an intensity measure versus an engineering demand parameter.

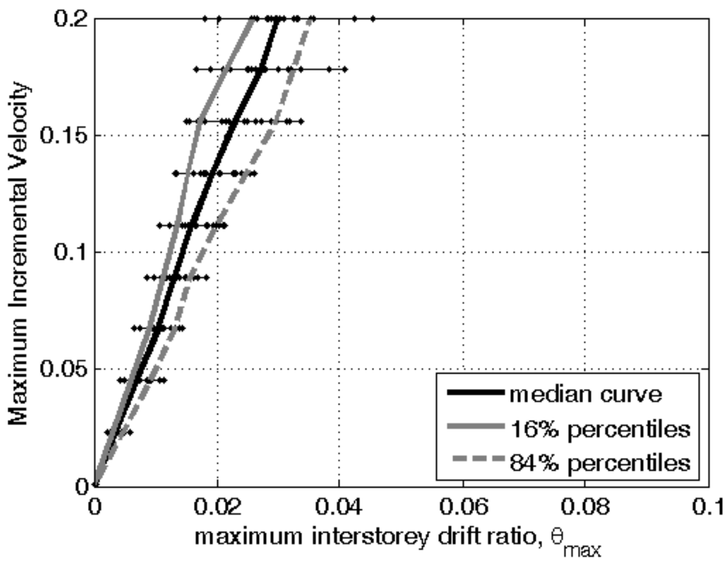

Figure 3.12: M-stripe analysis for the nine storey building considered in this dissertation.

Scaling to $S_a(T_1,5\%)$ at the natural period of the structure is a common approach. When matching of natural records is included, it is generally specified with regard to the ordinates of the acceleration response spectrum or in other words to the peak ground acceleration (PGA). The scaling procedure can be used with other intensity measures like the peak ground acceleration (PGA), the root Mean Square accelerations (RMS), maximum incremental velocity (MIV), spectrum intensity (SI), characteristic intensity (ChI).

In Figure 3.13 the scaling procedure of five different intensity measures is presented for a nine-storey steel moment-resisting frame: (a) Spectral acceleration ($Sa(T_1,5\%)$), (b) Peak Ground Acceleration (PGA), (c) Maximum Incremental Velocity (MIV), (d) Characteristic Intensity (ChI), (e) Spectrum Intensity (SI). It is observed that the selection of the intensity measure has a great impact on the shape of the curves. The dispersion of the values is smaller for maximum incremental velocity and for characteristic intensity and is larger for spectrum intensity and peak ground acceleration.

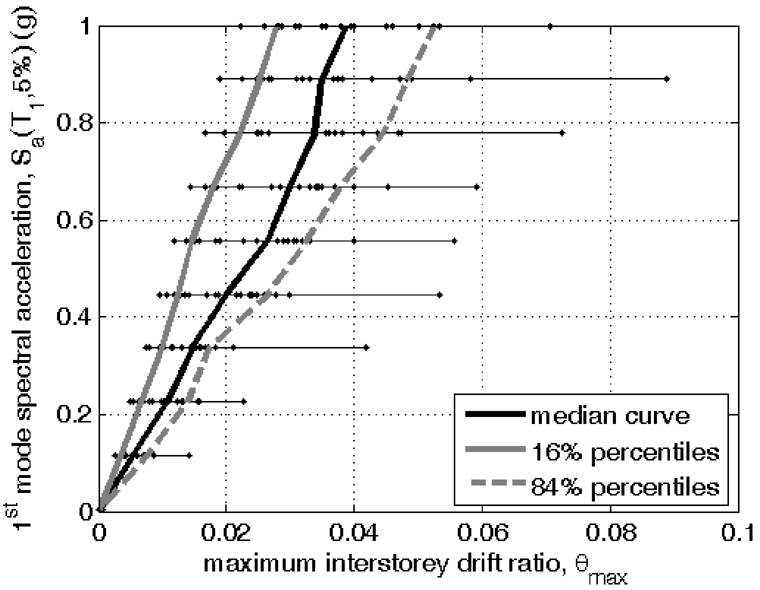

(a)

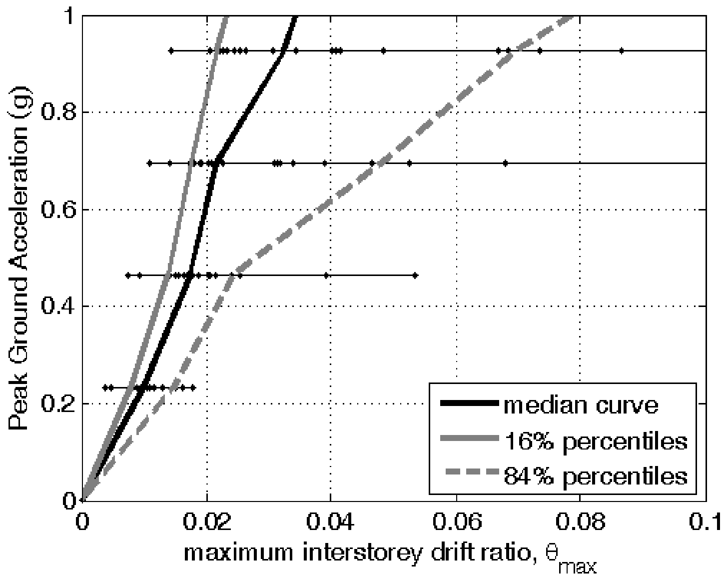

(b)

Figure 3.13: Scaling to different Intensity Measures such as: (a) Spectral acceleration, (b) Peak Ground Acceleration, (c) Maximum Incremental Velocity, (d) Characteristic Intensity, (e) Spectrum Intensity.

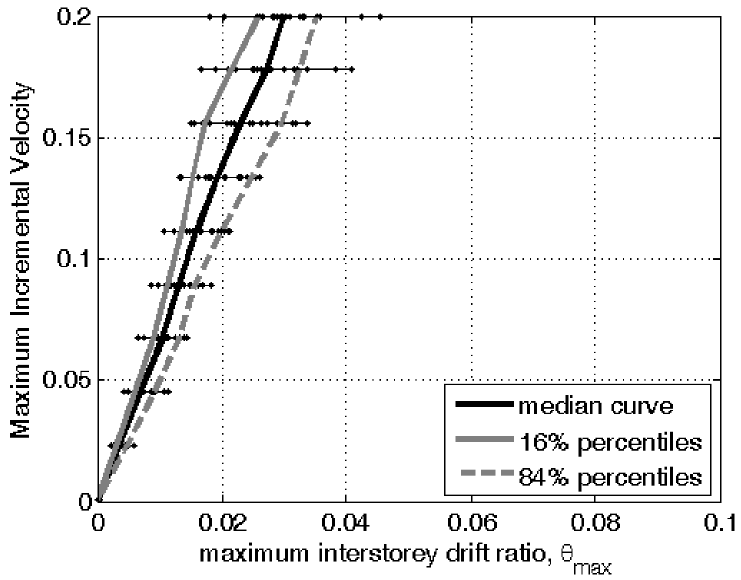

(c)

Figure 3.13 (cont'd): Scaling to different Intensity Measures such as: (a) Spectral acceleration, (b) Peak Ground Acceleration, (c) Maximum Incremental Velocity, (d) Characteristic Intensity, (e) Spectrum Intensity.

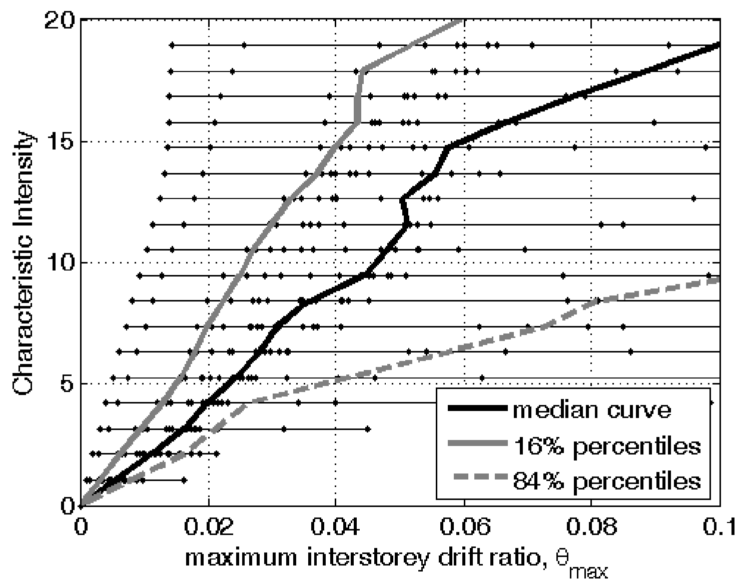

(d)

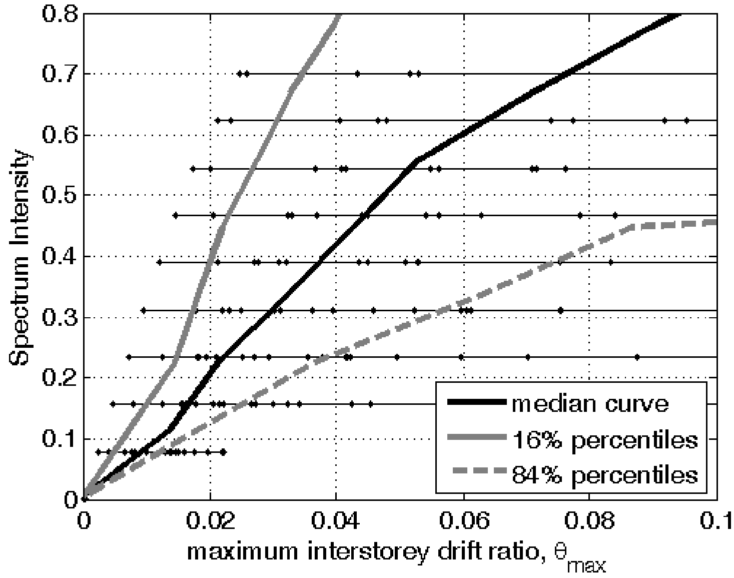

(e)

Figure 3.13 (cont'd): Scaling to different Intensity Measures such as: (a) Spectral acceleration, (b) Peak Ground Acceleration, (c) Maximum Incremental Velocity, (d) Characteristic Intensity, (e) Spectrum Intensity.

For the cases of spectrum intensity and peak ground acceleration intensity measures the dispersion increases as the spectrum intensity and peak ground acceleration increases. Large values of θ_{max} (bigger than 0.04) on average are achieved when the intensity measure is spectrum intensity, which is a fact that it is the most efficient intensity measure in terms of the width of $\theta_{max.}$ This observation agrees with Nau and Hall (1984), Martinez-Rueda (1998).

On the contrary the scaling of records using characteristic intensity and maximum incremental velocity as intensity measures does not lead to an amplitude of responses, namely to large θ_{max} values, as for the values of scaling that have been used, thus 0<MIV<0.2 and 1<ChI<3.

In the present investigation the spectral acceleration of the first mode period ($Sa(T_1,5\%)$) is used as the most common intensity measure in the literature and the antiseismic design codes (e.g. FEMA-356). As it can be seen from figure 3.13a the use of $Sa(T_1,5\%)$) is characterized by relatively small dispersion until θ_{max} =0.04 on average; thus allowing a satisfactorily reliable estimate of the response up to this value of EDP.

In the study of Shome et al. (1998), a five-DOF model of a steel structure was used, considering global and non-linear damage measures. The records used were scaled to the same intensity measured by the mean $Sa(T_1,5\%)$ at the fundamental period of the structure. The study concludes that when scaling to the median spectral acceleration predicted by an attenuation equation is done, the MDOF response does not depend on the magnitude and distance.

Scaling to $S_a(T_1,5\%)$ at the natural period of the structure is fundamental to code specifications. For the dynamic analysis most of the seismic design codes do not provide targets of records in terms on strong-motion parameters. When matching of real records is included, it is generally specified with regard to the ordinates of the acceleration response spectrum in the code. Bommer and Ruggeri (2002) summarise in their work the guideline recommendations in current seismic design codes for the use of time-histories in dynamic analysis. The New Zealand code specifies the matching in a descriptive manner over the period range of interest of the structure being analysed. The requirements of the Argentinian code are more specific with conditions of matching the areas of the two spectra between 0.05 and the fundamental period of the structure. In the French code the matching is done over the entire period for the value of the mean spectrum. More details about the requirements of the code mentioned previously are presented in Bommer and Ruggeri (2002) (Acevedo 2003).

The “strength” of an earthquake ground motion is often quantified by an intensity measure (IM), such as peak ground acceleration or spectral acceleration at a given period ($Sa(T_1,5\%)$). Here we use first-mode spectral acceleration. This IM is used to quantify both the rate of occurrence of future earthquake ground motions (hazard) and the effect of these ground motions on the structure (response).In this thesis we use single parameter, or scalar, IMs that are traditionally used.

The seismic risk analysis of a structure requires the assessment of both the rate of occurrence of future earthquake ground motions (hazard) and the effect of these ground motions on the structure (response). These two pieces are often linked with an intensity measure such as spectral acceleration. However, earth scientists typically use the geometric mean of the spectral accelerations of the two horizontal components of ground motion as the intensity measure for *hazard* analysis, while structural engineers often use spectral acceleration of a single horizontal component as the intensity measure for *response* analysis. This inconsistency in definitions is typically not recognized when the two assessments are combined, resulting in unconservative conclusions about the seismic risk of the structure.

However the effect of the selection of the intensity measure on the median curve depends greatly on the characteristics of the structure. Therefore the results already quoted cannot expand to every case. A wide dispersion of values to be scaled for a certain intensity measure implies that the EDP accomplished is sensitive to time histories used. Therefore, the use of an intensity measure that leads to a great dispersion probably is not safe when compared to an intensity measure which for the same scaling levels leads to smaller dispersions achieving however the desired width of θ_{max} on average. As desired θ_{max} we mean the under examination performance levels which we want the structure to accomplish (Immediate Occupancy, Life Safety, Collapse Prevention).

3.6.6 Incremental Dynamic Analysis

The concept of Incremental Dynamic Analysis (IDA) method was firstly conceived by Bertero (1977) and Nassar and Krawinkler (1991) and afterwards it was presented in different approaches (for example Luco and Cornell (2000); Mwafy and Elnashai (2001)). However, it has been established as a main method for the assessment of structural performance by Vamvatsikos and Cornell (2002). In analogy to the standard incremental static or pushover analysis where the side loads increase gradually, in the incremental dynamic analysis the structural model is subjected to properly selected ground motion records which are scaled to correspond to gradually increasing intensity levels. A series of dynamic analyses are performed and the corresponding response quantities are derived. In their work Vamvatsikos and Cornell (2002) used the older variations of the method in order to reach the best method for the performance-based design approach. The resulting IDA curves include the pairs of intensity measure versus response quantity for each level of intensity and each record. The main objective of an IDA analysis is to develop a curve that indicates the overall structural performance through a relation between the seismic intensity level and the corresponding maximum response of the structural system in a manner similar with the load-displacement curve of the static pushover analysis (Vamvatsikos and Cornell 2002).

The intensity level and the structural response are described by the intensity measure (IM) and engineering demand parameter (EDP), respectively. The implementation of IDA involves the following steps: (a) development of the nonlinear finite-element model which is necessary to perform nonlinear dynamic analyses; (b) selection of a suite of earthquake records consistent with a design scenario; (c) selection of a proper intensity measure and an engineering demand parameter; (d) application of an algorithm which chooses the best scaling factors in order to perform IDA with the least required nonlinear dynamic analyses; (e) scaling of the sample records to test structural response from elastic response to collapse; (f) performing the dynamic analyses of the structural model and evaluation of the engineering demand parameter that corresponds to each intensity level; (e) using of a suitable technique to summarize the multiple records results.

The selection of IM and EDP is an issue of critical importance for the IDA methodology. In the work by Giovenale *et al.* (2004) the significance of selecting an efficient IM is discussed The IM should be a monotonically scalable ground motion parameter like the PGA, PGV, the 5% damped spectral acceleration at the structure's first-mode period ($S_a(T_1,5\%)$) as well as many other single parameters, or even a combination of parameters, e.g., a vector (Baker and Cornell 2003). In this study the $S_a(T_1,5\%)$ is selected, since it is the most commonly used intensity measure in practice today for the analysis of buildings. An indicative $S_a(T_1,5\%)$ versus maximum inter-storey drift IDA curve is shown in figure 3.16.

We can quantify the damage by using any of the EDPs whose values can be related to particular structural damage states. Ghobarah *et al.* (1999) propose that the EDPs may be organized into four categories which are based on: maximum deformation; cumulative damage; a combination of maximum deformation and cumulative damage; global engineering demand parameters. The IDA analyses of this study were performed selecting maximum interstorey drift $\theta_{\max}$ as the engineering demand parameter. The maximum interstorey drift is selected because of the established relation between inter-storey drift values and performance-based descriptions such as immediate occupancy, life safety and collapse prevention (FEMA-273 (1997)). Also θ_{max} is directly related to joint rotations; thus, is usually considered as an appropriate EDP selection for multi-storey building response. Moreover, there is a defined relation between drift ratio and damage-states (Ghobarah (2004)).

The difference between IDA and multi-stripe analysis is that IDA is based on the time integration of every earthquake record separately while on multi-stripe analysis all records are scaled to the same intensity. Thus, each record uses different values of scaling factor and for each record a different IDA is incurred. The mean curve is generated by summarizing all these curves. This procedure, as shown in figure 3.16, is preferable because the response of every curve of the structure has significant differences in the maximum capacity in $S_a(T_1,5\%)$ which depends on the record.

In figure 3.14 three capacity curves, which came up from three different earthquake records, are presented for a nine-floor steel frame (Fragiadakis et al. 2006). It is obvious that the capacity curve depends not only on the structure but also on the earthquake record. For small values of the intensity measure, approximately 0.2g the outcome is elastic but the IDA curves don’t have a steady slope. As the intensity grows it is observed in some cases that the slope is reduced, as in the case of the static capacity curve and in some other cases the response has hardened and the slope is increased.

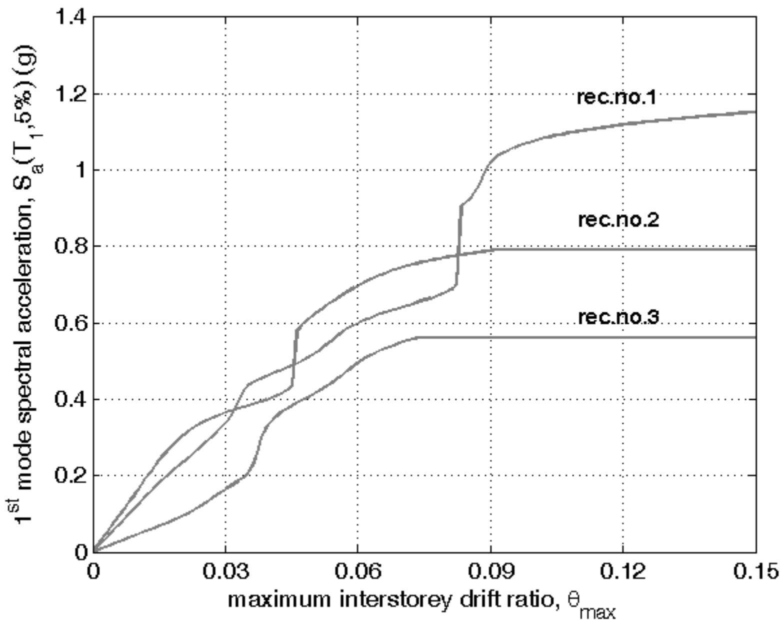

Figure 3.14: Incremental Dynamic analysis curves for three records for the nine-storey steel moment-resisting frame.

The increase of the slope of the capacity curve is due to the characteristics of the earthquake record. As the earthquake record is scaled the cycles in the beginning of the record, which were not intense may change the dynamic characteristics of the structure. Thus the impact of the next more intense loading cycles which of the record may provoke smaller impact θ_{max}. Especially in buildings with many floors the increase in loading often produce yielding in some stories at the base of the construction, relieving the higher floors which as it is observed, usually suffer from maximum interstorey drifts.

For the needs of the performance-based design and keeping in mind that the capacity curves differ from record to record, the mean curve is computed as well as the curves for 16 and 84 percentile. The median curve for 30 records is shown in figure 3.15 and in figure 3.14 the three curves of the thirty records are depicted. Except for the capacity curve we can easily obtain other information regarding the response of the structure depending on the intensity measure. As an example figure 3.11 shows the distribution of the interstorey drift which reflect the capacity curves of the figure 3.11 for the three levels of intensity measure $S_a(T_1,5\%)$.

IDA is sensitive to each seismic record characteristics. Significantly different $S_a(T_1,5\%)$ values are expected for different earthquake records; thus, different scaling factors are used for each seismic record to correspond to specific intensity levels and one IDA curve is associated to each seismic record. The median IDA capacity curve for a single structure is derived from the IDA curves of the whole range of the imposed seismic records. In Figure 3.14 three capacity IDA curves corresponding to a steel moment-resisting frame are depicted, in which seperate IDA analyses were performed for three different seismic records. It is obvious that the capacity curve depends not only on the type of the structure but also on the seismic record that is imposed on the structure. For lower values of the PGA in the vicinity of 0.4g the response of the structure can be considered almost elastic and the inclination of the curves are almost constant as shown in figure 3.14. However, as the intensity becomes higher the capacity curves began to differ significantly, presenting either stabilization at a certain value of PGA or $Sa(T_1,5\%)$ or increase of the inclination due to hardening.

The diversity in the curves' inclination depends on the seismic record and the inelastic response of the structure. This is explained by the fact that as the record is scaled up, weak cycles in the early part of the response time-history may become strong enough to provoke damage (yielding). During the subsequent strong cycles the dynamic characteristics of the structure have already been altered at a great extend; thus; the overall response is significantly different than that at lower intensity levels. “For multi-storey buildings, a stronger ground motion may lead to earlier yielding of one floor which in turn acts as a fuse to relieve another (usually higher) one. Even simple oscillators when caused to yield in an earlier cycle, may be proven less responsive in later cycles that had previously caused higher EDP values, as it is shown in record 3 in figure 3.14, possibly due to “period elongation”. The same phenomena account for the structural resurrection, an extreme case of hardening, where a system is pushed all the way to global collapse (i.e the analysis code cannot converge, producing ‘numerically infinite’ values of the EDPs) at some values of the IM, only to reappear as non-collapsing at a higher intensity level, displaying but still standing (e.g., figure 3.14-record 1)" (Vamvatsikos and Cornell, 2004).

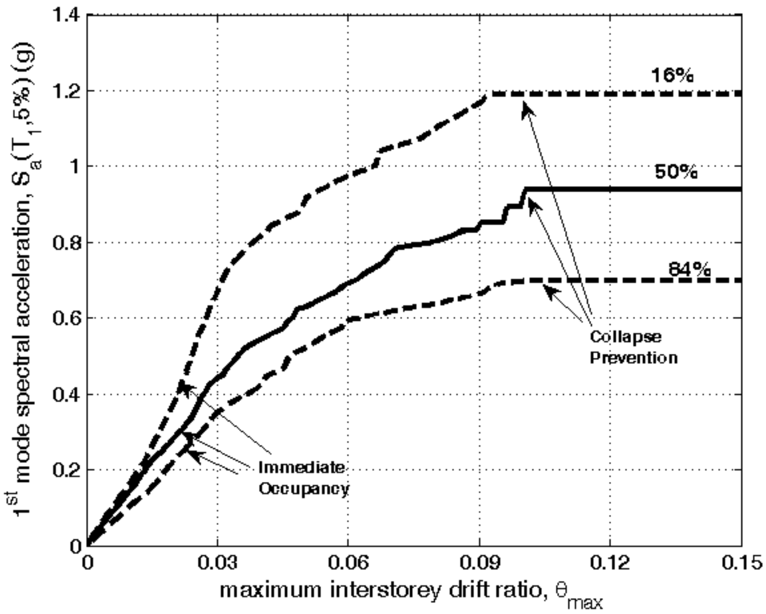

Figure 3.15: Median capacity curves and its 16% and 84% percentiles for the nine-storey steel moment-resisting frame.

Usually 12 to 14 analyses for each seismic record are enough in order to develop an IDA curve. These runs are performed by using the hunt and fill tracing algorithm, described in detail by Vamvatsikos and Cornell (2004). This algorithm allows a wise scaling of earthquake records in order to bound the IM parameter space, and then fills in the gaps, both capacity and demand-wise (Vamvatsikos and Cornell, 2004). The hunt-and-fill tracing algorithm ensures that the record scaling levels are appropriately selected to minimize the number of required runs, reducing the computational cost. Analyses are performed at rapidly increasing levels of IM until non–convergence of the direct integration procedure is occurred (denoting global dynamic instability). In order to sufficiently capture the global collapse and increase the accuracy at lower IMs additional analyses are performed at intermediate IM levels. The user only needs to specify the desired accuracy for demand and capacity, select the maximum tolerable number of dynamic analyses, and then wait for a few hours to get the results. (Vamvatsikos and Cornell, 2004).

The additional runs are being placed sequentially in the middle of the largest IM gaps. Thus the large gaps left by the initial increasing steps to the flatline are filled in; these additional runs ensure that the algorithm has not missed an earlier step collapse and increase the demand resolution. For the estimation of the demanded performance levels, it is essential to depict the limit states on the IDA curves (Vamvatsikos and Cornell (2004)).

In order to design the demand for different performance-based levels it is necessary to draw on the capacity curves the different limit states. As an example in the figure 3.15 the IDA curve is designed at the level of immediate occupancy and that of collapse prevention which are suggested from FEMA-350. In accordance with FEMA-350 for steel structures with full-moment connections, the level of immediate occupancy is exceeded when θ_{max}>10%. As shown in figure 3.15 the two limit states are broken when $S_a(T_1,5\%)>0.3g$ and $S_a(T_1,5\%)>0.91g$.

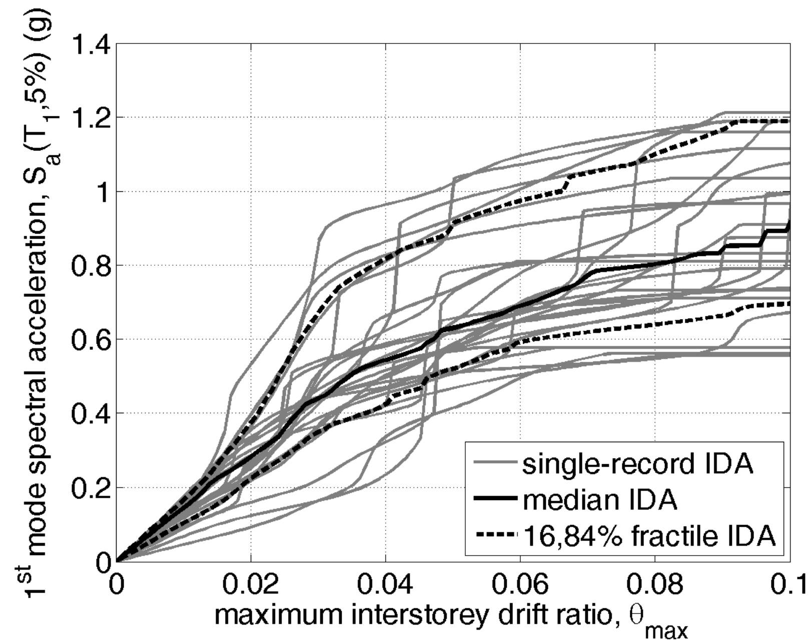

Figure 3.16: IDA curves-median and 16th with 84th percentiles for the nine-storey steel moment-resisting frame.

3.7 Conclusions

In this chapter performance assessment methods have been discussed. The nonlinear performance assessment methods are advantageous because they can predict more accurately the performance of a structure. The scaling procedure discussed based on the IM's is the most widely used by the engineers in order to scale seismic records. The IM which is mostly used is the first-mode spectral acceleration. Furthermore, the EDP chosen in this study is the maximum interstorey drift. The cloud analysis and IDA are also presented with the IDA being the most popular in recent studies. The difference between IDA and multi-stripe analysis is the scaling factor. IDA uses the hunt-and-fill algorithm which tracks down the scaling factor causing collapse of the structure and fills the remaining IDA curve with nonlinear response history analysis points. Multi-stripe analysis uses a constant step of the scaling factor.

3.8 References

Antoniou, S. and Pinho, R. (2004). "Development and Verification of a Displacement-based adaptive pushover procedure." *Journal of Earthquake Engineering*, Vol. 8(5), pp.643-661.

ASCE/SEI Standard 41-06; 2006. Seismic Rehabilitation of Existing Buildings, prepublication edition, Structural Engineering Institute, American Society of Civil Engineers.

ASCE/SEI Standard 41-13; 2014. Seismic Evaluation and Retrofit of Existing Buildings, Structural Engineering Institute, American Society of Civil Engineers.

Aschheim, M., Tjhin, T., Comartin, C., Hamburger, R., Inel, M. (2007). "The scaled nonlinear dynamic procedure", Engineering Structures, Vol. 29(7), 1422-1441.

ATC-40 (1996). "Seismic Evaluation and Retrofit of Concrete Buildings." California Seismic Safety Commission, Report No. SSC 96-01, Applied Technology Council, Redwood City, California, USA.

Baker, J.W., Cornell C.A. (2006) "Vector-Valued Ground Motion Intensity Measures for Probabilistic Seismic Demand Analysis", John A. Blume

Earthquake Engineering Center. Report No. 150 Report#150, Stanford, CA.

Bracci, J.M., Kunnath, S.K., and Reinhorn, A.M. (1997). “Simplified Seismic Performance and Retrofit Evaluation.” Journal of Structural Engineering, Vol. 123(3), pp. 3-10.

Benjamin, J.R. and C.A. Cornell, (1970), *Probability, Statistics, and Decision for Civil Engineers*, McGraw-Hill, New York.Bertero, V.V. (1977). “Strength and deformation capacities of buildings under extreme environments.” In Structural Engineering and Structural Mechanics, Pister KS (ed.). Prentice-Hall: Englewood Cliffs, NJ, pp. 211-215.

Chopra, A.K. (2001). “Dynamics of Structures: Theory and Applications to Earthquake Engineering (2nd edn).” Prentice-Hall, Englewood Cliffs, N.J.

Chopra, A.K. and Goel, R.K. (2001). “Direct Displacement-Based Design: Use of Inelastic vs. Elastic Design Spectra.” Earthquake Spectra, Vol. 17(1), pp. 47-65.

Chopra, A.K. and Goel, R.K. (2002). ”A modal pushover analysis procedure for estimating seismic demands for buildings.” Earthquake Engineering & Structural Dynamics, Vol. 31(3), pp. 561-582.

Cornell, C.A. and Krawinkler, H. (1999) “Advancing Performance-Based Earthquake Engineering”, PEER Center News 2(1),January 1999 pp. 1-3.

Eberhard, M.O., and Sozen, M.A. (1993). “Behavior-Based Method to Determine Design Shear in Earthquake-Resistant Walls.” Journal of the Structural Division, ASCE, Vol. 119(2), pp.619–640.

Eurocode 3 (1993). “Design of steel structures. Part1.1: General rules for buildings.” European Committee for Standardisation. Brussels.

Eurocode 8 (2003). “Design of structures for earthquake resistance, Part 1, European standard, CEN 1998-1, Draft No. 6”, European Committee for Standardization, Brussels.

Fajfar, P., and Fischinger, M. (1988). “N2—A Method for Non-Linear Seismic Analysis of Regular Structures.” Proceedings of the Ninth World Conference on Earthquake Engineering, Tokyo-Kyoto, Japan.

Fajfar, P. and Gaspersic, P. (1996). “The N2 method for the seismic damage analysis for RC buildings”, Earthquake Engineering & Structural Dynamics, 25:23-67.

Fajfar, P. (1999). “Capacity spectrum method based on inelastic demand spectra.” Earthquake Engineering & Structural Dynamics, Vol. 28 (9), pp. 979-99.

FEMA-273, NEHRP Guidelines for the Seismic Rehabilitation of Buildings, Building Seismic safety Council for the Federal Emergency Management Agency, Washington DC,1997.

FEMA-356 (2000). Prestandard and commentary for the seismic rehabilitation of buildings. Federal Emergency Management Agency, Washington DC, SAC Joint Venture.

FEMA-440 (2005): Improvement of Nonlinear Static Seismic Analysis Procedures. Federal Emergency Management Agency: Washington, DC.

Fragiadakis, M., Papadrakakis, M. (2008) “Modeling, analysis and reliability of seismically excited structures: Computational issues.” International Journal of Computational Methods; 5(4): 483-511.

Freeman, S.A. (1998). “Capacity spectrum method as a tool for seismic design”, Proceedings of the Eleventh European Conference on Earthquake Engineering, A.A. Balkema, Rotterdam.

Ghobarah A, Abou-Elfath H, Biddah A. 1999. “Response-based damage assessment of structures”, Earthquake Engineering and Structural Dynamics, 28(1):79-104.

Ghobarah, A., (2004) “On drift limits associated with different damage levels, International Workshop on Performance-Based Seismic Design”, June 28-July 1.

Giovenale P, Cornell CA, Esteva L. (2004) “Comparing the adequacy of alternative ground motion intensity measures for the estimation of structural responses”, Earthquake Engineering and Structural Dynamics, 33(8):951-979.

Goel, R.K. (2005). “Evaluation of Modal and FEMA Pushover Procedures Using Strong-Motion Records of Buildings.” Earthquake Spectra, Vol. 21(3), pp. 653-684.

International Code Council (ICC) (2000). International Building Code (IBC), Falls Church, VA.

Jalayer, F., Cornell, C.A., 2002 “Alternative Nonlinear Demand Estimation Methods for Probability-Based Seismic Assessments.” Earthquake Engng. Struct.Dyn.,00:1-6.

Katsanos, E.I., Sextos, A.G., Manolis, G.D. (2010) “Selection of Earthquake Ground Motion Records: a State-of-the-art review from a structural engineering perspective.” Soil Dynamics and Earthquake Engineering 30(4) 157-169.

Krawinkler, H. and Miranda, E. (2004). “Performance-based earthquake engineering, In Earthquake Engineering: From Engineering Seismology to Performance-based Earthquake Engineering” (Y.Bozorgnia and Vitelmo V. Bertero (Eds), CRC Press)

Krawinkler, H and Seneviratna, G.D.P.K. (1998). “Pros and cons of a pushover analysis of seismic performance evaluation.” Engineering Structures, Vol. 20(4-6), pp. 452-464.

Kottke, A. Rathje, E.M. (2008). “A semi-automated procedure for selecting and scaling recorded earthquake motions for dynamic analysis”, Earthquake Spectra, 24(4): 911-932.

Luco, N. and Bazzurro, P. (2007). “Does amplitude scaling of ground motion records result in biased nonlinear structural drift responses?” Earthquake Engineering and Structural Dynamics, 36(13), 1813-1835.

Luco, N. and Cornell, C.A. (2000). “Effects of connection fractures on SMRF seismic drift demands.” ASCE Journal of Structural Engineering, Vol. 126, pp. 127-136.

Maniatakis, Ch.A., Psycharis, I.N., Spyrakos, C.C., Effect of higher modes on the seismic response and design of moment-resisting RC frame structures, Engineering Structures 56, 417-430, (2013).

Martinez-Rueda, J.E. (1998) “Scaling procedure for natural accelerograms based on a system of spectrum intensity scales”, Earthquake Spectra, 14(1): 135-152.

Mitropoulou Ch.Ch, Lagaros N.D, Papadrakakis M. (2010). “Economic building design based on energy dissipation: a critical assessment”, Bulletin of Earthquake Engineering, 8(6): 1375-1396.

Mitropoulou Ch.Ch (2011). “Advanced computational methods for seismic design and assessment of reinforced concrete structures” National Technical University of Athens, School of Civil Engineering, Institute of Structural Analysis and Antiseismic Research, Athens,Greece.

Mwafy, A.M. and Elnashai, A.S. (2001). “Static pushover versus dynamic collapse analysis of RC buildings.” Engineering Structures, Vol. 23(5), pp. 407-424.

Nau, J.M. and W.J.Hall, (1984) “Scaling methods for earthquake response spectra” Journal of Structural Engineering. 110: 1533-1548.

Newmark N.M., Rosenblueth E. (1971) “Fundamentals of Earthquake Engineering”, Prentice-Hall, Englewood Cliffs, NJ.

Penelis, G.G. and Kappos, A.J. (1997). “Earthquake-resistant concrete structures”, E&FN SPON (Chapman & Hall), London.

PEER (2008). PEER NGA Database. Pacific Earthquake Engineering Research Center. available from http://peer.berkeley.edu/smcat/, last accessed on 2008.

Priestley, M.J.N, Calvi, G.M., Kowalsky, M.J. (2007) “Displacement Based Seismic Design of Structures”, IUSS Press.

Vamvatsikos, D., Cornell, C.A. (2002). “Incremental dynamic analysis”, Earthquake Engineering and Structural Dynamics, 31(3), 491–514.

Vamvatsikos, D., Cornell, C.A. (2004). “Applied incremental dynamic analysis”, Earthquake Spectra, 20(2), 523–553.

Watson-Lamprey, J, Abrahamson, N. (2006). “Selection of ground motion time series and limits on scaling”, Soil Dynamics and Earthquake Engineering, 26(5), 477-482.

CHAPTER 4

Uncertainty in structural engineering

4.1 Theoretical approaches to uncertainty

Natural sciences, which arise from the mathematical interpretation of natural phenomena, used in the past to interpret the random results of experiments as a deficiency of the mathematical models rather than as a property of nature itself. In those times, uncertainty was rejected as a natural phenomenon because of the enthusiastic illusion of a science being able to provide exact answers. The foremost example of this deterministic world-view was Newtonian physics and classical mechanics as developed by Galileo and Newton.

However, in later times, the introduction of mathematical models for probability and randomness became an absolute necessity in order to explain physical phenomena in thermodynamics and quantum mechanics. From that point on, the old paradigm of an exact science was abandoned in those areas where the evidence and the magnitude of randomness could no longer be ignored.

Two broad types of uncertainties can be considered in general: (i) *aleatory* uncertainty; and (ii) *epistemic* uncertainty. The word aleatory derives from the latin word *alea*, which means the rolling of dice. Thus, an aleatory uncertainty is one that is presumed to be the intrinsic randomness of a phenomenon arising because of natural, unpredictable variation in the performance of the system under study. The word epistemic derives from the Greek word «*επιστήμη*», which means science. Thus, an epistemic uncertainty is one that is presumed as being caused by lack of knowledge (or data) about the behavior of the system. Most problems of engineering interest involve both types of uncertainties. The distinction between these two types can be useful in engineering analysis because epistemic uncertainty is reducible. Although some have suggested that a clear distinction between the two types can be made, in the modeling phase it is often difficult to determine whether a particular uncertainty should be put in the aleatory category or the epistemic one and thus the distinction is rather determined by our modeling choices (Der Kiureghian and Ditlevsen 2009). It has been found that both aleatory and epistemic uncertainty can be treated and analyzed, either separately or combined, using probability theory and statistics.

4.2 Uncertainty in structural mechanics

Uncertainties in structural mechanics, analysis and design play an extremely important role. They affect not only the safety and reliability of structures and mechanical components, but also the quality of their performance. Structural engineering requires safety levels that correspond to extremely low probabilities of significant consequences on the structures. Although this has been mankind's prime structural safety requirement for centuries, the means to achieve it has varied widely over time. In an effort to increase safety and structural reliability, safety factors were adopted by code committees in the 1970s in a subjective manner - without a probability basis - and they applied reasonably well to standard common structures. These factors developed through experience and have been adjusted over the years as confidence developed in the various building methods and systems. When confidence in a system was high and good performance has been shown over the years, the safety factors were gradually reduced by small increments over a number of versions of the applicable code. On the other hand, when accidents or failures occurred, there was a corresponding increase in safety factors. The codes we use today for structural engineering design have been largely formed based on this slow, evolutionary process.

The trial and error process described above, for the determination of safety factors, is slow and costly and it is quite incapable to adapting to new technologies and new environments in time. As we enter into periods of rapid technology developments, this adaptive method has become unable to account for our increasing needs. Probability-based methods, with the means to apply measures to uncertainty, are the obvious choice for the development of safety factors for these new technologies, providing the means to accommodate new loadings, materials and systems and to drive the appropriate information acquisition to the proper design of such systems.

Nowadays, there are fields of science where the consideration of randomness is well established, such as quantum mechanics and other branches of modern physics. Safety factors in all modern design codes are based on probability and uncertainty. Only the seismic codes have been left behind.

It can be said that randomness has been in fact considered in structural design in the past, but not in a systematic manner from an analytical - mathematical point of view. While in conventional, deterministic procedures the qualitative assessment of uncertainties is considered to be sufficient, more modern developments concentrate on their rational assessment, i.e. by quantification. This is accomplished by applying methods of statistics and probability and more recently also methods based on fuzzy sets. The fields which emerged from those developments are denoted as *Computational Stochastic Mechanics* as well as *Structural Reliability*.

It should be noted that the basic objective of these methods is not only to account for the probabilities, but mainly to make decisions about structural safety issues, thus probabilities are to be used in a decision making context. It is obvious that the reliability requires a scientifically-oriented calculation, whereas safety factors are a mere practical tool for producing a qualified product. Probability-based safety analysis should become the basis for safety factors in codes of practice and standards, and it is increasingly used to set structural safety requirements for specific structural systems. Its application is rational, in the sense that it uses probability theory to deal with uncertainty. It permits the code committees and individuals responsible for setting safety standards, with the means to be accountable. It permits the evolution of safety standards to proceed by adapting to new information without waiting for unfortunate events to occur in order to trigger changes in safety levels, as was the case in the past. Therefore, in the near future, probability-based safety analysis is bound to move into the mainstream of structural engineering practice.

4.3 Reliability analysis of structures

In this dissertation the formal probabilistic framework for seismic design and assessment of structures and its application to steel moment-resisting frame buildings is used. This is the probabilistic basis for the 2000 SAC Federal Emergency Management Agency (FEMA) steel moment frame guidelines. The framework is based on realizing a performance objective expressed as the probability of exceeding a specified performance level. Performance levels are quantified as expressions relating generic structural variables "demand" and "capacity" that are described by nonlinear, dynamic displacements of the structure. Common probabilistic analysis tools are used to convolve both the randomness and uncertainty characteristics of ground motion intensity, structural "demand", and structural system "capacity" in order to derive an expression for the probability of achieving the specified performance level. Stemming from this probabilistic framework, a safety-checking format of the conventional "load and resistance factor" is developed with load and resistance terms being replaced by the more generic terms "demand" and "capacity", respectively. This framework also allows for a format based on quantitative confidence statements regarding the likelihood of the performance objective being met. This format has been adopted in the SAC/FEMA guidelines (Cornell *et al.* 2002).

Consistent with modern seismic assessment procedures in the nuclear community (DOE 1994), the probabilistic analysis separately characterizes both the randomness and the uncertainty in demand and capacity. Based on these assessments the engineer is provided in these guidelines with a confidence statement with respect to the likelihood of unacceptable behavior. A more detailed presentation of this and other such frameworks is provided by Jalayer and Cornell (1998, 2002).

4.4 State-of-art assessment and design frameworks

In contrast to typical static (or quasi-static) loading situations, the infrequent nature of seismic loads and their nearly unbounded magnitude invariably introduces the dimension of time. Thus, the basic safety inequality assessment of action versus resistance does not provide an adequate description of seismic safety. Given that when a ground motion violates the inequality we cannot necessarily assume that the building has failed, the real question is how often is such an event going to happen in the lifetime of the structure, and what consequences this violation of the safety inequality (or failure) will have.

Furthermore, nowadays structural assessment is not only about estimating the structural response. Engineering quantities such as displacements, accelerations, plastic rotations, shear forces and moments make very little sense to stakeholders (e.g., building owners, insurance companies or governments). Non-engineers typically communicate in financial terms, such as the net present value of an investment. This shift in the focus of assessment marks the advent of modern “performance-based” (or “consequence-based”) earthquake engineering that has essentially become the mainstay of contemporary earthquake research. In this section, we discuss important elements of such methodologies, focusing on the measurement/definition of structural performance over the lifetime of the structure.

4.4.1 Deterministic versus Probabilistic frameworks

Typically, seismic intensity for a given mean annual frequency, structural demand for a given intensity and structural capacity/resistance to inelastic deformation, are modeled by lognormal random variables characterized by heavy right tails and large probabilities of exceeding values to the right of the mean. Such distributions are represented by the mean and standard deviation of their logarithmic values, or equivalently by their median μ and dispersion β, the latter being numerically very similar to the coefficient of variation (for values less than 0.7). Natural record-to-record dispersion is typically in the order of 30-40% at least, compounded with seismic hazard values whose uncertainty exceeds 100%. Thus, accurately quantifying and propagating such sources of variability all the way to structural response and performance estimates has become an important issue. While the consideration of multiple ground motion records, e.g., through IDA, may take care of the record-to-record variability, structural model uncertainty is still an open problem in earthquake engineering (Vamvatsikos and Fragiadakis (2010), Dolsek (2009), Kazantzi *et al* .(2008), Der Kiureghian and Ditlevsen (2009), Liel *at al.* (2009), Mehanny and Ayoub (2008)).

Nevertheless, seismic assessment is at its core a discipline that is practiced by professional engineers and it has deep roots in the tradition of infrastructure design over many decades. Therefore, seismic codes and guideline documents typically emphasize a deterministic approach where probabilistic aspects are roughly (and hopefully conservatively) approximated through “appropriate” choices of load levels and safety factors. Thus, all codified nonlinear static procedure (NSP) approaches essentially lack any trace of variability. The obvious shortcomings and constraints placed by such simplifying assumptions have been recognized over the years, contributing to the emergence of performance-based earthquake engineering, where, among others, proper characterization of structural response, damage and loss are essential features. Perhaps the best introduction to this never-ending discussion is offered by Bazzurro et al. (Bazzuro et al. (1998)) who compare the three fundamental frameworks for assessing structural performance, comparing the deterministic NSP against the conditional and the non-conditional probabilistic approaches.

Conditioning on the value of the intensity measure (IM), as already discussed, effectively separates the tasks of the seismologist and the structural engineer. At the cost of selecting a sufficient IM that can incorporate all the necessary seismological information without biasing the analysis, this also has the effect of massively reducing the number of required structural analyses. It is no wonder, then, that conditional approaches have dominated the scene from the very start. Arguably, the two most prominent such frameworks are offered by the PEER Center and the SAC/FEMA guidelines.

4.4.2 The PEER framework

Adopting a Poisson model for earthquake events allows expressing the structural performance via annualized earthquake-related losses. These may be quantified, e.g., by the triptych of repair costs, downtime and casualties that has been adopted by the Pacific Earthquake Engineering Research (PEER) Center in the form of the Cornell-Krawinkler framing equation (Cornell and Krawinkler (2000)):

$$\lambda(DV) = \iiint G(DV \mid DM) \cdot \left|\mathrm{d}G(DM \mid EDP)\right| \cdot \left|\mathrm{d}G(EDP \mid IM)\right| \cdot \left|\mathrm{d}\lambda(IM)\right| . \qquad (4.1)$$

DV is a single or a vector of decision variables, such as cost, time-to-repair or human casualties that are meant to enable decision making by stakeholders. *DM* represents the damage measures, typically discretized in a number of Damage States (e.g. red/yellow/green) of structural or non-structural elements and building contents. *EDP* contains the engineering demand parameters such as interstory drift or peak floor acceleration and *IM* is the seismic intensity, for example the 5%-damped first-mode pseudo spectral acceleration $Sa(T_1,5\%)$. The function $\lambda(y)$ provides the mean annual frequency (MAF) of exceedance of y, while $G(x)$ is the complementary cumulative distribution function (CCDF) of variable x.

The simplified formulation of Eq. (4.1) has received some criticism (Der Kiureghian (2005)), yet its usefulness has been proven in many ways in the past years. One of its most important applications is the probabilistic estimation of losses from seismic events (Yang *et al*. (2009)). This has originally appeared in the form of the assembly-based vulnerability method of Porter *et al.* (2001) for assessing repair losses and downtime. It was further improved and integrated with the PEER methodology by Aslani and Miranda (2005) who also incorporated the dichotomy of collapse versus non-collapse. Finally, Ramirez and Miranda (2012) provided the third generation loss assessment framework by adding the influence of residual displacements on the probability of demolition and the associated decommissioning costs. This is a rapidly evolving area of research and many improvements are expected to appear over the next few years.

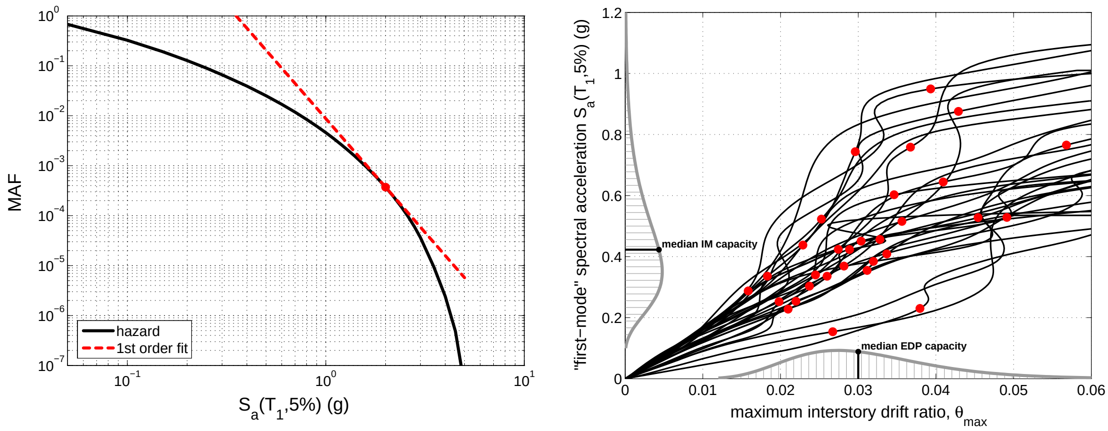

(a) (b)

Figure 4.1 (a) Sa seismic hazard curve of Van Nuys, CA for T = 2.35s and its power law fit, (b) IDA curves, collapse points and EDP_c, IM_c lognormal distributions for a 9-story steel frame (from D.Vamvatsikos (2014)).

4.4.3 The SAC/FEMA framework

Despite the usefulness of the comprehensive PEER approach, defining performance without involving any *DV* or the closely related *DM often* makes more sense for practice. Engineering quantities may be preferable, especially when working at the level of design, to discern the superior structure. This may be best achieved by moving to the familiar territory of limit-states: Let *DV* and *DM* be indicator variables that become unity when a given limit-state (LS) is exceeded, Eq. (4.1) simplifies to estimate λ_{LS}, the MAF of violating the limit-state (Jalayer and Cornell, 2009):

$$\lambda_{\mathrm{LS}} = \int_0^{+\infty} \left[\int_0^{+\infty} F(EDP_c \mid EDP)\, f(EDP \mid IM)\, \mathrm{d}EDP \right] \cdot \left| \frac{\mathrm{d}\lambda(IM)}{\mathrm{d}IM} \right| \mathrm{d}IM \qquad (4.2)$$

where F is the cumulative distribution function (CDF), f the probability density function (PDF) and EDP_c is the limit-state capacity expressed in terms of the EDP. The nested integral is often represented as $F(IM_c|IM)$, the CDF of the IM capacity for the limit-state, better known as the fragility function. In general, EDP_c and IM_c are intimately related probabilistic quantities that characterize a limit-state for a given structural system, best visualized on the IM-EDP coordinates of the familiar IDA curves (Figure 4.1b).

Eq. (4.2) may be less complex than the PEER framework, yet it is not simple enough for practical application. The breakthrough came with the work of Cornell *et al.* (2002) who, motivated by the failures observed in steel frames during the 1994 Northridge earthquake, developed a closed-form solution for the SAC/FEMA guidelines (FEMA-350 (2000), FEMA-351 (2000)). Therein, the hazard curve function $\lambda(IM)$ is approximated by a linear fit in log-log coordinates (see figure 4.1a) with a slope of k. If the EDP demand is lognormal with a conditional median of:

$$EDP_{50} \cong a \cdot (IM)^b \qquad (4.3)$$

and dispersion β_d, while the EDP capacity is also assumed lognormal with parameters EDP_{c50} and β_c, Eq. (4.2) becomes:

.

$$\lambda_{LS} \cong \lambda\left[\left(\frac{EDP_{c50}}{a}\right)^{\frac{1}{b}}\right]\exp\left[\frac{k^2}{2b^2}\left(\beta_d^2 + \beta_c^2\right)\right] \qquad (4.4)$$

The effect of epistemic uncertainty of demand and capacity can also be incorporated either by appropriately inflating the argument of the exponential to estimate either an overall mean, or value that will not be exceeded with a given confidence.

Such expressions offer a direct estimate of structural performance by capitalizing on the power of nonlinear static or dynamic analyses (Jalayer and Cornell (2009)) and PSHA to offer useful intuition into the effect of hazard, structural behavior and associated uncertainties on the estimated MAF of limit-state exceedance. The SAC/FEMA formulas have thus become the state-of-art in the attempt to provide a performance basis for seismic design and assessment. Subsequent work, though, has shown them to be prone to errors (Aslani and Miranda 2005), especially when the curvature of λ(IM) is significant (Bradley and Dhakal (2008)). A biased fit that better matches the hazard to the left of the median capacity (Dolsek and Fajfar (2008)), or, even better, a second-order fit paired with improved closed-form expressions (Vamvatsikos D. (2012)) can reduce such errors substantially, opening the road for wide-spread implementation.

4.5 <u>Basic Approach: Probability Assessment Formulation</u>

The objective is to show how the demand and capacity factors γ and φ, as well as *v*, the confidence factor in the SAC guidelines, have been derived by elementary probability theory from representations of the three random elements of the problem. These elements begin with the ground motion intensity, characterized here by the level of the spectral acceleration Sa at approximately the first natural period of the structure, and 5% or higher damping (Shome et al. 1998). The spectral displacement S_D may be a more natural choice for this displacement scheme but we shall retain the more commonly available measure Sa; the results and conclusions are the same. The other two random elements are the displacement demand D and the displacement capacity C. Both demand and capacity will be presumed here to be measured in terms of the maximum interstorey drift angle, i.e., the largest drift. The likelihood of various levels of future intense ground motions at the site are represented in the standard way by the hazard function $H(s_a)$, which gives the annual probability that the random intensity *Sa* at the site will equal or exceed Sa. This is provided by earth scientists on a site specific or mapped regional basis. The prediction of the drift demand given any particular level of ground motion and the estimation of the capacities of various “failure modes” are essential for structural engineers. The developments here focus on these two elements and specifically on their probabilistic representations. Finally, it must be recognized that all such probabilistic predictions and representations are uncertain estimates; explicit quantification and analysis of these uncertainties will be addressed subsequently.

The goal is to provide criteria based on desired performance objectives which are defined as specified probabilities of exceeding the performance level, such as the collapse-prevention damage state (Yun et al. 2002) and life safety damage state. To do so one must fold together the probabilistic representations of the three elements above. In keeping with the general design approach of separately considering demand and capacity, comparison at the displacement or drift level, this folding together is done in two steps. The first step couples the first two basic elements Sa hazard and drift demand (versus or conditional on Sa), to produce a (structure specific) drift hazard curve $H_D(d)$. This curve provides the annual probability (or strictly speaking the mean annual frequency) that the drift demand D exceeds any specified value d. The second step combines this curve with the third element, the drift capacity representation, to produce P_{PL}, the (annual) probability of the performance level not being met (e.g., the annual probability of collapse or the annual probability of exceeding the life safety level).

Using the total probability theorem (Benjamin and Cornell 1970), $H_D(d)$ becomes, in discrete form:

$$H_D(d) = P[D \geq d] = \sum_{all x_i} P[D \geq d \mid S_a = x_i] P[S_a = x_i] \tag{4.5}$$

To facilitate the computations, the probability of interest has been expanded by conditioning on all possible levels of the ground motion as can be seen in Eq.4.5.

The second factor within the sum, the likelihood of a given level of spectral acceleration $P[S_a = x_i]$, can easily be obtained from the standard hazard curve *H(s_a)*. In the first factor $P[D \geq d \mid S_a = x_i]$ one sees what the structural response analysis must be responsible for providing: the likelihood that the drift exceeds *d* given that the value of S_a is known. In continuous, integral form Eq.4.5 is

$$H_D(d) = \int P[D \geq d \mid S_a = x] \left| dH(x) \right| \tag{4.6}$$

In which the notation $\left| dH(x) \right|$ means the absolute value of the derivative of the site's spectral acceleration hazard curve times *dx*, i.e., loosely the likelihood that S_a=x. (The absolute value is needed only because the derivative is negative).

Using the total probability theorem again P_{PL} itself becomes (in discrete form)

$$P_{PL} = P[C \leq D] = \sum_{all d_i} P[C \leq D \mid D = d_i] P[D = d_i] \tag{4.7}$$

The second factor, the likelihood of a given displacement demand level P[D=*d*], can be determined from the drift hazard curve derived in Eq. (4.2). The first factor, the likelihood that the drift capacity is less than a specified value *d* given that the drift demand equals that value, $P[C \leq D \mid D = d]$ can to a first approximation be assumed to be independent of the information about the drift level itself, permitting this term to be simplified as below:

$$P_{PL} = \int P[C \leq d] \left| dH_D(d) \right| \tag{4.8}$$

The second factor $\left| dH_D(d) \right|$ is defined as above for the ground motion hazard curve: as the absolute value of the differential of the drift demand hazard curve.

4.6 Probabilistic calculations in performance-based earthquake engineering

In a reliability analysis problem, the purpose is to calculate the limit-state probability of failure or the limit-state mean annual frequency of exceedance. For earthquake engineering problems where the performance based design concept is implemented, the probability has to be determined for every performance level. Therefore, the term “failure probability” is replaced by “probability of exceedance conditional on the limit-state”, or simply by “limit-state probability of exceedance”. The probability is calculated by applying the total probability theorem and conditioning the probabilities on the parameter that expresses the intensity of the seismic action IM.

The mean annual frequency of exceeding a limit-state refers to the annual rate that an engineering demand parameter (EDP) exceeds a given capacity level (*edp*). The MAF of a limit-state is denoted as *v* and is calculated using the total probability theorem:

$$v_{LS}(edp \le EDP) = \int_{0}^{+\infty} P(edp \le EDP \mid IM = im) \left| \frac{dv(IM)}{dIM} \right| \mathrm{d}IM \qquad (4.9)$$

where $P(EDP > edp \mid IM = im)$ is the limit-state probability that an engineering demand parameter exceeds a threshold value, conditional on a given intensity value *im*; the second term of the integral of Eq.4.9 is the slope of the hazard curve or, in other words, it is the mean annual rate of ground motion intensity, IM. The absolute value is used because the slope has a negative value. Eq.4.9. allows the integration of the results of structural analysis with data produced by seismologists. The first term of the integral of Eq.4.9 is also known as ‘fragility’ or vulnerability curve.

MAF is the convolution integral of the limit-state fragility curve with the site hazard curve. Thus, the MAF calculation consists of a structural engineering part, which is the calculation of the limit-state fragilities, and an engineering seismology part that refers to estimating the site hazard curve. The seismic hazard at a site is obtained through probabilistic seismic hazard analysis (PSHA) and is represented by a hazard curve (figure 4.1a). A limit-state is assumed exceeded when the engineering demand parameter (EDP) chosen exceeds the corresponding threshold value.

The calculation of Eq. 4.9 requires first to determine the limit-state fragilities, while the slope $d\nu(IM)/dIM$ is extracted from the site hazard curve. In order to calculate analytically the fragility, it is assumed that the maximum interstorey drift, at a given intensity $S_a(T_1,5\%)$ level, follows the lognormal distribution. Thus, the probabilities are calculated as follows:

$$P(EDP > edp \mid IM = im) = \Phi\left[\frac{\ln(edp) - \ln(\hat{\theta}_{\max})}{\hat{\delta}}\right] \tag{4.10}$$

where $\ln(\hat{\theta}_{\max})$ and $\hat{\delta}$ are the logarithmic mean and the standard deviation of $\hat{\theta}_{\max}$, respectively, given the intensity level $Sa(T_1,5\%)$.

For performance-based design, pairs of hazard levels and corresponding performance levels have to be set, depending on the type of the structure. Therefore, the response is evaluated for a number of objectives, following the FEMA-356 (2000) terminology: immediate occupancy (IO), life safety (LS) and collapse prevention (CP). Each objective corresponds to a given probability of being exceeded during the life span of a structure, typically considered equal to 50 years. A usual assumption is that the immediate occupancy level corresponds to a 50% probability of exceedance, the life safety level to a 10% probability and the collapse prevention to 2% probability of being exceeded, all referring to a 50-year time window.

4.7 References

Aslani, H., Miranda, E., (2005) “Probabilistic earthquake loss estimation and loss disaggregation in buildings", Report No. 157, The John A. Blume Earthquake Engineering Research Center, Stanford University, Stanford, CA.

Aslani, H., Miranda, E., (2005) “Probability-based seismic response analysis.” Engineering Structures 27 (8): 1151–1163.

Bazzurro, P., Cornell, C.A., Shome, N., Carballo, J.E., (1998) “Three proposals for characterizing MDOF nonlinear seismic response”, Journal of Structural Engineering ASCE 124(11): 1281–1289.

Benjamin, J.R. and C.A. Cornell, (1970), *Probability, Statistics, and Decision for Civil Engineers*, McGraw-Hill, New York.

Bradley, B.A., Dhakal, R.P. (2008) “Error estimation of closed-form solution for annual rate of structural collapse.” Earthquake Engineering and Structural Dynamics 37: 1721-1737.

Cornell, C. A., Jalayer, F., Hamburger, R.O, and Foutch, D. A., M.ASCE (2001) “Probabilistic basis for 2000 SAC Federal Emergency Management Agency Steel Moment Frame Guidelines”, J. Struct. Eng., 128(4), 526-533.

Cornell, C.A., Krawinkler, H., (2000) Progress and challenges in seismic performance assessment, PEER Center News 3 (2) URL http://peer.berkeley.edu/news/2000spring/index.html (accessed Oct 2012).

Cornell, C.A., Jalayer, F., Hamburger, R.O., Foutch, D.A., (2002) “The probabilistic basis for the 2000 SAC/FEMA steel moment frame guidelines”, Journal of Structural Engineering ASCE 128 (4): 526–533.

Der Kiureghian, A., Ditlevsen, O., (2009) “Aleatory or Epistemic? Does it matter?” Structural Safety 31: 105–112.

Der Kiureghian, A. (2005) “Non-ergodicity and PEER’s framework formula”, Earthquake Engineering and Structural Dynamics 34 (13): 1643–1652.

DOE (1994). “Natural phenomena hazards design and evaluation criteria for Department of Energy facilities” DOE-STD-1020-94, Washington, D.C.

Dolsek, M., (2009) “Incremental dynamic analysis with consideration of modelling uncertainties”, Earthquake Engineering and Structural Dynamics 38(6): 805–825.

Dolšek, M., Fajfar, P. (2008) “The effect of masonry infills on the seismic response of a four storey reinforced concrete frame-a probabilistic assessment.” Engineering Structures 30(11): 3186-3192.

FEMA-356: Prestandard and commentary for the seismic Rehabilitation of buildings, Federal Emergency Management Agency, Washington, DC, 2000.

Fib, Probabilistic performance-based seismic design, Bulletin 68, International Federation of Structural Concrete, Lausanne, CH, 2012.

Jalayer, F. and Cornell, A. (1998) “Development of a probability-based demand and capacity factor design seismic format.” Internal Technical Memo, Dept. of Civil and Environmental Engineering, Stanford Univ. Stanford, Calif.

Jalayer, F. and Cornell, A. (2002). “A technical framework for probability-based demand and capacity factor (DCFD) seismic formats” RMS Technical Rep. No 43 to the PEER center, Dept. of Civil and Environmental Engineering, Stanford, Calif.

Jalayer, F., Cornell, C.A., (2009) “Alternative non-linear demand estimation methods for probability-based seismic assessments”, Earthquake Engineering and Structural Dynamics 38 (8): 951–1052.

Kazantzi, A.K., Righiniotis, T.D., Chryssanthopoulos, M.K., (2008) “Fragility and hazard analysis of a welded steel moment resisting frame.” Journal of Earthquake Engineering 12(4) 596–615.

Liel, A.B., Haselton, C.B., Deierlein, G.G., Baker, J.W., (2009) “Incorporating modeling uncertainties in the assessment of seismic collapse risk of buildings”, Structural Safety 31 (2) 197–211.

Mehanny, S.S.F., Ayoub, A.S. (2008) “Variability in inelastic displacement demands: Uncertainty in system parameters versus randomness in ground records”, Engineering Structures 30: 1002–1013.

Porter, K.A., Kiremidjian, A.S., LeGrue, J.S. (2001) “Assembly-based vulnerability of buildings and its use in performance evaluation”, Earthquake Spectra 17 (2): 291–312.

Ramirez, C.M., Miranda, E. (2012) “Significance of residual drifts in building earthquake loss estimation”, Earthquake Engineering and Structural Dynamics 41:1477–1493.

SAC Joint Venture (2000). “Recommended seismic design criteria for new steel moment-frame buildings.” Report No. FEMA-350, prepared for the Federal Emergency Management Agency, Washington DC.

SAC Joint Venture (2000). “Recommended seismic evaluation and upgrade criteria for existing welded steel moment-frame buildings.” Report No.

FEMA-351, prepared for the Federal Emergency Management Agency, Washington DC.

Vamvatsikos, D. and Fragiadakis, M. (2010) “Incremental dynamic analysis for estimating seismic performance uncertainty and sensitivity”, Earthquake Engineering and Structural Dynamics 39 (2) 141–163.

Vamvatsikos, D., “Derivation of new SAC/FEMA performance evaluation solutions with second-order hazard approximation”, Earthquake Engineering and Structural Dynamics DOI: 10.1002/eqe.2265 (accepted).

Vamvatsikos, D., (2014) “Accurate application and second-order improvement of the SAC/FEMA probabilistic formats for seismic performance assessment”, Journal of Structural Engineering ASCE DOI: 10.1061/(ASCE)ST.1943-541X.0000774 (accepted).

Yang, T.Y., Moehle, J., Stojadinovic, B., Der Kiureghian, A. (2009) “Seismic performance evaluation of facilities: Methodology and implementation”, Journal of Structural Engineering ASCE 135 (10): 1146–1154.

Yun, S.-Y., Hamburger, R. O., Cornell, C.A. and Foutch, D. A. (2002). “Seismic Performance evaluation for steel moment frames” J. Struct. Eng. 128(4), 534-545.

CHAPTER 5

Assessment of the bias introduced in IDA due to scaling

5.1 Introduction

Nonlinear response history analysis (NRHA) lies in the core of the incremental dynamic analysis method (IDA) (Vamvatsikos and Cornell 2002), where the structure is subjected to a suite of ground motion records. Every record is scaled to multiple levels of intensity, producing the structure's capacity curve in terms of an engineering demand parameter (EDP) versus an intensity measure (IM). IDA provides a powerful performance estimation framework, which, however, is often questioned due to the scaling of records with factors that are considerably different from one. This practice leads to ground motions that may not represent a realistic physical process and may under- or over-estimate the demand, or in other words, may introduce bias (συστηματικό σφάλμα) in the capacity estimation.

IDA provides the median demand in EDP-IM terms and also calculates the corresponding dispersion. However, little information is available on whether the demand estimations offered are biased due to record scaling. The primary concern with record scaling is whether 'weak' records when scaled up will be representative of 'strong' records. The problem also depends on the intensity measure adopted and on the properties of the structure examined. This chapter systematically investigates the effect of record scaling and provides a rational approach for measuring the bias introduced when IDA analysis is performed.

5.2 Literature review

Past studies on the scaling practice propose limits on the scaling factors. The early studies of Vanmarcke (1979) and Krinitzsky and Marcuson (1983), report that in general, the scaling factor should lie between 0.5 and 2.0 or 0.25 and 4.0, respectively. In Shome *et al.* (1998) it is shown that small-to-moderate scaling factors do not introduce bias in the response estimation. It was also shown that there are structures for which scaling does not introduce bias, e.g. moderate period buildings in sites with no directivity. In their IDA paper, Vamvatsikos and Cornell (2002) discuss the “legitimacy” of the scaling practice stating that the problem depends on the structure, the EDP, the IM and the number of records. The bottom line of their discussion is that scaling is legitimate when the choice of the IM is such that the IM values, conditional on the EDP, are effectively independent of the magnitude and the distance scenario. Furthermore, Iervolino and Cornell (2005) suggest that, for magnitudes between 6.4 and 7.4, there is no need for a careful site-specific process of record selection by magnitude and distance. They also observed that scaling arbitrarily selected records to match the strength of stronger records does not introduce bias in the seismic demand estimations. Their findings were based on analyses with scale factors up to 4 and ductility demands up to 6. These conclusions were based on records divided into bins where the mean scaling factor of every bin was equal to one. Luco and Bazzuro (2007) observed biased responses when the mean scale factor of a bin was larger than one. They show that scaled records chosen with a magnitude-distance criterion can introduce bias in the median response that increases with the degree of scaling. They show that the amount of bias depends on the fundamental period of the structure, its strength and the sensitivity of the structure to higher modes. Furthermore, according to Baker (2007) when the number of records that are scaled up is approximately equal to the number of records that are scaled down unbiased median interstory drift ratios are obtained.

Other researchers have proposed approaches to select records that can be scaled without biasing the response (e.g. Watson-Lamprey and Abrahamson 2006). Baker and Cornell (2006) proposed selecting seismic records using the epsilon ‘ε’-method in order to reduce the bias. The epsilon parameter “ε” is defined as the number of standard deviations between the observed spectral value and the median value of a ground motion prediction equation. Other approaches for using scaled records in nonlinear response history analysis (NRHA) are presented by Aschheim et al. (2007) and Kottke and Rathje (2008), while Iervolino et al. (2010) compared different procedures for obtaining sets of spectral matching accelerograms. They show that artificial, or adjusted, accelerograms may underestimate the displacement response compared to original natural records. Grant and Diaferia (2013) investigate the possible bias introduced when using records that have been scaled to match the design spectrum. A review of alternative selection procedures based on established methods for incorporating strong ground motions records within the framework of seismic design of structures is given in Katsanos et al. (2010). Grigoriu (2011) presented theoretical arguments and analytical results implying that significant discrepancies from actual response may be introduced by scaling natural earthquake records. Rathje et al. (1998) studied the characterization of the frequency content of earthquakes with three parameters: T_m, mean period, predominant period T_p and the smoothed spectral predominant period T_0. It is shown that the mean period (T_m) is preferred.

The above studies focus on the bias introduced on the building’s performance estimation when nonlinear response history analysis with scaled records is performed. In this work we investigate this issue in the context of the Incremental Dynamic Analysis (IDA) method. To assess the bias due to record scaling in IDA, we obtain limit-state response statistics using a large number of both natural and synthetic ground motion records. The bias is assessed both quantitatively and qualitatively for the full range of limit-states, thus providing useful information about scaling and its legitimacy in the context of IDA.

5.3 Structural models

The building models considered are single- and multi-degree-of-freedom (SDOF and MDOF, respectively), covering a wide-range of building configurations. The SDOF oscillators vary from very stiff to soft systems of medium-to-long periods, while the MDOF systems are two well-known benchmark buildings.

5.3.1 Single-degree-of freedom structures

Six SDOF oscillators, having period values of T=0.1, 0.3, 0.5, 0.7, 1.0 1.5 and 2.0 were examined. The force-displacement (F-δ) relationship of the SDOFs is multilinear following the generic capacity curve of Figure 5.1. The capacity is fully described by five parameters: the elastic stiffness k_{el}, the hardening stiffness (k_h=$a_h k_{el}$), the capping ductility (δ_c =$\mu_c \delta_y$), the post-capping stiffness (k_c=$a_c k_{el}$) and the residual strength (F_r=λF_y) which begins at δ_r=$\mu_r \delta_y$. These systems are able to degrade exhibiting both cyclic and in-cycle degradation and therefore are able to realistically capture the response of a structure.

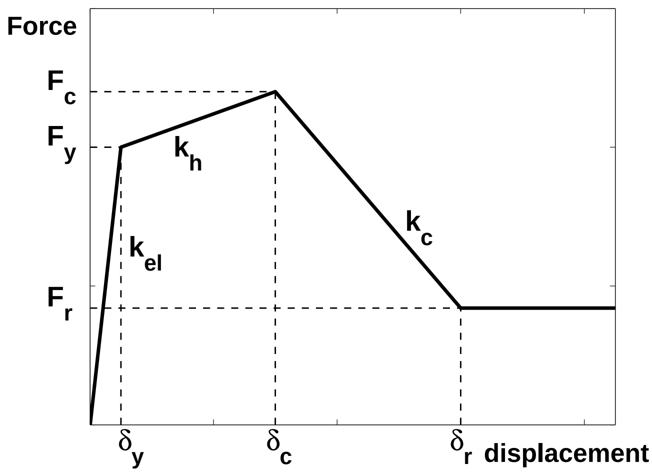

Figure 5.1: Force displacement curve of a quadrilinear SDOF oscillator

The SDOF systems were modeled using the “hysteretic” material model of the material library of the OpenSees platform (McKenna and Fenves 2001). This material allows for cyclic stiffness and strength degradation. Similar behavior is assumed in the positive and the negative directions. The damping ratio was considered equal to 5% of the critical, while for both models the assumed post-yield stiffness was a_{el}=0.01 and the yield strength F_y was taken 20% of the total weight. The remaining parameters that describe the response curve were set equal to: a_c=-0.5, μ_c=3, λ=0.5, while the pinching factor for strain and stress was assumed equal to 0.5 thus assuming moderate pinching. The material parameters that define damage due to ductility and energy absorption were set equal to zero.

If the curve in figure 5.1 stops at (δc, Fc), i.e. we have only two line segments: the line segment from point (0,0) to the point (δy, Fy) and the line segment from point (δy, Fy) to the point (δc, Fc), then we have the bilinear case of the oscillator.

5.3.2 Multi-degree-of-freedom structures-Steel Moment Frame Buildings

The MDOF structures considered are two steel moment-resisting frames that have been designed for a Los Angeles site according to the 1997 NEHRP (National Earthquake Hazard Reduction Program) provisions. The models (figure 5.2b) are denoted as LA3 (three-storey steel moment resisting frame) and LA9 (nine-storey steel moment resisting frame). The buildings have been designed following contemporary design code requirements, thus adhering to the strong-column, weak-beam design philosophy. For both structures, centerline models are used to model the two-dimensional exterior moment-resisting frame of each building, while the analyses were performed using the OpenSees platform. The cross sections and the geometry of the two buildings are shown in figure 5.2b. The fundamental periods of the frames are T_1=0.93s and T_1=2.34s, respectively. Both buildings are essentially first-mode dominated, although the LA9 building has some sensitivity to higher modes.

Geometric nonlinearities in the form of P-Δ effects were included in our analyses. The effect of the internal gravity frames was explicitly considered with a leaning column as suggested in the FEMA P-695 (2009) guidelines. The columns are assumed elastic, while component models are positioned at the beam-ends allowing plastic rotations to develop according to a moment-rotation relationship.

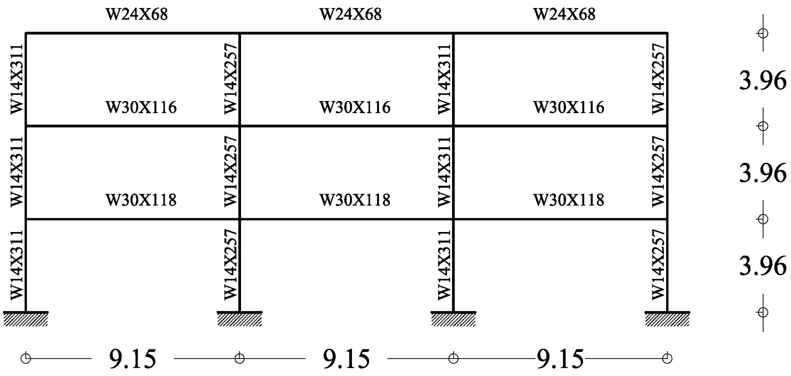

Figure 5.2.a: Geometry and cross-sections of steel moment resisting frames: three-storey (LA3) building

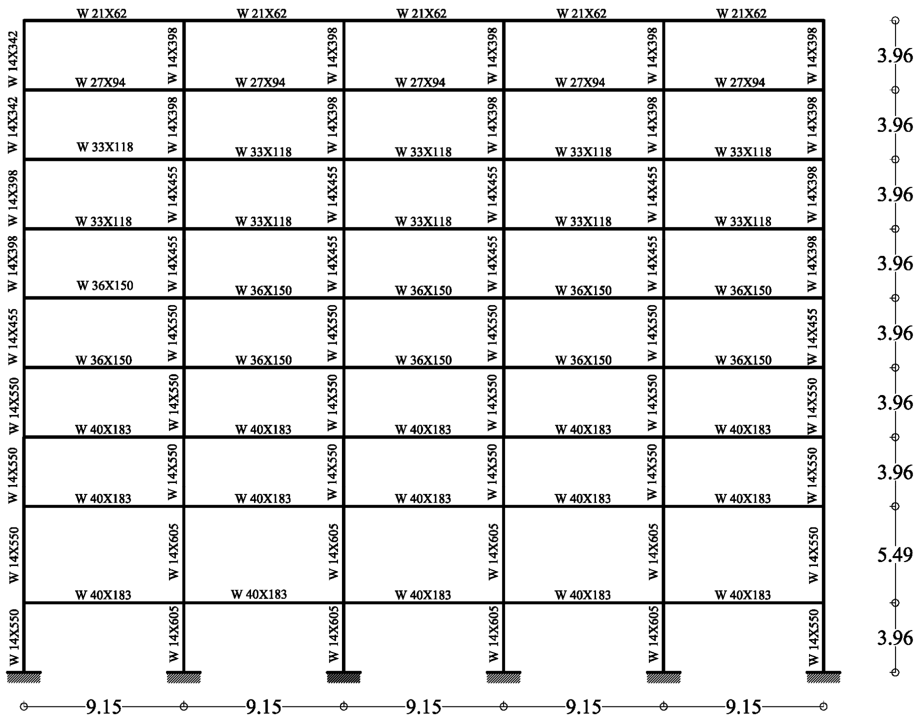

Figure 5.2b: Geometry and cross-sections of steel moment resisting frames: nine-storey (LA9) building.

The moment-rotation relationship assumed, is multilinear with a response curve that can be described with parameters similar to those of the degrading SDOF oscillators of figure 5.1 (assuming that the curve refers to moment-rotation instead of force-displacement quantities). The corresponding parameter values were set equal to a_h=0.01, μ_c=3, a_c=-0.5, λ=0.5, similar to those of the SDOFs.

5.4 Maximum scaling factor

The maximum scaling factors usually applied within an IDA can be estimated with some simple calculations. Figure 5.3 shows the $S_a(T_1,5\%)$ values for the set of ground motion records whose properties are discussed in section 'Ground motion records' and listed in Table 1. The records are unscaled and the $S_a(T_1,5\%)$ values considered refer to the peak ground acceleration (T_1=0sec), while T_1 is set equal to 0.93 and 2.3sec corresponding

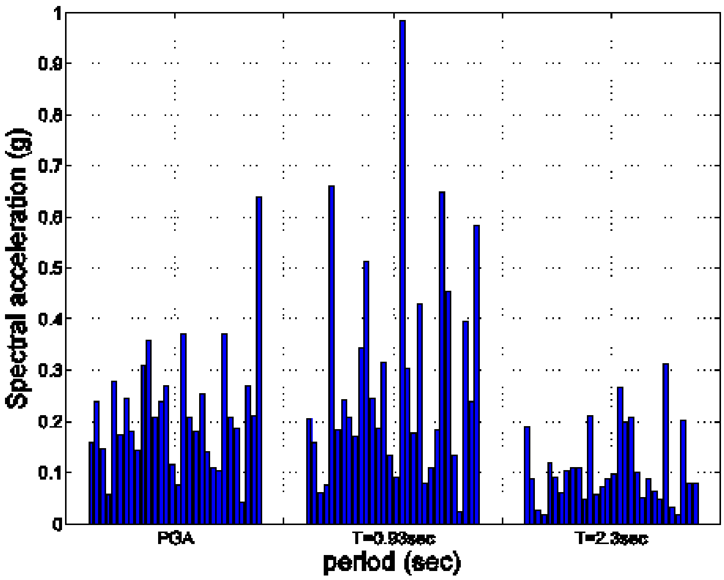

Figure 5.3: Spectral acceleration values for a typical 30-record suite of ground motions. PGA and Sa(T1,5%) values for T1=0.93 and 2.34sec are shown.

to the first mode period values of the LA3 and the LA9 building, respectively. In the numerical analysis section we also show that the median $S_a(T_1,5\%)$ collapse capacity of the LA3 frame is 1.6g and of the LA9 frame is 0.91g. According to Figure 5.3, the mean $S_a(T_1,5\%)$ of the whole ground motion set is 0.18g and 0.05g, for T_1=0.93 and T_1=2.3sec, respectively. This means that the average scale factors at collapse are 1.6/0.18=9 and 0.91/0.05=18.2, respectively. These are large and unrealistic values, thus making necessary the discussion on the effect of scaling in IDA. Moreover, it can be seen that due to the natural tendency of ground motion records to have smaller $S_a(T_1,5\%)$ values as T_1 increases, the scaling factors necessary to collapse a frame building are larger for more flexible structures. This observation is contrary to the fact that due to the shape of the design spectrum, stiffer structures are designed for a larger $S_a(T_1,5\%)$ demand.

5.5 Nonlinear regression

Nonlinear regression can be performed with the Loess or the Lowess (locally weighted scatterplot smoothing) algorithms. Both algorithms are strongly related non-parametric regression methods that combine multiple regression models in a *k*-nearest-neighbor-based meta-model. “Loess” is a later generalization of Lowess; although it is not a true initialism, it may be understood as standing for “LOcal regression”.

Loess and Lowess thus build on "classical" methods, such as linear and nonlinear least squares regression. They address situations in which the classical procedures do not perform well or cannot be effectively applied without undue labor. Loess combines much of the simplicity of linear least squares regression with the flexibility of nonlinear regression. It does this by fitting simple models to localized subsets of the data to build up a function that describes the deterministic part of the variation in the data, point by point. In fact, one of the chief attractions of this method is that the data analyst is not required to specify a global function of any form to fit a model to the data, only to fit segments of the data.

The trade-off for these features is increased computation. Because it is so computationally intensive, Loess would have been practically impossible to use in the era when least squares regression was being developed. Most other modern methods for process modeling are similar to Loess in this respect. These methods have been consciously designed to use our current computational ability to the fullest possible advantage to achieve goals not easily achieved by traditional approaches.

A smooth curve through a set of data points obtained with this statistical technique is called a **Loess Curve**, particularly when each smoothed value is given by a weighted quadratic least squares regression over the span of values of the y-axis scattergram criterion variable. When each smoothed value is given by a weighted linear least squares regression over the span, this is known as a **Lowess curve**; however, some authorities treat Lowess and Loess as synonyms.

5.5.1 Definition of a Loess model

Loess, originally proposed by Cleveland (1979) and further developed by Cleveland and Devlin (1988), specifically denotes a method that is also known as locally weighted polynomial regression. At each point in the data set a low-degree polynomial is fitted to a subset of the data, with explanatory variable values near the point whose response is being estimated. The polynomial is fitted using weighted least squares, giving more weight to points near the point whose response is being estimated and less weight to points further away. The value of the regression function for the point is then obtained by evaluating the local polynomial using the explanatory variable values for that data point. The Loess fit is complete after regression function values have been computed for each of the n data points. Many of the details of this method, such as the degree of the polynomial model and the weights, are flexible. The range of choices for each part of the method and typical defaults are briefly discussed next.

5.5.2 Localized subsets of data

The **subsets** of data used for each weighted least squares fit in Loess are determined by a nearest neighbors algorithm. A user-specified input to the procedure called the "bandwidth" or "smoothing parameter" determines how much of the data is used to fit each local polynomial. The smoothing parameter, α, is a number between $(\lambda+1)/n$ and 1, with λ denoting the degree of the local polynomial. The value of α is the proportion of data used in each fit. The subset of data used in each weighted least squares fit comprises the n*a* points (rounded to the next largest integer) whose explanatory variables values are closest to the point at which the response is being estimated.

Parameter α is called the smoothing parameter because it controls the flexibility of the Loess regression function. Large values of α produce the smoothest functions that wiggle the least in response to fluctuations in the data. The smaller α is, the closer the regression function will conform to the data. Using too small a value of the smoothing parameter is not desirable, however, since the regression function will eventually start to capture the random error in the data. Useful values of the smoothing parameter typically lie in the range 0.25 to 0.5 for most Loess applications.

5.5.3 Degree of local polynomials

The local polynomials fit to each subset of the data are almost always of first or second degree; that is, either locally linear (in the straight line sense) or locally quadratic. Using a zero degree polynomial turns Loess into a weighted moving average. Such a simple local model might work well for some situations, but may not always approximate the underlying function well enough. Higher-degree polynomials would work in theory, but yield models that are not really in the spirit of Loess. LOESS is based on the ideas that any function can be well approximated in a small neighborhood by a low-order polynomial and that simple models can be fit to data easily. High-degree polynomials would tend to overfit the data in each subset and are numerically unstable, making accurate computations difficult.

5.5.4 Weight function

As mentioned above, the weight function gives the most weight to the data points nearest the point of estimation and the least weight to the data points that are furthest away. The use of the weights is based on the idea that points near each other in the explanatory variable space are more likely to be related to each other in a simple way than points that are further apart. Following this logic, points that are likely to follow the local model best influence the local

model parameter estimates the most. Points that are less likely to actually conform to the local model have less influence on the local model parameter estimates.
The traditional weight function used for LOESS is the tri-cube weight function,

$W(x)=(1-|x|^3)^3$ and in general $[|x|<1]$.

However, any other weight function that satisfies the properties listed in Cleveland (1979) could also be used. The weight for a specific point in any localized subset of data is obtained by evaluating the weight function at the distance between that point and the point of estimation, after scaling the distance so that the maximum absolute distance over all of the points in the subset of data is exactly one.

5.5.5 Advantages of Loess

As discussed above, the biggest advantage Loess has over many other methods is the fact that it does not require the specification of a function to fit a model to all of the data in the sample. Instead the analyst only has to provide a smoothing parameter value and the degree of the local polynomial. In addition, Loess is very flexible, making it ideal for modeling complex processes for which no theoretical models exist. These two advantages, combined with the simplicity of the method, make Loess one of the most attractive of the modern regression methods for applications that fit the general framework of least squares regression but which have a complex deterministic structure.

Although it is less obvious than for some of the other methods related to linear least squares regression, Loess also accrues most of the benefits typically shared by those procedures. The most important of those is the theory for computing uncertainties for prediction and calibration. Many other tests and procedures used for validation of least squares models can also be extended to Loess models.

5.5.6 Disadvantages of Loess

Loess makes less efficient use of data than other least squares methods. It requires fairly large, densely sampled data sets in order to produce good models. This is because Loess relies on the local data structure when performing the local fitting. Thus, Loess provides less complex data analysis in exchange for greater simulation costs.

Another disadvantage of Loess is the fact that it does not produce a regression function that is easily represented by a mathematical formula. This can make it difficult to transfer the results of an analysis to other people. In order to transfer the regression function to another person, they would need the data set and software for Loess calculations. In nonlinear regression, on the other hand, it is only necessary to write down a functional form in order to provide estimates of the unknown parameters and the estimated uncertainty. Depending on the application, this could be either a major or a minor drawback to using Loess. In particular, the simple form of Loess cannot be used for mechanistic modeling where fitted parameters specify particular physical properties of a system.

Finally, as discussed above, Loess is a computationally intensive method. This is not usually a problem in our current computing environment unless the data sets being used are very large. Loess is also prone to the effects of outliers in the data set, like other least squares methods. There is an iterative, robust version of Loess [Cleveland (1979)] that can be used to reduce Loess' sensitivity to outliers, but too many extreme outliers can still overcome even the robust method.

5.6 Nonlinear regression on the cloud

Single or multiple “cloud analysis” may be adopted to estimate the conditional demand (or capacity) (Cornell *et al.* 2002, Jalayer and Cornell 2009). When cloud analysis is adopted, the records are scaled using a common scale factor thus forming a cloud in the IM-EDP plane (figure 5.4a) or not scaled at all. Both versions have appeared. Multiple cloud analysis refers to the case where all records are scaled more than once with a common, increasing scale factor.

A building capacity curve in EDP-IM terms can be obtained with the aid of linear or nonlinear regression as we discuss below.

To evaluate the bias in the median capacity estimations of IDA analysis, we perform cloud analysis leaving the records unscaled, i.e. assuming a scale factor equal to one. Given the limitation of cloud analysis to provide the conditional dispersion, we are limited to studying the bias on the median $S_a(T_1,5\%)$ capacities. Moreover, when only natural records are used, the data tend to become scarce for large $S_a(T_1,5\%)$ values. This is due to the lack of recorded ground motions capable to produce large demands (e.g. for $\theta_{max}>0.4$), especially when medium to long period structures founded on dense soil are studied. For such period ranges unscaled ground motions with $S_a(T_1,5\%)$ values above 0.5g are rare. To overcome this problem and obtain statistically significant estimates of the median, we have augmented our ground motion database with synthetic records.

Nonlinear regression is performed on the cloud of the EDP-IM data using the Loess (locally weighted scatterplot smoothing) algorithm (Cleveland and Delvin 1988). The algorithm requires specifying the span of the moving average in order to define a window of neighbouring points that will be included in the calculation. The sensitivity of the regression process to the span value is shown in figure 5.4a. For comparison we also show the least squares fit of the data. A large span of the moving average will increase the smoothness, while a small span will decrease the smoothness and will give a curve that is more sensitive to the data set.

The regression process and the selection of the span value is a source of additional bias on the performance estimation process. To reduce this effect we chose an optimum span value using the *k*-fold cross-validation algorithm (Efron and Tibshirani 1993). According to this method, the cloud is randomly partitioned to *k* subsamples. A single subsample is retained as the validation cloud set and the remaining *k*-1 subsamples are used as the training set to generate the Loess curve. The square of the distance between the Loess curve produced with the training set and the curve produced by the testing set gives the mean-squared error. This approach allows the evaluation of the goodness-of-fit as function of the span value. Figure 5.4b shows the variation of the sum of squared errors against the span. The optimum span value is the one that minimizes the sum of the errors.

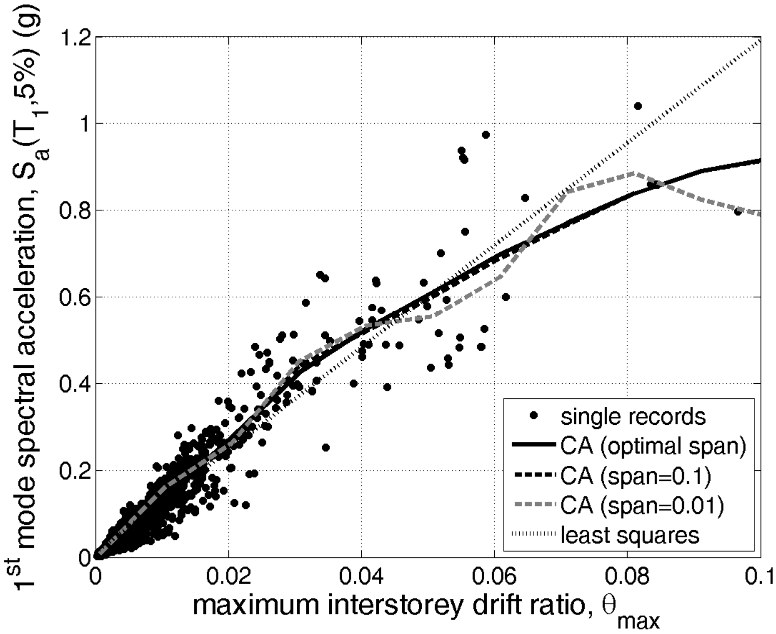

Figure 5.4a: Capacity curves for different span values of the Loess fit.

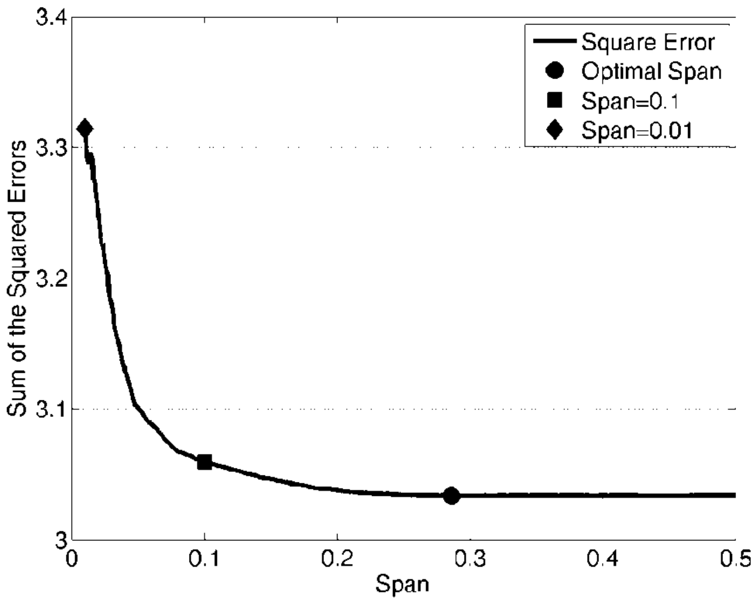

Figure 5.4b: Square error of the Loess fitting as function of the span value of the nine-storey.

5.7 Bootstrap analysis

5.7.1 Generally

Statistics is changing. Modern computers and software make it possible to look at data graphically and numerically in ways previously inconceivable. They let us do more realistic, accurate, and informative analyses than can be done with pencil and paper.

The bootstrap and other resampling methods are part of this revolution. Resampling methods allow us to quantify uncertainty by calculating standard errors and confidence intervals. They require fewer assumptions than traditional methods and generally give more accurate answers (sometimes very much more accurate).

- Fewer assumptions. For example, resampling methods do not require thatdistributions be Normal or that sample sizes be large.
- Greater accuracy. Some bootstrap methods are more accurate in practice than classical methods.
- Generality. Resampling methods are remarkably similar for a wide range of statistics and do not require new formulas for every statistic. You do not need to memorize or look up special formulas for each procedure.
- Promote understanding**.** Bootstrap procedures build intuition by providing concrete analogies to theoretical concepts.

Resampling has revolutionized the range of problems accessible to business people, statisticians, and students. It is beginning to revolutionize our standards of what is acceptable accuracy in high-stakes situations such as legal cases, business decisions, and clinical trials.

5.7.2 Statistical inference

Statistical inference is based on the sampling distributions of sample statistics. The bootstrap is first of all a way of finding the sampling distribution, at least approximately, from just one sample. The procedure consists of the following steps:

Step 1: Resample. Create hundreds of new samples, called bootstrap samples or resamples, by sampling with replacement from the original random sample. Each resample is the same size as the original random sample.

Sampling with replacement means that after we randomly draw an observation from the original sample, we put it back before drawing the next observation. This is like drawing a number from a hat, then putting it back before drawing again. As a result, any number can be drawn once, more than once, or not at all. If we sampled without replacement, we'd get the same set of numbers we started with, though in a different order.

Step 2: Calculate the bootstrap distribution. Calculate the statistic for each resample. The distribution of these resample statistics is called *bootstrap distribution.*

Step 3: Use the bootstrap distribution. The bootstrap distribution gives information about the shape, center, and spread of the sampling distribution of the statistic.

5.7.3 Why does bootstrapping work?

It might seem that the bootstrap creates data out of nothing. This seems suspicious. But we are not using the resampled observations as if they were real data—the bootstrap is not a substitute for gathering more data to improve accuracy. Instead, the bootstrap idea is to use the resample means to estimate how the sample mean of a certain sample from this population varies because of random sampling.

Using the data twice—once to estimate the population mean, and again to estimate the variation in the sample mean—is perfectly legitimate. Indeed, we've done this many times before: for example, when we calculated both $\overline{x}$ and $s/\sqrt{n}$ from the same data. What is different is that:

1. We compute a standard error by using resampling rather than the formula $s/\sqrt{n}$, and

2. We use the bootstrap distribution to see whether the sampling distribution is approximately Normal, rather than just hoping that our sample is large enough for the central limit theorem to apply.

The bootstrap idea applies to statistics other than sample means. To use the bootstrap more generally, we appeal to another principle—one that we have often applied without thinking about it.

5.7.4 The plug-in principle

To estimate a parameter, a quantity that describes the population, use the statistic that is the corresponding quantity for the sample.

The plug-in principle suggests that we estimate a population mean μ by the sample mean $\overline{x}$ and a population standard deviation σ by the sample standard deviation s. Estimate a population median by the sample median. To estimate the standard deviation of the sample mean for an SRS, $\sigma / \sqrt{n}$, plug in s to get $s / \sqrt{n}$. The bootstrap idea itself is a form of the plug-in principle: substitute the distribution of the data for the population distribution, then draw samples (resamples) to mimic the process of building a sampling distribution.

In many settings, we have no model for the population. We then appeal to probability theory, and we also cannot afford to actually take many samples. The bootstrap rescues us. Use the one sample we have as though it were the population, taking many resamples from it to construct the bootstrap distribution. Then use the bootstrap distribution in place of the sampling distribution.

In practice, it is usually impractical to actually draw all possible resamples. We carry out the bootstrap idea by using 1000 or so randomly chosen resamples. We could directly estimate the sampling distribution by choosing 1000 samples of the same size from the original population. But it is very much faster and cheaper to let software resample from the original sample than to select many samples from the population. If we had the ability to perform many analyses, we would prefer to spend it on obtaining a single larger sample rather than many smaller samples. A larger sample gives a more precise estimate.

In most cases, the bootstrap distribution has approximately the same shape and spread as the sampling distribution, but it is centered at the original statistic value rather than the parameter value. The bootstrap allows us to calculate standard errors for statistics for which we don't have formulas and to check normality for statistics that theory does not easily handle.

5.7.5 Summary

1. To bootstrap a statistic (for example, the sample mean), draw hundreds of resamples with replacement from the original sample data, calculate the statistic for each resample, and inspect the bootstrap distribution of the resampled statistics.
2. The bootstrap distribution approximates the sampling distribution of the statistic. This is an example of the plug-in principle: use a quantity based on the sample to approximate a similar quantity from the population.
3. Bootstrap distributions usually have approximately the same shape and spread as the sampling distribution but are centered at the statistic (from the original data) when the sampling distribution is centered at the parameter (of the population).
4. Use graphs and numerical summaries to determine whether the bootstrap distribution is approximately Normal and centered at the original statistic and to get an idea of its spread. The bootstrap standard error is the standard deviation of the bootstrap distribution (Efron B., Tibshirani R. (1993)).
5. The bootstrap does not replace or add to the original data. We use the bootstrap distribution as a way to estimate the variation in a statistic based on the original data.

For most statistics, bootstrap distributions approximate the shape, spread, and bias of the actual sampling distribution.

Bootstrap distributions differ from the actual sampling distributions in the location of their centers. The sampling distribution of a statistic used to estimate a parameter is centered at the actual value of the parameter in the population, plus any bias. The bootstrap distribution, generated by resampling from a single sample, is centered at the value of the statistic for the original sample, plus any bias. The two biases are similar even though the two centers are not.

5.7.6 Two sample problems

Two-sample problems are among the most common statistical settings. In a two-sample problem, we wish to compare two populations, such as male and female customers, based on separate samples from each population. The bootstrap can also compare two populations, without the normality condition and without the restriction to comparison of means. The most important new idea is that bootstrap resampling must mimic the “separate samples” design that produced the original data.

Bootstrap for comparing two populations:

Given independent simple random samples (SRSs) of sizes and from two populations:

1. Draw a resample of size with replacement from the first sample and a separate resample of size from the second sample. Compute a statistic that compares the two groups, such as the difference between the two sample means.
2. Repeat this resampling process hundreds of times.
3. Construct the bootstrap distribution of the statistic. Inspect its shape, bias, and bootstrap standard error in the usual way.

The patterns displayed by the scatterplot smooth are not just chance. We can use the bootstrap distribution of the smoother’s curve to get an idea of how much random variability there is in the curve. Each resample “statistic” is now a curve rather than a single number. The spread of the resample curves about the original curve shows the sampling variability of the output of the scatterplot smoother.

Nearly all the bootstrap curves mimic the general pattern of the original smooth curve. This suggests that these patterns are real, not just chance.

Bootstrap distributions mimic the shape, spread, and bias of sampling distributions. The bootstrap standard error is the standard deviation of the bootstrap distribution. It measures how much a statistic varies under random sampling. The bootstrap estimate of bias is the mean of the bootstrap distribution minus the statistic for the original data. Small bias means that the bootstrap distribution is centered at the statistic of the original sample and suggests that the sampling distribution of the statistic is centered at the population parameter.
The bootstrap can estimate the sampling distribution, bias, and standard error of a wide variety of statistics, such as the trimmed mean.
To bootstrap a statistic that compares two samples, such as the difference in sample means, we draw separate resamples from the two original samples. The interval between the 2.5th and 97.5th percentiles of the bootstrap distribution of a statistic is a 95% bootstrap percentile confidence interval for the corresponding parameter.

5.7.7 Use of the bootstrap

We use the bootstrap method (Efron and Tibshirani 1993) to investigate the significance of our numerical results. Bootstrap is a tool easy to implement that allows calculating the bias or the confidence interval of a response statistic. Bootstrapping is the practice of estimating the properties of a response statistic by random sampling with replacement from the original dataset. For example, if we have an initial population $\mathbf{x}=(x_1, ..., x_n)$ we resample with replacement to get m new populations $\mathbf{x}^m=(x_1^m, ..., x_n^m)$. Sampling with replacement means that some members of $\mathbf{x}$ may appear more than once in $\mathbf{x}^m$. The response statistic of interest is calculated for every sample $\mathbf{x}^m$ to obtain its bootstrap distribution, which contains valuable information about the shape, the center and the spread of the sampling distribution of the response statistic of interest.

This procedure can be also applied in the two-dimensional space, such as smoothed scatter plots. Both IDA and cloud analysis use smoothed scatter plots that consist of points in the EDP-IM space. In this case, **x** contains the coordinates of the data and smoothing is repeated for every bootstrap sample $\mathbf{x}^m$. We then perform Loess on every bootstrap sample on the $\mathbf{x}^m$ bootstrap samples. Confidence intervals can be easily calculated for both IDA and cloud analysis. Let $\bar{S}_a(T_1, 5\%)$ be the median $S_a(T_1,5\%)$ of every smoothed curve, which is always conditional on the EDP (θ_{max}). The subscript '(α)' is used to denote the sample's α% fractile. The (1-α)100% confidence interval is calculated as:

$$\left[\left(\bar{S}_a(T_1, 5\%)\right)^{a/2} \quad , \quad \left(\bar{S}_a(T_1, 5\%)\right)^{(1-a/2)}\right] \tag{5.1}$$

In figure 5.5.a and 5.5.b the estimate of the median and the 95% confidence intervals are shown versus the initial scattered data (figure 5.5a), and 1000 capacity curves generated after bootstrapping the results of cloud analysis (figure 5.5b).

In both plots, the 95% confidence interval on the median is denoted with a dashed bold line, while the solid bold line is the corresponding median curve obtained through bootstrap.

Figure 5.5a and 5.5b show the bootstrap confidence intervals when cloud analysis is applied on the nine-storey steel moment frame. Figure 5.5a shows the initial scattered data obtained through cloud analysis, while figure 5.5b shows the 1000 bootstrap curves plotted as grey lines. For θ_{max} values beyond 0.06, the original data become scarce (Figure 5.5a). However, this occurs for large drift (or intensity) values and thus does not affect the limit-states that are usually of interest.

5.8 Ground motion records

All IDAs were performed with a set of thirty ground motion records. The records used and their properties are listed in Table 5.1. The table contains records of relatively large magnitudes M_w in the range between 6.5 to 6.9, have been recorded on dense soil and bear no marks of directivity. These are ground motion records that have been used in several IDA analyses in the past, e.g. Vamvatsikos and Cornell (2005). Figure 5.6 shows the response spectra of the ground motion set of Table 5.1.

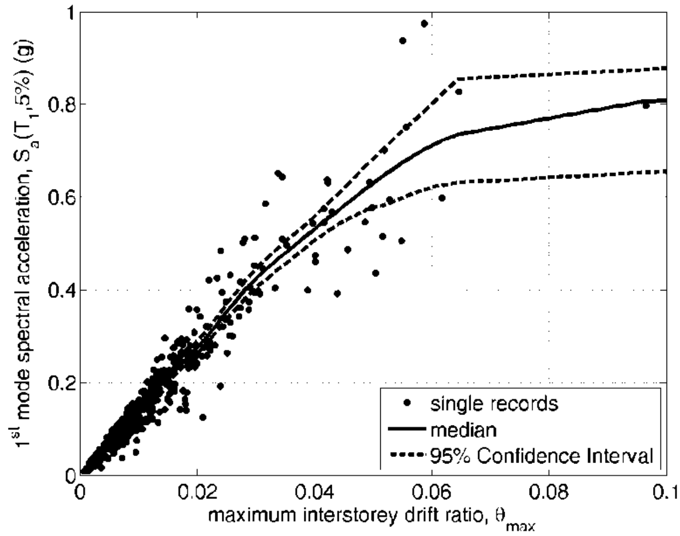

Figure 5.5a: Maximum interstorey drift versus 1^{st} mode spectral acceleration for the initial scattered data.

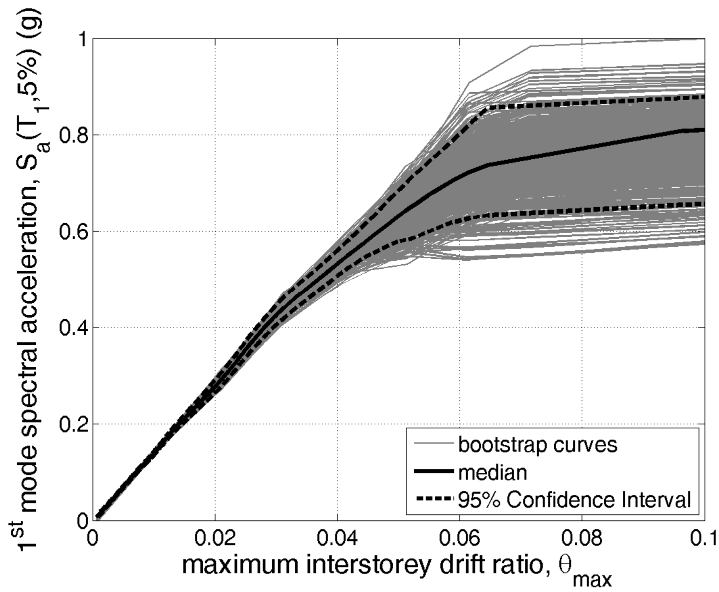

Figure 5.5b: Maximum interstorey drift versus 1st mode spectral acceleration for 1000 capacity curves generated after bootstrapping the results of cloud analysis. Also it can be seen from the figure that we have the 95% confidence interval on the median.

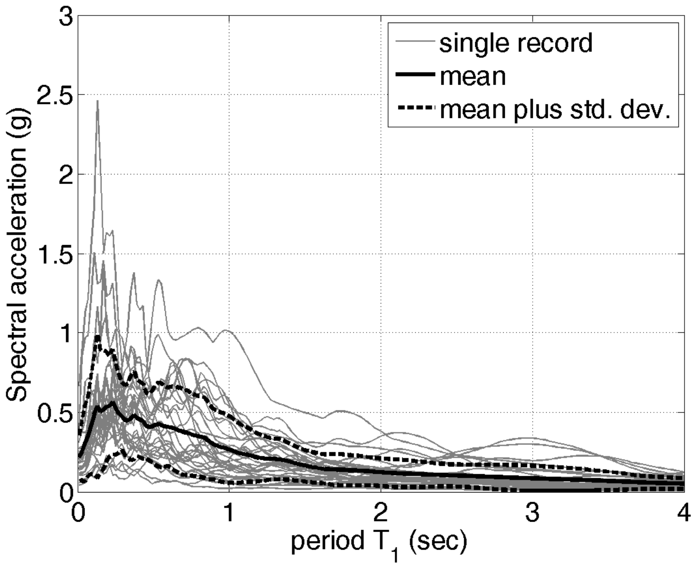

Figure 5.6: Response spectra of the thirty IDA records. The black lines refer to the mean (solid) and the mean plus and minus (dashed) one standard deviation curves.

For cloud analysis, both natural and synthetic ground motions are used. In all, 1480 natural and synthetic records were chosen to perform the NRHAs of cloud analysis. 1015 natural ground motions were selected from the PEER database (PEER NGA Database 2008), ensuring uniform processing, while figure 5.7a shows their response spectra. As discussed in Figure 5.3, only few ground motions have $S_a(T_1,5\%)$ values strong enough to exceed 1g for periods beyond 1sec. Such $S_a(T_1,5\%)$ intensities are not strong enough to cause yielding or collapsing for most of our structures. To overcome this problem we have augmented the ground motion dataset with 465 synthetic records. The response spectra of the synthetic records are shown in figure 5.7b.

In figure 5.7a, 5.7b the response spectra of the natural ground motion (5.7a) and the synthetic ground motion (5.7b) are shown. The black lines refer to the mean plus and minus one standard deviation.

Published results have indicated that simulated ground motions can be used to complement ground motion records for inelastic structural analyses (Luco and Rezaeian 2013). In this study, we used the broadband ground motion simulation model by Liu et al. (2006), a hybrid method that achieves computational efficiency by combining deterministic inelastic simulations in the low-frequency range (<1Hz) with stochastic frequency-domain simulations for higher frequencies (1-10Hz).

Table 5.1. Thirty ground motion records used for IDA.

No	Event	Station	φ^{o} [1]	Soil[2]	M [3]	R [4] (km)	PGA (g)
1	Loma Prieta, 1989	Agnews State Hospital	090	C,D	6.9	28.2	0.159
2	Northridge, 1994	LA, Baldwin Hills	090	B,B	6.7	31.3	0.239
3	Imperial Valley, 1979	Compuertas	285	C,D	6.5	32.6	0.147
4	Imperial Valley, 1979	Plaster City	135	C,D	6.5	31.7	0.057
5	Loma Prieta, 1989	Hollister Diff. Array	255	–,D	6.9	25.8	0.279
6	San Fernando, 1971	LA, Hollywood Stor. Lot	180	C,D	6.6	21.2	0.174
7	Loma Prieta, 1989	Anderson Dam Downstrm	270	B,D	6.9	21.4	0.244
8	Loma Prieta, 1989	Coyote Lake Dam Downstrm	285	B,D	6.9	22.3	0.179
9	Imperial Valley, 1979	El Centro Array #12	140	C,D	6.5	18.2	0.143
10	Imperial Valley, 1979	Cucapah	085	C,D	6.5	23.6	0.309
11	Northridge, 1994	LA Hollywood Storage FF	360	C,D	6.7	25.5	0.358
12	Loma Prieta, 1989	Sunnyvale Colton Ave	270	C,D	6.9	28.8	0.207
13	Loma Prieta, 1989	Anderson Dam Downstrm	360	B,D	6.9	21.4	0.24
14	Imperial Valley, 1979	Chihuahua	012	C,D	6.5	28.7	0.27
15	Imperial Valley, 1979	El Centro Array #13	140	C,D	6.5	21.9	0.117
16	Imperial Valley, 1979	Westmoreland Fire Station	090	C,D	6.5	15.1	0.074
17	Loma Prieta, 1989	Hollister South & Pine	000	–,D	6.9	28.8	0.371
18	Loma Prieta, 1989	Sunnyvale Colton Ave	360	C,D	6.9	28.8	0.209
19	Superstition Hills, 1987	Wildlife Liquefaction Array	090	C,D	6.7	24.4	0.180
20	Imperial Valley, 1979	Chihuahua	282	C,D	6.5	28.7	0.254
21	Imperial Valley, 1979	El Centro Array #13	230	C,D	6.5	21.9	0.139
22	Imperial Valley, 1979	Westmoreland Fire Station	180	C,D	6.5	15.1	0.11
23	Loma Prieta, 1989	Halls Valley	090	C,D	6.9	31.6	0.103
24	Loma Prieta, 1989	WAHO	000	C,D	6.9	16.9	0.37
25	Superstition Hills, 1987	Wildlife Liquefaction Array	360	C,D	6.7	24.4	0.2
26	Imperial Valley, 1979	Compuertas	015	C,D	6.5	32.6	0.186
27	Imperial Valley, 1979	Plaster City	045	C,D	6.5	31.7	0.042
28	Loma Prieta, 1989	Hollister Diff. Array	165	C,D	6.9	25.8	0.269
29	San Fernando, 1971	LA, Hollywood Stor.	090	C,D	6.6	21.2	0.21
30	Loma Prieta, 1989	WAHO	090	C,D	6.9	16.9	0.638

[1] Component
[2] USGS, Geomatrix soil class
[3] Moment magnitude
[4] Closest distance to fault rupture

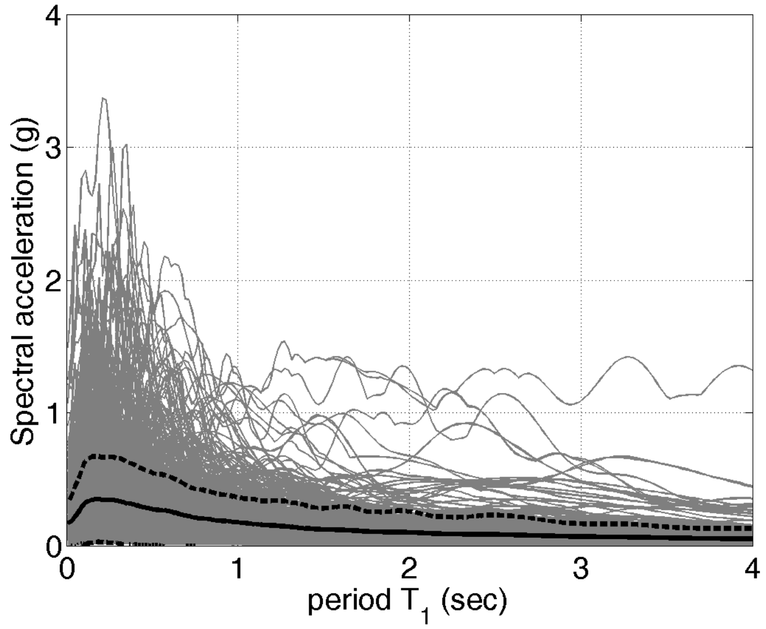

Figure 5.7a: Response spectra for natural ground motion.

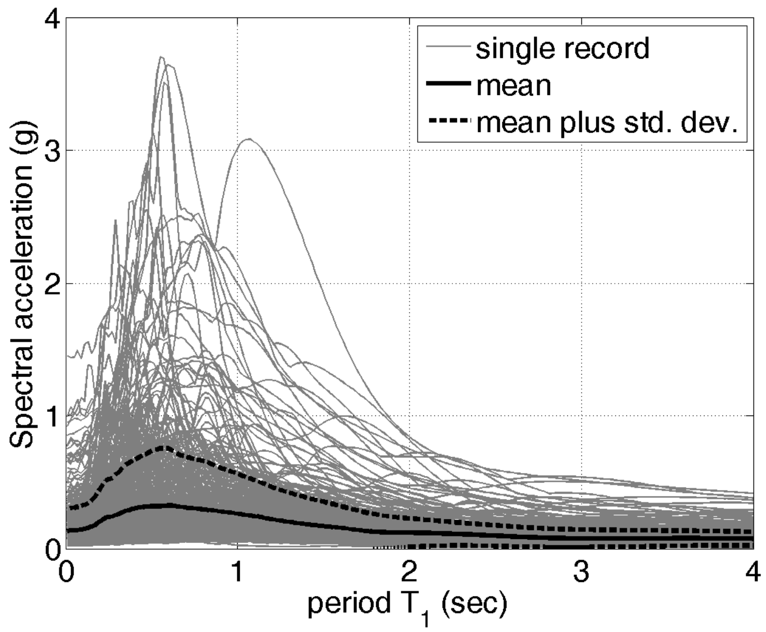

Figure 5.7b: Response spectra for synthetic ground motion.

Although such hybrid models provided until recently the most realistic simulation of broadband ground motions (among others Olsen and Mayhew, 2010; Graves and Pitarka, 2010), physics-based earthquake models are nowadays enabling deterministic simulations that produce ground motion time histories with comparable frequency content (<10Hz) (for example Cui et al. 2013). Still, the computational time and modeling effort required for the latter renders them less attractive for problems involving multiple realizations such as the study presented here.

Using the Liu et al. (2006) model, we simulated a series of weak, medium and large earthquake scenarios (M_w=5÷7.5), and computed three-component seismograms on a surface station grid at distances 2-75km from the surface projection of the fault. More information on the source and crustal models in these simulations can be found in Assimaki *et al.* 2008. Simulated ground motions were initially computed for rock outcrop conditions, namely for average shear wave velocity in the top 30m, $V_{s,30}$=760m/sec. To account for realistic site response –and particularly for nonlinear effects that characterize the response of sediments to strong earthquakes– we then deconvolved the simulated records to 100m depth; and used the motion at depth as input in nonlinear site response analyses for three characteristic soil profiles in Southern California. More details on the nonlinear soil model and soil profiles used can be found in Assimaki *et al.* (2008).

In this study, the synthetic records that were used as part of a combined record set consisted of horizontal components with Magnitudes 6, 6.5, 7.5 each within a PGA range of 0.1~2.0g. 465 out of 3150 ground motions fulfilled the PGA.

5.9 <u>Numerical results</u>

Figure 5.8 shows the results for the seven SDOF systems with T_1=0.1s, 0.2s, 0.3s, 0.5s, 0.7s, 1.0s, 1.5s. The grey lines refer to the results of IDA, where the median drawn with a grey solid line and the grey dashed lines denote its 95% confidence intervals. The results of cloud analysis are presented in a similar fashion with black lines. Since many records produce excessive ductility demands, we have set a ductility threshold at μ_u=10 beyond which we consider the structure as collapsed. In IDA this situation is also handled by setting a threshold in the EDP (Vamvatsikos and Cornell 2002). Moreover, in

IDA the collapse capacity is that of the ultimate horizontal plateau. Therefore, in cloud analysis we divide our data to “non-collapsed” and “collapsed” simulations. The curves shown in figures 5.8 correspond to the “non-collapsed” case, while the “collapsed” simulations are also shown in figures 5.8 as black dots stacked on μ_u=10. In Table 5.2 we examine separately the case of “collapsed” simulations. In figures 5.8a, 5.8b, 5.8c, 5.8d, 5.8e, 5.8f, 5.8g are shown the IDA and cloud analysis curves and their 95% confidence intervals for SDOF oscillators.

As it can be seen in those figures median IDA and cloud analysis curves are close for all period values and for ductility values of up to 3. More specifically, for systems with T_1=0.1s, 0.3s and 0.5s they coincide until μ=2 which corresponds to the capping ductility μ_c. Also, for systems with T_1= 0.7, 1.0 and 1.5 they coincide until μ=3, which, is the limit that the equal displacement rule applies. Beyond this ductility value, differences in the *R* capacities are observed. The capacity curves start to become horizontal for ductility values near 4.5, indicating that the system has reached its maximum *R* capacity.

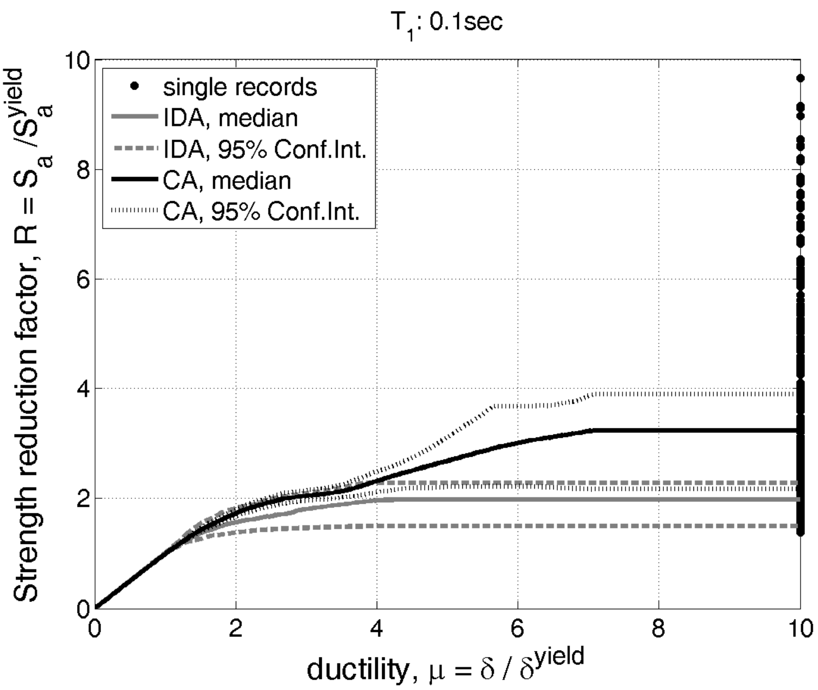

Figure 5.8a: Strength reduction factor versus ductility for T_1=0.1sec.

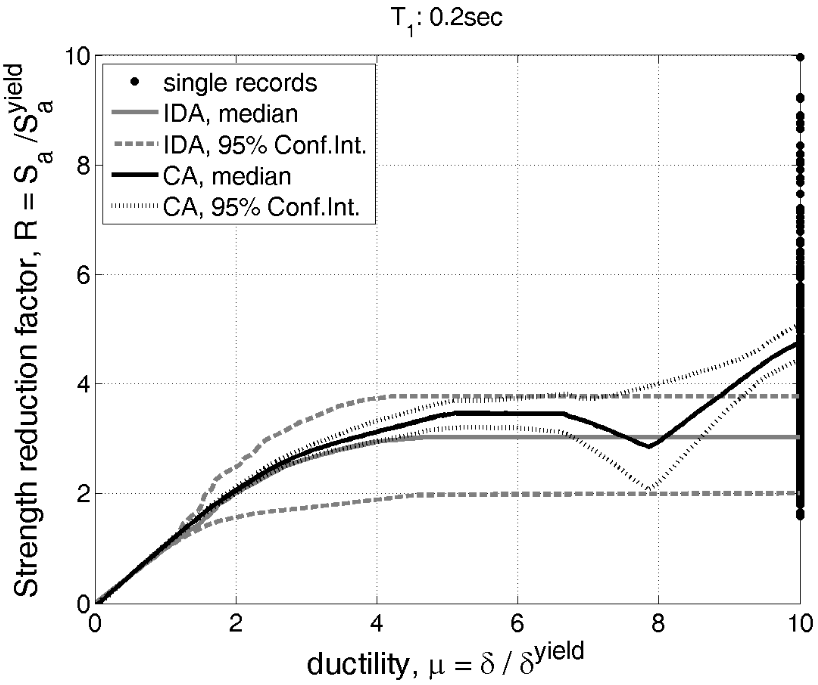

Figure 5.8b: Strength reduction factor versus ductility for for T_1=0.2sec.

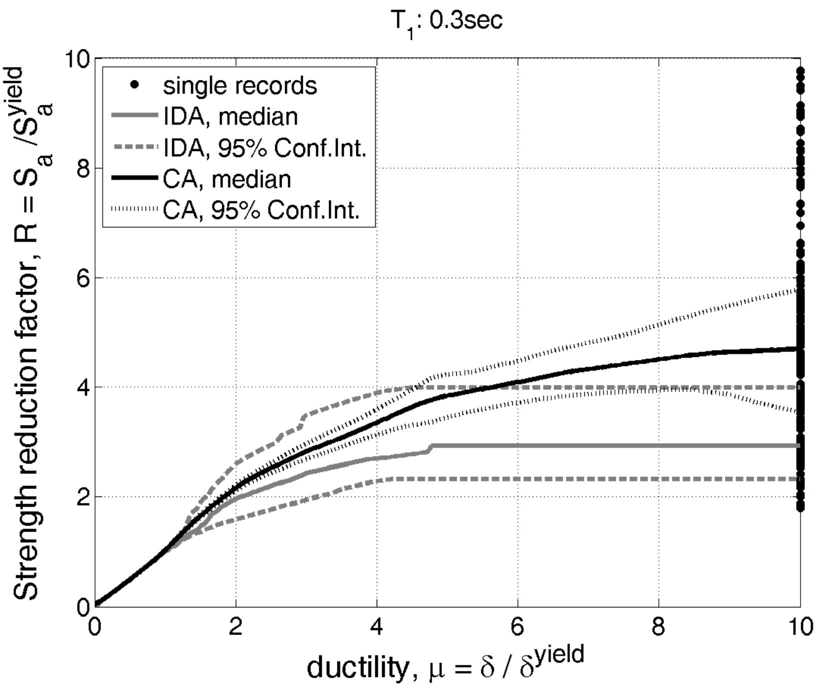

Figure 5.8c: Strength reduction factor versus ductility for T_1=0.3sec.

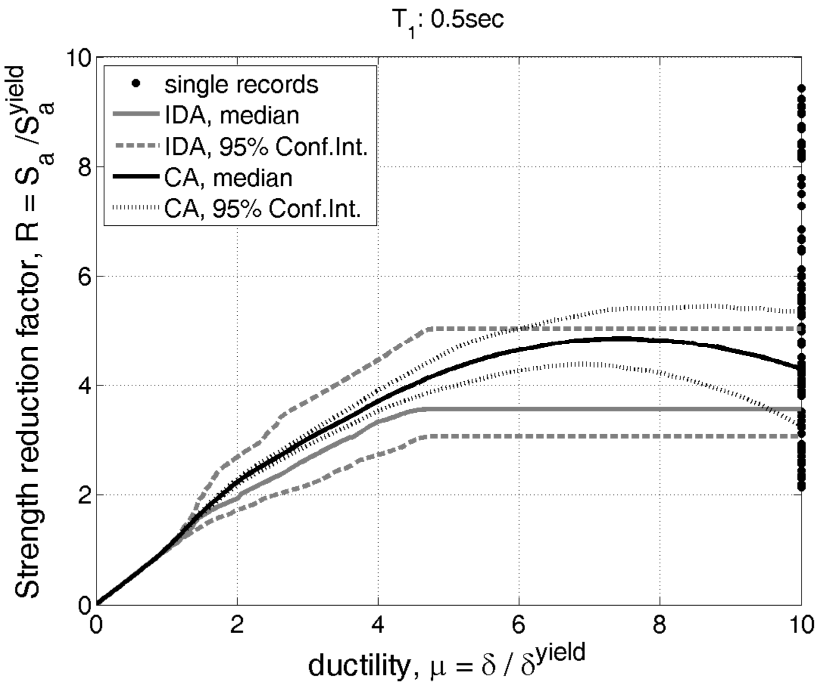

Figure 5.8d: Strength reduction factor versus ductility for T_1=0.5sec.

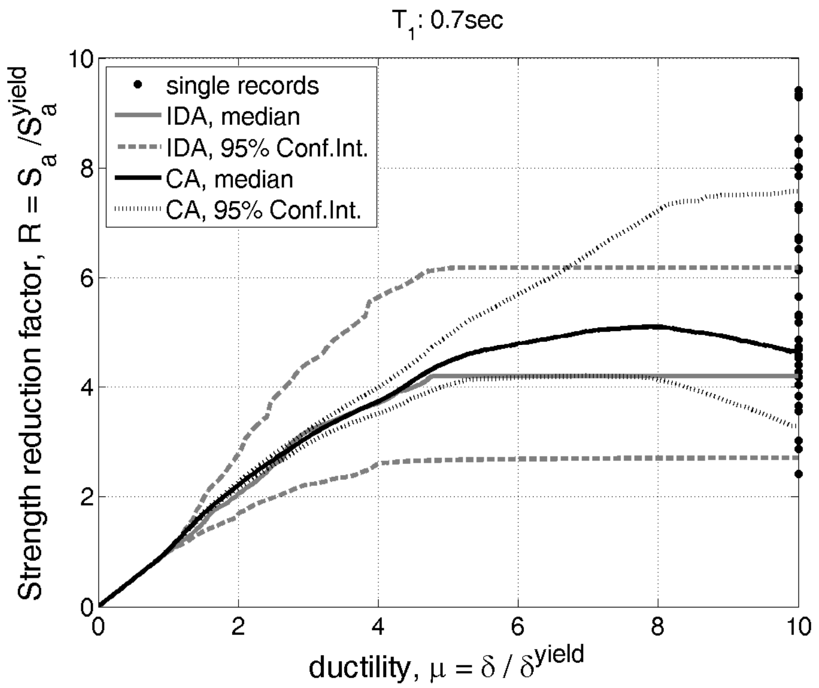

Figure 5.8e: Strength reduction factor versus ductility for T_1=0.7sec.

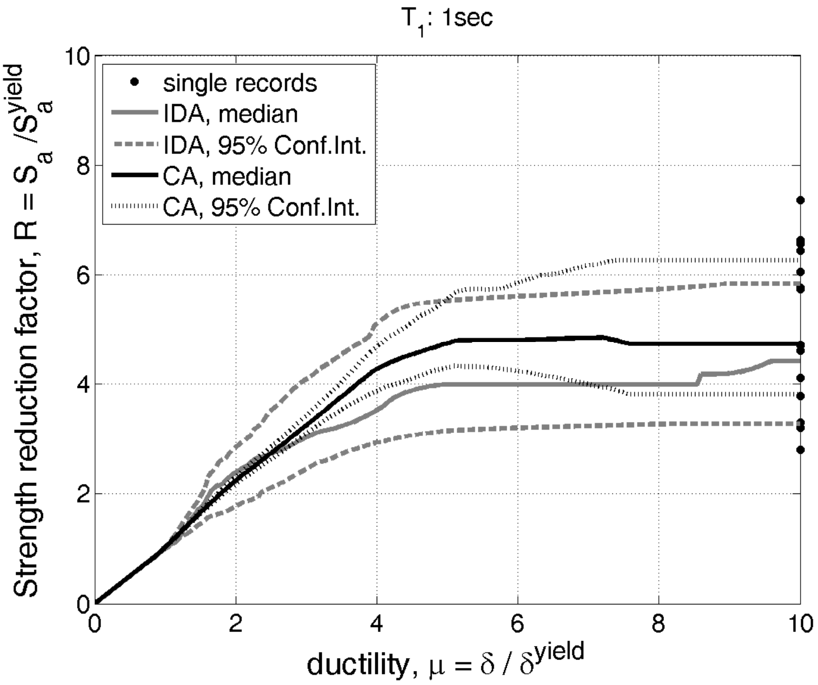

Figure 5.8f: Strength reduction factor versus ductility for T_1=1.0 sec.

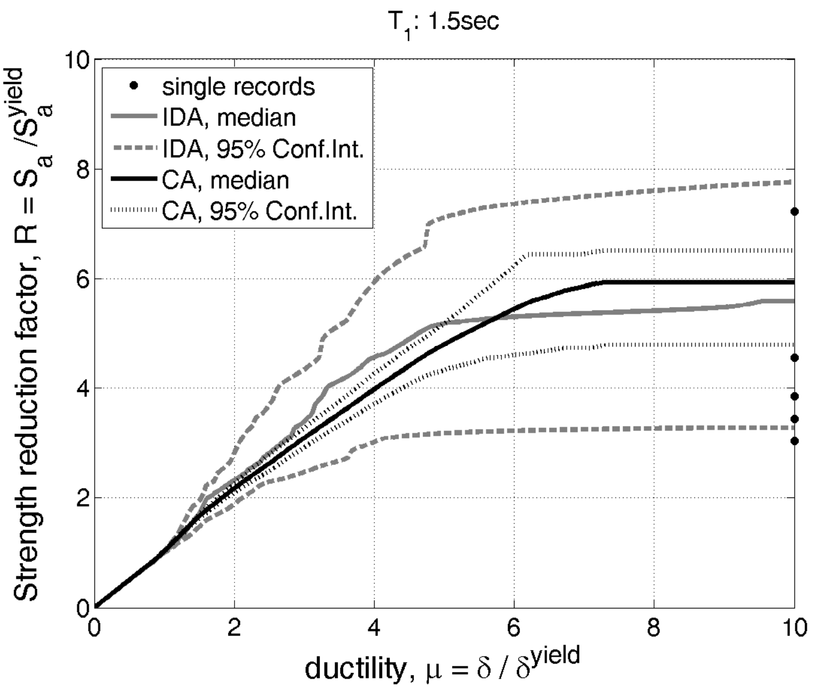

Figure 5.8g: Strength reduction factor versus ductility for T_1=1.5 sec.

As discussed above, with the increase of the ductility demand, the differences between the median IDA and the cloud analysis curves also increase. It becomes apparent that for small period values, T_1=0.1s and 0.3s, IDA underestimates the R capacities, while for medium to large periods, T_1=0.5s, 0.7s and 1.0s, IDA still underestimates the capacity but to a lesser degree. For T_1 =1.5sec the difference is small and the demand is slightly overestimated for μ<6 and underestimated when μ>6.

In figures 5.8 we show the 95% confidence intervals in order to provide an estimate of the dispersion. In general, for T_1>0.3 the intervals of IDA are wider compared to those of cloud analysis. Moreover, the width of the confidence intervals increases as the ductility demand increases and also as the period increases. In the linear elastic range the width is practically zero but grows quickly at ductilities beyond μ=1 for IDA and μ=3 for cloud analysis. If we consider an arbitrary ductility value, e.g. μ=8, comparing oscillators with T_1 equal to 0.1 and 1.5sec, it is seen that the width of the confidence intervals of IDA varies considerably. This implies that the observations regarding the median IDAs, are valid approximately, since there may be ground motions where the demand could lie anywhere within the confidence interval.

In figures 5.10 we also show the 95% confidence intervals in order to provide an estimate of the dispersion. According to figure 5.10, the intervals are wider in the case of IDA and relatively narrow for cloud analysis except when the first mode period equals 0.1sec. In general the width of confidence intervals increases as the ductility demand increases also with the period. For the linear elastic range the width is zero, but grows quickly after μ=1. In the figures 5.10 the median capacity curves and their 95% confidence intervals for quadrilinear SDOF oscillators is shown. In figure 5.10d and for a quadrilinear SDOF of T_1=0.5sec there is a non-monotonicity observed in high ductility values approximately over μ=7. This is an issue of LOESS and it questions the accuracy of the median LOESS curve. Still it is not of great interest because over μ=7 there is scarcity of data so we cannot give accurate answers.

In figures 5.11 we also show the 95% confidence intervals in order to provide an estimate of the dispersion. According to figure 5.11, the intervals are wider in the case of IDA and relatively narrow for cloud analysis for the bilinear case. In general the width of confidence intervals increases as the ductility demand increases also with the period. For the linear elastic range the width is zero, but grows quickly after μ=1. In the figures 5.11 below the median capacity curves and their 95% confidence intervals for bilinear SDOF oscillators is shown. Furthermore, figures 5.11a to 5.11h show the case of the bilinear oscillator.

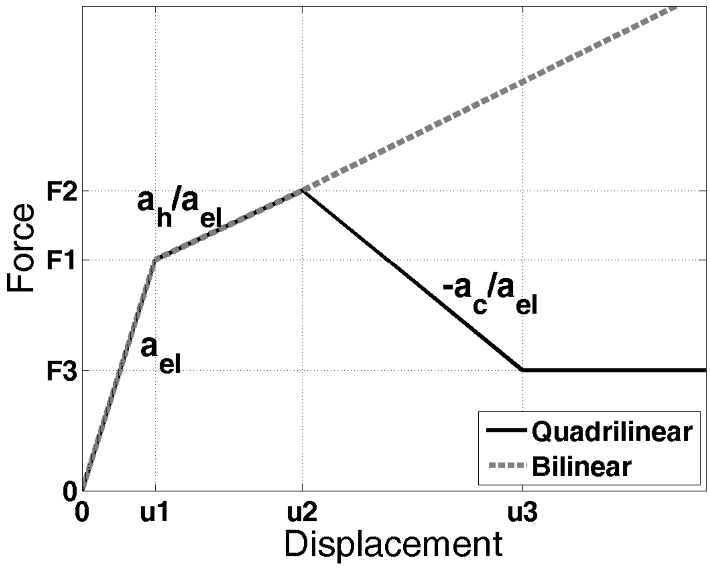

Figure 5.9: Force versus displacement for the quadrilinear and the bilinear case.

Comparing the two cases of quadrilinear and bilinear oscillators (Figure 5.9), it is clear that the single-analysis results, shown as dots, are more scattered and cover more evenly the whole range of interest in the case of bilinear observations. Looking at the multilinear oscillators results, some dots are shown to be concentrated on the μ=10 vertical line. For these records the demand is very close or has exceeded μ=10 indicating that the system collapses. Moreover, for large periods, e.g. for T_1=1.5sec, the number of dots shown is smaller compared to that of smaller periods. This is due to the limited availability of records that above 1 sec have large *Sa*(T_1,*5%*) values and are strong enough to cause large ductility demand. In this case, sufficient data are available for ductility values that not exceed 5 or 6 and therefore beyond these values we cannot be confident for our findings.

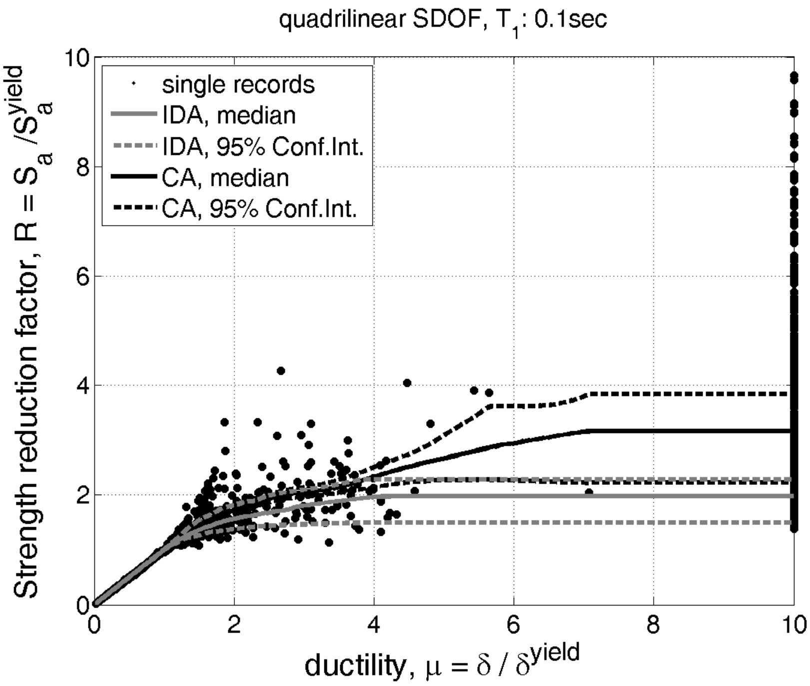

Figure 5.10a: Strength reduction factor versus ductility for a quadrilinear SDOF and for T_1 =0.1 sec.

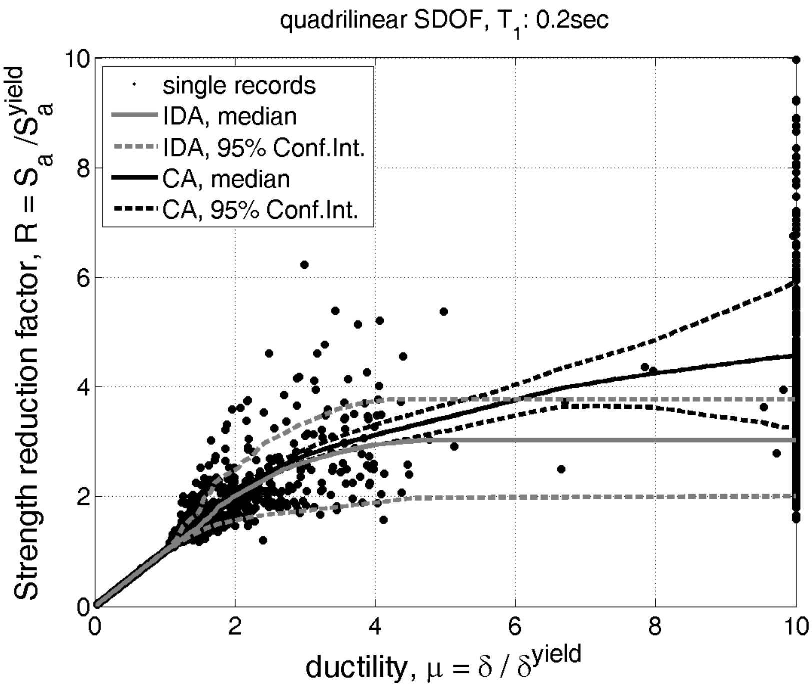

Figure 5.10b: Strength reduction factor versus ductility for a quadrilinear SDOF and for T_1 =0.2sec.

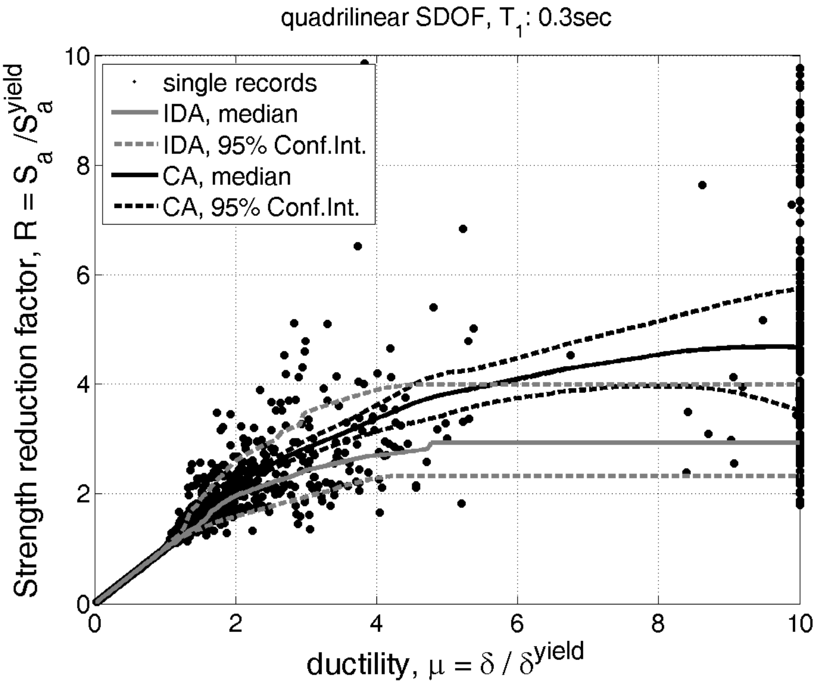

Figure 5.10c: Strength reduction factor versus ductility for a quadrilinear SDOF and for T_1=0.3sec.

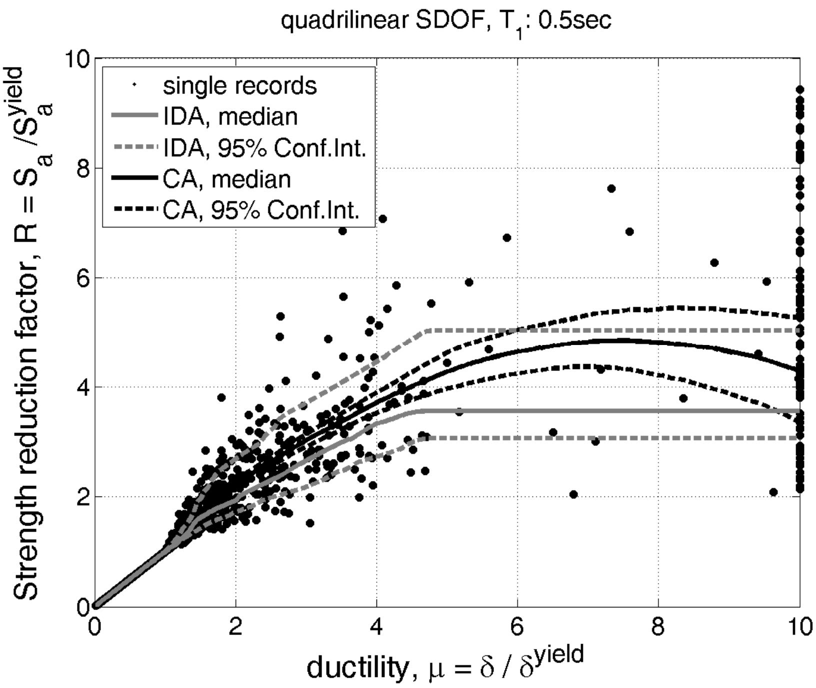

Figure 5.10d: Strength reduction factor versus ductility for a quadrilinear SDOF and for T_1=0.5sec.

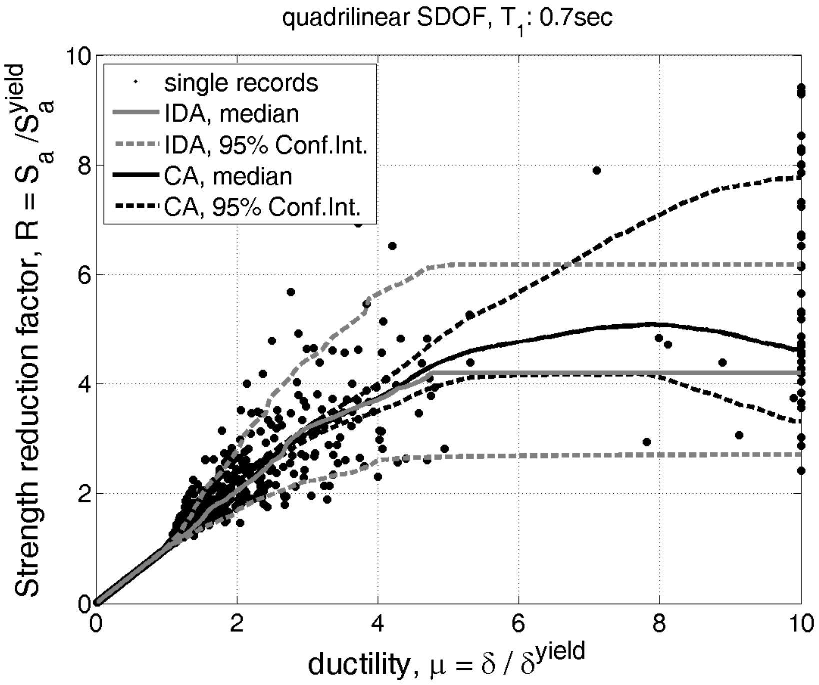

Figure 5.10e: Strength reduction factor versus ductility for a quadrilinear SDOF and for T_1=0.7sec.

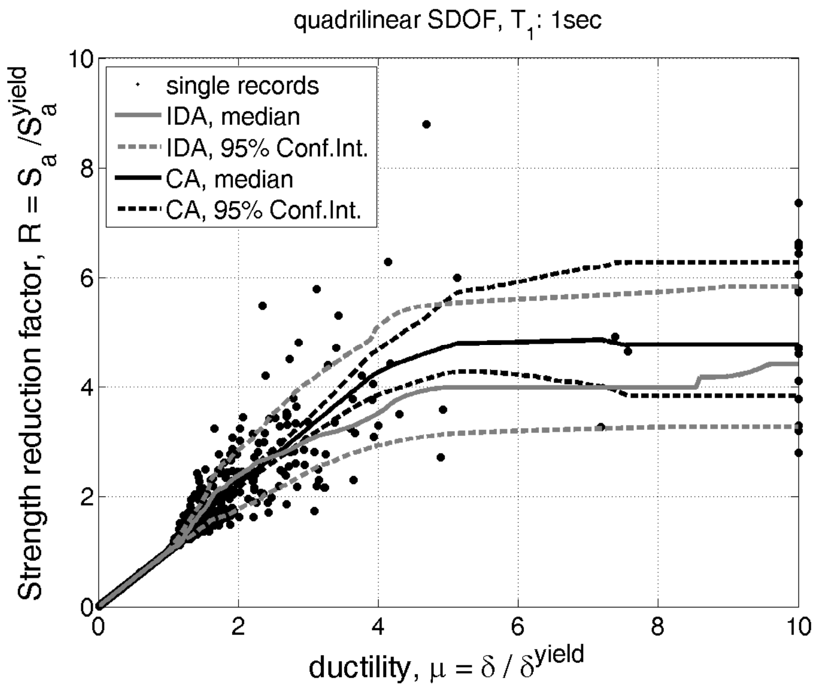

Figure 5.10f: Strength reduction factor versus ductility for a quadrilinear SDOF and for T1=1.0 sec.

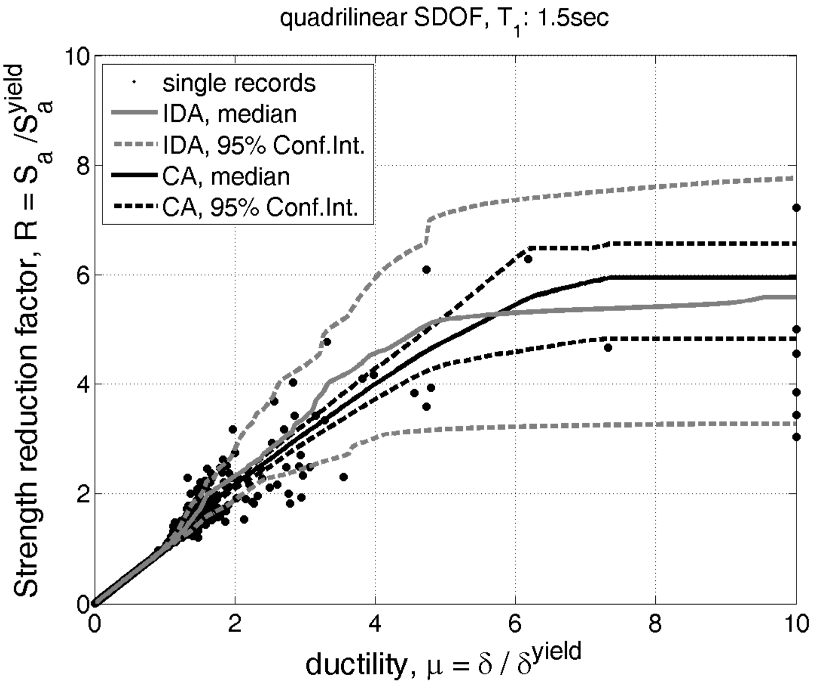

Figure 5.10g: Strength reduction factor versus ductility for a quadrilinear SDOF and for T1=1.5sec.

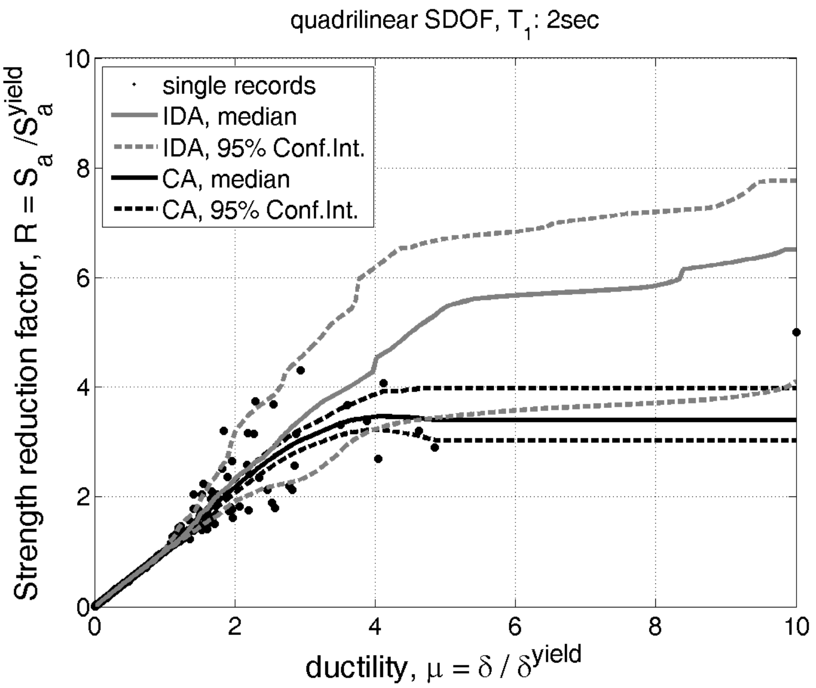

Figure 5.10h: Strength reduction factor versus ductility for a quadrilinear SDOF and for T_1=2.0sec.

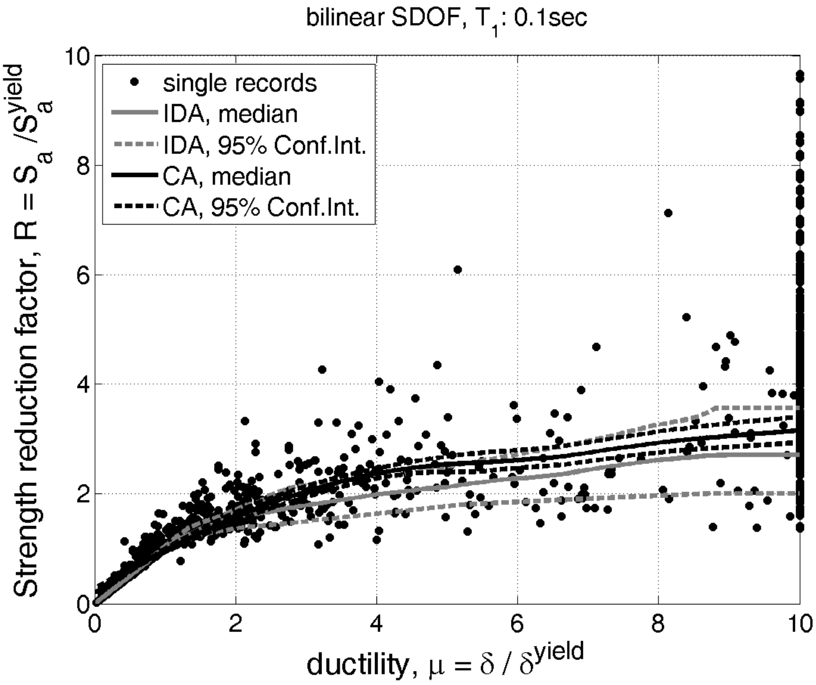

Figure 5.11a: Strength reduction factor versus ductility for a bilinear SDOF and for T_1=0.1sec.

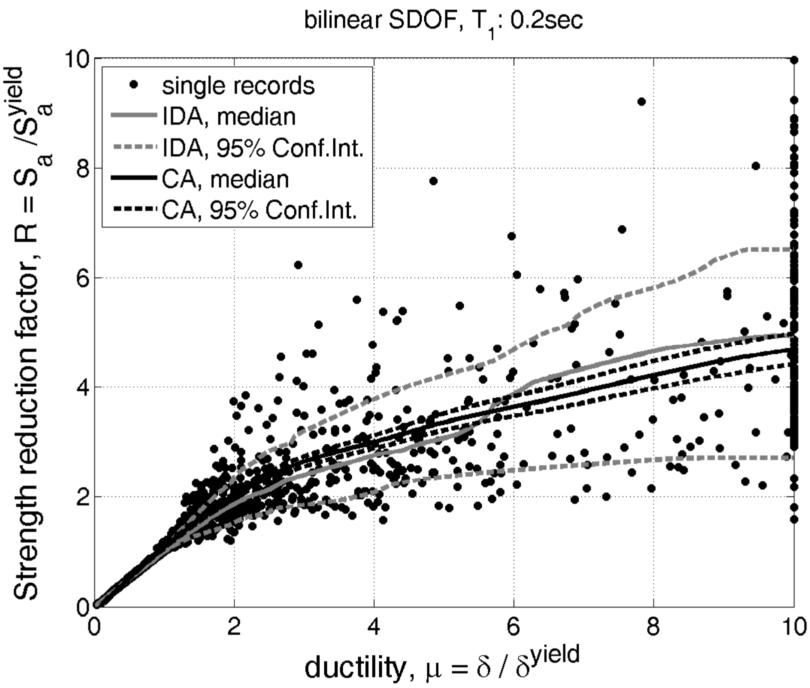

Figure 5.11b: Strength reduction factor versus ductility for a bilinear SDOF and for T_1=0.2sec.

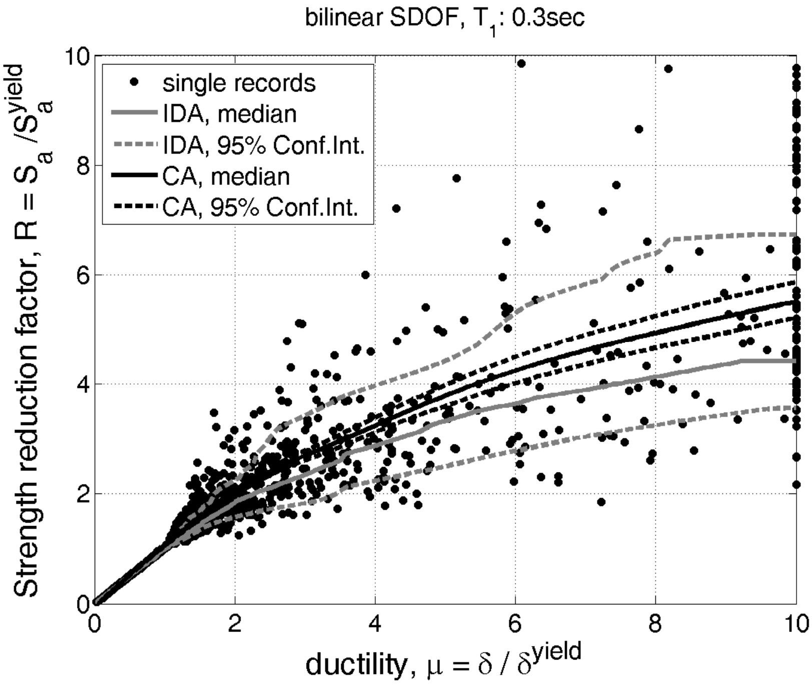

Figure 5.11c: Strength reduction factor versus ductility for a bilinear SDOF and for T_1=0.3sec.

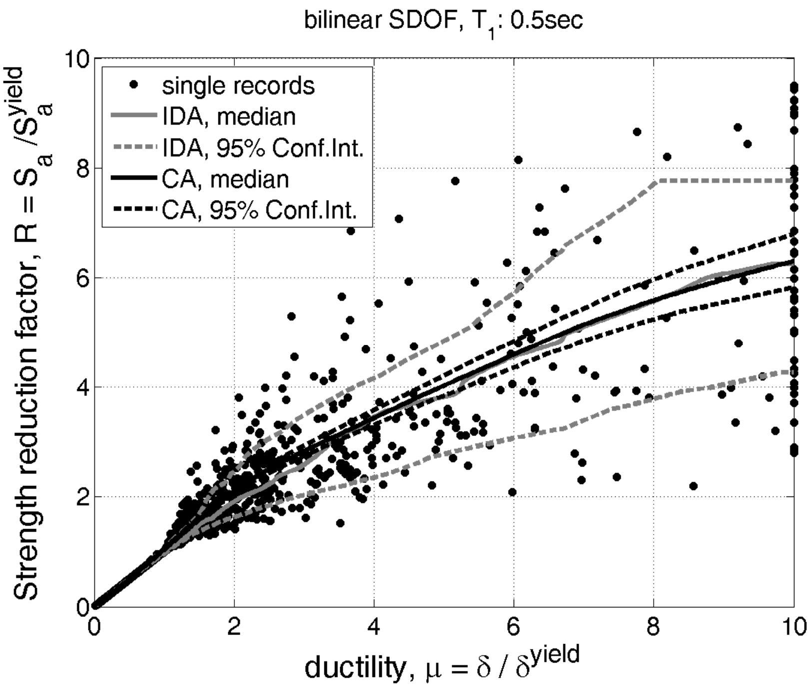

Figure 5.11d: Strength reduction factor versus ductility for a bilinear SDOF and for T_1=0.5sec.

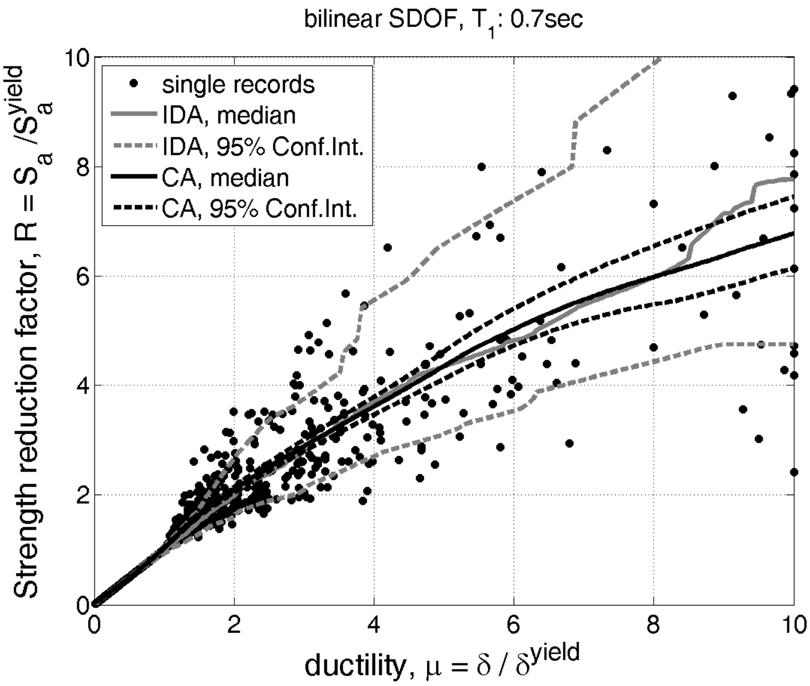

Figure 5.11e: Strength reduction factor versus ductility for a bilinear SDOF and for T_1=0.7sec.

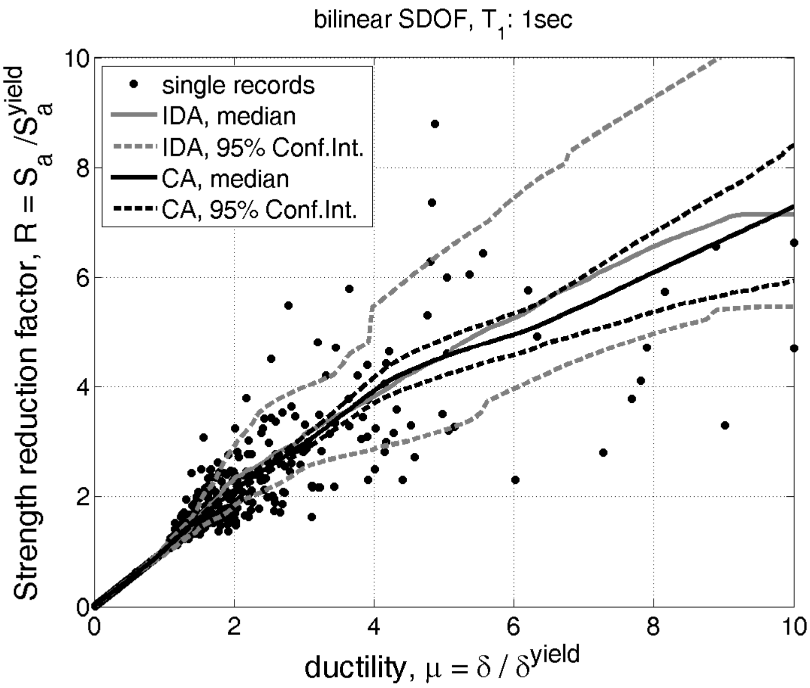

Figure 5.11f: Strength reduction factor versus ductility for a bilinear SDOF and for T_1=1.0sec.

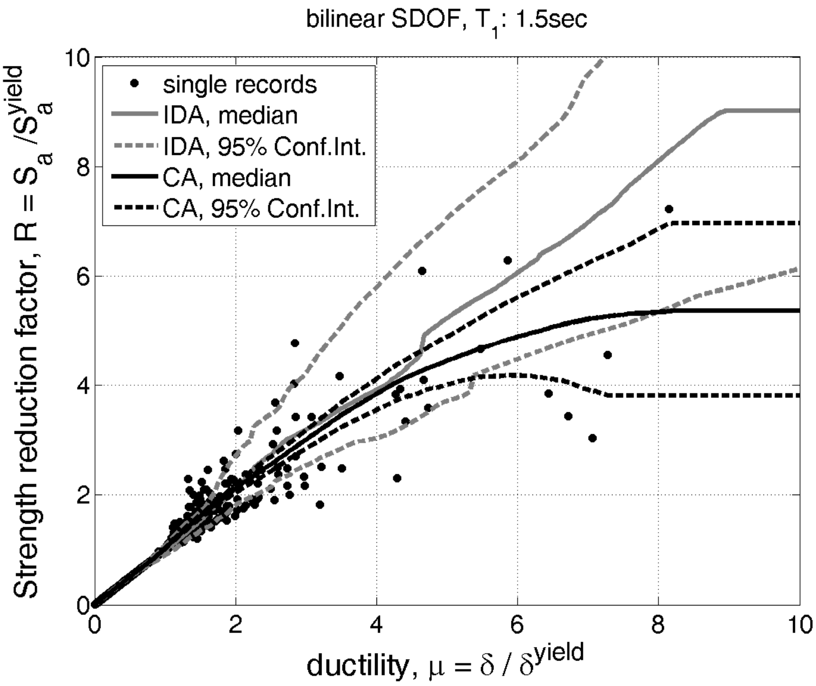

Figure 5.11g: Strength reduction factor versus ductility for a bilinear SDOF and for T_1=1.5sec.

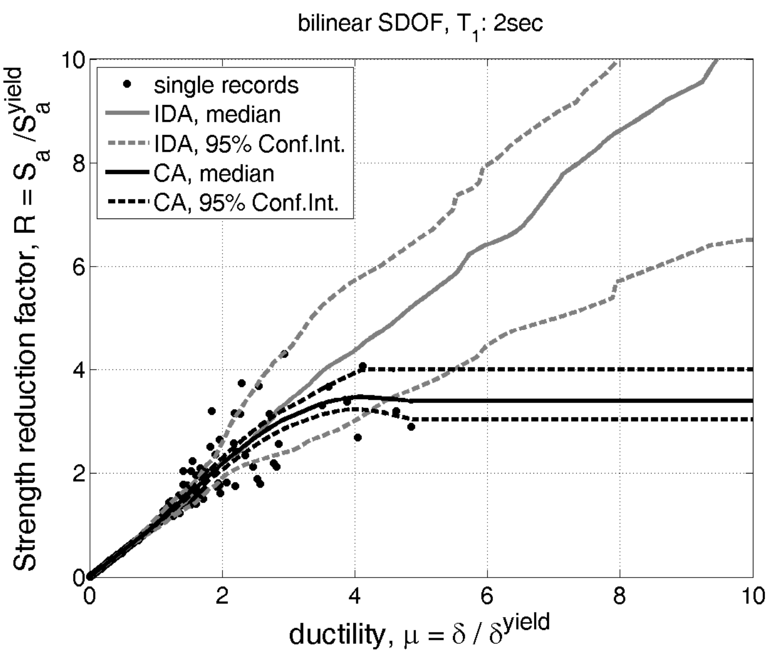

Figure 5.11h: Strength reduction factor versus ductility for a bilinear SDOF and for T_1=2.0 sec.

Besides, in the above figures 5.10a to 5.10f we have isolated the quadrilinear case, and arbitrarily select a ductility value, e.g. μ=8, the width of the confidence intervals of the IDA's varies from R=2 to 6, for the oscillators with T1=0.1sec and 2.0 sec respectively. This means that the above observations regarding the accuracy of the median IDA's, are valid on average since there may be isolated cases that the medians may differ. For T1=0.1sec, 0.3sec and for SDOFs that follow both the quadrilinear and the bilinear hysteretic rule the confidence intervals of the Loess generated curves are not entirely captured in the confidence intervals of the IDA.

Table 5.2 shows the *R* capacities of the collapsed simulations. The first two rows refer to the median *R* capacities of IDA and cloud analysis, respectively, while the third row shows their ratio. Although the differences in the "non-collapsed" simulations were small, indicating little bias, in the case of "collapsed" simulations, there is a clear trend that IDA underestimates the collapsed capacities. The only exception is the value referring to T_1=1.5s, but as shown in figure 5.10, this case should be discarded since it has been obtained from a rather small number of simulations. This means that IDA is conservative in general (i.e. it overestimates EDPs) so it can be used safely. This means that we are consistent with similar works (Luco and Bazzuro (2007)).

In the figures 5.12a and 5.12b below we compare the median IDA and cloud analysis curves for the three-storey and the nine-storey steel moment resisting frames. For the three-storey frame the median IDA and cloud analysis curves coincide until θ_{max} =0.03. Beyond this value the difference gradually increases until θ_{max}=0.12, while beyond this value we cannot make a safe observation.

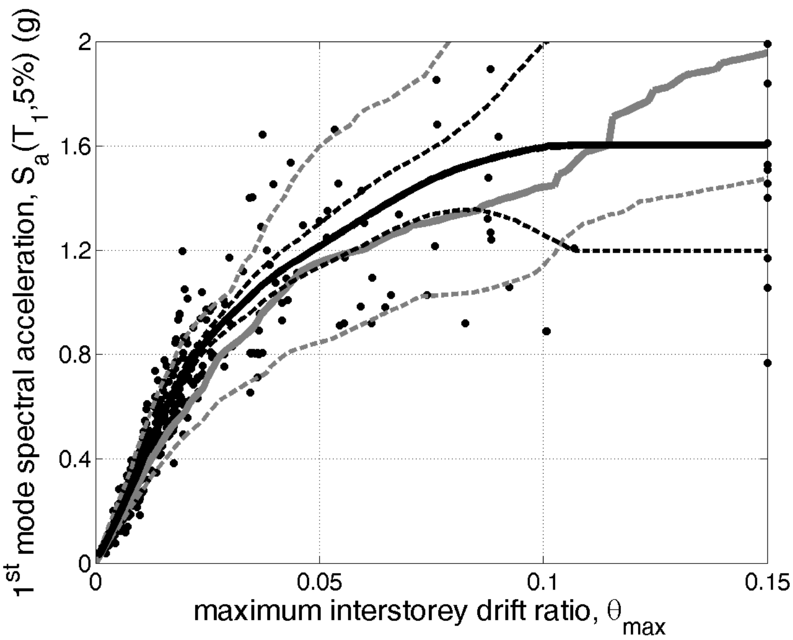

Figure 5.12a: Median capacity curves and their 95% confidence intervals for three-storey steel frame

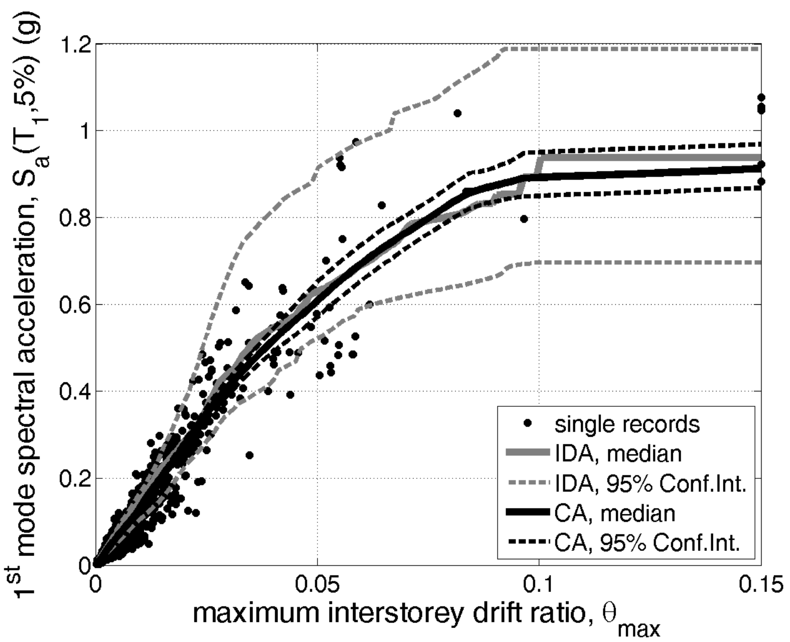

Figure 5.12b: Median capacity curves and their 95% confidence intervals for the nine-storey steel frame.

Table 5.2. Collapsed *R*-capacities of the SDOF oscillators.

	T_1 (sec)					
	0.1	0.3	0.5	0.7	1.0	1.5
R^{IDA}	1.98	2.92	3.56	4.2	4.41	5.59
R^{Cloud}	3.13	4.74	4.36	4.64	4.74	5.93
R^{IDA}/R^{Cloud}	0.63	0.62	0.82	0.91	0.93	0.94

For the nine-storey building (figure 5.12b) both curves are identical even though beyond θ_{max}=0.07 and above $S_a(T_1, 5\%)$=0.8g our data become scarce. This is due to the limited availability of records that are strong enough to cause large drift demand at this period and thus we cannot reach to safe conclusions. Moreover, for the nine-storey frame the median IDAs lies within the confidence interval of cloud analysis, while this is not the case for the three-storey frame. Both cloud analysis and IDA produce estimates of the capacities that are close, apart from the case of the nine-storey frame, at large limit-states.

Comparing Figure 5.12a with the corresponding SDOF case (Figure 5.8e), in both plots the median IDA curve of the LA3 building, after yielding, slightly exceeds the estimate of cloud analysis. The reverse of this trend is observed at large drifts (θ_{max}>0.12) in Figure 5.12a, but it is not present in Figure 5.8. However, as also discussed above, safe conclusions cannot be made for such large drifts. For the LA9 frame, again the effect of scaling is quite small (Figure 5.12b). This trend was also observed as the period of the SDOFs is increased (Figure 5.8)

As already shown for the SDOFs in Table 5.2, in Table 5.3 the $Sa(T_1$,5%) capacities of the collapsed simulations are shown. The ratio of collapsed capacities for both frames has values close to 1 (fourth row), which indicates that the capacity estimation at collapse is practically unbiased.

The data of Table 5.3 should be interpreted with caution, since a small number of unscaled ground motions were able to produce collapse.

Table 5.3 Collapsed $S_a(T_1$,5%)-capacities of the MDOF buildings.

	three-storey (LA3)	nine-storey (LA9)
S_a^{IDA}	2.0	0.94

S_a^{Cloud}	1.6	0.91
S_a^{IDA}/ S_a^{Cloud}	1.2	1.03

5.10 Bias estimation

Bias of $S_a(T_1)$ intensity measure can be seen as the systematic under or over-estimation of the R or $S_a(T_1,5\%)$, capacity. We quantify the bias assuming that the unbiased response is that of the cloud analysis since this method leaves the records unscaled. Thus, the bias of $S_a(T_1)$ on capacity, conditional on the EDP, is measured as the ratio:

$$\text{bias}=\frac{(R)_{IDA}}{(R)_{cloud}}, \text{ or } \text{bias}=\frac{\left(S_a\left(T_1,5\%\right)\right)_{IDA}}{\left(S_a\left(T_1,5\%\right)\right)_{cloud}} \tag{5.2}$$

where $S_a(T_1,5\%)_{IDA}$ is the $S_a(T_1,5\%)$ capacities of IDA and $S_a(T_1,5\%)_{cloud}$ is the capacity obtained from cloud analysis. In order to assess the statistical significance of the bias and calculate the corresponding confidence intervals, we perform bootstrap on the bias values of Eq. (2). We are thus able to monitor the bias of $S_a(T_1)$ for the full range of limit-states (EDP values). The confidence intervals of the bias add further confidence on our observation regarding the effect of scaling within the framework of IDA.

Figures 5.13 and figures 5.14 show the confidence intervals of the bias conditional on the EDP and allow some general observations. When the whole confidence interval is clearly above, or below the unity line then we are certain that the capacity is over or under-estimated. On the other hand, if the confidence interval contains evenly the unity line we have no evidence of bias. Moreover, the width of the confidence intervals is a measure that reveals the sensitivity of the conditional capacity to scaling which increases in agreement with the capacity curves of figures 5.8 and figure 5.10. Bootstrap can be also used to calculate the bootstrap median of Eq. (2) which adds further confidence to our results.

5.10.1 Single-Degree-of-Freedom systems

Figures 5.13 show the confidence intervals of the conditional bias of the SDOF oscillators. For short-period oscillators, T_1= 0.1, 0.3 and 0.5 sec, the capacities are clearly biased for the whole range of demand. More specifically, IDA underestimates the capacities on average by 20-25%. For the early limit-states (until μ=5), the ratio is close to 0.75, while beyond this value it becomes smaller indicating that for stiff oscillators considerable bias should be expected at large ductilities. However, for medium period SDOFs (T_1=0.7sec and 1sec) the bias is certainly less pronounced.

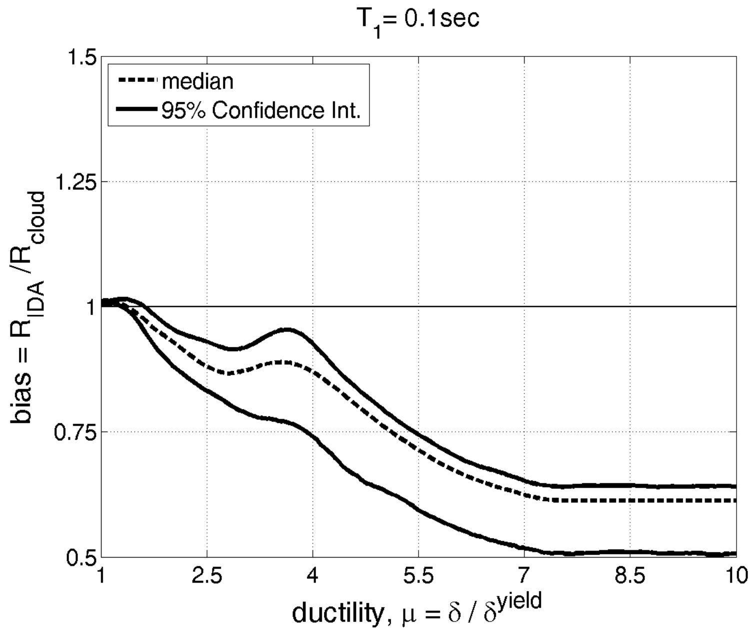

Figure 5.13a: Bootstrap 95% confidence intervals on the ratio of the median $Sa(T_1,5\%)$-capacities given θ_{max} of the IDA case over the cloud analysis case for the quadrilinear SDOF oscillators of T_1=0.1sec.

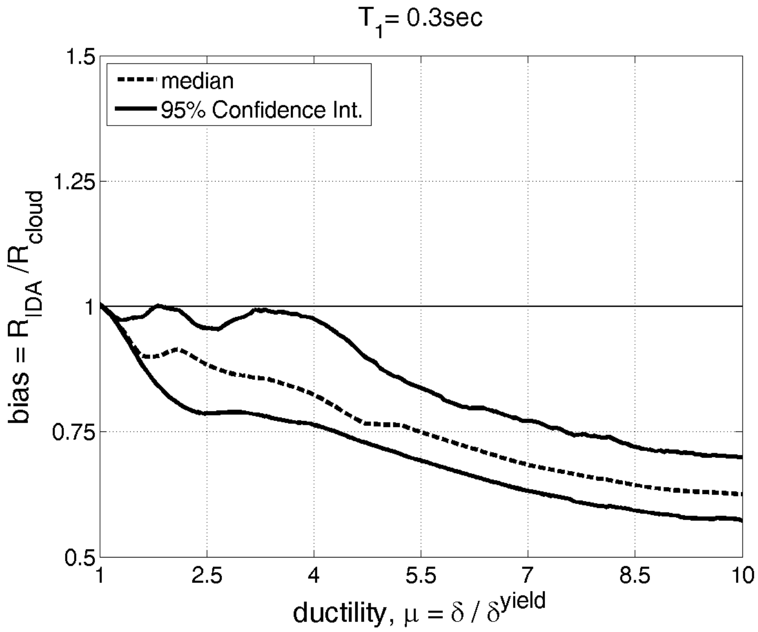

Figure 5.13b: Bootstrap 95% confidence intervals on the ratio of the median *S*a(T_1,5%)-capacities given θ_{max} of the IDA case over the cloud analysis case for the quadrilinear SDOF oscillators of T_1=0.3sec.

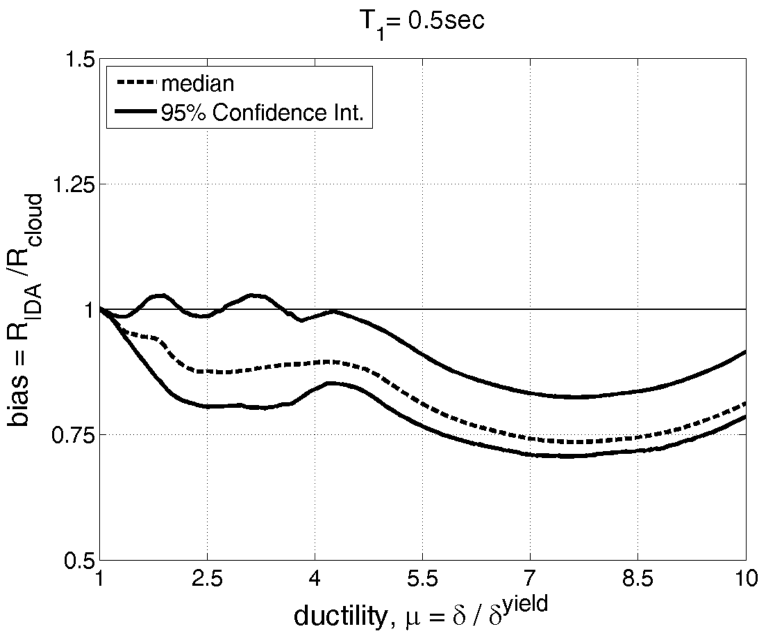

Figure 5.13c: Bootstrap 95% confidence intervals on the ratio of the median *S*a(T_1,5%)-capacities given θ_{max} of the IDA case over the cloud analysis case for the quadrilinear SDOF oscillators of T_1=0.5sec.

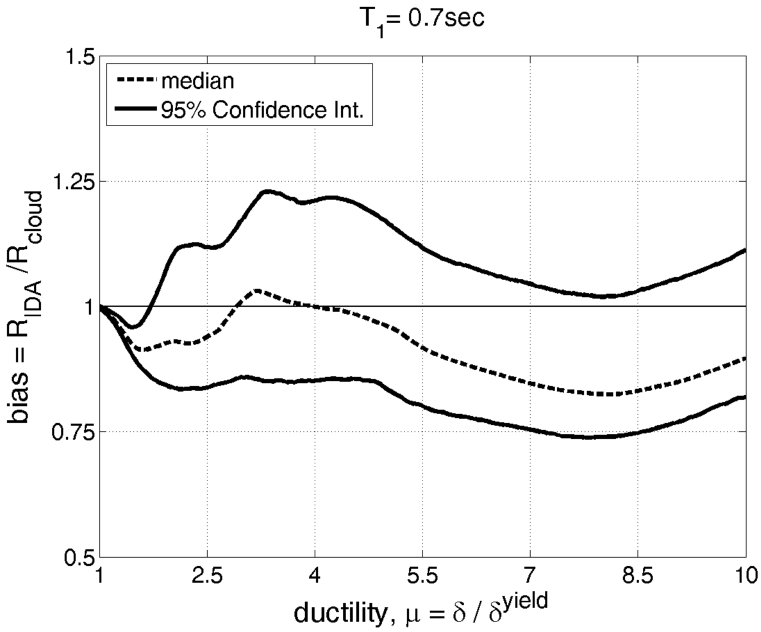

Figure 5.13d: Bootstrap 95% confidence intervals on the ratio of the median *S*a(T_1,5%)-capacities given θ_{max} of the IDA case over the cloud analysis case for the quadrilinear SDOF oscillators of T_1=0.7sec.

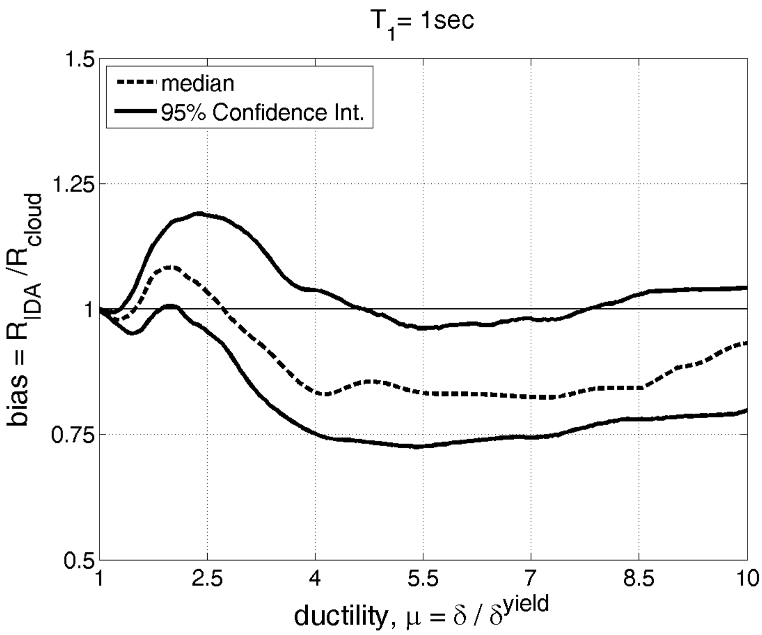

Figure 5.13e: Bootstrap 95% confidence intervals on the ratio of the median *S*a(T_1,5%)-capacities given θ_{max} of the IDA case over the cloud analysis case for the quadrilinear SDOF oscillators of T_1=1.0sec.

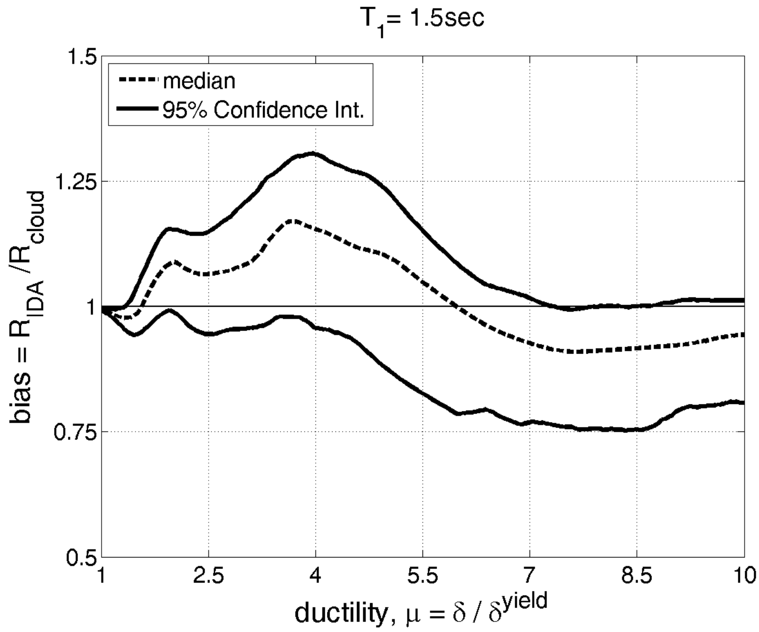

Figure 5.13f: Bootstrap 95% confidence intervals on the ratio of the median *S*a(T_1,5%)-capacities given θ_{max} of the IDA case over the cloud analysis case for the quadrilinear SDOF oscillators of T_1=1.5sec.

In the case of the bilinear oscillator we have respectively the below figures:

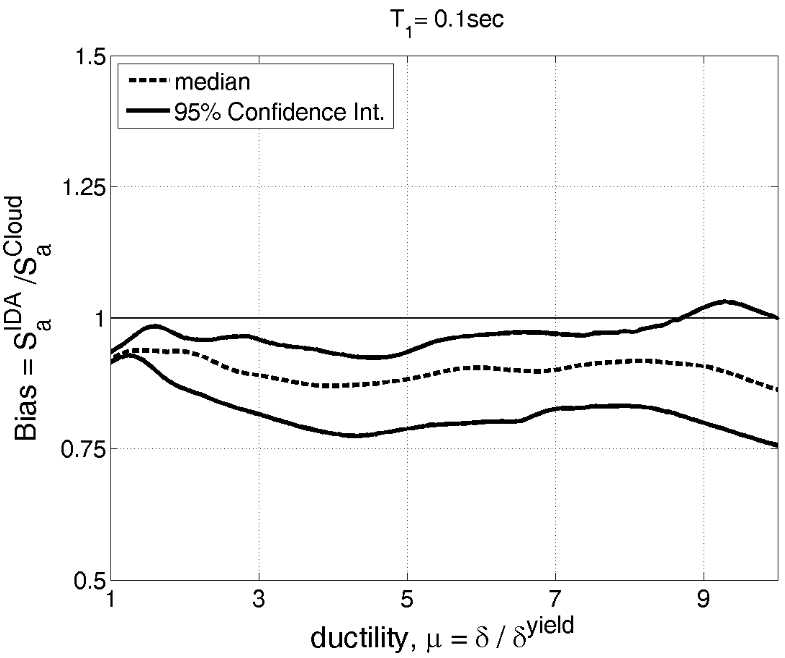

Figure 5.14a: Bootstrap 95% confidence intervals on the ratio of the median $Sa(T_1,5\%)$-capacities given θ_{max} of the IDA case over the cloud analysis case for the bilinear SDOF oscillators of T_1=0.1sec.

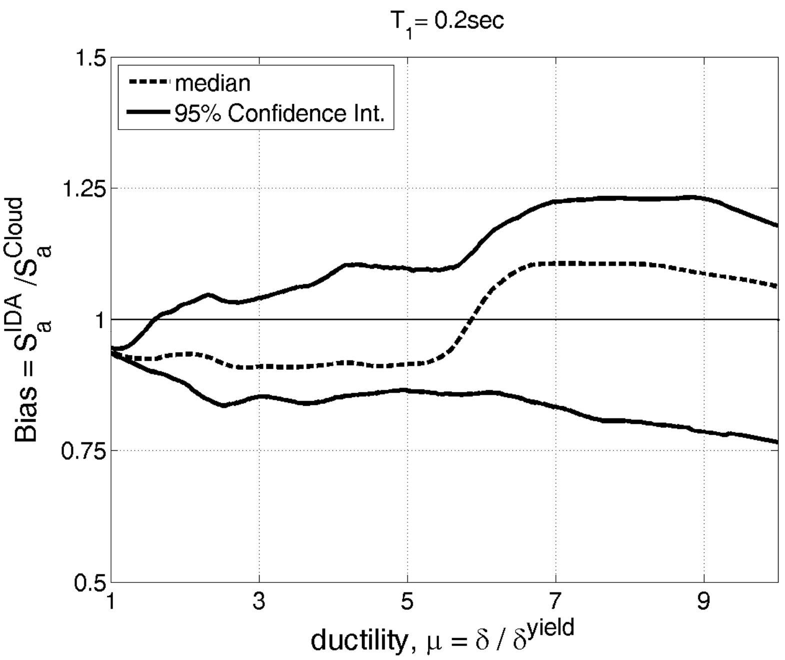

Figure 5.14b: Bootstrap 95% confidence intervals on the ratio of the median $Sa(T_1,5\%)$-capacities given θ_{max} of the IDA case over the cloud analysis case for the bilinear SDOF oscillators of T_1=0.2sec.

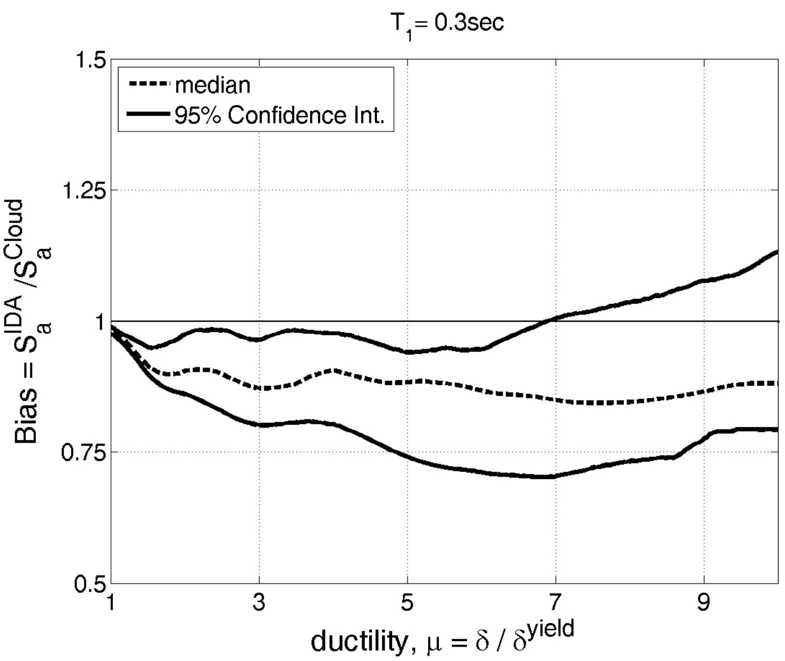

Figure 5.14c: Bootstrap 95% confidence intervals on the ratio of the median $Sa(T_1,5\%)$-capacities given θ_{max} of the IDA case over the cloud analysis case for the bilinear SDOF oscillators of T_1=0.3sec.

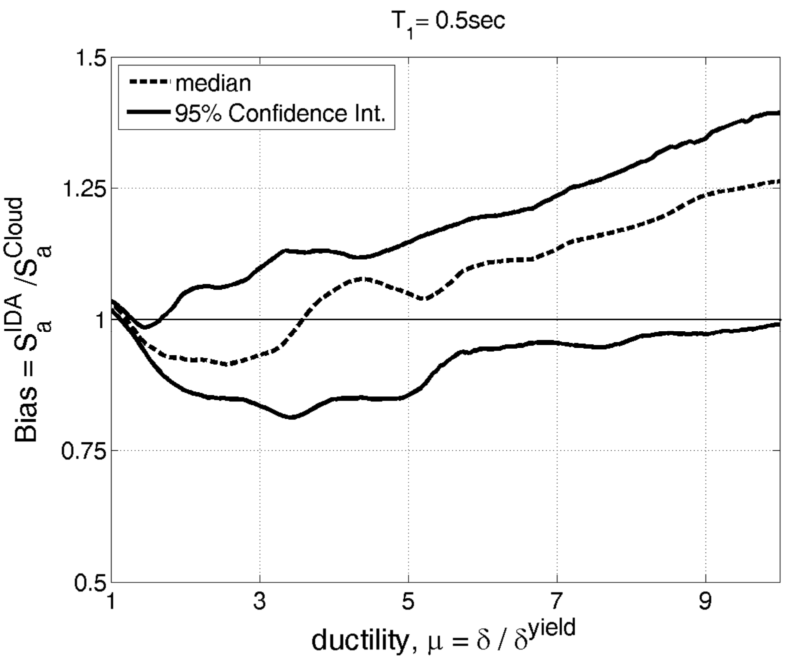

Figure 5.14d: Bootstrap 95% confidence intervals on the ratio of the median $Sa(T_1,5\%)$-capacities given θ_{max} of the IDA case over the cloud analysis case for the bilinear SDOF oscillators of T_1=0.5sec.

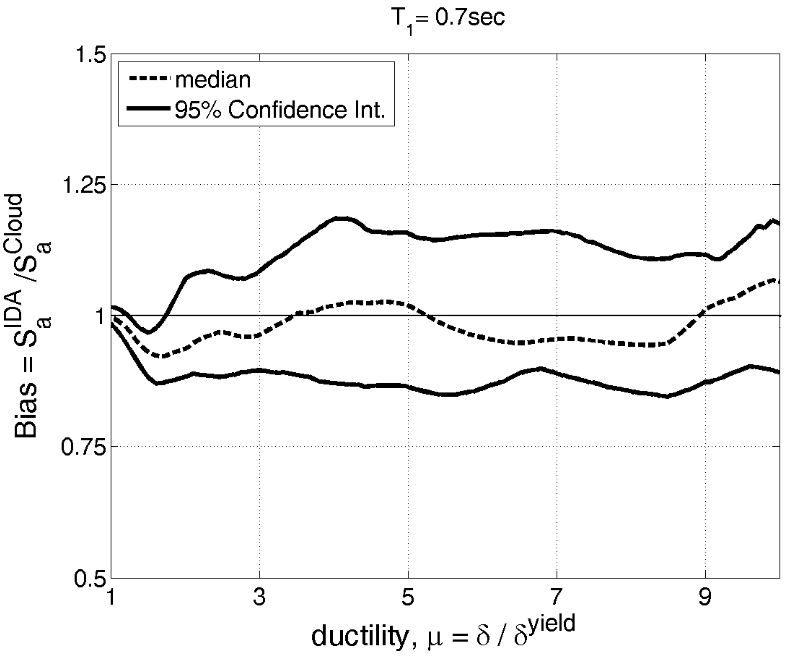

Figure 5.14e: Bootstrap 95% confidence intervals on the ratio of the median Sa(T1,5%)-capacities given θmax of the IDA case over the cloud analysis case for the bilinear SDOF oscillators of T1=0.7sec.

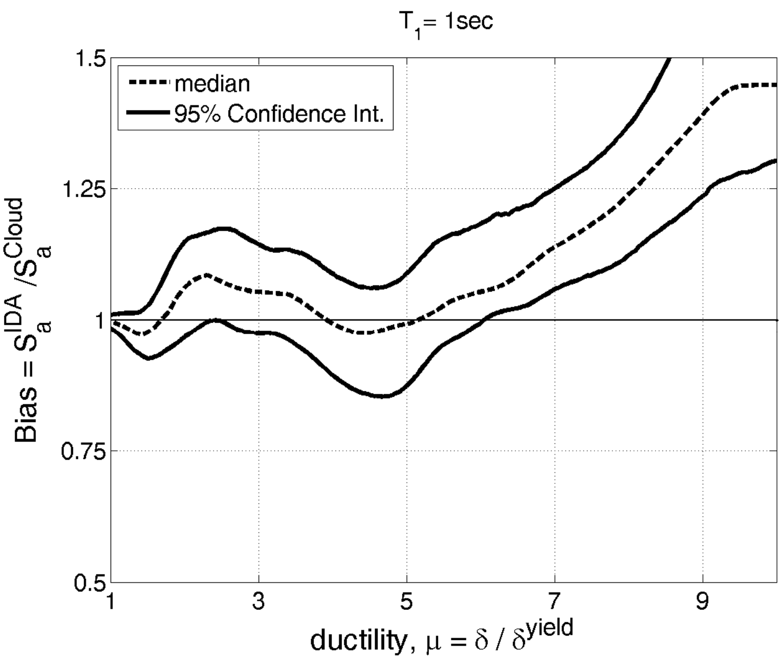

Figure 5.14f: Bootstrap 95% confidence intervals on the ratio of the median *Sa*(T_1,5%)-capacities given θ_{max} of the IDA case over the cloud analysis case for the bilinear SDOF oscillators of T_1=1.0 sec.

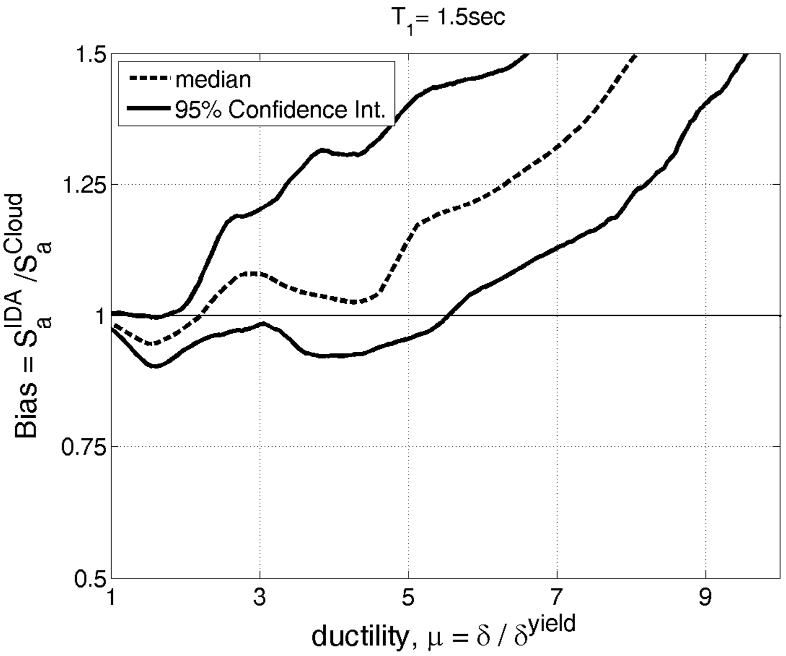

Figure 5.14g: Bootstrap 95% confidence intervals on the ratio of the median $Sa(T_1,5\%)$-capacities given θ_{max} of the IDA case over the cloud analysis case for the bilinear SDOF oscillators of T_1=1.5 sec.

For the T_1=0.7sec SDOF, there is no evidence of bias, while for the T_1=1.0sec oscillator, mild bias of Sa(T_1) can be identified. In the latter case, the response is overestimated for early limit-states and underestimated for μ values beyond 3. This behavior is also observed for the T_1=1.5sec oscillator, where the early overestimation is more pronounced and can be seen for μ values up to 6.

The bootstrap median for most oscillators lies approximately at the center of the intervals, indicating that the bootstrap empirical distribution is practically symmetric.

5.10.2 Multi-Degree-of-Freedom buildings

Figure 5.15 shows the results of the bias of $S_a(T_1)$ on the conditional $S_a(T_1,5\%)$ capacities for the three-storey (LA3) in figure 5.15a and in figure 5.15b the nine-storey (LA9) steel moment resisting frames. For both frames the bias is approximately constant for the whole range of limit-states. For the three-storey building the demand is underestimated, approximately by 10%.

This is a small bias and is always acceptable for engineering purposes. Moreover, some sensitivity is observed for early limit-states, i.e. θ_{max}=0.02. On the other hand, small overestimation of the demand is seen for the nine-storey frame, but in this case the intervals contain the unity line, indicating that we can consider our capacity estimations as unbiased. Again the bootstrap median is at the center of the intervals and its value is approximately 0.9 for three-storey frame and ranges from 1.1 to 0.98 for the nine-storey frame. Moreover, it can be seen that the MDOF results, give close qualitatively predictions to those of the SDOF.

The bias observed may be attributed also to duration and frequency characteristics of the records selected. It is true that no single parameter such as $Sa(T_1,5\%)$ can adequately characterize strong motion characteristics including frequency content, energy content and duration (Jennings 1985).
However:

1. The present work attempts to evaluate the scaling procedure as it is usually applied. For example no special care is paid, regarding the duration and frequency characteristics, for the selection of the record-set to perform IDA analyses (Vamvatsikos and Cornell 2005)
2. Also a large number of earthquake records with a variety of frequency content, energy content and duration have been included in the analyses; thus, the effect of any single strong motion parameter may be assumed that is relatively small.
3. Another issue of interest is the fact that increasing the requirements to be satisfied from the earthquake records may lead to significant decrease in the number of available earthquake records which may be controversial to accuracy in this type of reliability analyses.

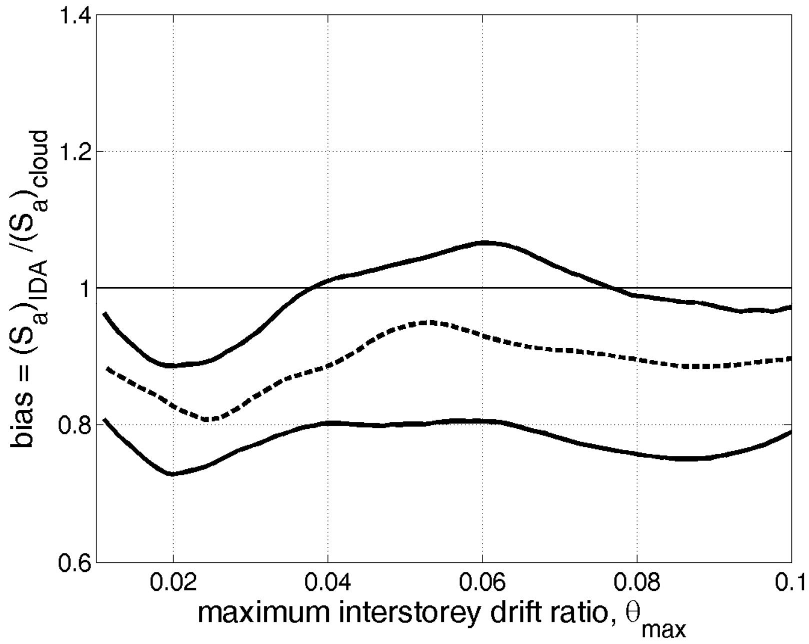

Figure 5.15a: Bootstrap 95% confidence intervals on the ratio of the median $S_a(T_1,5\%)$-capacities given θ_{max} of the IDA case over the cloud case for the LA3 building.

The use of a record-set with relatively equal frequency content and duration which could be achieved through the use of a suitable parameter, e.g., of the mean period T_m [Rathje *et al.* 1998] could be an issue of a forthcoming research.

A methodology for the evaluation of the bias of $S_a(T_1,5\%)$ intensity measure introduced due to record scaling in incremental dynamic analysis has been presented. The results of the bias assessment show that the SDOF oscillators underestimate the Sa capacity of IDA for first mode periods T1=0.1, 0.3 and 0.5sec, while IDA gave unbiased response estimates for SDOFs with T1=0.7, 1.0 and 1.5sec. This indicates that for small periods there is significant bias and the IDA method underestimates the response. As the period increases, the bias tends to become considerably smaller. In the latter case, and for early limit-states (ductilities up to 5) there may also be some bias, but now the response is overestimated. For the three- and nine-storey steel moment resisting frames IDA does not bias the seismic capacity estimates. The effect of bias for MDOF buildings can be extracted from the plots of the SDOF oscillators, but there will always be differences due to the complexity of the MDOF models compared to the simplified SDOF oscillators.

The bias estimation of MDOF structures, such as the LA3 and the LA9 buildings, is an issue that deserves further study due to the inherent complexity of the problem. Among the factors that complicate (compared to the SDOF case) this effort are the contribution of higher-modes, the difficulty to have a single response parameter capable to characterize the response (EDP), the difficulty to have an appropriate IM and the complex non-linear response due to the different plastic mechanisms and dynamic instabilities that may affect the collapse mechanism. Therefore, we here provide a first evaluation of the effect of record scaling within the frameworkof the IDA method based on the study of only two MDOF structures.

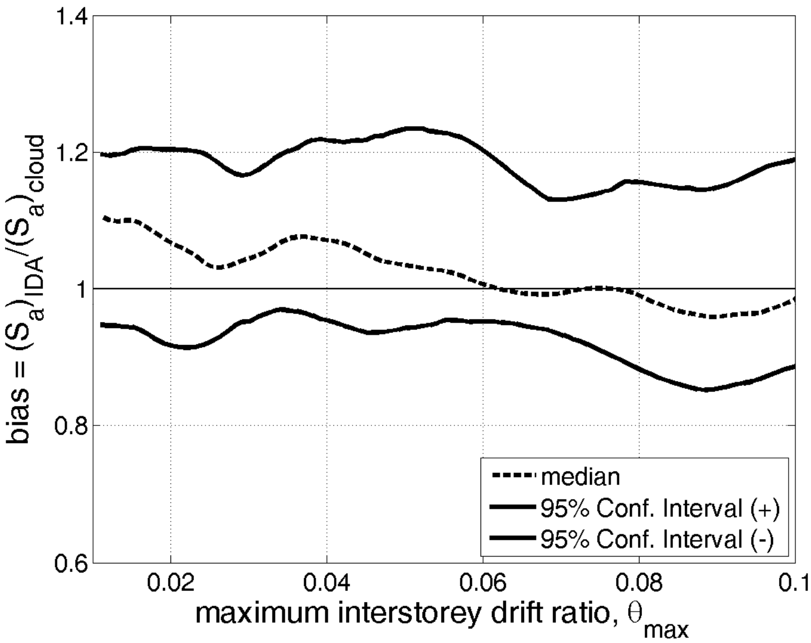

Figure 5.15b: Bootstrap 95% confidence intervals on the ratio of the median $S_a(T_1,5\%)$-capacities given θ_{max} of the IDA case over the cloud case for the LA9 building.

5.11 References

Aschheim, M., Tjhin, T., Comartin, C., Hamburger, R., Inel, M. (2007). “The scaled nonlinear dynamic procedure”, Engineering Structures, 29(7): 1422-1441.

Assimaki, D., Li, W., Steidl, J., Schmedes, J. (2008). “Quantifying nonlinearity susceptibility via site-response modeling uncertainty at three sites in the Los Angeles basin”, Bulletin of the Seismological Society of America, 98 (5): 2364-2390.

Baker J.W. (2007). “Measuring bias in structural response caused by ground motion scaling” in Proceedings, 8th Pacific Conference on Earthquake Engineering, Nangyang Technological University, Singapore, 8 pp.

Baker, J.W., Cornell C.A. (2006). “Vector-Valued Ground Motion Intensity Measures for Probabilistic Seismic Demand Analysis”, John A. Blume Earthquake Engineering Center. Report No. 150 Report#150, Stanford, CA.

Cleveland, W.S. (1979). "Robust Locally Weighted Regression and Smoothing Scatterplots". Journal of the American Statistical Association 74 (368): 829–836. doi:10.2307/2286407.

Cleveland, W.S. (1981). "LOWESS: A program for smoothing scatterplots by robust locally weighted regression". The American Statistician 35 (1): 54.

Cleveland, W.S., Delvin, S.J. (1988). “Locally-weighted Regression: An approach to Regression Analysis by local fitting”, J. Amer. Statist. Assoc., 83(403): 596-610.

Cornell, C.A., Jalayer, F., Hamburger, R.O., Foutch D.A. (2002). “The probabilistic basis for the 2000 SAC/FEMA steel moment frame guidelines”, Journal of Structural Engineering, 128(4): 526-533.

Cui, Y., Poyraz, E., Olsen, K.B. Zhou, J., Withers, K., Scott, K. Callaghan, S., Larkin, J., Clark C. Guest, C.C., Choi, D.J., Chourasia, A., Shi, Z., Day, S.M., Maechling, P., Jordan, T.H. (2013). “Physics-based seismic hazard analysis on petascale heterogeneous supercomputers.” SC2013:70(http://www.informatik.unitrier.de/~ley/pers/hk13/d/Day:Steven_M==; last accessed 20 Jan. 2014).

Efron B., Tibshirani R. (1993). “An introduction to the Bootstrap”. New York, Chapman & Hall.

FEMA P-695 (2009). “Quantification of Seismic Performance Factors”, FEMA P-695 Report, prepared by the Applied Technology Council for the Federal Emergency Management Agency, Washington, D.C.

Fox J., (2002) “Nonparametric Regression: Appendix to An R and S-PLUS Companion to Applied Regression”.

Grant, D.N., Diaferia, R. (2013). “Assessing the adequacy of spectrum-matched ground motions for response history analysis”, Earthquake Engineering & Structural Dynamics, 42: 1265-1280.

Graves, R.W, Pitarka A. (2010). “Broadband ground motion simulation using hybrid approach”, Bulletin of Seismological Society of America. Bull. Seism. Soc. Am., 100, 5A, 2095-2123.

Grigoriu, M. (2011). “To Scale or Not to scale Seismic Ground-Acceleration Records”, J. Eng. Mech,137(4):284-293.

Hesterberg, T., Monaghan, S., Moore, D.S., Clipson, A., Epstein, R., (2003). “Bootstrap methods and permutation tests” W.H. Freeman and company, New York.

Iervolino, I., Cornell, C.A. (2005). “Record selection for nonlinear seismic analysis of structures.” Earthquake Spectra, 21(3): 685–713.

Iervolino, I., De Luca, F., Cosenza, E. (2010). “Spectral shape-based assessment of SDOF nonlinear response to real, adjusted and artificial accelerograms”, Engineering Structures, 32(9): 2776-2792

Jalayer, F., Cornell, C. A. (2009). “Alternative non-linear demand estimation methods for probability-based seismic assessments”, Earthquake Engineering & Structural Dynamics, 38(8): 951-972.

Jennings PC. (1985). “Ground motion parameters that influence structural damage”. In: Scholl RE, King JL, editors. Strong ground motion simulation and engineering applications, EERI Publication 85-02. Berkeley, CA: Earthquake Engineering Research Institute;

Katsanos, E.I., Sextos A.G., Manolis G.D., (2010). “Selection of earthquake ground motion records: A state-of-the-art review from a structural engineering perspective”, Soil Dynamics & Earthquake Engineering, 30(4): 157-169.

Kottke, A. Rathje, E.M. (2008). “A semi-automated procedure for selecting and scaling recorded earthquake motions for dynamic analysis”, Earthquake Spectra, 24(4): 911-932.

Krinitzsky, E.L. and Marcuson, W.F. (1983). “Principles for selecting earthquake motions in engineering design”. Bulletin of the Association of Engineering Geologists, 20(3): 253–265.

Liu, P., Archuleta, R.J., Hartzell, S.H. (2006). “Prediction of broadband ground-motion time histories: Hybrid low/high-frequency method with correlated random source parameters”, Bulletin of the Seismological Society of America, 96(6): 2118-2130.

Luco N., Rezaeian S. (2013). “Progress of the SCEC Ground Motion Simulation Validation (GMSV) Technical Activity Group (TAG), 2013 Cosmos Annual Meeting”, http://www.cosmos-eq.org/technicalsession/5_Luco.pdf (last accessed 01.02.2014)

Luco, N. and Bazzurro, P. (2007). “Does amplitude scaling of ground motion records result in biased nonlinear structural drift responses?” Earthquake Engineering & Structural Dynamics, 36(13): 1813-1835.

McKenna, F., Fenves, G.L. (2001). “The OpenSees Command Language Manual -Version 1.2”, Pacific Earthquake Engineering Research Centre, University of California, Berkeley.

Olsen, K.B., Mayhew J.E. (2010). “Goodness-of-fit Criteria for Broadband Synthetic Seismograms, With Application to the 2008 Mw5.4 Chino Hills, CA, Earthquake”, Seism. Res. Lett. 81, 715-723.

PEER (2008). PEER NGA Database. Pacific Earthquake Engineering Research Center. available from http://peer.berkeley.edu/smcat/, last accessed on 2008.

Ratje, E.M., Abrahamson, N.A., Bray, J.D. (1998) “Simplified Frequency Content Estimates of Earthquake Ground Motions”, J. Geotech. Geoenviron. Eng. 124: 150-159.

Shome, N., Cornell, C.A., Bazzurro, P., Carballo, J.E. (1998). “Earthquakes, records, and nonlinear MDOF responses”, Earthquake Spectra, 14(3): 469–500.

Spyrakos, C., Koutromanos, I.A. and Maniatakis, Ch.A., (2009) “Seismic Response of Base-Isolated Buildings Including Soil-Structure Interaction”, Soil Dynamics and Earthquake Engineering, Vol.29, pp. 658-668.

Spyrakos, C., Maniatakis, Ch.A. and Koutromanos, I. A., (2009) “Soil-Structure Interaction Effects on Base-Isolated Buildings Founded on Soil Stratum”, Engineering Structures Journal, Vol.31, pp.729-737.

Vamvatsikos, D., Cornell, C.A. (2002). “Incremental Dynamic Analysis”, Earthquake Engineering & Structural Dynamics, 31(3): 491–514.

Vamvatsikos, D., Cornell, C.A. (2005). “Developing efficient scalar and vector intensity measures for IDA capacity estimation by incorporating elastic spectral shape information”, Earthquake Engineering & Structural Dynamics, 34(13): 1573-1600.

Vanmarcke, E.H. (1979). “State-of-the-art for assessing earthquake hazards in the United States: Representation of earthquake ground motion: scaled accelerograms and equivalent response spectra” Miscellaneous Paper S-73-1, Report 12, US Army Corps of engineers Waterways Experiment Station, Vicksburg, Mississippi.

Watson-Lamprey, J., Abrahamson, N. (2006). “Selection of ground motion time series and limits on scaling”, Soil Dynamics & Earthquake Engineering, 26(5): 477-482.

CHAPTER 6

Structural optimization

6.1 Introduction

The term “optimum design of structures” is of unclear meaning unless someone interprets it correctly. Therefore structural mechanics gives a clear meaning of the terms ‘structure’ and ‘optimum design’. The baseline of structural mechanics interprets the term “structure” as a description of the arrangement of the elements and the materials that creates a system capable to undertake the loads imposed by the design requirements. This procedure is iterative and when it is implemented for the design of structure its aim is to reach the optimum design. Structural engineering aims at the construction of structural systems like bridges, aircrafts etc. The progress of computer technology created more demands in structural engineering as well. In this way the design of a structural system that satisfies the structural requirements related to safety and economy are of great importance to be optimally designed. The term “optimum design’’ is used for a design that satisfies the serviceability requirements and also complies with criteria like the cost or the weight of the system that has to have the less possible values.

The aim of the engineer is to optimize (minimize) one (or more) objective function(s). This can be done by finding a combination of independent design variables that may take real or integer values. In structural mechanics, such optimization problems usually impose restrictions on the random variables, which refer to the range of every parameter, which define the search space. Moreover, the restrictions are imposed on other constraint functions, like those imposed on stresses and strains, which determine the space of acceptable solutions for the problem at hand.

For the calculation of an optimal design the engineers have to perform two steps: find the mathematical formulation of the optimization problem and implement an optimization algorithm. The first step involves the definition of the design parameters, the relationship between these parameters, determining the optimization function as well as defining the constraints of the problem. The second step is to choose a suitable optimization algorithm which will be combined with structural and optimization models. A basic premise for the case of structural optimal design is to express in mathematical terms the structural behavior (structural model). In the case of structural systems behavior this refers to the response under static and dynamic loads, such as displacements, stresses, eigenvalues, buckling loads, etc.

The fact that efficient optimization algorithms exist guaranties that the problem of optimal design will be adequately addressed. An important parameter for the proper use of these algorithms is the experience of the engineer. The design procedure is an iterative process where repetition is considered as the sequential test of candidate designs. Also, it evaluates whether they are superior or not compared to the past ones, while satisfying the constraints of the problem. The conventional procedure used by engineers is the ‘‘trial and error’’ procedure. The use of such empirical techniques with increased complexity and magnitude does not lead to the optimal solution of the problems. This was the reason that led to automatic the design of buildings by exploiting the developments in computer technology and the advances in optimization algorithms. Nowadays, these tests can be performed automatically and with greater speed and accuracy.

6.2 A review on optimization in engineering

New and more efficient methods have been developed recently still the history of optimization dates hundreds of years from the era of Euclid until today. Euclid (300B.C.) confronted with the problem of finding the shortest distance which may be drawn from a point to a line (Russo, 2004), while Heron of

Alexandria (100B.C.) studied the optimization problem of light travelling between two points by the shortest path (Russo, 2004). Cauchy (1847) presented for the first time a minimization procedure (Steepest Descent Method) implementing function derivatives. The development of calculus provided the means for the development of the mathematical theory for optimization. The pioneering works of Courant (1943) on penalty functions, Danzig (1951) on linear programming, Karush (1993) as well as Kuhn and Tucker (1951) on optimality conditions for constrained problems initiated the modern era of optimization.

Optimization methods for solving nonlinear problems were introduced mostly in the 60's. We begin with Rosenbrock (1960) who presented the method of orthogonal directions, Rosen (1960) suggested the gradient projection method, Zoutendijk (1960) formed the feasible directions method. In 1961 Hooke and Jeeves developed the pattern search method, Davidon, Fletcher and Powell (1963) stated the variable metric method. We continuou with Fletcher and Reeves (1964) presented the Conjugate Gradient method, Powel (1964) introduced the method of conjugate directions, Nelder and Mead (1965) suggested their Simplex method. Finally, Box (1965) introduced his homonymous technique, while Fiacco and McCormick (1966) formed the so called Sequential Unconstrained Minimization technique.

In the 70's structural optimization has been the subject of intensive research. This fact encloses several different approaches for optimal design of structures which has been advocated (Sheu and Prager (1968); Pope and Schmit (1971); Spunt (1971); Galagher and Zienkiewicz (1973); Venkayya et al. (1973); Haug and Arora (1974); Moses (1974)). The methods presented here are of deterministic character; that is when applied to the same initial design vector the result is always the same final design vector. The non-existence of randomness is the reason for this. As a result, there is also the probability of getting trapped in local minima. Mathematical programming (MP) methods make use of local curvature information derived from linearization of the original functions. This is done by using their derivatives, with respect to the design variables at points obtained in the process of optimization, to construct an approximate model of the initial problem. On the contrary the application of combinatorial optimization methods based on probabilistic searching do not need gradient information and therefore avoid to perform the computationally expensive sensitivity analysis step. Gradient based methods present a satisfactory local rate of convergence, but they cannot assure that the global optimum can be found, while combinatorial optimization techniques are generally more robust and present a better global behavior than the mathematical programming methods. They may suffer, however, from a slow rate of convergence towards the global optimum (Mitropoulou et al. 2011).

In contrast to the deterministic optimization methods, stochastic optimization algorithms allow for randomness to appear. In this way, it is possible to get different final design vectors, even though the initial vector is the same. In this category, the most known and widely applied methods are the genetic algorithms (GA), originating from Holland (1975) and Goldberg (1989), the simulated annealing (SA) by Kirkpatrick (1984), evolutionary programming (EP) (Fogel et. al, 1966), and the evolutionary strategies (ES) (Rechenberg, 1973; Schwefel, 1981).The main characteristic of these methods is the wider exploration and exploitation of the domain, which in turn increases both the probability of locating the global minimum and the computational cost. Both GA and ES imitate biological evolution and combine the concept of artificial survival of the fittest with evolutionary operators to form a robust search mechanism. Apart from the pure deterministic or pure stochastic procedure, hybrid schemes have been introduced as well. The main idea behind the hybridism is to combine the advantages of both categories of methods in order for a better result to be obtained (Papadrakakis et. al, 1999; Lagaros et. al, 2002, Mitropoulou et al, 2011).

6.3 Formulation of an optimization problem

In an automatic seismic design algorithm, the whole design process is nested within the framework of an optimization algorithm. The main benefit of using a structural optimization environment is that the optimization algorithm locates the most efficient design is serving as a “search engine” among a vast number of possible design solutions. To use such algorithms it is first necessary to set up the mathematical formulation of the optimization problem.

In its simplest form the formulation of the generic Single *Objective Optimization Problem (SOP)* can be written as follows:

$$\min F(s)$$
$$\text{s.t.}\begin{cases} g_i(\mathbf{s}) \geq 0, i = 1,...,l \\ s_j \in R^d, j = 1,...,m \end{cases} \tag{6.1}$$

where $F(\boldsymbol{s})$ is the objective function to be minimized and g_i are the l deterministic constraints of the problem, $\boldsymbol{s}$ is the vector of m design variables that take their values from a discrete set denoted as R^d. The aim of sizing optimization is to minimize the objective function, which usually is proportional to the cost of the structure. The design variables of Eq. 6.1 are discrete since they refer to the cross-sections of the structural members, while R^d refers to the table of commercial structural sections. Due to engineering practice demands, the structural members (beams and columns) are divided into groups of design variables, thus providing a trade-off between the use of more material and the need for symmetry and uniformity due to practical considerations.

Equality constraints rarely appear in nature and therefore are used scarcely in real world problems. Mostly we use inequality constraints. If the objective function is the weight of the structure, then it is given by:

$$f(x) = \rho \cdot \sum_{i=1}^{N_e} A_i \cdot L_i \tag{6.2}$$

where ρ is the material density, N_e is the number of elements of the model and A_i, L_i are the cross sectional area and the length of each structural element, respectively.

6.4 Objective Function

A large number of designs ranging from feasible to infeasible while only one solution is the best to describe every optimization problem. This distinction between good and better designs necessitates a criterion which will compare and evaluate the designs. This criterion is defined by a function that takes a specific value for any given design and it is called objective function. This objective function depends on the design variables (see equation (6.1)). Equation 6.1 refers to a minimization problem. A maximizing problem of the function F(**s**) can be transformed into a minimization problem of the objective function -*F*(**s**). An objective function that is to be minimized it is often called as the weight function.

Selecting the objective function is a very important step. It is as important as the proper selection of the design variables. Possible objective functions reported in the literature are: minimizing the cost, the weight optimization problem, the energy losses problem and maximizing the profit. When these functions are applied as a single-objective in the optimization problem they form a single-objective design. Also, in many cases the formulation of the optimization problem is defined with the simultaneous optimization of two or more objective functions that form conflicting targets. As an example, of this type of optimization problem is the case where the objective is to find an optimum design with minimum weight and simultaneously to have minimum stress or displacement fields in some parts of the structural system. These type of problems are called optimization problems with multiple objective functions (multi-objective design or Pareto optimum design).

6.5 Design variables

A fully defined design requires the correct selection of certain parameters called design variables. A design is called infeasible when it does not fullfil the requirements of the problem while when the requirements are fulfilled the design is called feasible.

A feasible design is the one that is able to be implemented and not necessarily the best. In order to tackle the mathematical problem correctly we ought to have selected the correct design variables. The incorrect selection of the design variables in the worse case it will give an infeasible design. As the 'degrees of freedom' of the mathematical model of the structure of the optimization problem is increased, it is desirable to select more design variables that are necessary for the problem formulation. In such problems it is possible to remove the additional design variables by designating to them specific values for the next steps of the optimization procedure.

6.6 Discrete and continuous design variables

The design variables which are used in structural design optimization due to manufacturing limitations are discrete (Makris *et al.* 2006) since cross-sections have to belong to a certain predefined set provided by the manufacturers. There are also cases where for the same problem the design variables are mixed, continuous and discrete, e.g. in a topology-sizing optimization problem where the design variables include nodal coordinates (continuous) as well as beam cross-sectional sizes (discrete). With the general formulation of Eq. (6.1), the design variables may have continuous, discrete or integer values, or a combination of them, with the restriction:

$$x_i \in \mathrm{X}_i \quad \text{for } i = 1, \ldots, n \tag{6.3}$$

where X_i is the set of x_i, which may be continuous or discrete. When discrete design variables are only used, then the available set of values is clearly defined. When continuous design variables are considered, then the above restriction is usually written as:

$$x^L \leq x \leq x^U \tag{6.4}$$

where x^L and x^U are two vectors of length n containing the lower and upper bounds of the design variables, respectively.

Various methods have been proposed for dealing with mixed problems, with continuous and discrete design variables (Bremicker *et al.* 1990). Usually discrete variables are handled as equivalent continuous variables, and at the end of the optimization process the design variables are given the appropriate discrete values, as close as possible to the optimal continuous values (Hager and Balling 1988). In case of a discrete problem where the design space can be univocally arranged for all the characteristics of the cross sections, the above method can give a good approximation of the discrete optimum solution. Nevertheless, in realistic engineering problems this may not be the case. Most the methods that have been proposed convert the mixed problem to a series of continuous problems that are solved consecutively (Cai and Thierauf 1993a; Cai and Thierauf 1993b; Fu et al. 1991).

6.7 Constraint Functions

The design of a structural system is achieved when the design parameters take specific values. Design can be considered any arbitrarily defined structural system, such as a circular cross section with a negative radius, or a ring cross section with a negative wall thickness, as well as any non-constructible building system. All engineering or code provisions are introduced in the mathematical optimization model in the form of inequalities and equalities which are called constraint functions. These constraint functions in order to have meaningful contribution on the mathematical formulation of the problem should be at least dependent on one design variable. The constraint functions that are usually imposed on the structural problems are stress and strain constraints, whose values are not allowed to exceed certain limits. Sometimes the engineers impose additional constraint functions that may be useless, which they are either dependent on others or they remain forever in the safe area, this is due to the existence of uncertainties on the definition of the problem or due to inexperience. The use of additional constraint functions may result to calculations requiring additional computational effort without any benefit especially in the case of mathematical programming methods that they require to perform sensitivity analysis.

One inequality constraint function $g_j(\mathbf{s}) \leq 0$ is considered as active at the point $\mathbf{s}^*$in the case that the equality is satisfied, i.e. $g_j(\mathbf{s})=0$. Accordingly, the above constraint function is considered as inactive for the design $\mathbf{s}^*$ for the case that the inequality is strictly satisfied, i.e. $g_j(\mathbf{s}^*)<0$. The inequality constraint function is considered that it is violated for the design $\mathbf{s}^*$if a positive value that $g_j(\mathbf{s}^*)>0$, corresponds to the value of the constraint function. Similarly, an equality constraint function $h_j(\mathbf{s})$ is considered that it is violated for the design $\mathbf{s}^*$ if the equality is not satisfied, i.e. $\mathrm{h_j}(\mathbf{s}*)\neq 0$.Therefore, an equality constraint function might be active or violated. From all the description provided related to the active or the inactive constraint functions it is clear that any feasible design is defined by active or inactive inequality constraint functions and active equality constraint functions.

At each step of the optimization process it is unlikely that all constraint functions are active. The engineers are not able to determine in advance which of these functions will become active and which of them will become inactive at each step. For this reason, when solving optimization problems it is necessary to use different techniques to address more effectively the constraint functions, techniques that greatly improves the efficiency of the optimization procedure and reduce significantly the time required for the calculations. Especially when the problem is relatively large, i.e. the formulation of the problem is defined with many design variables and constraint functions, any possibility of reducing the calculations of the values required and the derivatives of constraint functions has significant impact on the efficiency of the performance of the optimization procedure. So it is crucial to identify at each step of the optimization procedure the constraint functions that are located within the safe area, i.e. they are inactive, which they do not affect the process of finding of an improved design in order to continue the optimization process with only the active constraint functions.

An active constraint function suggests that its presence significantly affects the improvement of the current design. By definition, the equality constraint functions should be fulfilled at each step of the optimization procedure;

therefore they are considered always among the active constraint functions (Arora, 1989; Gill and Murray, 1981). An active inequality constraint function means that at this stage it should be fulfilled as equality or even approximately. When a constraint function is inactive then it means that its presence is not important at that part of the optimization procedure, since the active constraint functions fullfil the needs of the design. This does not mean, though, that this constraint function is redundant as in another optimization step can be activated. Usually, in order to increase the effectiveness of the mathematical algorithms, only the active constraint functions are taken into account. On the other hand other optimal design methods like the fully-stressed design method are based on exploiting the presence of active constraint functions.

In order to identify the active constraint functions the values of the constraint functions should be normalized first (Vanderplaats, 1984) to have a single reference system regardless of the type of the constraint function. For example, it is likely that the value of a displacement constraint function to take values in the order of 0.1-2.0 cm, while the value of a stress displacement constraint function to take values is in the order of 25,000 kPa, so readily it is apparent that it is necessary to homogenize the sizes of the two constraint functions. The normalization of the value constraint functions takes place in accordance with the following relations:

$$g_j^N(\mathbf{s}) = \frac{g_j^l - g_j}{\left|g_j^l\right|} \leq 0 \qquad (6.5)$$

for a constraint function limited with a lower bound, $g_j^l \leq g_j$, and:

$$g_j^N(\mathbf{s}) = \frac{g_j - g_j^u}{\left|g_j^u\right|} \leq 0 \qquad (6.6)$$

for a constraint function limited with an upper bound, $g_j \leq g_j^u$. Thus, if the normalized value of the constraint function is equal to +0.50 then it violates its permissible value by 50%, while if its normalized value is equal to -0.50 then this constraint is 50% below the allowable value. Usually among the active constraint functions are included those with normalized value greater than -0.1 to -0.01 (Arora, 1989). Furthermore, it is also allowed a small tolerance when the constraint functions violate the minimum allowable value (-0.005 to 0.001) since the process of simulation, analysis, design and construction involves many uncertainties.

6.8 Global and local minimum

A common problem for all mathematical optimization methods is that due to the deterministic nature of the operators used they may be directed to identifying a local minimum, in contrast to the methods that are based on probabilistic operators where random search procedures are implemented and they are more likely to locate the global minimum of the problem at hand. The definitions of the local and the global minimum in mathematical terms can be as follows:

Local minimum. A point s*in the design space is considered as a local or a relative minimum if the design satisfies the constraint functions and the relationship $F(s^*) \leq F(s)$ is valid for every feasible design point in a small region around the point s*. If only the inequality is valid, $F(s^*) < F(s)$, then the point s* is called as a strict or a unique or a strong local minimum.

Global minimum. A point s* the design space is defined as the global or absolute minimum for the problem at hand if this design satisfies the constraint functions and the relation $F(\mathbf{s}^*) \leq F(\mathbf{s})$ is valid for every feasible design point. If only the inequality is valid. $F(\mathbf{s}^*) < F(\mathbf{s})$, then the point s* is called as a strict or a unique or a strong global minimum.

If there is no constraint functions then the same definitions can be used, but they are valid throughout the design space and they are not restricted only in the region of feasible designs. Generally it is difficult to foretell in advance the existence of local or global minimum in every optimal design problem. However, if the objective function F(**s**) is continuous and the region of feasible designs is nonempty, closed and bounded, then there is a global minimum for the objective function F(**s**) (Arora, 1994). The region of feasible is defined as not empty when there are no conflicting constraint functions or when there are not redundant constraint functions. If the optimization algorithm cannot to identify any feasible point then it can be said that the region of feasible designs is empty and therefore the problem should be reformulated by removing or defining some constraint functions to be more flexible. The region of feasible designs is defined as closed and fixed when the constraint functions are continuous and there are not 'strict' inequality constraint functions (g(**s**)<0). The existence of minimum designs is not cancelled if these conditions are not satisfied, simply the minimum designs cannot be established mathematically, but these optimum designs can be obtained during the optimization process.

6.9 Types of structural optimization problems

There are mainly three classes of structural optimization problems: (i) sizing; (ii) shape; and (iii) topology optimization.

6.9.1 Sizing Optimization

In sizing optimization problems the aim is mainly to minimize the weight of the structure under certain behavioral constraints on stresses and displacements. The design variables are most frequently chosen to be dimensions of the cross-sectional areas of the members of the structure. Due to engineering practice demands the members are divided into groups having the same design variables. This grouping of elements results in a trade-off between the use of more material and the need of symmetry and uniformity of structures due to practical considerations. Furthermore, it has to be taken into account that due to fabrication limitations the design variables may not be continuous but discrete since cross-sections belong to a certain predefined set, provided by the manufacturers. In this dissertation we are mainly occupied with this category of optimization problems.

6.9.2 Shape Optimization

In structural shape optimization problems the aim is to improve the performance of the structure by modifying its boundaries and therefore its shape. This can be numerically achieved by minimizing an objective function subjected to certain constraints (Hinton and Sienz (1994); Ramm *et al*. (1994)). The design variables are either some of the coordinates of the key points in the boundary of the structure or some other parameters that influence the shape of the structure. When shape optimization is considered, the structural domain is not fixed but has a predefined topology.

6.9.3 Topology Optimization

Structural topology optimization assists the designer to define the type of structure, which is best suited to satisfy the operating conditions for the problem at hand. It can be seen as a procedure of optimizing the rational arrangement of the available material in the design space and eliminating the material that is not needed. Topology optimization is usually employed in order to achieve an acceptable initial layout of the structure, which is then refined with a shape optimization tool. Various methods have been proposed for topology optimization problems, employing the following main approaches (Hinton and Sienz 1993): (i) Ground structure approach (Pedersen 1993; Schwefel 1981); (ii) homogenization method (Bendsoe and Kikuchi 1988; Hinton and Hassani 1995; Suzuki and Kikuchi 1993); (iii) bubble method (Eschenauer et al. 1993); and (iv) fully stressed design technique (Van Keulen and Hinton 1996; Xie and Steven 1993). The first three approaches behave as normal optimization techniques. On the other hand, the fully stressed design technique is not an optimization algorithm in the conventional sense, as it proceeds by removing inefficient material, and therefore optimizes the use of the remaining material in the structure, in an evolutionary process.

6.10 Genetic Algorithms

Evolutionary algorithms (EA) are able to handle complicated optimization problems at the expense of more optimization cycles. Their rapid development made feasible the solution of complex and realistic nonlinear structural optimization problems. Evolutionary–based optimizers do not require the calculation of gradients of the constraints, as opposed to mathematical programming algorithms, and thus structural design code checks can be implemented in a straightforward manner as constraints. Several recent publications using different algorithms for the optimum seismic design of steel structures can be found in the literature. For example, Liu *et al.* (2006), and Rojas *et al.* (2007), presented seismic multi-criteria design approaches considering reliability-based design methodologies using a genetic algorithm (GA). Another popular optimization algorithm is the evolution strategies (ES) which has been successfully used by several researchers (Lagaros *et al*. 2002, among others). A promising option would also be the use of the harmony search algorithm which imitates the musician who searches for a better state of harmony. This algorithm had been recently used to optimize large-scale steel frames (Hasancebi *et al.* 2010, Lagaros and Papadrakakis (2011)).

In this study the optimization problem is solved using a genetic algorithm. GA is a general search and optimization methodology inspired by the process of natural selection (Goldberg 1989) and is currently the most widely used evolutionary algorithm. The algorithm is based on Darwin's theory of evolution, with the central concept being that one could start with a primordial mess and end up with the incredibly diverse set of biological solutions seen today. Its metaphor to engineering optimization, results to a numerical tool that can be used for general purposes and does not need the calculation of gradients as traditional mathematical optimizers do. Implementations of this model typically use fixed-length character strings (binary or real valued) to represent their genetic information, together with a population of individuals which undergo mutation and crossover in order to guide the search process towards the optimum. A string, which represents a member of the genetic population, is referred as a genotype or a chromosome.

6.10.1 The three main steps of the basic GA

Step 0 initialization: The first step in the implementation of any genetic algorithm is to generate an initial population. In most cases the initial population is generated randomly. In this study in order to perform a comparison between various optimization techniques the initial population is fixed and is chosen in the neighborhood of the initial design used for the mathematical programming method. After creating an initial population, each member of the population is evaluated by computing the representative objective and constraint functions and comparing it with the other members of the population.

Step 1 selection: Selection operator is applied to the current population to create an intermediate one. In the first generation the initial population is considered as the intermediate one, while in the next generations this population is created by the application of the selection operator.

Step 2 generation (crossover–mutation): In order to create the next generation, crossover and mutation operators are applied to the intermediate population to create the next population. Crossover is a reproduction operator, which forms a new chromosome by combining parts of each of the two parental chromosomes. Mutation is a reproduction operator that forms a new chromosome by making (usually small) alterations to the values of genes in a copy of a single parent chromosome. The process of going from the current population to the next population constitutes one generation in the evolution process of a genetic algorithm. If the termination criteria are satisfied the procedure stops, otherwise, it returns to step 1.

The steps of the GA-based design algorithm we used in this dissertation are briefly summarized as follows:

1. ***Initialization**:* Random generation of an initial population of the vectors of the design variables s_j (j=1,.., m). The vectors are encoded as binary strings.
2. ***Fitness evaluation - "Analysis steps"***: perform all necessary calculations to assess the capacity of the structure. If some problem constraints are violated, penalize the objective function. The analysis step and the calculation of the penalties are discussed in the paragraphs that follow.
3. ***Selection, Generation and Mutation***: Apply the GA operators (selection, generation, mutation) to create the members of the next generation t^j (j=1,…, m).
4. ***Final check**:* Stop if a pre-specified number of generations has been reached, or a convergence criterion has been met, otherwise return to step 2.

6.11 Methods for handling the constraints

Although genetic algorithms were initially developed to solve unconstrained optimization problems, during the last decade several methods have been proposed for handling constrained optimization problems as well. The methods based on the use of penalty functions are employed in the majority of cases for treating constraint optimization problems with GA. In this study methods belonging to this category have been implemented and will be briefly described in the following section.

The methods based on the use of penalty functions are employed in the majority of cases for treating constraint optimization problems with GA. In this study methods belonging to this category have been implemented and will be briefly described in the following section.

6.11.1 Method of static penalties

In the method of static penalties the objective function is modified as follows:

$$F'(s)=\begin{cases}F^{(n)}(s),\text{if } \mathbf{s}\in R^{\mathrm{d}}\\ F^{(n)}(s)+p\cdot viol^{(n)}(s), otherwise\end{cases} \tag{6.7}$$

where p is the static penalty parameter, viol is the sum of the violated constraints and F is the objective function to be minimized, both normalized in [0,1], while F is the feasible region of the design space.

$$viol(s)=\sum_{j=1}^{m}h_j(s) \tag{6.8}$$

The sum of the violated constraints is normalized before it is used for the calculation of the modified objective function. The main advantage of this method is its simplicity. However, there is no guidance on how to choose the single penalty parameter p. If it is chosen too small the search will converge to an infeasible solution, otherwise, if it is chosen too large, a feasible solution may be located but it would be far from the global optimum. A large penalty parameter will force the search procedure to work away from the boundary where the global optimum is usually located and divides the feasible region from the infeasible one.

6.11.2 Method of dynamic penalties

The method of dynamic penalties was proposed by Joines and Houck (1994) and applied to mathematical test functions. As opposed to the previous method, dynamic penalties are implemented in this case. Individuals are evaluated (at the generation g) by the following formula:

$$\begin{aligned}F'(s)&=F^{n}(s)+(c\cdot g)^{a}\,\mathrm{viol}^{(n)}(s)\\ \mathrm{viol}(s)&=\sum_{j=1}^{m}h_j^{\beta}(s)\end{aligned} \tag{6.9}$$

where c, a and b are constants. A reasonable choice for these parameters was proposed as follows: c =0.5–2.0, a= b= 1 or 2. For high generation number, however, the $(c\cdot g)^{a}$ component of the penalty term takes extremely large values which make even the slightly violated designs not to be selected in subsequent generations. Thus, the system has little chances to escape from local optima. In most experiments reported by Michalewicz (1991) the best individual was found in early generations.

When a constraint is violated, a penalty p is calculated and used to penalize the objective function. The penalty depends on the difference of the value obtained from analysis with the acceptable threshold. Penalizing the objective function will: (a) make the problem unconstrained, and (b) worsen the fitness of the design and thus reduce the probability of its members to participate in a future generation. In this work the objective function is penalized as:

$$\bar{F}(\mathbf{s}) = \max(p)F(\mathbf{s}) \tag{6.10}$$

where $\bar{F}(\mathbf{s})$ is the penalized objective function and max(p) is the maximum value of the penalty p, obtained when one or more constraints have been violated. The calculation of the penalty parameter p is very significant. A large penalty will force the design procedure to work away from the region where the global optimum is located, while a small penalty will make the algorithm converge to an infeasible solution. Moreover, the penalty parameter adjusts the weight of the penalty imposed on the objective function during the optimization process. In our study the penalties are calculated as:

$$p = \left|q - q_{\mathrm{lim}}\right| / q_{\mathrm{lim}} \tag{6.11}$$

where q_{lim} is the threshold value of the quantity on which the constraint is set, and q is the value obtained during the “analysis” step.

6.12 References

Arora, J.S., (1989) “Introduction to optimum design”, McGraw-Hill, New York.

Arora, J.S., (1994) “Methods for optimization of large-scale systems,” in Papadrakakis, M. (ed.), Solving Large-Scale Problems in Mechanics, John Wiley, 391-430.

Bendsoe M.P., and Kikuchi N., (1988), “Generating optimal topologies in structural design using a homogenization method”, Computer Methods in Applied Mechanics and Engineering, 71: 197-224.

Box, M.J. (1965). “A New Method of Constrained Optimization and a Comparison with Other Methods.” Computer J, Vol.8, pp. 42-52.

Bremicker, M., Papalambros, P.Y., and Loh, H.T., (1990), “Solution of Mixed-Discrete Structural Optimization Problems with a New Sequential Linearization Algorithm,” Computers & Structures, 37(4): 451-461.

Cai, J., and Thierauf, G., (1993), “Discrete optimization of structures using an improved penalty function method” Engineering Optimization Journal, 21:293-306.

Cauchy, A. (1847) “Methode generale pour la resolution des systems d’equation simultanes” Compt. Rend., 25:536-538.

Courant R. (1943). “Variational methods for the solution of problems of equilibrium and vibrations.” Bull Amer. Math. Soc, 49:1-23.

Dantzig, G. B. (1951) “Maximization of a linear function of variables subject to linear inequalities.” Activity Analysis of Production and Allocation, Koopman (Ed.), Cowles Commission Monograph, 13, John Wiley and Sons, New York.

Davidson, R., Fletcher, R., Powell, M.J.D. (1963). “A rapidly convergent descent method for minimization.” Computer J., Vol. 6(2): 163-168.

Eschenauer H.A., Schumacher A. and Vietor T., (1993), “Decision makings for initial designs made of advanced materials,” in Bendsoe M.P. and Soares C.A.M (eds.) NATO ARW ‘Topology designs made of advanced materials,’ Sesimbra, Portugal, Kluwer Academic Publishers, Dordrecht, Netherlands, 469-480.

Fiacco, A.V., McCormick, G.P. (1966). “Extension of SUMT for nonlinear programming: equality constraints and extrapolation.” Management Science, 12:816-828.

Fletcher, R., Reeves, C.M (1964) “Function Minimization by Conjugate Gradients”. Computer J., 7:149-154.

Fogel L.J., Owens A.J., and Walsh M.J., (1966), “Artificial intelligence through simulated evolution”, Wiley, New York.

Fu, J., Fenton, R.G., and Cleghorn, W.L., (1991), “A mixed integer-discrete-continuous programming method and its applications to engineering design optimization”, Engineering Optimization Journal, Vol. 17:263-280.

Gallagher R.H. and Zienkiewicz).C., (1973), "Optimum Structural Design: Theory and Applications", John Wiley & Sons, New York, USA.

Goldberg, D.E, (1989) "Genetic Algorithms in search, optimization and machine learning", Addison-Wesley.

Hager, K., Balling R. (1988). "A New Approach for Discrete Structural Optimization." ASCE Journal of Structural Engineering, 114(5), 1120-1134.

Haug E.J and Arora J.S., (1974) "Optimal mechanical design techniques based on optimal control methods", ASME paper No 64-DTT-10, Proceedings of the 1st ASME design technology transfer conference, 65-74, New York, October.

Hinton E., and Hassani B., (1995) "Some experiences in structural topology optimization", in B.H.V Topping (ed.) Developments in Computational Techniques for Structural Engineering, CIVIL-COMP Press, Edinburgh, 323-333.

Hinton E., and Sienz J., (1993) "Fully stressed topological design of structures using an evolutionary procedure", Journal of Engineering Computations, 12: 229-244.

Hinton E., and Sienz J., (1994) "Aspects of adaptive finite element analysis and structural optimization," in Topping B.H.V. and Papadrakakis M. (eds) Advances in Structural Optimization, CIVIL-COMP Press, Edinburgh, 1-26.

Holland J., (1975), "Adaptation in natural and artificial systems" University of Michingan Press, Ann Arbor, USA.

Hooke, R., Jeeves, T.A. (1961). "Direct Search Solution of Numerical and Statistical Problems." J of the ACM, 8: 212-229.

Joines J., Houck C., (1994), "On the use of non-stationary penalty functions to solve non-linear constrained optimization problems with Gas", in Michalewicz, Z., Schaffer, J.D., Schwefel, H.-P., Fogel, D.B., Kitano, H., (eds), Proceedings of the 1st IEEE International Conference on Evolutionary Computation, IEEE Press, 579-584.

Karush, W. (1939). "Minima of Functions of Several Variables with Inequalities as Side Conditions." MS Thesis, Dept. of Mathematics, University of Chicago, Chicago IL.

Kirkpatrick, S. (1984), "Optimization by simulated annealing: quantitative studies", J Statist Phys, 34: 975-986.

Kuhn, H.W, Tucker A.W. (1951). “Non-linear Programming.” In J.Neyman (Ed.), Proceedings of the Second Berkeley Symposium on Mathematical Statistics and Probability, University of California Press, Berkeley, CA, 481-493.

Lagaros, N.D., Papadrakakis, M., Kokossalakis, G., (2002) “Structural optimization using evolutionary algorithms”, Computer & Structures, 80(7-8), 571-587.

Makris P.A., Provatidis C.G., Venetsanos D.T. (2006) “Structural optimization of thin-walled tubular trusses using a virtual strain energy density approach”, Thin-Walled Structures, 44:235-246.

Michalewicz Z., Janikow C.Z., (1991) “Handling constraints in genetic algorithms”, In Belew, R.K., and Booker, L.B., (eds.), Proceedings of the 4th International Conference on Genetic Algorithms, Morgan Kaufmann, 151-157.

Mitropoulou, Ch., (2011) “Advanced computational methods for seismic design and assessment of reinforced concrete structures”, PhD Dissertation at NTUA.

Moses F., (1974) “ Mathematical programming methods for structural optimization”, ASME Structural Optimisation Symposium AMD 7: 35-48.

Nelder, J.A., Mead, R. (1965). “A Simplex Method for Function Minimization.” Computer Journal, Vol. 7, pp. 308-313.

Papadrakakis, M., Tsompanakis, Y., Lagaros, N.D., (1999). “Structural shape optimization using Evolution Strategies”, Engineering Optimization, 31: 515-540.

Pedersen P., (1993). “Topology optimization of three dimensional trusses”, in Bendsoe M.P., and Soares C.A.M (eds.), NATO ARW ‘Topology design of structures’, Sesimbra, Portugal, Kluwer Academic Publishers, Dordrecht, Netherlands, 19-31.

Pope G.G. and Schmit L.A. (eds.) (1971), “Structural Design Applications of Mathematical Programming Techniques”, AGARDO graph 149, Technical Editing and Reproduction Ltd., London.

Powell, M.J.D. (1964). “An efficient Method for finding the minimum of a function of several variables without calculating derivatives.” Computer Journal, 7(4): 303-307.

Ramm E., Bletzinger K.-U., Reitinger R., and Maute K., (1994) “The challenge of structural optimization,” in Topping B.H.V. and Papadrakakis M. (eds) Advances in Structural Optimization, CIVIL-COMP Press, Edinburgh, 27-52.

Rechenberg I., (1973), “Evolution strategie: optimization of technical systems according to the principles of biological evolution”, Frommann-Holzboog, Stuttgart.

Russo, L. (2004) “The forgotten revolution: How science was born in 300BC and why it had to be reborn.” Springer, Berlin.

Rosen, J. (1960). “The Gradient Projection Method for Nonlinear Programming, I. Linear Constraints.” Journal of the Society for Industrial and Applied Mathematics, 8:181-217.

Rosenbrock, H.H (1960). “An Automatic Method for finding the Greatest or Least Value of a function” Comp J, 3:175-184.

Schwefel H.P., (1981) “Numerical optimization for computer models”, Wiley & Sons, Chichester,U.K.

Sheu C.Y. and Prager W., (1968), “Recent development in optimal structural design” Applied Mechanical Reviews, 21(10): 985-992.

Spunt L., (1971), “Optimum structural design”,Prentice-Hall, Englewood Cliffs, New Jersey, 41-42.

Suzuki K., and Kikuchi N., (1993) “Layout optimization using the homogenization method”, in Rozvany G.I.N (ed.), NATO/DFG ASI ‘Optimization of large structural systems’, Berchtesgaden, Germany, Kluwer Academic Publishers, Dordrecht, Netherlands, 157-175.

Van Keulen F. and Hinton E., (1996) “Topology design of plate and shell structures using the hard kill method” in B.H.V. Topping (ed.) Advances in optimization for Structural Engineering, CIVIL-COMP Press, Edinburgh, 177-188.

Vanderplaats, G.N., (1984), “Numerical optimization techniques for engineering design”, McGraw-Hill, New York, USA.

Venkayya V.B., Khot N.S and Berke L., (1973) “Application of optimality criteria approaches to automated design of large practical structures” 2nd Symposium of Structural Optimization AGARD-CP-123, Milan, Italy.

Veselago, V.G. (2002) “Formulating Fermat’s principle for light travelling in negative refraction materials”. PHYS-USP, Vol. 45(10): 1097-1099.

Xie Y.M., and Steven G.P., (1993). “A simple evolutionary procedure for structural optimization” Computers & Structures, 49: 885-896.

Zoutendijk, G. (1960). “Methods of Feasible Directions.” Elsevier

CHAPTER 7

Reliability-based optimum seismic design of structures

7.1 Introduction

This chapter discusses the use of simplified performance estimation methods within the framework of an optimization algorithm. Such methods will allow to make inexpensive estimates of the reliability-based constrains of the problem. The proposed algorithm, called «GeneticStructuralOptimization_using_IDA-SPO2IDA» (GSO_IDA-SPO2IDA), is efficient and is able to provide designs with improved properties. The Genetic Algorithm (GA) serves as a search engine capable of locating the most efficient building design that satisfies all design requirements. More specifically, the resource-demanding IDA method is replaced by the Static Pushover to Incremental Dynamic Analysis (SPO2IDA) approach in order to provide fast estimates of the demand at various performance levels. The design problem is examined with two optimization formulations: the deterministic-based design optimization (DBO), and the reliability-based design optimization (RBO). In the DBO formulation the constraints are imposed directly on the engineering demand parameters (EDP's), e.g. interstorey drift, hinge rotations, stress resultants. In the RBO case, additional constraints associated with the limit-state mean annual frequencies (MAF's) of the EDP's under consideration are implemented instead. A three and nine-storey steel moment-resisting frames (SMRF) are used to demonstrate the proposed methodology.

7.2 Literature review of approximate methods

More specifically, Dolsek & Fajfar (2007) proposed the IN2 method, which is a simplified procedure that combines nonlinear static analysis with the response spectrum approach aiming to substitute the ‘exact’ I Vamvatsikos & Cornell (2005) developed the SPO2IDA tool (Static Pushover to Incremental Dynamic Analysis) in an effort to approximate the IDA curve taking advantage information extracted from the static pushover backbone. Han & Chopra (2006) proposed the MPA-based IDA method which in essence is a variation of the Modal Pushover Analysis (MPA) method that aims to provide inexpensive response estimations. Azarbakht and Dolsek (2007) proposed the use of a limited number of ground motions, selected using equivalent single-degree-of-freedom (ESDOF) systems. The ESDOFs are used to identify a small number of records whose median IDA curve is close to that of the full set of records. Dolsek and Fajfar (2007) proposed the IN2 method, a simplified procedure that combines nonlinear static analysis with the response spectrum approach. In this work the SPO2IDA tool was implemented for the evaluation of the designs generated by the genetic algorithm. The SPO2IDA tool enables an accurate estimation of the fractile IDA curves even close to collapse without needing any nonlinear dynamic analysis. Latest research by Vamvatsikos et al. (2009) has shown that the error introduced in the IDA estimation when the SPO2IDA tool is used is equal to the accuracy achieved in the performance estimation of an IDA using ten ground motions. Furthermore, SPO2IDA is easily attainable from the internet. All the above methods are approximate and their results compare well to those of IDA, while their cost and efficiency varies.

7.3 Approximate seismic performance-estimation methods

7.3.1 The IN2 method

Simplified inelastic procedures used in seismic design and assessment combine the nonlinear static (pushover) analysis and the response spectrum approach. One of such procedures is the N2 method, which has been implemented into the Eurocode 8 standard. The N2 method can be employed also as a simple tool for the determination of the approximate summarized

IDA (incremental dynamic analysis) curve. Such analysis is called the incremental N2 method (IN2) (Dolsek and Fajfar 2007).

In general, an IN2 curve is intended to approximate a summarized IDA curve and is not calculated for a single ground motion. The term ‘summarized’, when related to IN2 curves, applies only to mean or median curves, since the proposed simplified approach is not intended for the determination of dispersion. Therefore, default values for the dispersion measures for randomness and uncertainty in displacement demand and capacity have to be used. Simplified pushover-based approaches for determination of approximate IDA curves have been explored also in Incremental N2. IN2 method is a relatively simple nonlinear method for determination of approximate IDA curves. IN2 method is, like the IDA analysis, a parametric analysis method. An IDA curve is determined with nonlinear dynamic analyses, while each point of an IN2 curve (approximate IDA curve), which corresponds to a given seismic intensity, is predicted with the N2 method. All limitations which apply to the N2 method apply also to IN2 method.

In order to determine an IN2 curve, first the ground motion intensity measure and the demand measure have to be selected. The most appropriate pair of quantities is the spectral acceleration and the top (roof) displacement, which allow also the visualization of the procedure (Figure 7.1). Other relevant quantities, like maximum storey drift, rotation at the column and beam end, shear force in a structural element and in a joint, and story acceleration, can be employed as secondary demand measures. They are related to roof displacement and can be uniquely determined if roof displacement is known. The secondary demand measures can be used, together with the main demand measure, for performance assessment at different performance levels.

Roof displacement and other relevant demand measures for a chosen series of spectral accelerations are determined by the N2 method. This step represents the main difference in comparison with IDA analysis because the N2 method is used for the determination of seismic response. Therefore the shape of the IN2 curve depends on the inelastic spectra applied in the N2 method, which are based on the relation between strength reduction factor, ductility and period (the $R-\mu-T$ relation). If a simple $R-\mu-T$ relation, based on equal displacement rule in the medium- and long-period range, is used, the IN2 curve is linear for structures with period higher than $C\ T$ and bilinear for structures with period lower than $C\ T$.

A more complex $R-\mu-T$ relation was proposed for infill RC frames. In this case IN2 curve is four-linear. Considering the piecewise linearity of the IN2 curve, only a few points have to be determined in order to obtain the complete N2 curve.

Usually the inelastic spectra, used in the N2 method, represent mean spectra and consequently the IN2 curve represents a mean curve. More specifically, the $R-\mu-T$ relation for infill frames represents an idealization of the $R-\mu-T$ relation, calculated for mean ductility given the reduction factor. The schematic construction of the IN2 curve for a SDOF model in acceleration-displacement (AD) format is presented in figure 7.1. The capacity diagram (multi-linear curve) shown in figure 7.1 is characteristic for infill RC frames and represents the idealized pushover curve of an equivalent SDOF model. As an example, two points (P_1 and P_2) of the IN2 curve, corresponding to two different ground motion intensities, are schematically constructed with the N2 method. The radial line from origin and crossing yield point represents the elastic system with period T. Elastic seismic demand in terms of elastic spectral acceleration ($S_{ae,1}$ or $S_{ae,2}$) and corresponding elastic spectral displacement ($S_{de,1}$ or $S_{de,2}$) is determined as the intersection of this line with the elastic spectrum for the appropriate ground motion intensity. The inelastic displacement demand ($S_{d,1}$ or $S_{d,2}$) is then determined with the N2 method. It corresponds to the point where the horizontal line, at the acceleration S_{ay}, intersects the appropriate inelastic spectrum. A point of the IN2 curve (e.g. the points P_1 and P_2) is defined with the pairs: elastic spectral acceleration on the Y-axis and the corresponding inelastic displacement demand on the X-axis (figure 7.1). If inelastic displacements are determined for many levels of elastic spectral acceleration, the complete IN2 curve can be obtained.

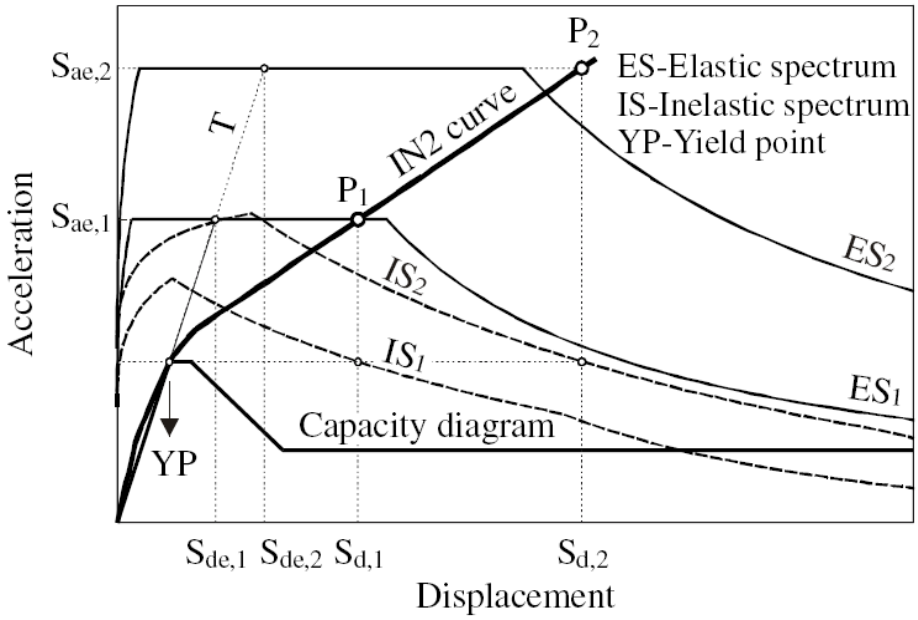

Figure 7.1: Schematic construction of an IN2 curve. (Dolsek and Fajfar 2004)

7.3.2 <u>Progressive incremental dynamic analysis</u>

The aim of this methodology is to decrease the number of ground motion records needed for the prediction of a median IDA curve (Azarbakht and Dolsek (2007)). In addition to the MDOF model, which is employed in the IDA analysis, the advantages of the simple model (e.g. the SDOF model), which is not computationally demanding, are taken into account. Such an approach is employed in many other approximate methods. These methods use the response of the simple model, in combination with the pushover analysis, to predict the seismic response of the MDOF model. However, the methodology described employs the simple model only to predict the precedence list of ground motion records. Single-record IDA curves are then calculated, step by step using the MDOF model from the precedence list of ground motion records until acceptable tolerance for the median IDA curve is reached. The main steps of the methodology can be described as follows:

1. Select a set of ground motion records based on the earthquake scenario. This is the same step as in an IDA analysis. The number of

records within the given set can, if so desired, be high, since, when using the methodology, there is no need to compute the seismic response of the MDOF model for all records in order to obtain a good prediction of the median IDA curve.

2. Create a MDOF mathematical model that can be used for the simulation of the realistic seismic response of the structure under investigation.
3. Define a simple mathematical model, e.g. a SDOF model. This model should be a good representative of the linear and nonlinear characteristics of the MDOF mathematical model, yet simple enough for it to be possible to perform a large number of nonlinear time-history analyses, without the need for very time-consuming calculations.
4. Compute single-record IDA curves for the simple model, for all the ground motion records within the given set. Because of the simplicity of the chosen simple model, this should not be a time-consuming task.
5. Based on the results obtained in step 4, arrange the ground motion records within the given set in order to obtain a good precedence list. This is an optimization problem. The objective of the optimization is to minimize the differences between the 'original' and the 'selected' median IDA curves. The 'original' median IDA curve is obtained from all the single-record IDA curves (step 4), whereas the 'selected' median IDA curves are obtained only for the first s ground motion records from the precedence list, where s is the number of 'selected' ground motion records. The number of median IDA curves, based on the s ground motion records, is thus equal to the number of ground motion records in the set being used.
6. Compute a single-record IDA curve for the MDOF model, starting with the first record from the precedence list. After computation of the single-record IDA curves for the s^{th} record from the precedence list (where s is a number greater than or equal to two), compute the 'selected' median IDA curve and compare it with the 'selected' median IDA curve obtained from the $(s-1)^{th}$ records.
7. Repeat step 6 until the difference between the 'selected' median IDA

curves, determined for the s^{th} and $(s-1)^{th}$ records, is less than the acceptable tolerance, and then stop performing the IDA analysis on the MDOF model.

8. The ‘selected’ median IDA curve, calculated from the *s* single-record IDA curves with dispersion responses based on SDOF IDAs, can be used for further seismic performance assessment.

The described procedure can significantly reduce the number of nonlinear time-history analyses needed to predict the median IDA curve with sufficient accuracy. However, the efficiency of the procedure depends on the ability of the simple model to predict the damage measure of the MDOF model, as well as on the ability of the optimization algorithm to find the best precedence list of ground motion records. The median IDA curve, obtained from the described procedure by employing a limited number of ground motion records, is usually a good approximation to the ‘original’ median IDA curve for the MDOF model, which is calculated from all the single-record IDA curves.

The choice of the simple mathematical model is important, since the precedence list of ground motion records is obtained from the IDA analysis on the simple model. It is, therefore, desirable that IDA curves determined by using the simple model do not differ significantly from the IDA curves determined by using the MDOF model, although the problem is constrained by the fact that analyses with the simple model should not be time consuming. Note that the simple model cannot capture the failure mechanisms that are present in the more realistic MDOF model. However, the ground motion records, which can be used to predict a good median IDA curve for the simple model, are just good representatives for the prediction of the median IDA curve for the MDOF model.

It can also be mentioned that the procedure can be easily applied to other problems, and not just to the problem of minimizing the number of records for the sufficiently accurate prediction of the median IDA curve. For example, the procedure can be applied for the selection of a certain number of records for a purpose of an experiment as well as for a particular design purpose. For the latter case, many codes recommend using a certain number of records for the prediction of the most critical actions and/or a different number of records (usually more) for the prediction of the mean or median response. In this case, the described approach can significantly reduce the bias in the seismic response which is present because of the limited number of ground motion records prescribed for nonlinear dynamic analyses (Azarbakht and Dolsek 2007).

7.3.3 MPA-based IDA

Summarized below are a series of steps used to estimate the peak inelastic response of a symmetric-plan, multistory building about two orthogonal axes to earthquake ground motion along an axis of symmetry using the MPA procedure:

1. Compute the natural frequencies ω_n and modes φ_n, for linearly elastic vibration of the building.
2. For the n^{th}-mode, develop the base shear-roof displacement, V_{bn} -u_{rn}, pushover curve for force distribution according to the relation:

   $$s_n^* = \boldsymbol{m}\phi_n ,$$

   where $\boldsymbol{m}$ is the mass matrix of the structure.

3. Idealize the pushover curve as a bilinear curve. If the pushover curve exhibits negative postyielding stiffness, idealize the pushover curve as elastic-perfectly-plastic.
4. Convert the idealized pushover curve to the force displacement for the nth-“mode” inelastic SDF system:

   F_{sn}/L_n - D_n , by using the relations:

   $$\frac{F_{sny}}{L_n} = \frac{V_{bny}}{M_n^*} , \tag{7.1}$$

   $$D_{ny} = \frac{u_{rny}}{\Gamma_n \phi_{rn}} , \tag{7.2}$$

$$\Gamma_n = \phi_n^T \boldsymbol{m} 1 / \phi_n^T \boldsymbol{m} \phi_n \, . \tag{7.3}$$

where M_n^* is the effective modal mass, ϕ_{rn} is the value of ϕ_n at the roof.

5. Compute peak deformation D_n of the n^{th}-“mode” inelastic SDF system defined by the force deformation relation and damping ratio ζ_n. The elastic vibration period of the system is :

$$T_n = 2\pi \left(\frac{L_n D_{ny}}{F_{sny}} \right)^{1/2} \tag{7.4}$$

For a SDOF system with known T_n and ζ_n, D_n can be computed by nonlinear response history analysis (RHA) or from the inelastic design spectrum (Chopra, 2001).

6. Calculate peak roof displacement u_{rn} associated with the n^{th}-“mode” inelastic SDF system from the relation:

$$u_{rn} = \Gamma_n \phi_{rn} D_n \tag{7.5}$$

7. From the pushover database (Step 2), extract values of desired responses r_n: floor displacements, story drifts, plastic hinge rotations, etc.
8. Repeat Steps 3-7 for as many modes as required for sufficient accuracy. Typically, the first two or three ‘modes’ will suffice.

9. Determine the total response (demand) by combining the peak “modal” responses using the SRSS rule (relation 7.6):

$$r = \left(\sum_n r_n^2 \right)^{1/2} \tag{7.6}$$

In the MPA-based approximate procedure to determine IDA curves, the MPA procedure is used to estimate seismic demands due to each ground motion at each intensity level instead of nonlinear RHA. Although modal analysis theory is strictly not valid for inelastic systems, the fact that elastic modes are coupled only weakly in the response of inelastic systems (Chopra and Goel 2002) permitted development of the MPA procedure. The MPA procedure provides a computationally efficient, although approximate, alternative to non-linear RHA.

In MPA, the effective earthquake forces (relations 7.7 and 7.8):

$$\mathbf{m}\ddot{\mathbf{u}}+\mathbf{c}\dot{\mathbf{u}}+\mathbf{f}_s\left(\boldsymbol{u}, sign\,\dot{u}\right)=-\boldsymbol{mi}\,\ddot{u}_g(t) \tag{7.7}$$

$$\mathbf{p}_{\mathrm{eff}}(t)=\ -\mathbf{m}\boldsymbol{i}\,\ddot{u}_g(t) \tag{7.8}$$

are expanded into their modal components. This spatial (height-wise) distribution of the effective earthquake forces over the building is defined by the vector **s** ≡ **m*i*** and their time variation by $\ddot{u}_g(t)$. The force distribution can be expanded as a summation of modal inertia force distributions $\mathbf{s}_n$:

$$s=\sum_{n=1}^{N} s_n \tag{7.9}$$

$$s_n \equiv \Gamma_n m\phi_n \tag{7.10}$$

where ϕ_n is the nth-mode of natural vibration and $\Gamma_n = \phi_n^T \boldsymbol{mi} / \phi_n^T \boldsymbol{m}\phi_n$. Thus

$$\mathbf{p}_{\mathrm{eff,n}}(t)=\ -s_n\,\ddot{u}_g(t) \tag{7.11}$$

is the n^{th}-mode component of effective earthquake forces.

In the MPA procedure, the peak response of the building to $\mathbf{p}_{\mathrm{eff},n}(t)$ — or the peak 'modal' demand r_n — is determined by a non-linear static or pushover analysis using the modal force distribution based on the relation:

$\mathbf{s}^*n = \mathbf{m}/n$

at the peak roof displacement u_{rn} associated with the n^{th}-mode inelastic SDF system. The peak modal demands r_n are then combined by an appropriate modal combination rule to estimate the total demand. This procedure is directly applicable to the estimation of deformation demands (e.g. floor displacements and storey drifts).

The MPA procedure has been described in a convenient step-by-step form beforehand. This approximate procedure has been shown to estimate seismic demands to a useful degree of accuracy for the SAC 9- and 20-storey buildings, generic frames (vertically ‘regular’ as well as vertically ‘irregular’) of height varying from 3 to 18 stories.

Based on structural dynamics theory, the MPA procedure is computationally attractive because it avoids non-linear RHA of the structure. Instead, computing each modal demand r_n requires one non-linear static analysis of the structure and a non-linear RHA of a ‘modal’ SDF system; and ‘modal’ demands need to be determined only for the first few (generally 2 or 3) ‘modes’ of the structure. Because the MPA procedure leads to a unique SPO for each mode, it bypasses the search for the ‘worst’ SPO mentioned earlier. Furthermore, the elastic stiffness of the force–deformation curve for the modal SDF system is uniquely defined as the modal frequency squared, thus avoiding the complications in the simplified IDA procedure.

In applying MPA to obtain IDA curves for all fractiles, an n^{th}-mode pushover analysis of the structure is implemented only once. The resulting database provides all the response information needed to estimate seismic demands due to any ground motion scaled to any intensity level. The ‘modal’ response is extracted from this database at the roof displacement u_{rn} due to the selected ground motion at the selected intensity level (Han and Chopra (2006)).

7.4 <u>The Static PushOver to Incremental Dynamic analysis (SPO2IDA) method</u>

According to the Incremental Dynamic Analysis (IDA) method the mathematical model of the structure is subjected to a suite of ground motion records incrementally scaled to different levels of seismic intensity (Vamvatsikos *et al.* 2002). Recent research has shown that the scaling practice is legitimate and introduces small bias on the prediction of the structural response (Zacharenaki *et al.* 2009). The building’s capacity can be viewed using the curve of an EDP which characterizes the demand (e.g. maximum interstorey drift ratio) versus an Intensity Measure (IM), e.g. the 5%-damped, first-mode spectral acceleration $S_a(T_1,5\%)$, representing the seismic intensity. A complete representation of the capacity is given through the estimation of the 16%, 50% and 84% summarized curves. Performance limit-states are defined on these curves by appropriate limits which are set on the EDP values. The results of IDA can be combined with probabilistic seismic hazard analysis in order to estimate the mean annual frequency (MAF) of a limit-state being exceeded.

Based on the established method of using SDOF oscillators to approximate MDOF systems, we have investigated the SPO-to-IDA connection for simple oscillators. The SDOF systems studied were of short, moderate and long periods with moderately pinching hysteresis and 5% viscous damping while they featured backbones ranging from simple bilinear to complex quadrilinear with an elastic, a hardening and a negative-stiffness segment plus a final residual plateau that terminated with a drop to zero strength. The oscillators were analyzed through IDA and the resulting curves were summarized into their 16%, 50%, 84% fractile IDA curves which were in turn fitted by flexible parametric equations (Vamvatsikos and Cornell 2005). Having compiled the results into the SPO2IDA tool, which is available on line (Vamvatsikos 2002), an engineer user is able to effortlessly get an accurate estimate of the performance of virtually any oscillator without having to perform the costly analyses almost instantaneously recreating the fractile IDAs in normalized coordinates defined by the relation $R=S_a(T_1,5\%)/S_a^y(T_1,5\%)$, where $S_a^y(T_1,5\%)$ is the $S_a(T_1,5\%)$ value to cause first yield, versus ductility *μ.*

The Static Pushover to IDA (SPO2IDA) tool (Vamvatsikos and Cornell 2006) provides an approximate estimation of the IDA curve using the backbone of the static pushover (SPO). The SPO2IDA tool has been verified using SDOF systems and MDOF structures and can be considered as a powerful *R-μ-T* relationship. More specifically, the static pushover is approximated with a trilinear (figure 7.2a), or a quadrilinear, curve in order to extract the parameters that describe the SPO curve (figure 7.2b). The extracted parameters are then given as input to SPO2IDA to provide the fractile IDAs in normalized coordinates of strength reduction factor R versus ductility μ. The final approximate IDA curves $S_a(T_1,5\%)$-θ_{max} coordinates with the aid of simplified calculations on the available R-μ data (Fragiadakis and Vamvatsikos 2010).

In order to obtain an approximate IDA curve, first a static pushover (SPO) with a lateral load pattern proportional to the first-mode is performed. The SPO capacity curve is then approximated with a trilinear, or a quadrilinear, envelope (e.g. figure 7.2b). The backbone of the SPO is described by five parameters, shown in figure 7.2b. More specifically, the backbone initially allows for an elastic behaviour up to F_y, then hardens with a non-negative normalized slope until ductility μ_c while beyond this point a negative stiffness segment starts having a slope $-\alpha_c$. These parameters are given as input to SPO2IDA to obtain the median IDA curve and its fractiles. Since SPO2IDA capacities are in dimensionless R-μ coordinates, they have to be scaled to another pair of *IM-EDP* coordinates, such as the 5%-damped, first-mode spectral acceleration, $S_a(T_1,5\%)$ and the maximum interstorey drift ratio (θ_{max}).

The scaling from R-μ to $S_a(T_1,5\%)$-θ_{max} is easily performed with simple algebraic calculations:

$$\mathbf{S}_a(T_1,5\%) = \mathbf{R}\, S_a^{yield}(T_1,5\%) \tag{7.12}$$

$$\boldsymbol{\theta}_{roof} = \boldsymbol{\mu}\theta_{roof}^{yield} \tag{7.13}$$

where $\boldsymbol{\theta}_{roof}$ is the roof drift and $S_a^{yield}(T_1,5\%)$ and θ_{roof}^{yield} are the spectral acceleration and the roof drift at yield.

Once $\boldsymbol{\theta}_{roof}$ is known, $\boldsymbol{\theta}_{max}$ can be extracted from the results of the SPO, since for every load increment the correspondence between the two EDPs is always available.

Note that bold fonts are used to denote quantities that differ in every increment of the SPO and are available from its results. Thus the only unknown parameters in Eq. 7.12 and 7.13 are $S_a^{yield}(T_1,5\%)$ and θ_{roof}^{yield}. To determine $\theta_{\text{roof}}^{\text{yield}}$, we assume that is equal to the yield roof drift of the SPO and therefore after approximating the SPO curve is always available. $S_{\text{a}}^{\text{yield}}(\text{T}_1, 5\%)$ can be calculated if the elastic "stiffness" (or slope) of the median IDA curve plotted with θ_{roof} as the EDP is known. Thus the stiffness, k_{roof} , is the median stiffness value obtained using elastic response history analysis with a few ground motion records, or alternatively by using standard response spectrum analysis. Moreover, an approximate relationship for k_{roof} is proposed in Fragiadakis and Vamvatsikos (2010):

$$k_{\text{roof}} = \frac{4\pi^2 H}{C_0 T_1^2 g} \tag{7.14}$$

where H is the height of the building, T_1 is its fundamental period and C_0 is defined in ASCE-41 (2006) and is equal to the first mode participation factor. This relationship is good for first-mode dominated structures, otherwise C_0 will be inaccurate and consequently k_{roof} will be inaccurate.

Finally, $S_{\text{a}}^{\text{yield}}(T_1, 5\%)$ will be:

$$S_{\text{a}}^{\text{yield}}(T_1, 5\%) = k_{\text{roof}}\theta_{\text{roof}}^{\text{yield}} \tag{7.15}$$

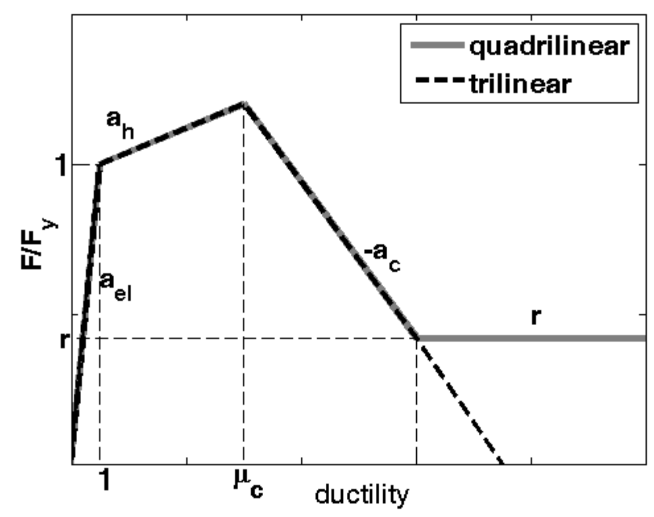

Figure 7.2a: Definition of the parameters that define the backbone of the SPO curve.

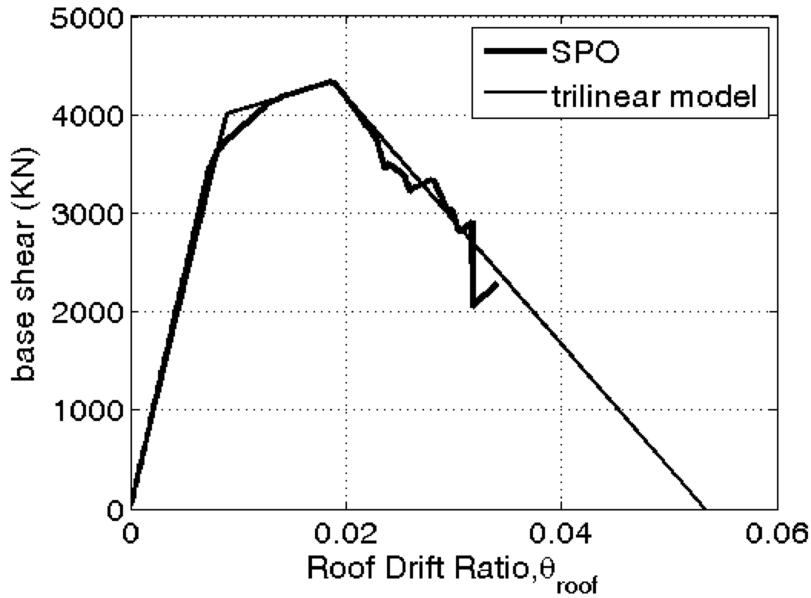

Figure 7.2b: The SPO curve and its approximation with a trilinear model.

In summary, the process of producing an approximate IDA curve from a single static pushover run involves the following steps. Initially perform a static pushover analysis with a first-mode lateral load pattern and then approximate it with a trilinear model. Next SPO2IDA will provide the IDA curves in normalized R-μ coordinates which have to be transformed in terms of $S_a(T_1,5\%)$ versus θ_{max}. This requires the elastic slope of the actual IDA, k_{roof} when θ_{roof} is the EDP. With the aid of Equations 7.12-7.15 we obtain the IDAs in $S_a(T_1,5\%)$-θ_{roof} coordinates. The final IDA curves are obtained using the mapping between θ_{roof} and θ_{max}, available from the results of the static pushover. Since SPO2IDA produces the median and the 16, 84% fractiles, a single SPO run will provide the median and the corresponding dispersion through the above calculations.

7.5 <u>Mathematical formulation of the optimization problem</u>

The problem formulation of Eq. 6.1 is a deterministic optimization problem, since all constraints are deterministic, i.e. the value an EDP must not exceed a prespecified threshold. On the other hand, a discrete reliability-based (RBO) optimization problem is a problem where reliability-based constrains are also included. In the latter case, the constraint is set on the probability that the threshold value of the EDP will be exceeded. In earthquake engineering problems, the limit-state mean annual frequencies (MAFs) can be used instead of probabilities.

Thus an RBO problem is mathematically formulated as follows:

$$\min F(\mathbf{s})$$
$$\text{subject to} \quad \begin{cases} g_i(\mathbf{s}) \geq 0, i = 1,...,l \\ s_j \in R^d, j = 1,...,m \\ h_k(v_{\text{EDP}}(\mathbf{s}) \leq v_{\text{EDP}}^{\text{lim}}(\mathbf{s})), k = 1,...,n \end{cases} \tag{7.16}$$

where h_k are the n probabilistic constraints and v is the MAF of the k_{th} limit-state of the EDP, which usually is the maximum interstorey drift (θ_{max}).

7.6 <u>Outline of the “analysis” step</u>

The steps of the GA-based design algorithm are given in detail in chapter 6 in paragraph 6.10.

Analysis step refers to the step used to evaluate the performance of a building design and not to a single, static or dynamic, finite element analysis. The flowchart of the analysis step is shown in figure 7.3. According to the flowchart, a number of design checks based on Eurocode 3 (EN 2005) and Eurocode 8 (EN 2003) are taken into consideration. For every candidate design, preliminary checks are performed first. These checks include examining whether the design complies with the “strong-column-weak-beam” philosophy. Checks whether the sections chosen are of class 1 are also carried out in order to ensure that the members are able to develop their full plastic moment and rotational ductility. Moreover, restrictions that ensure the proper connection of beams and columns with respect to the geometry of their cross-sections are performed.

The next step is to check the structure against load combinations that do not contain seismic actions, e.g. gravity and live loads. For these combinations, all EC3 checks regarding the capacity of beams and columns must be satisfied. For example for columns against bending with the presence of axial load, the following relationship should be satisfied:

$$\frac{N_{\mathrm{sd}}}{\chi_{\min} N_{\mathrm{pl,Rd}}} + \frac{k_{\mathrm{y}} M_{\mathrm{sd}}}{M_{\mathrm{pl,Rd}}} \leq 1 \tag{7.17}$$

where $\chi_{\min}$ is the reduction factor for flexural buckling taken equal to 0.7 because moment-frame columns are rarely prone to buckling if well designed, and k_y is a correction factor to allow for the combined effect of axial load and moment, taken equal to 1. Plastic capacities for each member section are determined as:

$$M_{pl.Rd} = w_{pl} f_y / \gamma_{\mathrm{M0}} \tag{7.18}$$

$$N_{pl.Rd} = A f_y / \gamma_{\mathrm{M1}} \tag{7.19}$$

where γ_{M0} and γ_{M1} are considered equal to 1.10 (ENV 1994). A number of other checks ensuring that the design complies with all EC3 requirements for the gravity load combination are also included. In every check where the constraints are violated the resulting design is updated so as to obtain one design that satisfies the check.

Subsequently, the capacity of the structure against seismic loads is assessed by performing Static pushover or IDA. The gravity loads are present according to the EC1 (ENV 1994) seismic load combination. The procedure followed to obtain the capacity and the corresponding constraints depend on whether the deterministic (DBO) or the probabilistic (RBO) formulation is implemented. For the RBO case, the procedure and all calculations are discussed in the next section. For the DBO case, performance criteria that refer to the local member level, such as plastic hinge rotations or member chord rotations, can be used. Alternatively, storey level criteria, such as on maximum interstorey drift, can also be adopted. Suggested values for plastic hinge rotations and maximum interstorey drift values are given for steel moment resisting frames by FEMA-356 (2000) and FEMA-350 (2000) respectively. Since nonlinear analysis is performed, the P–Δ effects are taken into account explicitly. In the present study, another restriction adopted is that the applied axial force on columns should not exceed 50% of the member capacity given by Eq. 7.19, in order to allow ductile structural behavior.

7.7 Risk-based calculations

The reliability-based formulation of Equation 7.16 requires the calculation of the mean annual frequency (MAF) for a number of prespecified limit-states. Usually in reliability-based optimization problems the thresholds are set on the limit-state probabilities, i.e. the probability of the near collapse limit-state should not be less than 90%. However, in earthquake engineering applications it is preferable to set the constraints on the limit-state MAF. More specifically, the reciprocal of the MAF is the return period, in years, that a limit-state is exceeded and the MAF provides how many times in one year a limit-state is exceeded.

In this work the EDP assumed is the maximum interstorey drift $\theta_{\max}$, but other EDPs, or a combination of EDPs, can be also adopted. The limit-state MAF is denoted as v_{LS} and is calculated using the total probability theorem (Jalayer 2002):

$$v_{LS}(edp \leq EDP) = \int_{0}^{+\infty} P(edp \leq EDP \mid IM = im) \left| \frac{dv(IM)}{dIM} \right| dIM \qquad (7.20)$$

Equation 7.20 is calculated numerically since the analytical integration is not always possible. According to Dolsek and Vamvatsikos (2010) there are two ways to calculate the MAF. The first is to calculate the probability that the demand exceeds the capacity of the structure, called the direct or EDP-based method, and the second is the indirect, or the IM-based, approach. The IM-based approach refers to calculating the probability that the IM will be above the random IM capacity of the structure. In this work the IM-based approach has been followed.

Here we examine the three-storey steel moment-resisting frame for the Hazard curve and T_1= 1.12 sec (figure 7.4a), and typical the median IDA curves and its 16th and 84th fractiles obtained from the approximate procedure (figure7.4b).

In order to calculate the conditional probabilities of Equation 7.20 using

$$P\left(IM_C < IM \mid IM = im\right) \qquad (7.21)$$

the conditional building response statistics should be available. As response statistics we refer to the conditional median and the 16%, 84% fractiles, which are readily available if the IDA curves are known. In an optimum design framework we use the IDA curves obtained with the aid of the SPO2IDA tool and following the procedure discussed in the previous section. Typical curves are shown in figure 7.4b.

Assuming a lognormal distribution, and if $\ln(\hat{\theta}_{\max})$ and $\hat{\beta}$ are the logarithmic mean and the standard deviation of $\hat{\theta}_{\max}$ for a given intensity $S_a(T_1,5\%)$, the following expression can be used for the dispersion (Vamvatsikos and Fragiadakis 2010):

$$\hat{\beta} = \frac{1}{2}\left(\ln S_a^{84\%} - \ln S_a^{16\%}\right) \approx \left(\ln S_a^{84\%} - \ln S_a^{50\%}\right) \qquad (7.22)$$

The performance objectives adopted in this study are that of EC8, thus: damage limitation (DL), significant damage (SD) and near collapse (NC). The levels suggested in EC8 refer to the recurrence of ground acceleration that should be considered for performance-based calculations. In our study we adopt the same levels and notation for the damage that a building sustains. Therefore, the DL objective implies very light damage with minor local yielding and negligible residual drifts within a period of 50 years corresponding to a level of 50% probability of exceedance. SD and the NC objectives correspond to heavier damage states, as implied by their definitions. These levels correspond to exceedance probabilities equal to 50%, 10% and 2% in 50 years; briefly denoted hereafter as 50/50, 10/50 and 2/50 for DL, SD, and an NC limit states, respectively. The probabilistic constraints are applied on the annual rate that the EDP is exceeded, as suggested in Eq. 7.16. In particular, the rates used for the 50/50, 10/50 and 2/50 levels are related to the return period of the limit-state being exceeded as τ=1/v, where v is obtained using the Poisson formula, i.e. v_{LS} = (-1/t)ln(1-p). For example, for the DL objective v_{DL} = (-1/50) ln(1-0.5) = 0.014 and τ_{DL} = 1/0.014 = 72 years. Therefore, the constraints adopted in this paper will be (7.23):

$$\begin{aligned} &\tau_{DL} \geq 72\mathrm{yrs} \\ &\tau_{SD} \geq 475\mathrm{yrs} \\ &\tau_{NC} \geq 2475\mathrm{yrs} \end{aligned} \tag{7.23}$$

The conditional probability $P\left(IM_C < IM \mid IM = im\right)$ is finally calculated as:

$$P\left(IM_c < IM \mid IM = im\right) = \Phi\left(\frac{\ln(\theta_{\mathrm{lim}}) - \ln(\hat{\theta}_{\mathrm{max}})}{\beta}\right) \tag{7.24}$$

where θ_{lim} is the drift limit considered for the corresponding performance objective and Φ is the cumulative probability function of the Gaussian distribution.

At this point we consider that we can get increased accuracy using IDA and SPO2IDA within the genetic algorithm due to the fact that small bias is observed in IDA with intensity measure $S_{\mathrm{a}}(T_1)$ for the nine-storey steel moment-resisting frame (LA9).

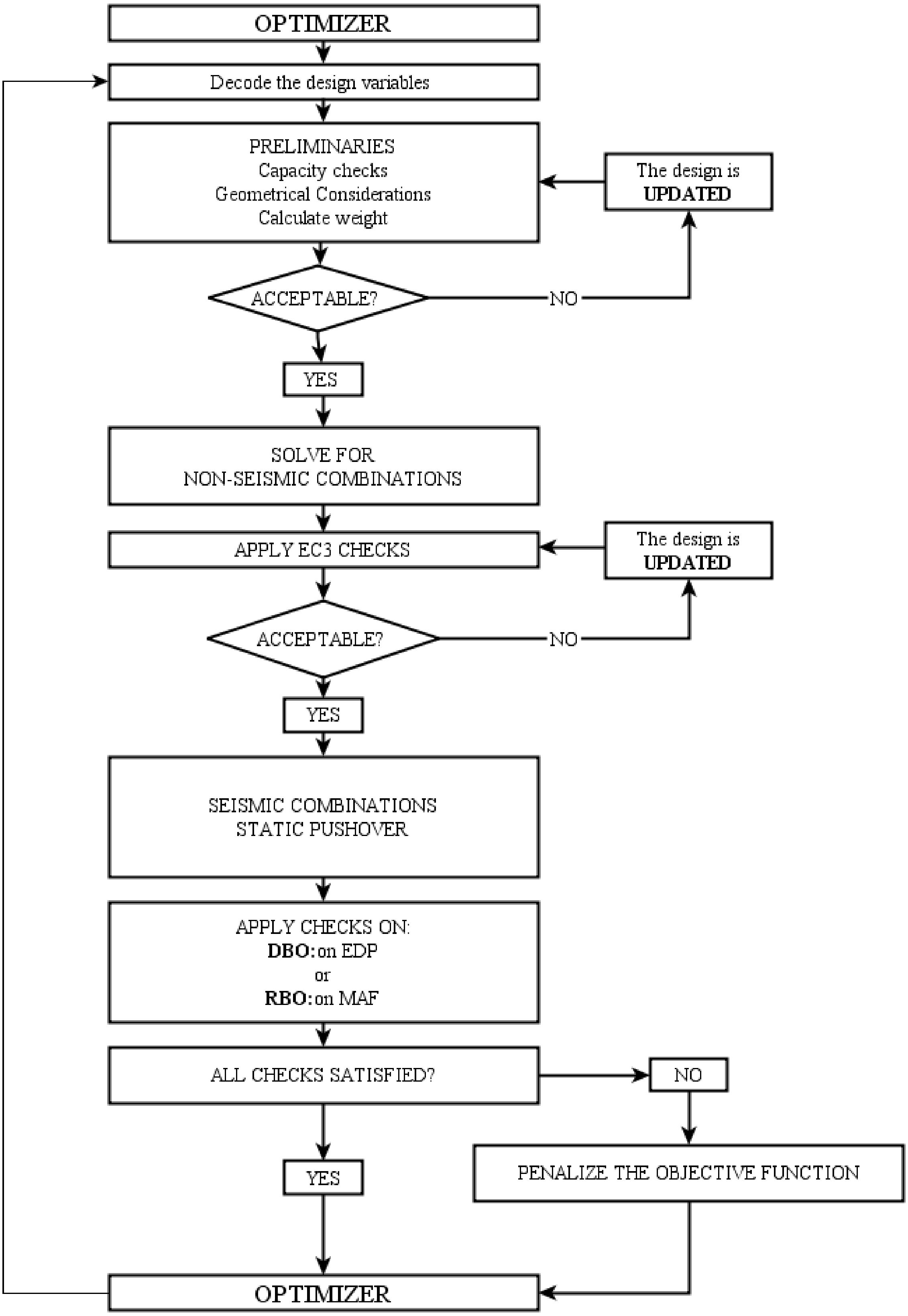

Figure 7.3: Flowchart of the analysis phase.

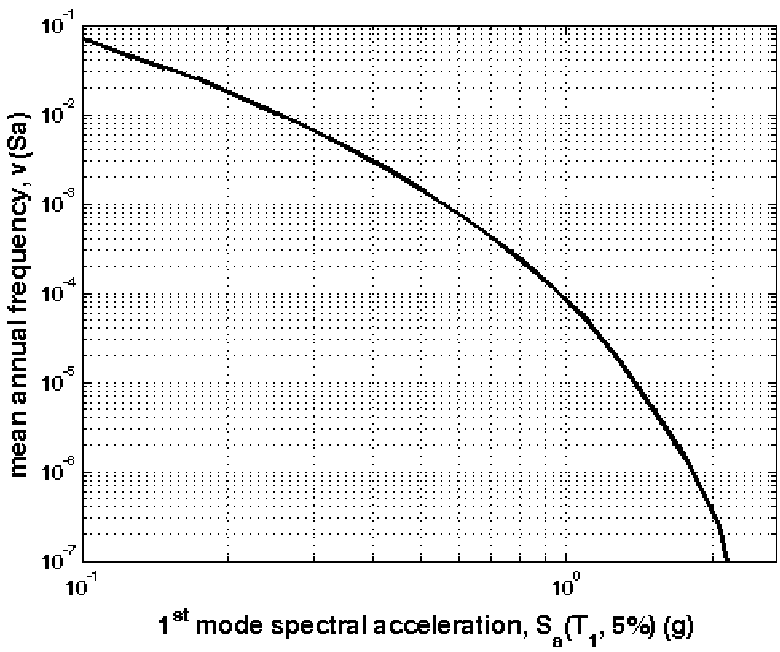

Figure 7.4a: 1st mode spectral acceleration versus mean annual frequency.

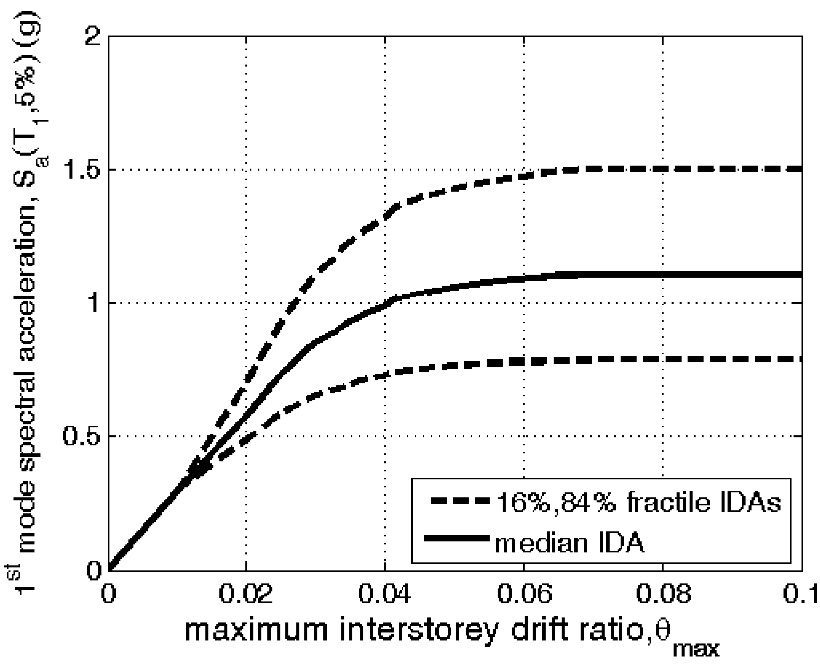

Figure 7.4b: maximum interstorey drift ratio versus 1st mode spectral acceleration.

7.8 Numerical results

The proposed methodology is demonstrated on a three- and a nine-storey steel moment-resisting frames. The two frames and the decision variables considered are shown in figures 7.5 and 7.6, respectively. Both frames are benchmark problems, originally designed for a Los Angeles site according to the 1997 NEHRP (National Earthquake Hazard Reduction Program) provisions and are known in the literature as LA3 and LA9 buildings, respectively. All sections are W-shaped, taken from tables of the American Institute of Steel and Construction (AISC) in order to be consistent with the original design. If full compatibility with the Eurocodes was desired instead, European or British cross section tables could have been used. The three-storey frame consists of four bays with span 9.15m and the height of every storey is 3.96m. The nine-storey frame has five bays with 9.15m span, and a basement. Apart from the first, all stories are 3.96m high, including the basement. The height of the first storey is 5.49m.

The objective function of Eq. 6.1 and 7.16 is the total weight of the frame, obtained as:

$$F(\mathbf{s}) = \gamma \sum_{i=1}^{n} A_i L_i \tag{7.25}$$

where γ is the specific weight of steel, A_i is the section area of the i^{th} member, L_i is the length of the i^{th} member and n is the total number of structural members. The dimension m of the design variable vector **s** is m=5 and 13 for the three- and the for nine-story frame, respectively. For the three-storey frame the members are divided to five groups: three for the beams and two groups for the columns (exterior and interior) as can be seen in Table 7.1 and figure 7.5. Similarly, 13 groups were considered for the nine-storey frame: five for the beams and four for the interior and the exterior columns, respectively (table 7.2 and figure 7.6). The grouping was decided following the initial design of each building (Foutch and Yun 2002), while, in general, this choice lies on the experience and/or the preference of the designer.

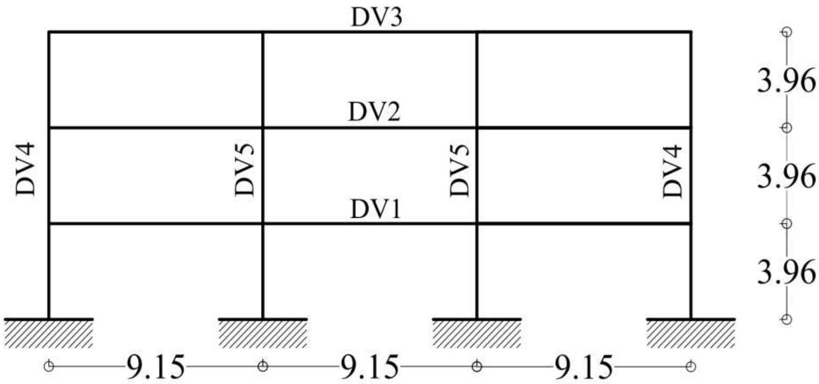

Figure 7.5: The three-storey steel moment resisting frame.

The effect of the internal gravity frames was explicitly considered with a leaning column as suggested in the FEMA P-695 (2009) guidelines. The columns are assumed elastic, while component models are positioned at the beam ends allowing plastic rotations to develop according to the moment-rotation relationship discussed in FEMA P-695 and assuming zero axial force. All analyses were performed on the OpenSees platform (McKenna and Fenves 2001). The modulus of elasticity was assumed equal to 200GPa and the yield stress 235MPa. Geometric nonlinearities in the form of P-Δ effects were included in our analyses explicitly. We also assume that sufficient lateral bracing for beams and columns is present, allowing the cross sections to develop their full plastic moment capacity without suffering of lateral torsional buckling first. More details about the model used for the nine-storey frame can be found in Fragiadakis and Vamvatsikos (2010).

Both frames are assumed to have rigid connections and fixed supports. The permanent load is taken as G=5KN/m^2 and the live load is considered equal to Q=2KN/m^2. The non-seismic load combination considered was 1.35G+1.50Q and the seismic combination was 1.0G+0.3Q+E, where E are the seismic actions. The EDP adopted is the maximum interstorey drift, θ_{max}, and the thresholds were 0.6, 1.5, and 3% for the DL, SD and NC objectives, respectively.

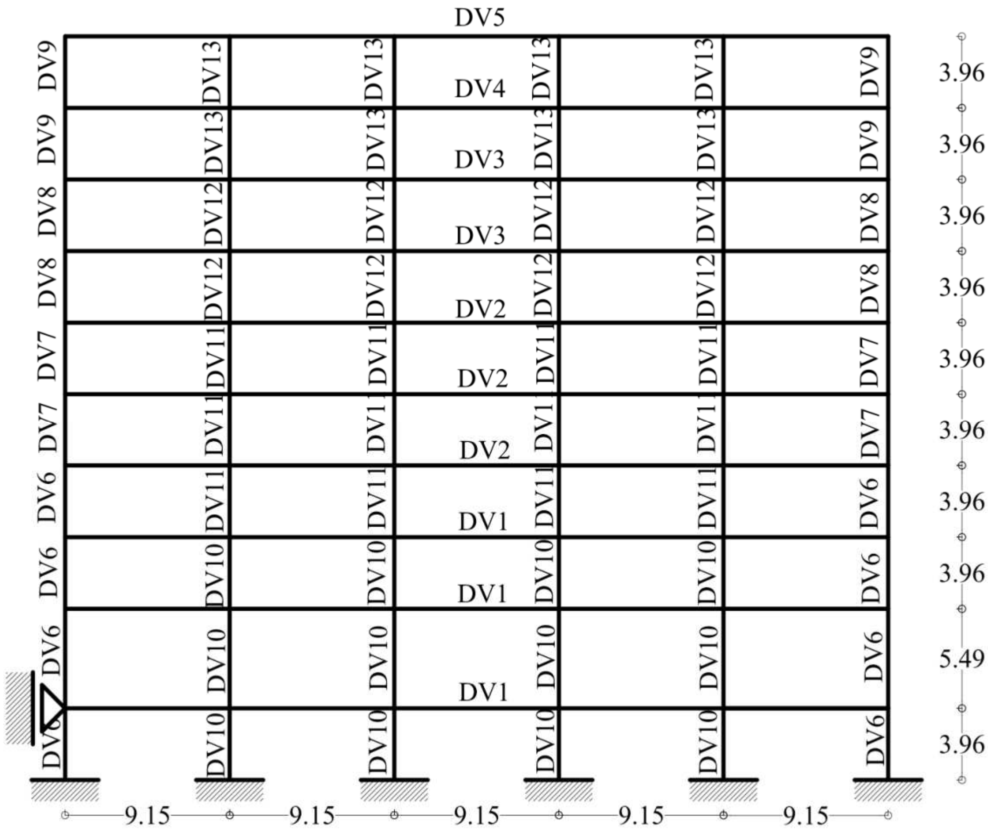

Figure 7.6: The nine-storey steel moment resisting frame.

The genetic algorithm employed for solving the optimization problem required 50 generations of a population size equal to 30 members. For the selection function the rank option was used, while the crossover fraction was 0.8 and the migration function was assumed equal to 0.2. For the mutation of the individuals the Gaussian mutation was used. The deterministic (DBO) and the reliability-based (RBO) optimization procedures were considered for both frame buildings. The results of the optimized structures are shown in Tables 1 and 2. For the three-storey frame the optimum designs have material volumes equal to 3.9m^3 and 4.10m^3 for the deterministic and the reliability-based procedure, respectively, while for the nine-storey frame the corresponding optimum design volumes are 25.75m^3 and 27.34m^3. It is clear that for both buildings the deterministic design procedure leads to designs with less material volume, since the reliability-based procedure takes under consideration the problem uncertainties and thus requires heavier cross-sections to satisfy these requirements.

Figure 7.7a shows the history of the optimization process for the three-storey building. For the three-storey frame, the GA algorithm converged to the optimum approximately after 35 generations for both the DBO and the RBO cases. The minor differences in the optimization histories of the DBO and the RBO formulation arise from the different constraints imposed to every design that is generated randomly by the genetic algorithm.

Moreover, to validate the accuracy and demonstrate the efficiency of the proposed methodology, we compare the optimization history of the proposed algorithm to that of using in every iteration a full IDA analysis instead of the proposed simplified procedure. In the full IDA case, a suite of ten ground motion records have been used. The records have been selected from a bin of relatively large magnitudes, between 6.5-6.9, and moderate distances ranging from 18km to 32km. The comparison of the optimization histories is shown in figure 7.7b for the three-storey steel frame.

Table 7.1 Optimal design results for the three-storey building.

DBO optimized design (volume=3.9m^3)					
Storey / Group	**Beams**	**Storey / Group**	**External columns**	**Storey / Group**	**Internal columns**
1 / DV1	W33×118	1 / DV4	W14×120	1 / DV5	W14×233
2 / DV2	W27×94	2 / DV4		2 / DV5	
3 / DV3	W21×57	3 / DV4		3 / DV5	
RBO optimized design (volume=4.1m^3)					
1 / DV1	W33×118	1 / DV4	W14×145	1 / DV5	W14×257
2 / DV2	W27×84	2 / DV4		2 / DV5	
3 / DV3	W21×68	3 / DV4		3 / DV5	

Table 7.2 Optimal design results the nine-storey building.

DBO optimized design (volume=25.75m^3)					
Storey / Group	**Beams**	**Storey / Group**	**External columns**	**Storey / Group**	**Internal columns**
0-2 / DV1	W36×182	0-3 / DV6	W14×398	0-3 / DV10	W14×398
3-5 / DV2	W33×241	4-5 / DV7	W14×370	4-6 / DV11	W14×370
6-7 / DV3	W27×178	6-7 / DV8	W14×132	7-8 / DV12	W14×132
8 / DV4	W21×201	8-9 / DV9	W14×132	8-9 / DV13	W14×132
9 / DV5	W21×223				
RBO optimized design (volume=27.34m^3)					
0-2 / DV1	W40×183	0-3 / DV6	W14×426	0-3 / DV10	W14×426
3-5 / DV2	W36×182	4-5 / DV7	W14×426	4-6 / DV11	W14×426
6-7 / DV3	W33×169	6-7 / DV8	W14×211	7-8 / DV12	W14×257
8 / DV4	W27×217	8-9 / DV9	W14×109	8-9 / DV13	W14×109
9 / DV5	W21×132				

According to the figure 7.7b, for the three-storey frame, the proposed methodology achieves satisfactory results with respect to the full IDA procedure, resulting to optimum designs with material volumes equal to 3.9m^3 and 4.2m^3, respectively. Again, the small differences observed were expected and are due to the random nature of the GA algorithm and the approximations inherent in static pushover methods. A comparison of the median IDA curves of the optimum designs of the standard IDA and the approximate SPO2IDA-based procedure is shown in figure 7.8. The good agreement demonstrates the capacity of the approximate SPO2IDA method to reproduce the results of IDA and is in agreement with results published elsewhere (e.g. Vamvatsikos and Cornell 2005, 2006, Fragiadakis and Vamvatsikos 2010). So, here we present the three-storey SMRF for Generation evolution for the DBO and the RBO formulations using simplified methods (figure 7.7a) and the comparison of the optimization histories using full-IDA and the proposed method (figure 7.7b).

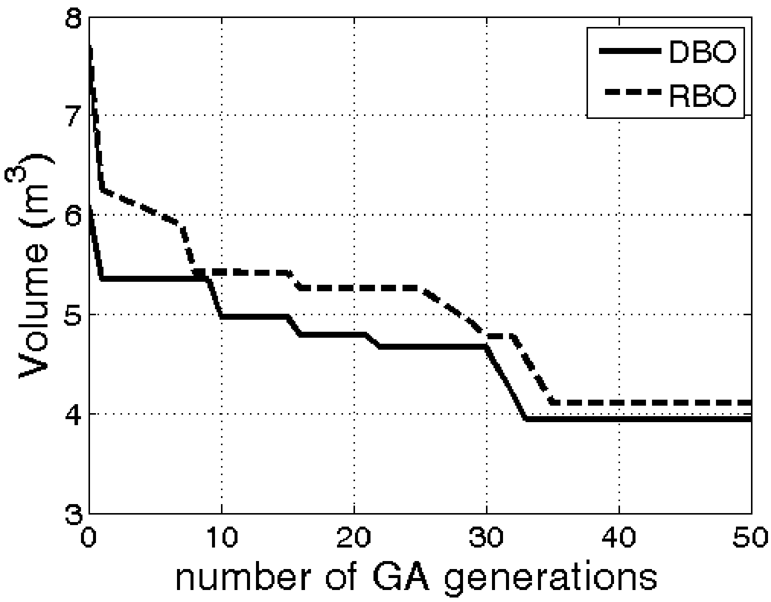

Figure 7.7a: number of GA generations versus volume for the DBO and the RBO formulations.

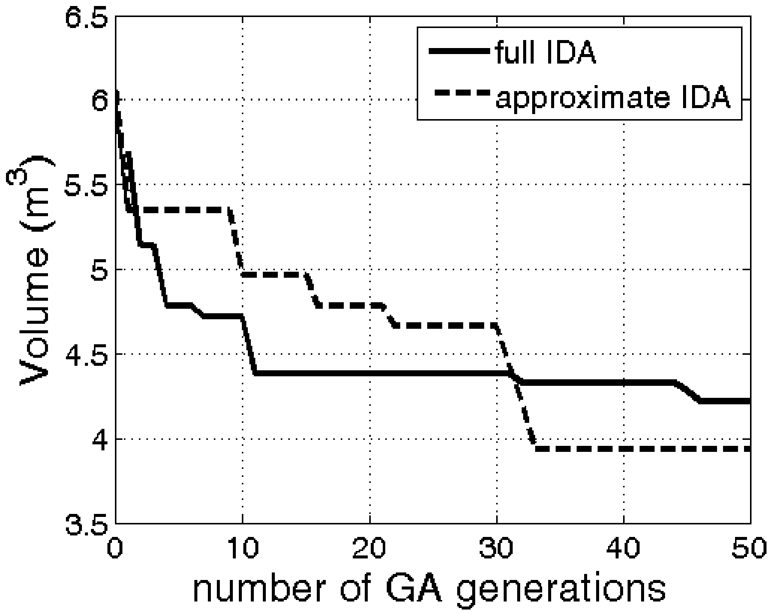

Figure 7.7b: number of GA generations versus volume using full-IDA and the proposed method.

In the sequel we give the median IDA curves using the full-IDA and the approximate SPO2IDA-based case for the three storey SMRF.

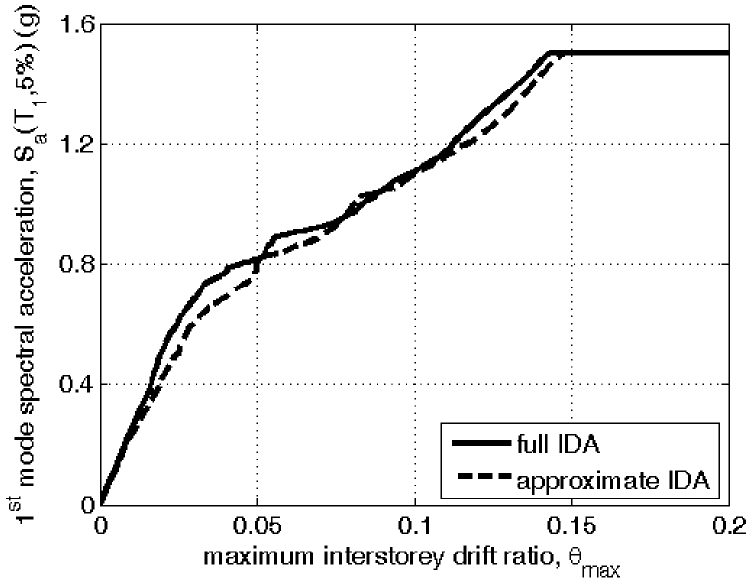

Figure 7.8: Maximum interstorey drift ratio versus 1st mode spectral acceleration. Three-storey SMRF: Median IDA curve using the full-IDA and the approximate SPO2IDA-based case.

For the three-storey frame, an Intel Core 2 Duo processor required 1.5 weeks to run the deterministic problem formulation (DBO) using the standard/full IDA procedure, while the proposed pushover-based deterministic algorithm required 12 hours. In both cases, the analysis was terminated after 50 generation, while a population size equal to 30 was adopted. In total 1850 and 1910 pushover analyses were performed for the DBO and the RBO problem, respectively, while the RBO problem was solved after 12.6 hours. Since the cost of performing full IDA analysis is prohibitive for the engineering practice, the proposed algorithm is a very good alternative as it drastically decreased the computational time and provided close estimates of the response using a state-of-the-art seismic performance estimation method. In the near future, the constantly increasing computing power is expected to make the application of such methods even more appealing.

Figure 7.9 compares the profiles of median maximum interstorey drifts for the DBO and the RBO optimum designs of the three-storey steel frame. The drift distribution provides an insight to the height-wise distribution of the damage. For both DBO and RBO designs and for every limit-state, the median drifts are close to the deterministic threshold.

However, for the RBO case this was achieved implicitly, since the constraints were set on the MAF and not on the drift. Figure 7.9d compares the drift demand of the DBO and the RBO design using the ratio of θ_{max} demand of the two design procedures. The two design formulations converged to building configurations with close properties and therefore the difference in the drift demand is not significant.

Here we present the three-storey SMRF: Drift profiles for optimum design for the damage limitation (DL) limit-state (figure 7.9a), structural damage (SD) limit-state (figure 7.9b), and near collapse (NC) limit-state (figure 7.9c). ratio of DBO over RBO maximum interstorey drifts for the three limit-states (figure 7.9d). The vertical dashed lines in (7.9a), (7.9b) and (7.9c) show the deterministic drift threshold.

We present the nine-storey SMRF: Drift profiles for optimum design for the damage limitation (DL) limit-state (figure 10a), (b) structural damage (SD) limit-state (figure 7.10b), and (c) near collapse (NC) limit-state (figure 7.10d) and the ratio of DBO over RBO maximum interstorey drifts for the three limit-states (figure 7.10d). The vertical dashed lines in (7.10a), (7.10b) and (7.10c) show the deterministic drift threshold.

In figure 7.8 we observe that the curves of the results of the maximum interstorey drift ratio versus 1st mode spectral acceleration for the three-storey SMRF and for the two methods:

a) median IDA curves using the full-IDA and

b) the approximate SPO2IDA-based case, are approximately similar.

In figure 7.9 we also see the distribution of the maximum interstorey drift ratio along the height of the frame for the three limit-states of the three-storey SMRF and for the two methods:

a) Deterministic-based optimization (DBO) and

b) Reliability- based optimization (RBO), are approximately similar.

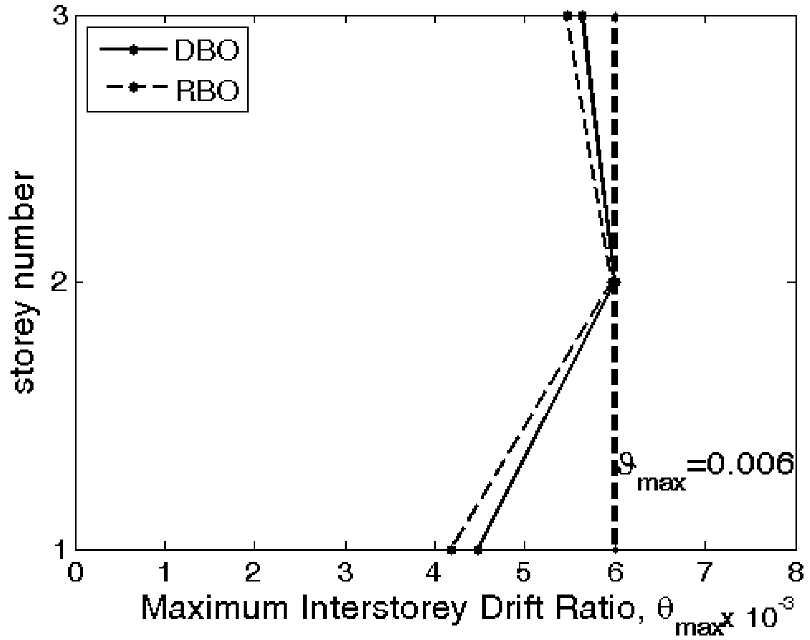

Figure 7.9a: Maximum interstorey drift ratio versus storey number for the damage limitation (DL) limit-state.

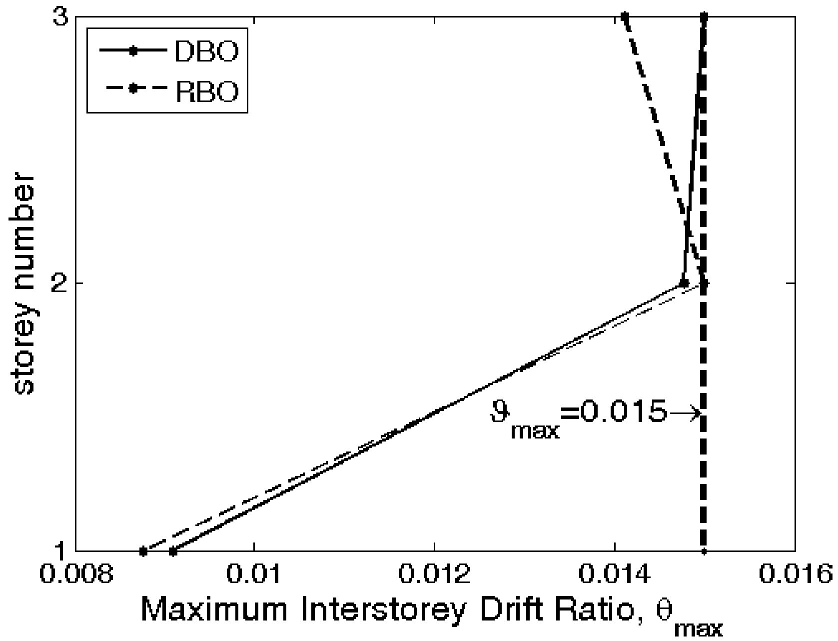

Figure 7.9b: Maximum interstorey drift ratio versus storey number for the structural damage (SD) limit-state.

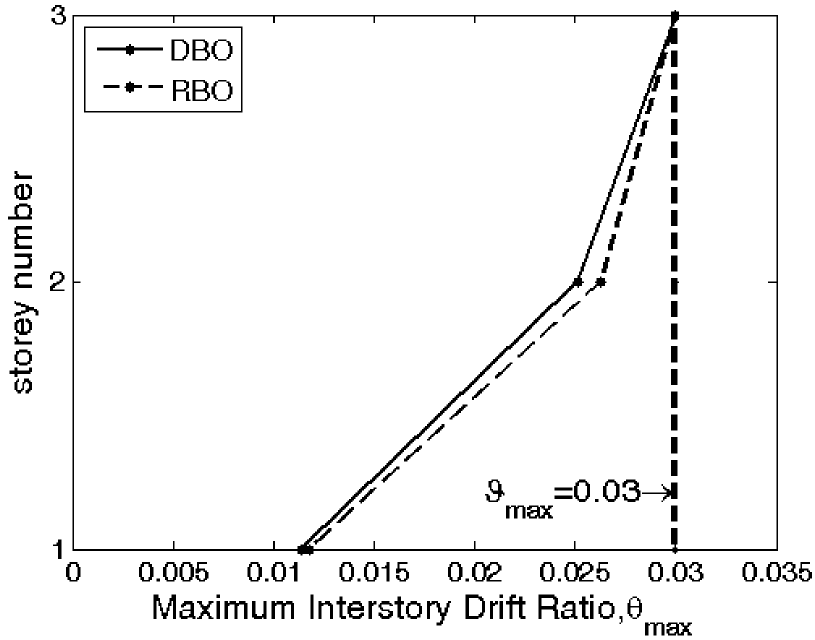

Figure 7.9c: Maximum interstorey drift ratio versus storey number for the near collapse (NC) limit-state.

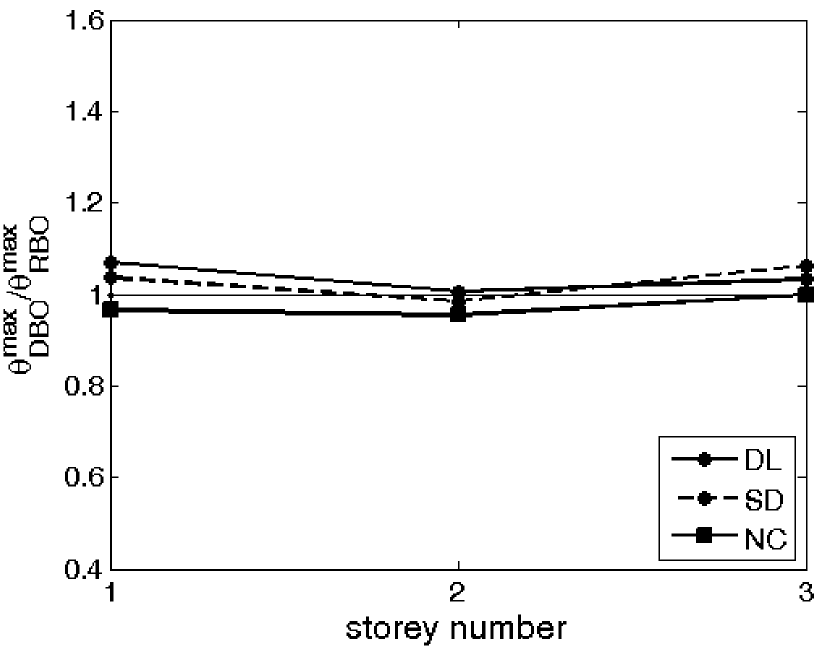

Figure 7.9d: Ratio of DBO over RBO maximum interstorey drifts for the three limit-states.

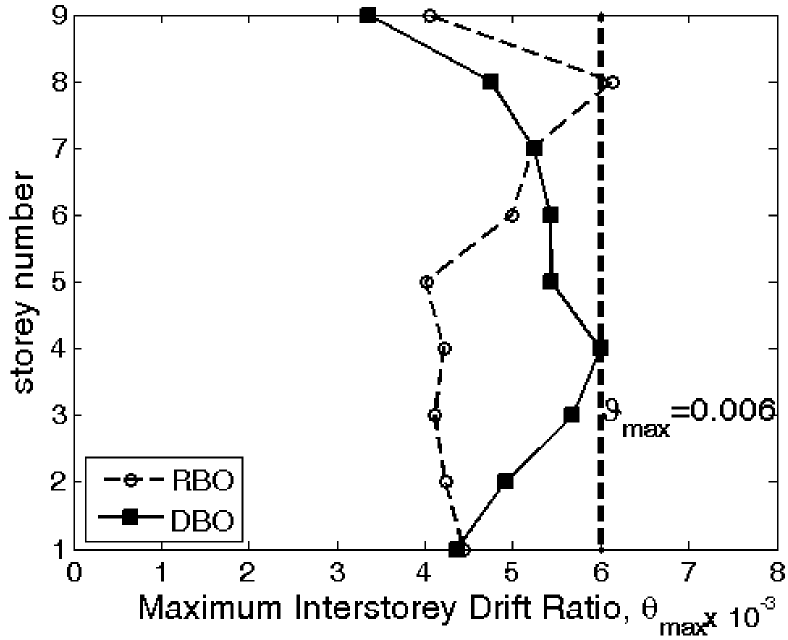

Figure 7.10a: Maximum interstorey drift ratio versus storey number for the damage limitation (DL) limit-state.

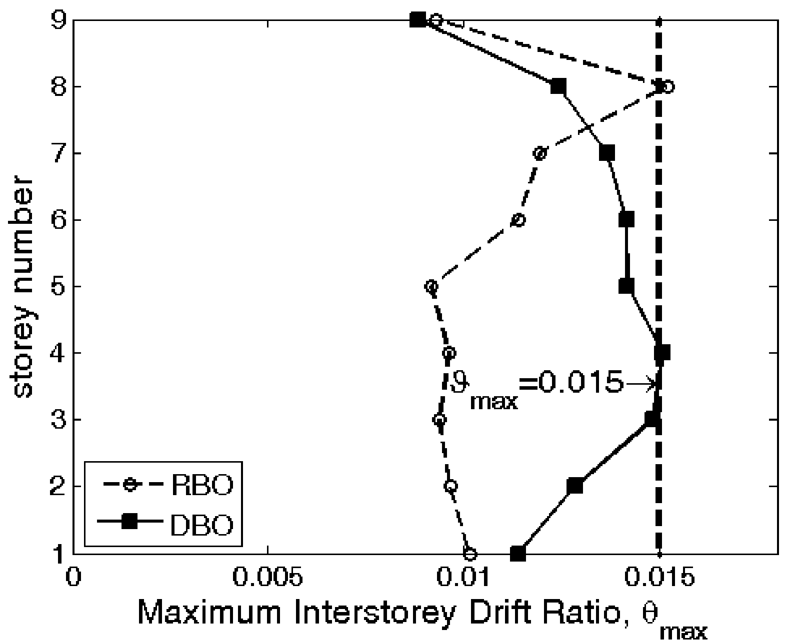

Figure 7.10b: Maximum interstorey drift ratio versus storey number for the structural damage (SD) limit-state.

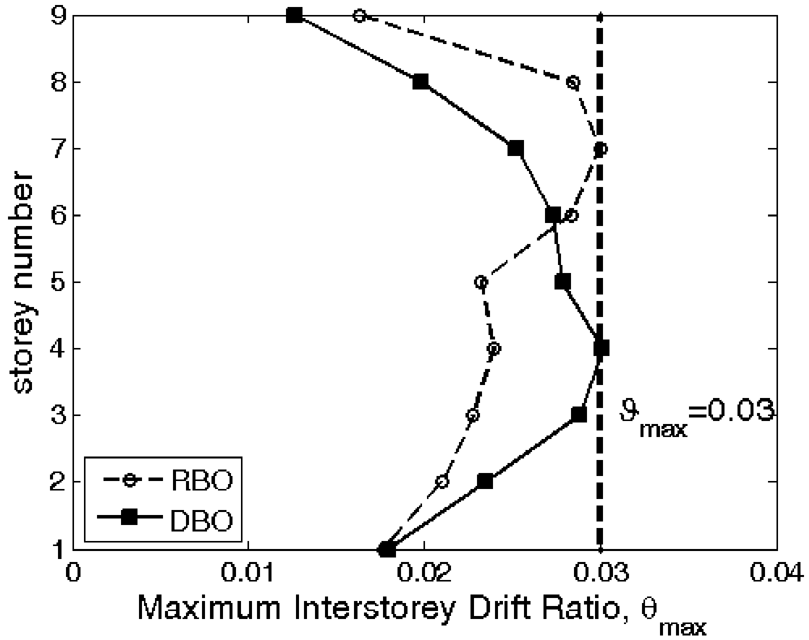

Figure 7.10c: Maximum interstorey drift ratio versus storey number for the near collapse (NC) limit-state.

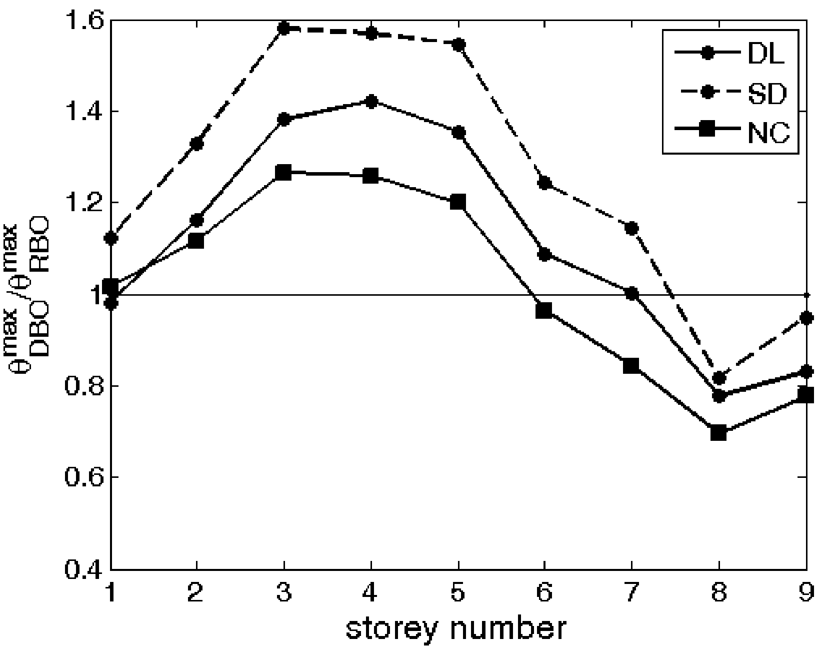

Figure 7.10d: Ratio of DBO over RBO maximum interstorey drifts for the three limit-states.

In figure 7.10a, 7.10b, 7.10c the profiles of the drifts versus the maximum interstorey drift ratio of the nine-storey are presented for the two methods:

a) Deterministic-based optimization (DBO) and

b) Reliability- based optimization (RBO), are approximately similar.

Therefore for larger more complicated building designs, the two procedures are likely to converge to designs that differ. For all three performance levels considered, the height-wise drift distribution differs, while for the DBO design the critical stories are the third and the fourth and for the RBO building the maximum demand is observed at the top (seventh and eighth storey). Moreover, for both buildings, the drift thresholds are reached for every performance level.

Finally, Table 3 shows the limit-state MAFs and in parenthesis the corresponding return periods. Also, with bold fonts we show the cases that the corresponding MAF thresholds have been violated. For both frames the RBO designs satisfy the constraints of Equation 7.17, while the DBO designs violate them for the SD and NC limit-states. Regarding the RBO buildings that have been designed having explicit limits on the allowable MAFs, it seems that the SD and NC limit-states are somewhat close to the thresholds, i.e. 475 and 2475 years respectively.

Table 7.3: Mean annual frequencies for the DBO and the RBO formulation. In parenthesis the corresponding return periods τ are given.

Design objective	DBO	RBO	RBO expectations
Three-storey steel frame			
DL	0.00435 (230 yrs)	0.00425 (235 yrs)	72
SD	0.00183 (547 yrs)	0.00174 (575 yrs)	475
NC	0.00040 (2478 yrs)	0.00034 (2921 yrs)	2475
Nine-storey steel frame			
DL	0.0295 (340 yrs)	0.00142 (702 yrs)	72
SD	**0.0295 (340 yrs)**	0.00142 (702 yrs)	475
NC	**0.0012 (834 yrs)**	0.00040 (2530 yrs)	2475

7.10 References

ASCE/SEI (2007), Seismic rehabilitation of existing buildings. ASCE Standard ASCE/SEI 41-06, American Society of Civil Engineers/Structural Engineering Institute, Reston, Virginia.

Azarbakht, A., Dolsek, M. (2007). Prediction of the median IDA curve by employing a limited number of ground motion records. Earthquake Engineering & Structural Dynamics 36(15): 2401-2421.

Azarbakht, A., Dolsek, M. (2011). Progressive Incremental Dynamic Analysis for First-Mode Dominated Structures. Journal of Structural Engineering 137(3):445-455.

Balea, I.D., Hulea, R., Stavroulakis, G.E. (2013). Discrete optimization approach for steel frames and trusses, based on genetic algorithm. ECCOMAS Special Interest Conference-SEECCM 2013: 3rd South-East European Conference on Computational Mechanics, Proceedings-An IACM Special Interest Conference pp. 650-659.

Balea, I.D., Hulea, R., Stavroulakis, G.E., (2013), Implementation of eurocode load cases in optimization problems of steel frames, based on genetic algorithms, Applied Mechanics and Materials, 310,pp.609-613.

Chopra, A.K. and Goel, R.K. (2001). “Direct Displacement-Based Design: Use of Inelastic vs. Elastic Design Spectra.” Earthquake Spectra, Vol. 17(1), pp. 47-65.

Chopra, A.K. and Goel, R.K. (2002). ”A modal pushover analysis procedure for estimating seismic demands for buildings.” Earthquake Engineering & Structural Dynamics, Vol. 31(3), pp. 561-582.

Deb, K. (2000). “An efficient constraint handling method for genetic algorithms”, Computer Methods in Applied Mechanics in Engineering, 186(2-4): 311-338.

Dolsek, M., Fajfar P. (2004). IN2-A simple alternative for IDA, 13th World Conference on Earthquake Engineering, Vancouver, B.C., Canada August 1-6 2004, Paper No.3353.

Dolsek, M., Fajfar P. (2007). Simplified probabilistic seismic performance assessment of plan-asymmetric buildings, Earthquake Engineering & Structural Dynamics, 36(13): 2021–2041.

Dolsek, M. (2009). Incremental dynamic analysis with consideration of modeling uncertainties, Earthquake Engineering & Structural Dynamics, 38(6): 805–825.

EN 1991-1-4:2005 (2005) Eurocode 1: Actions on Structures-Part 1-4: General Actions-Wind Actions. European Committee for Standardisation, Brussels, Belgium.

EN 1993-1 (2005) Eurocode 3: Design of steel structures. Part 1.1: General rules for buildings, European Committee for Standardisation, Brussels, Belgium.

EN 1998-1:2003 (2003) Eurocode 8: Design of structures for earthquake resistance. Part 1: General rules, seismic ENV 1991 (1994) Eurocode 1 Basis of design and design actions on structures. European Committee for Standardisation, Brussels, Belgium.

FEMA P-695 (2009). Quantification of Seismic Performance Factors, FEMA P-695 Report, prepared by the Applied Technology Council for the Federal Emergency Management Agency, Washington, DC.

Foutch, D.A., Yun, S.-Y. (2002). Modelling of steel moment frames for seismic loads, Journal of Constructional Steel Research, 58, 529-564.

Fragiadakis, M., Lagaros, N. (2011). An overview to structural seismic design optimization frameworks, Computers & Structures, 89(11): 1155-1165.

Fragiadakis, M., Lagaros, N.D. and Papadrakakis, M. (2006). Performance-based optimum design of steel structures considering life cycle cost, Structural and Multidisciplinary Optimization, 32(1): 1-11.

Fragiadakis, M., Papadrakakis, M. (2008). Performance-based optimum seismic design of Reinforced Concrete Structures, Earthquake Engineering and Structural Dynamics 37(6): 825-844.

Fragiadakis, M., Vamvatsikos, D. (2010). Fast Performance Uncertainty Estimation via Pushover and Approximate IDA, Earthquake Engineering and Structural Dynamics, 39(6): 683-703.

Geem, Z.W., Kim, J.H, Loganathan, G.V. (2001). A new heuristic optimization algorithm: harmony search. Simulation, 76(2):60-68.

Geem, Z.W. (2009). Music-inspired harmony search algorithm: theory and applications, Springer, Berlin.

Goldberg, D.E. (1989). Genetic Algorithms in Search, Optimization, and Machine Learning. Addison-Wesley Longman Publishing Co.

Han, S.W., Chopra, A.K. (2006). Approximate incremental dynamic analysis using the modal pushover analysis procedure. Earthquake Engineering & Structural Dynamics, 35(15): 1853–1873.

Hasancebi, O., Ferhat, E., Saka M.P., (2010). Adaptive Harmony Search Method for structural optimization, Journal of Structural Engineering, 136(4):419-431.

Jalayer, F. (2003). Direct probabilistic seismic analysis: Implementing non-linear dynamic assessments. PhD Dissertation, Department of Civil and Environmental Engineering, Stanford University, Stanford, CA.

Lagaros, N.D., Fragiadakis, M., Papadrakakis M., Tsompanakis Y. (2006). Structural Optimization: A tool for evaluating seismic design procedures. Engineering Structures, 28(12): 1623-1633.

Liel, A.B., Haselton, C.B., Deierlein, G.G., and Baker, J.W. (2009). Incorporating Modeling Uncertainties in the Assessment of Seismic Collapse Risk of Buildings. Structural Safety, 31(2): 197-211.

Liu, M, Burns, SA, Wen, YK (2003). Optimal seismic design of steel frame buildings based on life cycle cost considerations. Earthquake Engineering and Structural Dynamics, 32(9), 1313-1332.

Maniatakis, Ch.A., Spyrakos, C.C. (2012). A new methodology to determine elastic displacement spectra in the near-fault region. Soil Dynamics and Earthquake Engineering, 35:41-58.

McKenna, F., Fenves, G.L. (2001) The OpenSees Command Language Manual, 1.2, Edition, 2001.

Perus, I., Klinc, R., Dolenc, M., Dolsek, M. (2013). A web-based methodology for the prediction of approximate IDA curves. Earthquake Eng. Struct. Dyn., 42(1), 43-60.

Rojas, H.A., Pezeshk. S., Foley, C.M. (2007). Performance-based optimization considering both structural and nonstructural components. Earthquake Spectra, 23(3): 685-709.

Spyrakos, C.C., Maniatakis, Ch.A., Smyrou, E. and Psycharis, I.N., (2012) “FRP Strengthened Brick-Infilled RC Frames: An Approach for their Proper Consideration in Design”, The Open Construction and Building Technology Journal, Vol. 6, (Suppl 1-M19), pp. 306-324.

Tsompanakis, Y., Lagaros, N.D., Stavroulakis, G.E., Soft computing techniques in parameter identification and probabilistic seismic analysis of structures, Advances in Engineering Software 39(7), pp. 612-624

Vamvatsikos D., Dolsek M. (2011). Equivalent constant rates for performance-based seismic assessment of ageing structures, Structural Safety, 33(1): 8-18.

Vamvatsikos, D. (2009). Optimal multi-objective seismic design of a highway bridge by selective use of nonlinear static and dynamic analyses, Proceedings of the 9th International Conference on Structural Safety and Reliability (ICOSSAR), September 13-17, 2009, Osaka, Japan.

Vamvatsikos, D., Cornell C.A. (2002). Incremental Dynamic Analysis. Earthquake Engineering & Structural Dynamics 31(3): 491–514.

Vamvatsikos, D., Cornell C.A. (2005). Direct estimation of seismic demand and capacity of multidegree-of-freedom systems through incremental dynamic analysis of single degree of freedom approximation. Journal of Structural Engineering, 131(4): 589–599.

Vamvatsikos, D., Cornell, C.A. (2006). Direct estimation of the seismic demand and capacity of oscillators with multi-linear static pushovers through Incremental Dynamic Analysis. Earthquake Engineering & Structural Dynamics 35(9): 1097–1117.

Vamvatsikos, D., Fragiadakis, M. (2010). Incremental Dynamic Analysis for Seismic Performance Uncertainty Estimation, Earthquake Engineering and Structural Dynamics 39(2): 141-163.

Zacharenaki A., Fragiadakis M., Assimaki D. and Papadrakakis M. (2009). The impact of using scaled ground motion records for seismic capacity assessment, ECCOMAS Thematic Conference on Computational Methods in Structural Dynamics and Earthquake Engineering, June 22–24, Rhodes, Greece.

Zacharenaki A., Fragiadakis M., Assimaki D. and Papadrakakis M.(2014), Bias assessment in Incremental Dynamic Analysis due to record scaling, Soil Dynamics and Earthquake Engineering (accepted for publication)

CHAPTER 8

Conclusions and future research

8.1 Contributions of this study

This study presents an investigation on the seismic loading of structures and on a design methodology that results on optimized designs. It begins with a general overview of the methods applied to define the external loading for structural design. Then proceeds until a presentation of the intensity measures, followed by the different interpretations that are given by earth scientists and engineers of the first mode spectral acceleration ($Sa(T_1,5\%)$). The seismic hazard curve of spectral acceleration and the seismic records used for design are discussed together with the three types of accelerograms: natural, synthetic and artificial. Emphasis is given on the natural records because they are the most representative of strong ground motions, since a limited strong motion database makes it difficult to find natural unscaled earthquakes at the desired intensity level near structural collapse. The obtained results in this study revealed that the use of synthetic records is a reliable alternative natural accelerograms in high intensities. The advantages of the different types of intensity measures are presented as opposed to the first-mode spectral acceleration, which is usually used as the main intensity measure when the structure experiences seismic loading.

A methodology for the evaluation of the bias introduced due to record scaling in incremental dynamic analysis (IDA) has been presented. We have compared response estimations obtained using unscaled natural and synthetic records against those of IDA. Our comparison was based on calculating conditional bootstrap confidence intervals through a novel approach. A variety of structures has been considered and the overall conclusion of this study is that the bias IDA introduces with IM= Sa(T_1) is small and acceptable for engineering calculations. However, there are structural systems, e.g. stiff oscillators at large limit-states, where IDA fails to give unbiased response estimates. In this context, our findings are briefly summarised as follows:

- Current ground motion databases contain only few ground motions capable to produce large inelastic demands on structures with periods that exceed 0.5sec. Hence the used synthetic records as well is necessary.

- The results of the bias assessment show that the SDOF oscillators underestimate the Sa capacity of IDA for first mode periods T_1=0.1, 0.3 and 0.5sec, while IDA gave unbiased response estimates for SDOFs with T_1=0.7, 1.0 and 1.5sec. Here there were issues at high ductilities.

- For the three- and nine-storey steel moment resisting frames IDA does not bias the seismic capacity estimates.

Furthermore, the performance-based seismic design of steel moment-resisting frames has been investigated and a novel reliability-based optimization (RBO) algorithm has been proposed.

- It was shown that deterministic and reliability-based criteria can be easily adopted within the performance-based design concept which enables the engineer to define the mean annual frequency (MAF) of preset performance levels as a design criterion. Within this context, a common language can be used between engineers and stakeholders in setting appropriate requirements for the design of a building. The proposed algorithm uses the static-pushover-to-incremental-dynamic-analysis (SPO2IDA) method as an approximate performance estimation tool in an effort to speed up the probabilistic calculations.

- It was also shown that the implementation of structural design code checks within the proposed design framework is possible and designs that meet seismic design code provisions can be obtained in a straightforward manner. A genetic algorithm was implemented to solve the resulting optimization problem.

- While in deterministic-based optimization (DBO), stress and displacement constraints are considered in accordance with the design code safety factors, in the RBO case probabilistic constraints are incorporated instead. The obtained designs can be quite different from those obtained within a deterministic optimization framework as shown in the case of the nine-storey steel frame. Therefore, the proposed RBO formulation can really ensure optimal weight, providing a truly reliability-based design procedure applicable to real-world structures leading to safe and economic designs which should be preferred to the deterministic-based (DBO) alternative.

8.2 Future research

- The antiseismic methods of design with irregular plan view structures has always been an important problem for the engineers. The application of the proposed design methodology to this type of structures could lead to usefull conclusions.

- The design procedures which are based in non-linear methods of analysis posess increasing computational cost. Recent advances on computational methods for reducing the cost of the analysis and design such problems or alternatively reliable approximate methods evaluation of inelastic displacements, are necessary for the implementation of non-linear methods of analysis for design problems in everyday practice. Regardless of future developments in the field of computational engineering, the methods presented in this thesis are very likely to become especially popular in the coming years given the growth of computational power of modern computers.

- In recent years significant developments in the field of earthquake engineering related to new, improved design procedures have emerged. Such design procedures involve the development of computational tools that make feasible the incorporation of nonlinear analysis methods in order to account for extreme seismic actions. This design approach can be easily applied in engineering practice.